

Optimisation of a deep drawing process with experimental validation

Applied to an automotive deep drawing process of a B-pillar

CTW.07/TM-5562

Graduation assignment

Ing. E.V. ter Wijlen

October 22, 2007

University of Twente
Faculty of Engineering Technology
Department of Mechanical Engineering
Section Mechanics of Forming Processes

Supervision:

Prof. Dr. Ir. J. Huétink (UT)

Dr. Ir. A.H. van den Boogaard (UT)

Dr. Ir. M.H.A. Bonte (Company)

Dr. Ir. M.A. Masen (UT)

Voorwoord

Het werk dat wordt beschreven in dit afstudeer verslag is uitgevoerd in de periode van Juli 2006 tot Oktober 2007. Hiermee komt een einde aan mijn studieperiode. Na de opleiding werktuigbouwkunde aan de Saxion Hogeschool in Enschede ben ik begonnen met de studie werktuigbouwkunde aan de Universiteit Twente.

Dit deed ik samen met een stel andere HBO'ers Teun, Sander, Rob, Thijs, Mathijs en Jasper. Welke ik graag wil bedanken voor de leuke jaren. Niet alleen het samen studeren, maar ook het soggen¹ en de vele feestjes zorgden voor een leuke tijd.

Dit dankwoord wil ik ook aangrijpen om allen te bedanken die mij geholpen danwel ondersteund op de UT. Bedankt voor de sterke koffie, mooie verhalen en gezelligheid tijdens mijn afstudeerperiode.

Van buiten de vakgroep wil ik graag Bart Carleer (AutoForm) en Eisso Atzema (Corus) bedanken voor de discussies en bijeenkomsten m.b.t. tot mijn project.

Als één van de laatste maar niet als minste wil ik Martijn Bonte, Ton van den Boogaard en Han Huétink bedanken voor de dagelijkse begeleiding tijdens mijn afstuderen.

Tot slot wil ik mijn familie en mijn vriendin Jacobijn bedanken, omdat zij mij altijd hebben ondersteund en geholpen waar het kon.

Enschede, Oktober 2007
Rik ter Wijlen

¹Studie ontwijkend gedrag

Samenvatting

Elke auto bevat tussen de 200 en 300 onderdelen gevormd uit metaalplaat. Deze zitten rond de body en het chassis van de auto. Voor het omvormen van metaalplaat wordt meestal een dieptrek proces gebruikt. In het verleden werd het productieproces ontworpen door 'trial-and-error' in de fabriek. Sinds de jaren 90 hebben de eindige elementen simulaties hun intrede gedaan. Sindsdien is de 'trial-and-error' verplaatst naar computers. De volgende slag is het optimaliseren van dit productieproces om een robuust proces te verkrijgen zonder uitval en tegen lage kosten.

De opdracht is het toepassen van de optimalisatie techniek op het dieptrek proces van een B-stijl van de auto. De opdracht wordt uitgevoerd doormiddel van vier taken:

- Toepassen van de optimalisatie technieken op het productie proces van de B-stijl voor het bepalen van de meest invloedrijkste parameters.
- Het evalueren van de materiaal modellen van AutoForm en Corus.
- Het bepalen van de numerieke trends van de variabelen op de responsie.
- Het valideren van de numerieke trends doormiddel van experimentele testen in Dortmund.

De optimalisatie strategie is toegepast op het productie proces van de B-stijl. De uitkomst is een wiskundig optimalisatie probleem met één impliciete randvoorwaarde en tien ontwerp variabelen. Het doel is om de spanningen zo ver mogelijk onder de grens vervormingskromme (FLC) met als impliciete randvoorwaarde om boven de plooi lijn te blijven. De meest invloedrijkste variabelen, voor dit probleem, zijn bepaald met OptForm en AutoForm Sigma wat leidde tot één proces variabele, de plooihouder kracht en drie geometricische variabelen.

Verschillende materialen worden gebruikt in het dieptrek proces. In samenwerking met Corus zijn drie materialen gekozen; TRIP700, H340LAD en DP600. De verschillen tussen de materiaal modellen van Corus en de materiaal modellen die standaard in AutoForm zitten zijn beschreven. De verschillen kunnen gevonden worden in de FLC, vloeï oppervlak en de versterkings kromme. Dit is de reden waarom de materiaal modellen in de database van AutoForm "sterker" zijn dan diegene van Corus.

De vier ontwerpvariablen zijn één voor één een hele range gevarieerd, terwijl de anderen op hun referentiewaardes zijn gezet, zodat er een duidelijk beeld wordt verkregen over het effect van de variabelen op de responsie. De uitkomst is het effect van de variabele op de responsie in een grafiek, een zogenaamde "scatter plot". Tevens zijn er ook twee variabelen tegelijkertijd gevarieerd terwijl de anderen op hun referentiewaardes zijn gezet. De uitkomst daarvan is opgeslagen in een oppervlakte grafiek. Een opmerkelijke conclusie is getrokken tijdens deze berekeningen. Een niet continue trend is zichtbaar in een deel van de B-stijl met de procesvariabele plooihouder kracht.

Voor het valideren van de trends welke gevonden zijn tijdens de eindige elementen simulaties zijn experimentele testen uitgevoerd. Dit is gedaan op de universiteit van Dortmund met H340LAD en DP600. De eerste doelstelling was het vaststellen van het procesvenster van de verschillende materialen. De bovengrens (scheuren) en de ondergrens (plooiën) zijn vastgesteld. De andere testen zijn uitgevoerd om de effecten van de geometrische variabelen te bepalen op het dieptrek proces van de B-stijl. De testen zijn uitgevoerd in 2 dagen. Met het materiaal DP600 zijn er grote verschillen, tussen de 2 dagen met de plooihouder kracht waarbij de B-stijl scheurde. Mogelijke verklaring voor dit verschillen zijn positie van de plaat en/of wrijving. De pers data is geevalueerd aan de hand van de effectieve stoot kracht. De uitkomst is dat de positie van de plaat invloed heeft op het effectieve stoot kracht. Een groot verschil is gevonden tussen de effectieve stoot kracht. De effectieve stoot kracht was op dag twee hoger m.b.t. de experimenten van DP600. De verklaring voor de stijging in effectieve stoot kracht is een stijgende wrijving. Wat de oorzaak van de verhoogde wrijving is, is op dat moment nog steeds een raadsel. Voor het evalueren van de effecten van de positie en wrijving zijn extra eindige elementen berekeningen uitgevoerd. Dit bevestigt het vermoeden van de grote invloed van wrijving.

De conclusie die getrokken kan worden is dat de trends van de eindige elementen berekeningen gelijk zijn aan de trends met de experimenten. De exacte waardes zijn echter verschillend. Dit is veroorzaakt door de variatie in experimenten en de beperking in eindige elementen berekeningen.

Summary

Each car contains between the 200 and 300 sheet metal formed parts. They can be found amongst others in the body and the chassis of vehicles. Sheet metal parts are generally manufactured by a deep drawing process. In the past designing such a deep drawing process was done by experimental trial-and-error in the factory. Since this trial-and-error process is very time-consuming and costly, Finite Element simulations have been developing to move the trial-and-error procedure from the factory to the computer which makes the process design much faster and cheaper. The next step is to optimise the manufacturing process in the automotive industry to obtain a robust process with no scrap and low costs.

The assignment is to apply optimisation techniques to a real automotive deep drawing process of a B-pillar. This will be done by executing four tasks:

- Applying the optimization strategies to determine the variables with the most influence on the B-pillar.
- To evaluate the material models which are included in AutoForm with the ones provided by Corus.
- To determine the numerical trends with the design variables.
- To verify the numerical trends with experimental tests.

The optimisation strategy is applied to the manufacturing process of the B-pillar. First the 7 step methodology is applied to model the manufacturing process of the B-pillar. The outcome is a mathematical optimisation problem with one implicit constraint and ten design variables. The objective is to maximize the distance of the strains to the forming limit curve but stay above the wrinkling line, constraint. The most influential variables, for this problem, are determined with OptForm and AutoForm Sigma which yielded to one process variable, the blank holder force and three geometrical variables.

Several different materials can be used in the deep drawing process. In cooperation with Corus, three materials were chosen out of their range, namely TRIP700, H340LAD and DP600. The difference between the Corus material models and the ones which are implemented in AutoForm are specified. The difference can be found in the FLC, yield surfaces and hardening curves. This is the reason why the material models in the database of AutoForm are, “stronger” than the ones provided by Corus.

The four design variables are varied one by one while the others are set to the reference setting, while recording their effect on the responses, necking and wrinkling. The outcome is the effect of the variable on the response in a graphical display, the so called scatter plots. Also two variables are varied while the other two are set to their reference setting, the outcome is recorded in a surface plot. A remarkable conclusion was drawn during this

investigation, a non continuous trend was discovered in a certain region in the B-pillar with the process variable, blank holder force.

To validate the trends, which are found with the FEM simulations, experimental tests are conducted at the University of Dortmund, with H340LAD and DP600. The first objective was to determine the process window of the different materials, the upper (necking) and lower (wrinkling) limit of the blank holder force. The other tests that are conducted were to determine the effect of the geometrical variables on the deep drawing of the B-pillar. The tests were conducted during two days. With the material DP600 a large difference, between the two days, was found. With the same blank holder force, the B-pillar showed a crack at day 2. Possible explanations for this difference are: the position of the blank and friction. To determine if these possibilities are responsible for the difference, in blank holder force, the press data was evaluated. To determine the effect of the different possibilities the effective punch force is evaluated. The outcome is that the position had some influence on effective punch force. If one compares the experiments, with the same blank holder force for DP600 at day 1 and day 2, the effective punch force increased. This is the reason that the B-pillar started to neck at a lower blank holder force at day 2 in comparison with day 1. The explanations for the increase in effective punch force is the increase of friction. What did cause this friction was unknown at that moment. To evaluate the effect of position and friction additional FEM simulations are performed. This endorses the statement of the large influence of friction.

The conclusion that can be drawn is that the trends of the FEM simulations are similar with the trends found with the experiments. But the exact values of the trends are different. This is caused by the variation in experiments and the limitation of FEM simulations.

Contents

| | |
|--|------------|
| Voorwoord | i |
| Samenvatting | iii |
| Summary | v |
| 1 Introduction | 1 |
| 1.1 Background | 1 |
| 1.2 Metal forming processes | 1 |
| 1.3 B-pillar | 2 |
| 1.4 Assignment | 3 |
| 1.5 Objective | 3 |
| 1.6 Outline | 3 |
| 2 Optimisation strategy applied to the B-pillar | 5 |
| 2.1 Modeling the optimisation problem | 5 |
| 2.1.1 Step 1: Determine the appropriate optimisation situation | 6 |
| 2.1.2 Step 2: Select the necessary responses | 6 |
| 2.1.3 Step 3: Select objective function and implicit constraints | 9 |
| 2.1.4 Step 4: Quantify the objective function and implicit constraints | 10 |
| 2.1.5 Step 5: Select the design variables | 11 |
| 2.1.6 Step 6: Define the ranges on the design variables | 12 |
| 2.1.7 Step 7: Identify explicit constraints | 13 |
| 2.1.8 Mathematical model | 13 |
| 2.2 Screening and sensitivity | 14 |
| 2.2.1 Difference between OptForm and AutoForm Sigma | 14 |
| 2.2.2 Screening with OptForm | 15 |
| 2.2.3 Sensitivity with AutoForm | 16 |
| 2.2.4 Final design variables | 18 |
| 2.3 Conclusion | 18 |
| 3 Material models | 19 |
| 3.1 Materials | 19 |
| 3.2 Corus vs AutoForm | 20 |
| 3.2.1 H340LAD | 21 |

CONTENTS

| | | |
|----------|---|-----------|
| 3.2.2 | DP600 | 22 |
| 3.2.3 | TRIP700 | 23 |
| 3.3 | Discussion | 24 |
| 3.4 | Conclusion | 26 |
| 4 | FEM simulations | 27 |
| 4.1 | Settings | 27 |
| 4.1.1 | Reference settings | 28 |
| 4.1.2 | Variable settings | 28 |
| 4.1.3 | Blank size | 28 |
| 4.2 | Scatter plots | 29 |
| 4.3 | Blank holder force (Process Window) | 29 |
| 4.3.1 | H340LAD | 30 |
| 4.3.2 | DP600 | 31 |
| 4.3.3 | TRIP700 | 32 |
| 4.3.4 | Discussion | 33 |
| 4.4 | Blank holder force (Split in edges) | 34 |
| 4.5 | Scatter plots dependent on geometrical variables | 37 |
| 4.5.1 | Scatter plots dependent of x_5 | 37 |
| 4.5.2 | Scatter plots dependent of x_6 | 38 |
| 4.5.3 | Scatter plots dependent of x_{72} | 38 |
| 4.6 | Surface plots | 39 |
| 4.6.1 | Surface plots dependent on BHF and x_5 | 39 |
| 4.6.2 | Surface plots dependent on BHF and x_6 | 40 |
| 4.6.3 | Surface plots dependent on x_5 and x_6 | 40 |
| 4.7 | Discussion: scatter and surface plots | 41 |
| 4.8 | Optimal settings | 42 |
| 4.8.1 | Discussion: Optimal settings | 43 |
| 4.9 | Conclusion | 43 |
| 5 | Experimental validation | 45 |
| 5.1 | Materials for experimental validation | 45 |
| 5.2 | Equipment | 46 |
| 5.3 | Validation | 47 |
| 5.4 | Blank holder force | 48 |
| 5.4.1 | H340LAD | 48 |
| 5.4.2 | DP600 | 51 |
| 5.5 | Geometrical variables x_5 and x_6 | 53 |
| 5.5.1 | Variation of geometrical variable x_5 | 53 |
| 5.5.2 | Variation of geometrical variable x_6 | 55 |
| 5.5.3 | Variation of geometrical variable x_5 and x_6 | 57 |
| 5.6 | Discussion: results experiments | 58 |
| 5.7 | Conclusion: results experiments | 59 |
| 5.8 | Verification of the experimental results | 60 |
| 5.8.1 | Friction | 62 |
| 5.8.2 | Position | 64 |
| 5.8.3 | Influence geometrical variables | 64 |
| 5.9 | Comparison of the experimental results with FEM | 66 |

| | | |
|----------|---|------------|
| 5.9.1 | Process window | 66 |
| 5.9.2 | Thickness | 69 |
| 5.9.3 | Strains | 72 |
| 5.9.4 | Sensitivity for noise variables | 73 |
| 5.9.5 | Variation in region A | 74 |
| 5.10 | Conclusion | 75 |
| 6 | Conclusion & recommendations | 77 |
| 6.1 | Conclusions | 77 |
| 6.2 | Recommendations | 78 |
| | Bibliography | 79 |
| A | FEM simulations | 81 |
| A.1 | Springback | 81 |
| A.2 | Blank size | 82 |
| A.3 | AutoForm Sigma Optimisation | 84 |
| B | AutoForm | 87 |
| B.1 | Material models | 87 |
| B.1.1 | Hardening Curve | 87 |
| B.1.2 | Yield surfaces | 89 |
| B.2 | AutoForm responses | 91 |
| B.2.1 | Failure | 91 |
| B.2.2 | Wrinkling criterion | 92 |
| C | Materials models and properties | 93 |
| C.1 | Material properties used in FEM | 94 |
| C.2 | Material properties for experimental validation | 97 |
| C.2.1 | DP600 batch FEM against Experiments | 98 |
| D | Simulation series | 99 |
| D.1 | Exact location of the Regions | 100 |
| D.1.1 | Region A | 100 |
| D.1.2 | Region B | 101 |
| D.1.3 | Split in edge (DP600) | 101 |
| D.2 | Scatter plots | 102 |
| D.3 | Surface plots | 122 |
| D.4 | FEM simulations 2 | 132 |
| D.4.1 | Exact location of the Regions (simulation series 2) | 132 |
| D.4.2 | Region A | 133 |
| D.4.3 | Region B | 134 |
| D.5 | Scatter plots | 135 |
| E | Experimental information | 137 |
| E.1 | Blank dimensions | 137 |
| E.2 | Position of the blank on the die | 139 |
| E.3 | Thickness measurements | 140 |
| E.3.1 | Blank holder force(H340LAD) | 141 |

CONTENTS

| | | |
|-------|--|-----|
| E.3.2 | Blank holder force(DP600) | 143 |
| E.3.3 | Scatter plots dependent of the geometrical variables | 145 |
| E.3.4 | Surface plots dependent of the geometrical variables | 151 |
| E.4 | Forming limit diagrams | 152 |
| E.4.1 | Blank holder force (H340LAD) | 152 |
| E.4.2 | Blank holder force (DP600) | 154 |
| E.4.3 | Geometrical variation(H340LAD) | 156 |
| E.5 | Pictures of the experiments | 162 |
| E.5.1 | H340LAD | 162 |
| E.5.2 | DP600 | 163 |

1

Introduction

In this chapter a short introduction will be given about the background of the assignment and the assignment itself. The objective and the outline will be given at the end of this chapter.

1.1 Background

Each car contains between the 200 and 300 sheet metal formed parts. They can be found amongst others in the body and the chassis of vehicles. Sheet metal parts are generally manufactured by a deep drawing process. In the past, designing such a deep drawing process was done by experimental trial-and-error in the factory. Since this trial-and-error process is very time-consuming and costly, Finite Element simulations have been developed to move the trial-and-error procedure from the factory to the computer which makes the process design much faster and cheaper. It has been observed by the major car manufacturers and part suppliers that one successful simulation is often not sufficient. Due to inherent material and process variation is it possible that a large percentage of the produced parts do not meet the requirements and will thus be rejected. Such high scrap rates are very expensive and should be overcome. A possibility is to optimise the process. Optimisation and robustness analysis are considered to be an important future direction for manufacturing in the automotive industry.

1.2 Metal forming processes

By metal forming a piece of material is formed into the desired shape between dies. Examples of metal forming are forging, rolling, deep drawing, extrusion, hydroforming and stamping. The B-pillar is formed by deep drawing. The process starts with deep drawing of a flat sheet of metal. This is clamped between a die and a blank holder. Then a punch moves down to deform the blank into the desired shape. The process is depicted in Figure 1.1. The final shape of the product depends on tool geometry, material properties of the blank and process parameters.

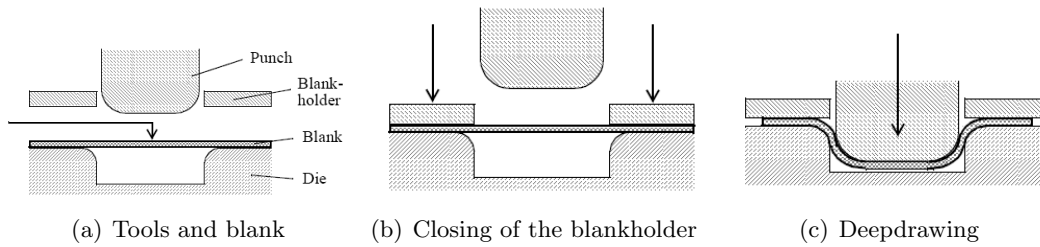


Figure 1.1: Schematic representation of a deep drawing process.

1.3 B-pillar

The definition of a B-pillar: the roof support between a car's front door window and rear side window [2].

The B-pillar is a structural part of a car, see Figure 1.2(e). It has to fulfill several structural loads during the use of a car. The customer wants to have a part without detectable cracks at the outside. Also certain surface defects are not accepted by the customer.

In Figure 1.2 a simplified manufacturing process of a B-pillar is shown, including a numerical simulation and the position of the B-pillar. The production process of a B-pillar starts with a coil of sheet metal. A blank is cut out of the coil. After that the blank is placed in a deep drawing press and it becomes a B-pillar. This part is placed in the automobile.

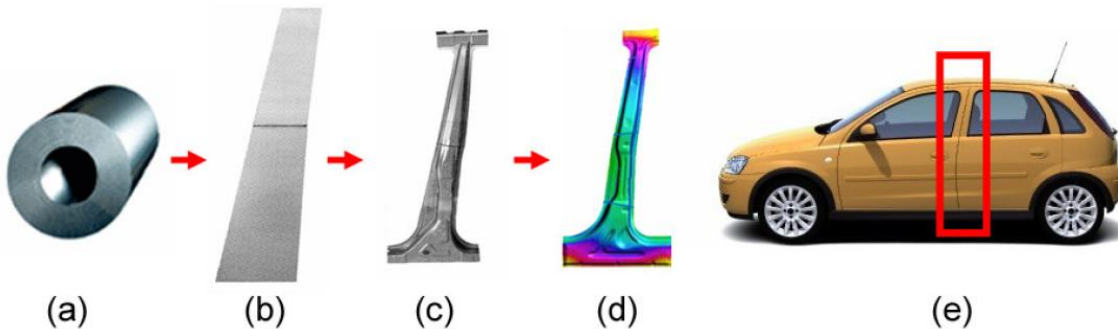


Figure 1.2: (a) sheet metal; (b) blank; (c) B-pillar; (d) FEM simulation; (e) position of the B-pillar in the car.

Many Finite Element Method (FEM) codes are available to simulate the manufacturing process. Depending on the code and type of calculation, one simulation may easily take hours or days to run. However this is much shorter compared to setting up and executing experiments. The FEM simulations which are done in this investigation are done with AutoForm. AutoForm is a specialized software for the simulation of sheet metal forming processes and for the design of complex sheet metal forming tools. AutoForm is the market leader regarding deep drawing simulation software for the automotive industry. The numerical simulation of the B-pillar takes about 1,5 hours.

1.4 Assignment

An optimization strategy is at the time being developed at the University of Twente. This assignment, applying the optimization strategies to a real deep drawing process, material model evaluation and experimental validation is a part of the project of the development of optimization strategies for metal forming processes. Cooperation exists with Corus Automotive, which will provide different materials for the experiments and with AutoForm which provides the simulation software and owns the dies for producing the B-pillar. The experimental validation will be done by performing a real deep drawing test at the University of Dortmund.

1.5 Objective

The main aim of this thesis is to provide useful information about the optimisation strategy. This will be done by executing four tasks:

- Applying the optimization strategies to determine the variables with the most influence on the B-pillar.
- To evaluate the material models which are included in AutoForm with the ones provided by Corus.
- To determine the numerical trends with the design variables.
- To verify the numerical trends with experimental tests.

1.6 Outline

The next chapter starts with applying the optimization strategies to the B-pillar. First the 7 step methodology is applied to the B-pillar manufacturing process. Second, different screening techniques has been used for selection and reduction of variables.

In Chapter 3 the material models of Corus and AutoForm are described and discussed. The most important differences are pointed out and the influence of these differences on the material models.

In Chapter 2 the variables are determined which had the most influence on the B-pillar. In Chapter 4 the variables are varied over a range to determine the effect on the response.

To validate of the effect of the variables experimental tests are preformed in Dortmund, this is described in Chapter 5. Also the difference between the experimental results and the numerical results is discussed. The conclusion and recommendations are listed in Chapter 6.

2

Optimisation strategy applied to the B-pillar

A three stage optimisation strategy is proposed by Bonte in [18]. The three stages are:

- 1: Modeling the optimisation problem
- 2: Screening to determine the most important design variables
- 3: Solving the optimisation problem

In this chapter the modeling of the optimisation problem and the screening to determine the most important design variables will be described applied to the B-pillar. Solving the optimisation problem has been excluded for this investigation.

2.1 Modeling the optimisation problem

For modeling we apply the 7 step methodology proposal that was introduced by Bonte [18]. This consist of the following 7 steps. These will be applied to the B-pillar.

- *Step 1: Determine the appropriate optimization situation;*
- *Step 2: Select only the necessary responses;*
- *Step 3: Select one response as objective function, the others as implicit constraints;*
- *Step 4: Quantify the objective function and implicit constraints;*
- *Step 5: Select possible design variables;*
- *Step 6: Define the ranges on the design variables;*
- *Step 7: Identify explicit constraints.*

2.1.1 Step 1: Determine the appropriate optimisation situation

The first step of the sequence is to determine the appropriate optimisation situation. The product development cycle applied to metal forming assist in doing this, see Figure 2.1.

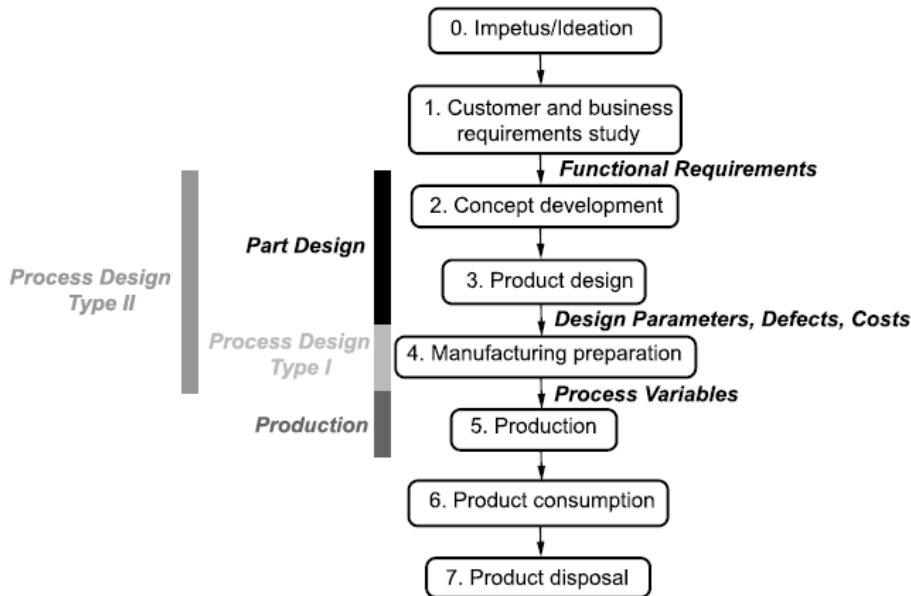


Figure 2.1: The product cycle applied to metal forming [18]

The aim is to optimize the B-pillar, therefore this is a Process Design Type I situation. This reduces the possible number of design variables to process variables only.

2.1.2 Step 2: Select the necessary responses

In step 1 it was determined that this is a Process Design Type I situation, this reduces input and output parameters. In this step only those responses will be selected that are necessary for optimising the problem. As one can see in Figure 2.1, the input and the output of this stage is mentioned. In Figure 2.2 the Input-Response for a design type I is mentioned.

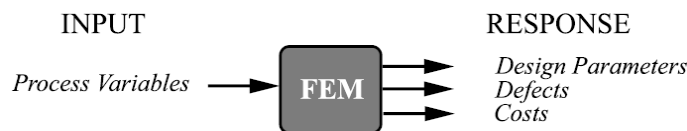


Figure 2.2: Input-response model for FE [18]

The possible responses are: design parameters, defects and costs, see Figure 2.3.

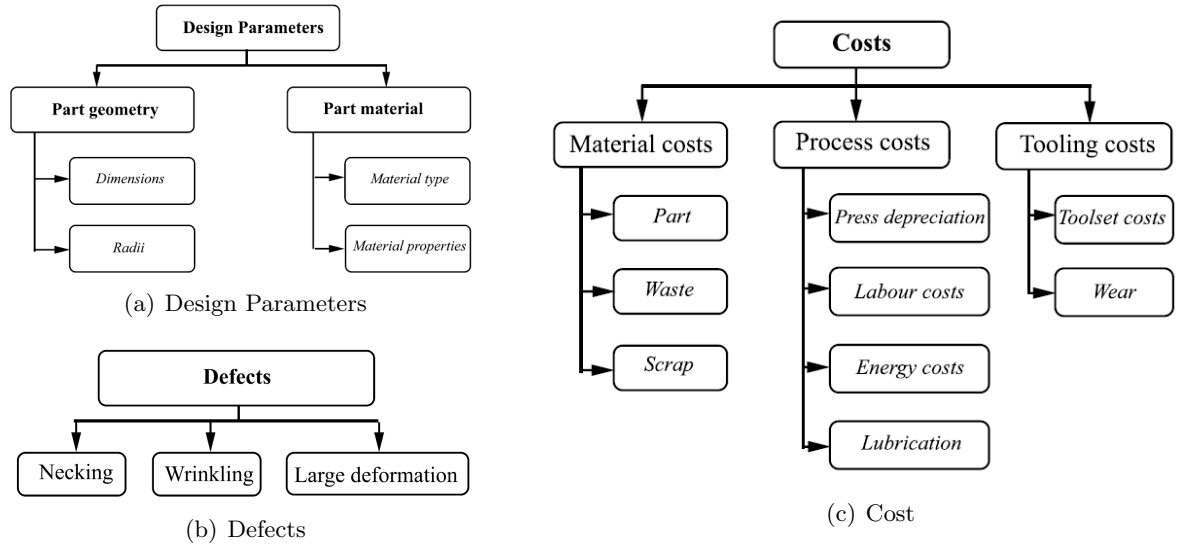


Figure 2.3: Top down structures for the responses from Bonte [1]

In Figure 2.3 top down structures for the possible responses that are mentioned in Figure 2.2 are presented.

If one looks at the top down structure of the design parameters, see Figure 2.3(a), two groups are distinguished. One can look at the part geometry, into dimension for example at the geometrical accuracy of the product. The other group is part material. Due to the fact that there are only 3 materials available for the experimental validation test. The 3 different materials will be considered independently. So therefore the group of part material will not be considered within the optimisation modeling.

Another possible response is the group of defects, see Figure 2.3(b), the possible responses are wrinkling, necking and large deformation. In an earlier project, the project of Veldman [20], experiences have been gained with large deformations. Experiences that have been obtained is that large deformation causes no trouble in the deformation process.

The last group of response is the group of costs, see Figure 2.3(c), these are divided into three different subgroups: material costs, process costs and tooling costs. These are not considered to be critical in this application.

After a discussion with all the participating groups a list of possible responses is made, see Table 2.1.

| Design Parameters | Defects | Costs |
|----------------------|----------------------------|----------------|
| Springback | Necking, measured in FLD | Material costs |
| Geometrical accuracy | Wrinkling, measured in FLD | Force Work |

Table 2.1: Possible responses

Although, the response of the group of costs is very interesting, it is not interesting to look after the effect. Therefore the possible responses are divided into two groups, design parameters and defects. Although the point of springback, see Appendix A.1, is very interesting the first focus will be on the strain space, FLD (wrinkling, necking).

The argument is that springback can be taken into account by a geometry effect and is

therefore much less important compared to product failure and wrinkles. Also the response group of costs is eliminated. The costs are very interesting if a new part is taking in production. If with optimisation the required force can be lowered and therefore a "smaller" press can be used this reduces the costs dramatically. In the case of the B-pillar the deep drawing press will be rented at the University of Dortmund and the material is provided by Corus.

Possible responses

As mentioned earlier the first focus will be on the strain space, this is the so called Forming Limit Diagram (FLD). These responses will be necking and wrinkling.

Necking

The necking of certain materials can be presented by means of a Forming Limit Diagram or FLD. An FLD consists of a number of measurements at which the material is stable, necked or fractured. A Forming Limit Curve (FLC) that denotes the boundary at which the material becomes unstable. The FLC of H340LAD is presented in Figure 2.4(c). The objective is to have a large safety margin to the FLC.

Wrinkling

Due to the fact that wrinkling is hard to predict with the use of FEM. Another approach has been chosen: to make the wrinkling a line in the FLD.

A FEM simulation is made with a minimum blank holder force. At the minimum blank holder force the chance is the highest that wrinkles occur. The FEM program is AutoForm, in this program also a wrinkling criterion is included. The larger the value of the wrinkling criterion at a given location on the sheet, the greater the possibility that wrinkles occur at that location [4], for more information see Appendix B.2.2. Because the wrinkling criterion in AutoForm is relative and it only indicates a possibility, a choice has been made to look at the FLD. Equal thickness can be indicated in the strain space, ($\epsilon_{major} = -\epsilon_{minor}$), as we assume that the reference process is feasible we translate this line to be the wrinkling line, see Figure 2.4(c).

In Figure 2.4(a) the red circled area is the area with the highest wrinkling criterion at the minimum blank holder force. Also a more detailed problem area, see Figure 2.4(b) is included with some red dots in it, here the maximum value of the wrinkling criterion occurs. These correspond with the red dots in the FLD, this will form the lower specification limit. A remark: in the FLD a lot of points are below the line of equal thickness ($\epsilon_{major} = -\epsilon_{minor}$), this means that thickening has taken place in the B-pillar.

The *Wrinkling line*, is made by moving the line of equal thickness to the left. An assumption is made that the reference process is feasible, the line is shifted to the left till all the points with the highest value of the wrinkling criterion are above this line. In Figure 2.4(c) one can see the wrinkling line in the FLD.

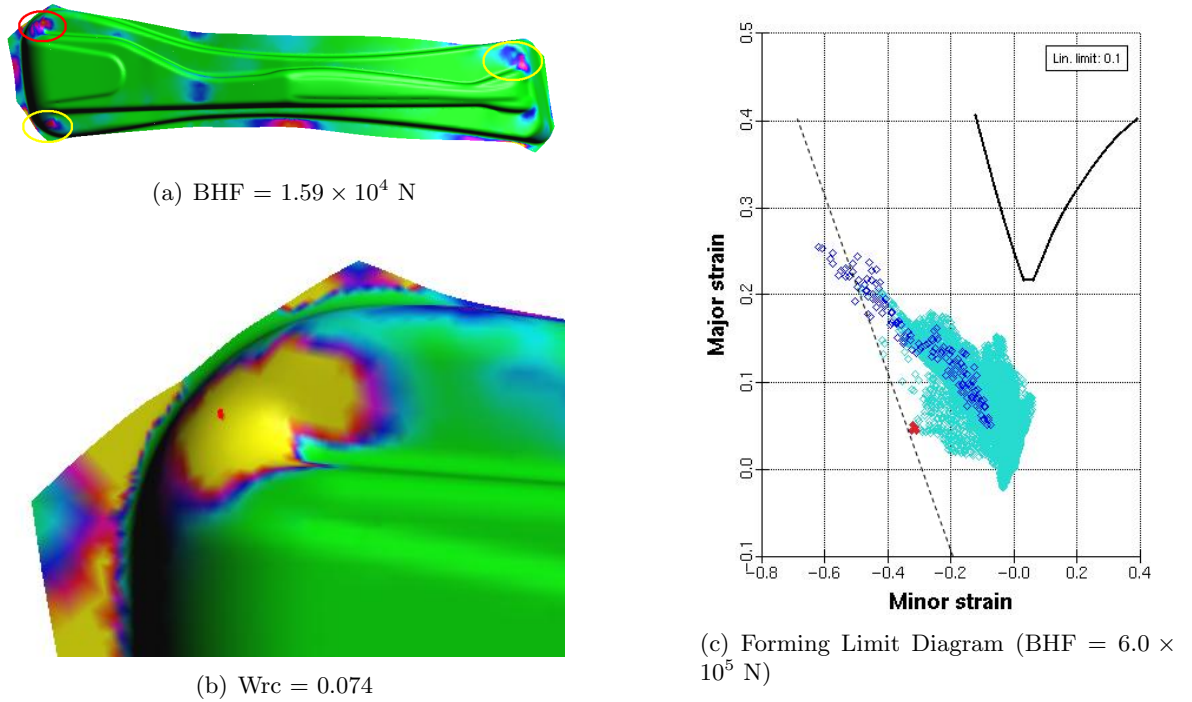


Figure 2.4: Minimum blank holder force and corresponding FLD

2.1.3 Step 3: Select objective function and implicit constraints

There are 2 different options as objective function, namely;

| | Objective function | implicit constraints |
|---|---------------------------|----------------------|
| 1 | max distance to FLC | wrinkling |
| 2 | max distance to wrinkling | FLC |

Table 2.2: Possible objective functions

Option 1: objective is to maximize the distance of the strains in the elements to the FLC and to stay above the implicit constraint the wrinkling line.

Option 2: objective is to maximize the distance of the strains in the elements above the wrinkling line and to stay beneath the FLC.

Conclusion

After a discussion a choice has been made for *Option 1*. The following arguments are used: Necking is more practical than wrinkling, a fracture is a more premium reason to reject a product than wrinkles. Considering the fact that the wrinkling criterion and also the wrinkling line only indicates a possibility for wrinkling. Another reason is that the optimum that will be found is close to the FLC and therefore has a low safety margin. This is not a solid base to start an optimisation.

Therefore the choice has been made for *option 1* to maximize the distance to FLC (f), and as implicit constraint the wrinkling criterion (g). This is the safest way to obtain good products with low risk on cracks (defects). Also if the product shows a crack, this is always a reason for scrap. However if wrinkles occur the product may be acceptable.

2.1.4 Step 4: Quantify the objective function and implicit constraints

All responses are distances in the FLD. The output from FEM are the major and minor strains. The distance to the FLC is defined as:

$$x_{dist2flc} = \epsilon_{maj}(\epsilon_{min}) - \epsilon_{flc}(\epsilon_{min}) \quad (2.1)$$

Where ϵ_{maj} and ϵ_{min} are the major and the minor strain at a certain location in the part, in the case of FEM simulations the major and minor strain in a certain element. A similar formulation can be made for the wrinkling line:

$$x_{dist2wrc} = \epsilon_{maj}(\epsilon_{min}) - \epsilon_{wrc}(\epsilon_{min}) \quad (2.2)$$

The mathematical formulation of the responses is done with the help of the response quantification of Bonte [18].

| Type of Response | Nodal/element value, critical | Applied to process |
|--------------------------|-------------------------------|---|
| Objective | $\max_n (X - USL)$ | $\max_n (\epsilon_{maj}(\epsilon_{min}) - \epsilon_{flc}(\epsilon_{min}))$ |
| Implicit constraint, LSL | $\max_n (LSL - X) \leq 0$ | $\max_n (\epsilon_{wrc}(\epsilon_{min}) - \epsilon_{maj}(\epsilon_{min})) \leq 0$ |

Table 2.3: Response quantification for B-pillar

The objective is to maximize the distance to the FLC. The element value $X = \epsilon_{maj}(\epsilon_{min})$ and the Upper Specification Limit (USL) is the FLC, $USL = \epsilon_{flc}(\epsilon_{min})$. The implicit constraint with a Lower Specification Limit (LSL). The LSL is the wrinkling line, $LSL = \epsilon_{wrc}(\epsilon_{min})$.

$$\epsilon_{wrc} = -\epsilon_{min} - 0.37 \quad (2.3)$$

The exact formulation of the wrinkling line, obtained from Figure 2.4(c).

2.1.5 Step 5: Select the design variables

This step is considered with the input for the FEM. From step 1 is known that the Process Variables are possible design variables (DV), see Figure 2.2. Variables that can be influenced in the manufacturing stage, can be subdivided in Geometry, Material and Process, see the top down structure in Figure 2.5:

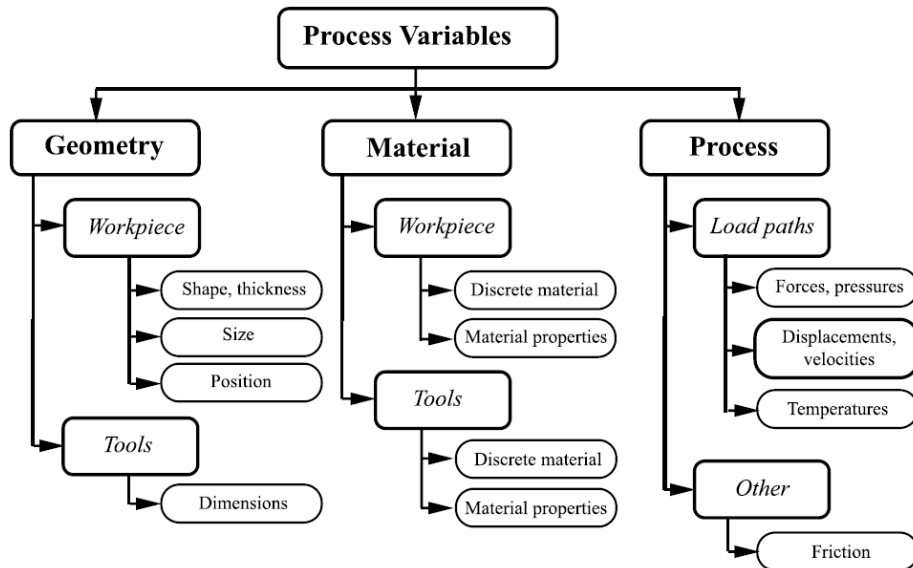


Figure 2.5: Possible process variables from Bonte [18]

If one looks at the top down structure, subgroups are also divided further. The process variable geometry is subdivided into workpiece and tool. It is not possible to change the dimensions of the tools due to fact of the high costs that are associated with the tooling costs. The possible variables must be found in the subgroup workpiece, we cannot change the thickness because we are limited with the test material, also we consider the different materials independently. The size is also no option, due to the fact that the minimum length of the blank to obtain a good product is 1500 mm this is also the length of the sheets that are available for the experimental validation.

If we consider the material parameters, the tools are modeled as rigid so therefore these are not taken into account. Because we consider the different materials independently, these are also not taken into account.

The third category in Figure 2.5 are process parameters, these are subdivided into load paths and other. As we take into account that with the current load path settings a good product can be obtained and the deep drawing press can be safely operated these will not be changed. The only variable in this process is the blank holder force.

Due to the fact that blanks are placed by hand on the blank holder and the blanks are oiled by hand. The friction and position are considered as noise variables. Therefore they are excluded as design variables. The remaining process variables of this investigation, are the blank holder force and the blank shape.

In the blank shape there is an infinite number of design variables, but the following ones are chosen, see Figure 2.6. In this figure the reference blank shape is shown with the design variables.

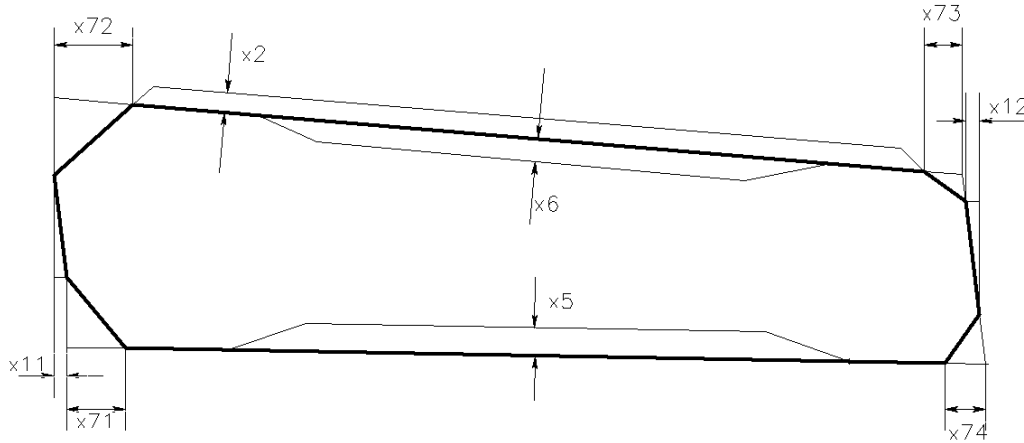


Figure 2.6: Blank shape variables (H340LAD)

2.1.6 Step 6: Define the ranges on the design variables

Upper and lower bounds have been specified for all the 10 design variables, 1 process variables and 9 geometry variables. These are included in Table 2.4.

| Design variable | Parameter | Reference process | Lower bound | Upper bound |
|-----------------|-----------|---------------------|-------------|---------------------|
| x_{01} | BHF | 6.0×10^4 N | 0 N | 4.0×10^6 N |
| x_{02} | x11 | 0 | 0 | 20 mm |
| x_{03} | x12 | 0 | 0 | 20 mm |
| x_{04} | x2 | 0 | 0 | 20 mm |
| x_{05} | x5 | 0 | 0 | 20 mm |
| x_{06} | x6 | 0 | 0 | 20 mm |
| x_{07} | x71 | 0 | 0 | 80 mm |
| x_{08} | x72 | 0 | 0 | 130 mm |
| x_{09} | x73 | 0 | 0 | 50 mm |
| x_{10} | x74 | 0 | 0 | 50 mm |

Table 2.4: Design variables and their ranges

2.1.7 Step 7: Identify explicit constraints

For this problem no relevant explicit constraints that describe impossible combinations of the design variables are present.

2.1.8 Mathematical model

The 7 step methodology now resulted in the following mathematically formulated optimisation model.

$$\begin{array}{llll}
 \max f (BHF, x_{11}, x_{12}, x_2, x_5, x_6, x_{71}x_{72}, x_{73}, x_{74}) & = & \epsilon_{maj}(\epsilon_{min}) - \epsilon_{flc}(\epsilon_{min}) & \\
 \text{s.t.} & & g_{impl} = \max_n (\epsilon_{wrc}(\epsilon_{min}) - \epsilon_{maj}(\epsilon_{min})) \leq 0 & \\
 0 \text{ N} & \leq & \text{BHF} & \leq 5000 \text{ kN} \\
 0 & \leq & x_{11} & \leq 20 \text{ mm} \\
 0 & \leq & x_{12} & \leq 20 \text{ mm} \\
 0 & \leq & x_2 & \leq 20 \text{ mm} \\
 0 & \leq & x_5 & \leq 20 \text{ mm} \\
 0 & \leq & x_6 & \leq 20 \text{ mm} \\
 0 & \leq & x_{71} & \leq 80 \text{ mm} \\
 0 & \leq & x_{72} & \leq 130 \text{ mm} \\
 0 & \leq & x_{73} & \leq 50 \text{ mm} \\
 0 & \leq & x_{74} & \leq 50 \text{ mm}
 \end{array}$$

Table 2.5: Optimisation model

By solving the optimisation model an attempt will be made to improve the reference process.

2.2 Screening and sensitivity

Following the sequence from Bonte [18], the following stage is to reduce the number of design variables further. A lot of design variables may be present which therefore makes the problem time consuming to solve. Therefore it will be worthwhile to reduce the number of design variables.

This will be done with two different methods, namely with the use of OptForm and AutoForm Sigma. To compare these two different methods to each other the problem areas are clearly pointed out. In Figure 2.7 the red circled area is the one where the highest value of the wrinkling criterion occurs. In Figure 2.7 the yellow circled areas is the one where the material first start to neck. On these areas the focus will lie for the screening. This is done with specific reasons, which will be shortly discussed. In the case of wrinkling 4 different zones are pointed out, see Figure 2.7 the red and grey circled areas. This is done for the fact that only the wrinkling in the product must be taken into account and not the wrinkling in the addendum. Also a focus area, see Figure 2.7 the yellow circled area, for the failure criterion is used for the fact to reduce the numerical noise in the response.

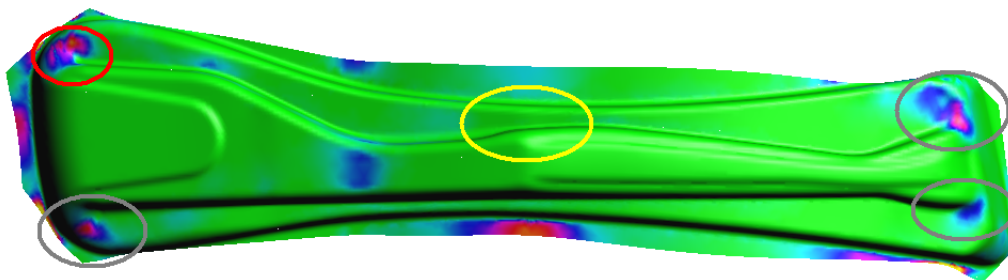


Figure 2.7: Focus areas for influence analysis

2.2.1 Difference between OptForm and AutoForm Sigma

With both procedures the FEM program that is used is AutoForm. However there are some differences between the use of OptForm with AutoForm and the use of AutoForm Sigma with AutoForm. These will be shortly explained.

Design Variables

The blank shape parameters in AutoForm Sigma are made with the help of the global modification mode. Whereas in OptForm the original input files are modified. Also with the variable blank holder force is varied in the Sigma analysis whereas in OptForm the force is exactly implemented.

Post-processing

With the AutoForm Sigma the results are analyzed with the help of function built in AutoForm Sigma, the performance mode. This will be further explained in the section concerning the AutoForm Sigma analysis. Whereas in the case of OptForm this is done with the help of AFprint and MATLAB. With the use of these two programs the values for the response

and constraints are obtained. For the objective the post-variable failure is used. The post-variable failure is defined as the ratio between the maximum major strain computed at an element and the major strain at which the FLC predicts failure at the corresponding minor strain (minor strain in the element). This implies that failure (splits) may be anticipated at a failure value of 1.0. For more information see Appendix B.2.1.

Also for the constraint wrinkling is implemented differently in the two programs. With the post processing of the results of AutoForm Sigma the wrinkling criterion is used, for more information see Appendix B.2.2. Whereas in OptForm the distance to the wrinkling line is used as defined in Table 2.5 is used, with the help of the major and minor strain of the elements in the different focus areas is used.

2.2.2 Screening with OptForm

To look at the linear effects of the design variables on the objectives and constraints a fractional factorial design is applied. Figure 2.8(a) shows a full factorial Design of Experiments (DOE) strategy for two levels and three factors (design variables). A LHD generally provides design points in the interior of the design space and less on the boundary, while a full factorial places DOE points right in the corners of the design space [12]. If one is only interested in linear effects the number of calculations can be reduced by applying fractional factorial DOE, see Figure 2.8(b), this is the case for screening with OptForm.

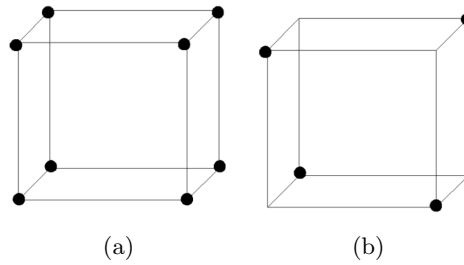


Figure 2.8: (a) 2^3 full factorial design; (b) 2_{III}^{3-1} factorial design

In the optimisation of the manufacturing process of the B-pillar 10 design variables are present. In the case of 10 design variables a so called resolution *III* design is applied in OptForm for screening. Therefore 2_{III}^{10-6} fractional factorial design is applied, therefore 16 FEM calculation have to be run to screen the importance of the design variables. The FEM calculation have to be run in the Finite Element program AutoForm. The FEM simulations have been run on a computer cluster and Pareto plots have been generated.

As mentioned earlier the Pareto plots are generated with the help of AFprint and MATLAB. The resulting Pareto plots for the objective function and implicit constraints are presented in Figure 2.9.

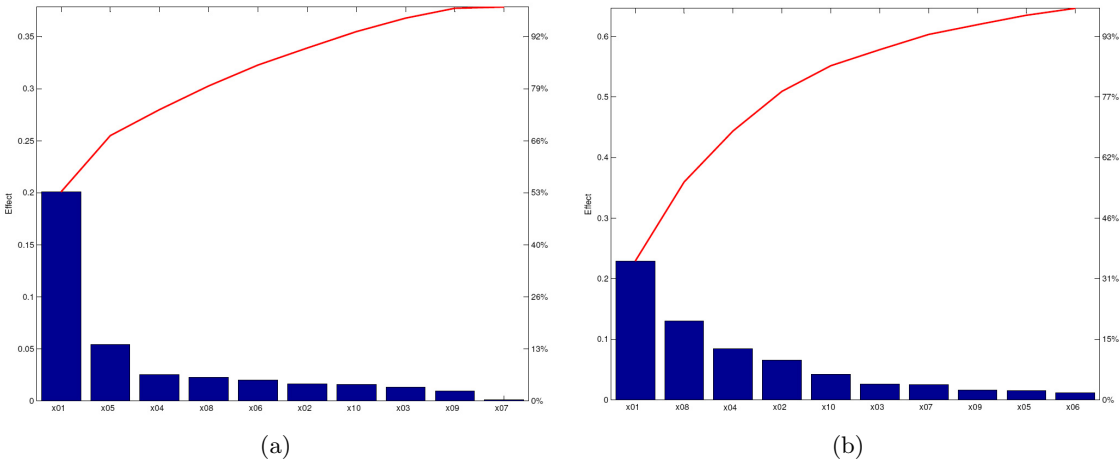
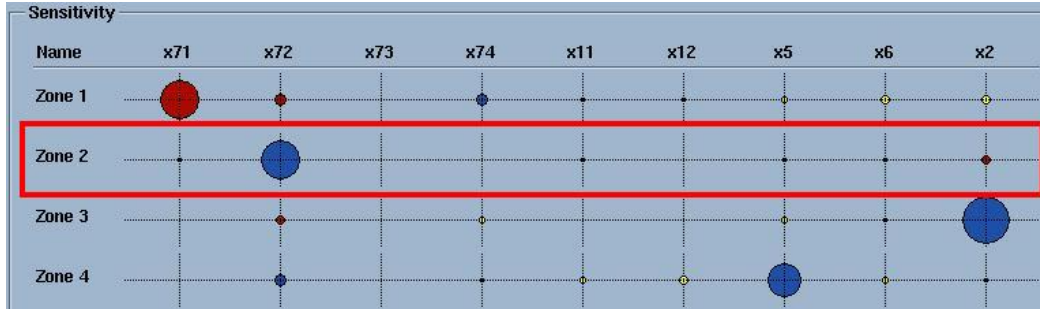


Figure 2.9: (a) Pareto plots of the influence of the design variables on the objective(a) and constraint (b)

Figure 2.9(a) indicates that the variables $x_{01} = BHF$ and $x_{05} = x_5$ have significant influence on the objective function. While Figure 2.9(b) indicates that the variables $x_{01} = BHF$, $x_{08} = x_{72}$ influence the implicit constraint.

2.2.3 Sensitivity with AutoForm

An influence/sensitivity analysis with AutoForm is executed with the 9 blank variables. The variation of the blank variables has been done with the global modification mode. The upper and lower limit of the blank variables are pointed out and with the help of the global modification the outline of the blank is varied. Due to many blank variables that must be taken into account 2 sensitivity analyses have been performed one at the minimum blank holder force and one at the maximum. In Figure 2.7 the red and grey circled areas are the focus area for the sensitivity analysis at the minimum blank holder force. In Figure 2.7 the yellow circled area is the focus area for the sensitivity analysis at the minimum blank holder force.

(a) BHF = 3.51×10^6 N, response Failure(b) BHF = 1.59×10^4 N, response Wrinkling criterion**Figure 2.10:** Sensitivity analysis with AutoForm

The sensitivity tab, see Figure 2.10 shows an influence/sensitivity matrix, which represents an overview of the strength of the influences of the design variables on the selected result variable in the defined zone. In the case of the two sensitivity analyses the result variable at the maximum blank holder force of 3.51×10^6 N is failure(maximum), for more information see Appendix B.2.1. In the case of the minimum blank holder force the result variable is the wrinkling criterion, for more information see Appendix B.2.2.

The area of the circles is proportional to the influence of the corresponding design variables on the appropriate zone of their dependency on the design variable. The blue circle refers to a negative sensitivity value, in AutoForm. The negative influence of the variables means that if the variables gets any larger the B-pillar will be more sensible for necking, see Figure 2.10(a) and wrinkling see Figure 2.10(b).

The yellow marked area is the focus area at the maximum blank holder force (Figure 2.10(a)). The red marked area is the focus area with the influence analysis at the minimum blank holder force (Figure 2.10(b)), this is also the red circled area in Figure 2.7.

Figure 2.10 indicates that the variable x_5 for the maximum blank holder force, see Figure 2.10(a) has a significant influence on the focus area for necking. While in Figure 2.10(b) indicates that the variable x_{72} for the minimum blank holder force has a significant influence.

The difference between the two influence/sensitivity analysis can be clarified through the fact of the different locations of the focus areas for the result variables.

2.2.4 Final design variables

With the screening with OptForm and sensitivity analysis with AutoForm the most important variables are determined. These were the blank holder force and the blank variables x_5 and x_{72} . The focus area for the constraint (wrinkling) is located in the corner of the product see Figure 2.7. It is physically clear that the geometrical variable x_{72} has a large influence on that area. The other geometrical variable x_5 is harder to clarify. A possible explanation is that the blank holder has a smaller area to enforce it is force on the blank. Therefore it will be "easier" to "pull" material through from the "problem" side of the blank. Another variable will also be considered, this will be x_6 . Due to the fact that with earlier experiments with the B-pillar this variable had some influence on the product. The outcome of the screening stage is that the mathematical optimisation model is reduced to 4 variables, which looks as follows, see Table 2.6. Another practical fact is that the sheets that are available for the experimental validation are in the dimensions of 1500 mm the blank cannot become any larger.

$$\begin{array}{rcll}
 \max f (BHF, x_5, x_6, x_{72}) & = & \epsilon_{maj}(\epsilon_{min}) - \epsilon_{flc}(\epsilon_{min}) & \\
 \text{s.t.} & & & \\
 \quad g_{impl} & = & \max_n (\epsilon_{wrc}(\epsilon_{min}) - \epsilon_{maj}(\epsilon_{min})) \leq 0 & \\
 \quad min & \leq & \text{BHF} & \leq \text{max kN} \\
 & & \text{Blank size} & \leq 1500 \text{ mm} \\
 & 0 \leq & x_5 & \leq 20 \text{ mm} \\
 & 0 \leq & x_6 & \leq 20 \text{ mm} \\
 & 0 \leq & x_{72} & \leq 130 \text{ mm}
 \end{array}$$

Table 2.6: Final optimisation model

2.3 Conclusion

Based on the 7 step methodology the B-pillar manufacturing process has been analyzed. The problem has been modeled. With OptForm and AutoForm the problem has been screened and the final optimisation model has been presented.

3

Material models

In the FE simulation program AutoForm several different material models are included, including H340LAD, TRIP700 and DP600. Also Corus provided their material models of H340LAD, TRIP700 and DP600. The following Sections 3.2.1-3.2.2 include the comparison of the three different materials independently. Only the differences are pointed out in these sections. In Section 3.3 the difference between the different models are further discussed. But first a short introduction of the different materials is given and why the materials are chosen.

3.1 Materials

Several different materials can be used in the deep drawing process. In cooperation with Corus, three materials were chosen out of their range, namely TRIP700, H340LAD and DP600. There are different reasons why the choice is made for these material:

- widely used in the automobile industry, see Figure 3.1
- available for experimental validation
- available in required dimensions

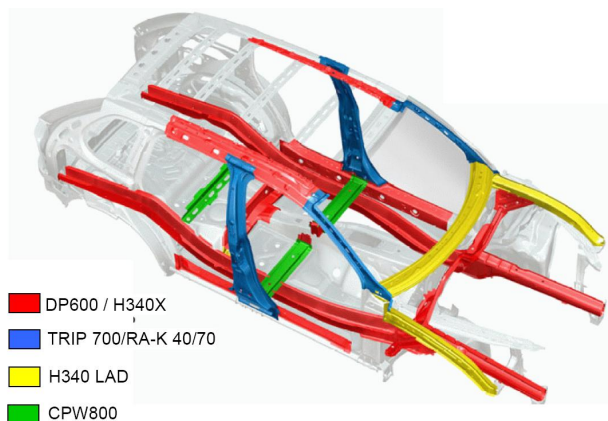


Figure 3.1: Materials in Porsche Cayenne [5]

3.2 Corus vs AutoForm

In this section the material models of the ones provided by Corus and the ones used in the database of AutoForm are compared to each other. In these files, 3 material properties are used, namely the hardening curve, the yield surface and the Forming Limit Curve (FLC) in the Forming Limit Diagram (FLD).

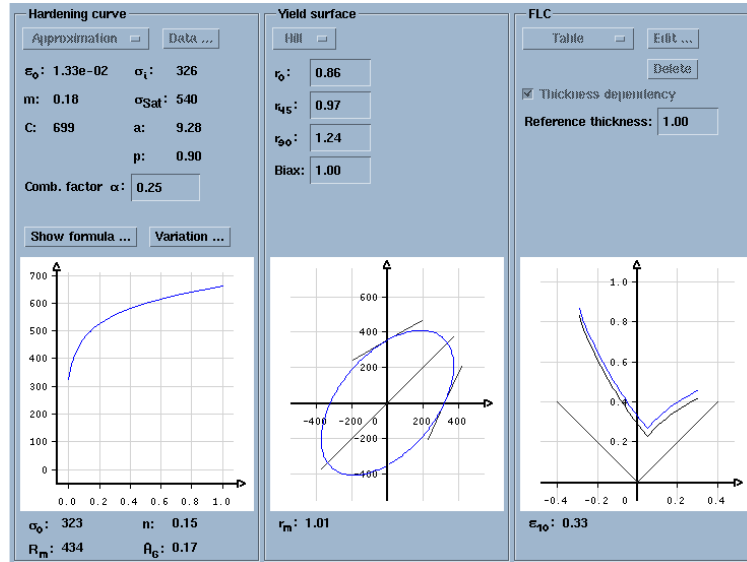
However it is not the aim of this project to compare the material models of the one used in AutoForm vs Corus. It was very instructive to do this, because it was a first introduction to AutoForm. At the same time, this is very useful information for AutoForm and Corus because specific differences between the material models are pointed out.

In AutoForm there are different methods to generate a material model. A difference that occurs in all the models is that the hardening curve of AutoForm is generated with the use of an approximation method. In the Corus model, the hardening curve is generated with the use of data generated by a tensile test. For the specific data sheets of the Corus models see Appendix C.1.

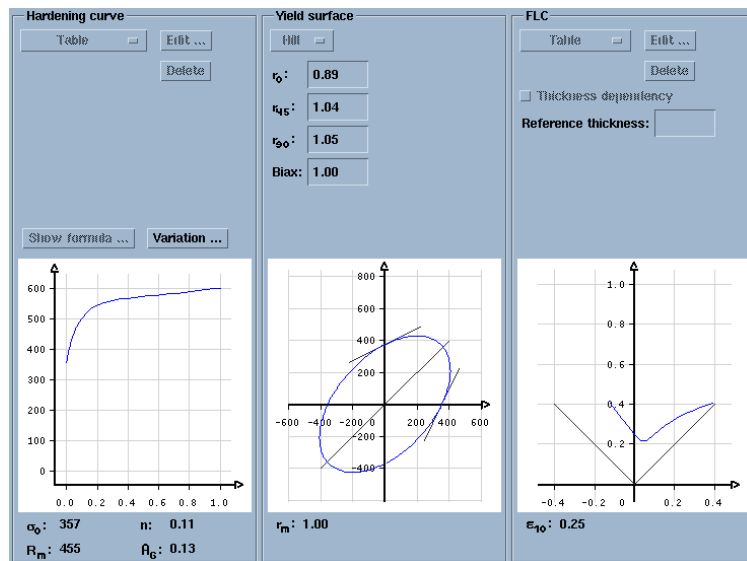
In the following sections the differences between the material models are pointed out. In Section 3.3 the effect of the differences on the material models is discussed.

3.2.1 H340LAD

In Figure 3.2 a comparison is made between two models of one material namely H340LAD. The two material models that are compared are the ones of Corus and AutoForm, this will also be the case in the following sections concerning the two other material models.



(a) AutoForm



(b) Corus

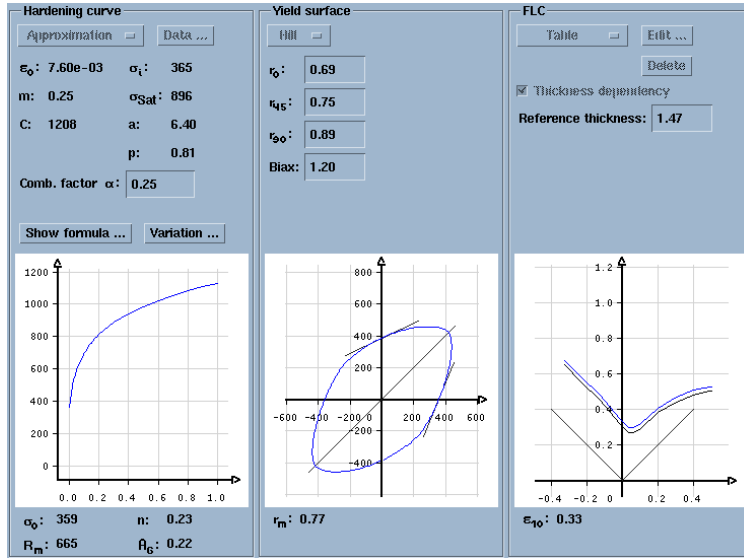
Figure 3.2: Material models of H340LAD

Conclusion

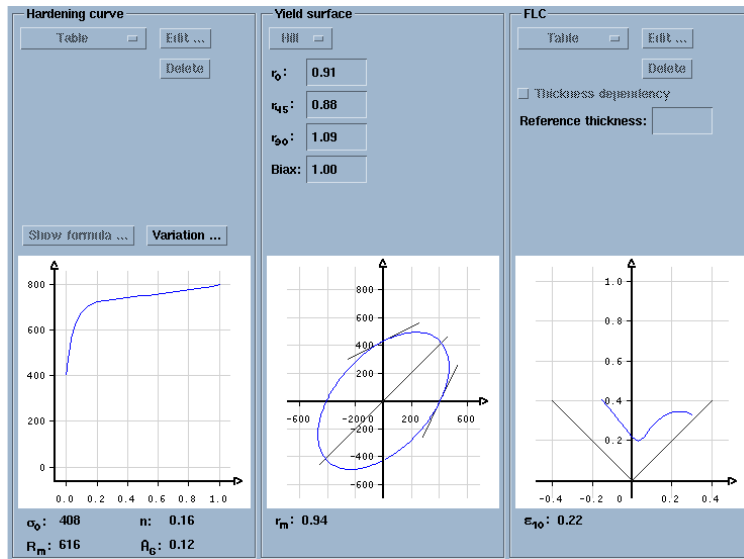
In Figure 3.2 it can be clearly seen that the FLC of the material model of Corus is different than the one used in the database of AutoForm. The FLC of the Corus model is situated lower than the one of AutoForm. Also there are some differences in the r values used in to create the yield surface. The biggest difference is in the r_{90} value.

3.2.2 DP600

In Figure 3.3 another comparison is made between two models of one material namely DP600.



(a) AutoForm



(b) Corus

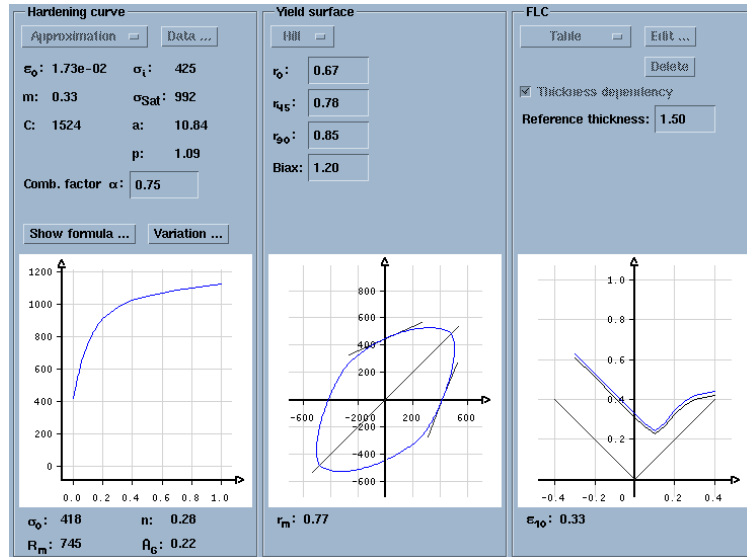
Figure 3.3: Material models of DP600

Conclusion

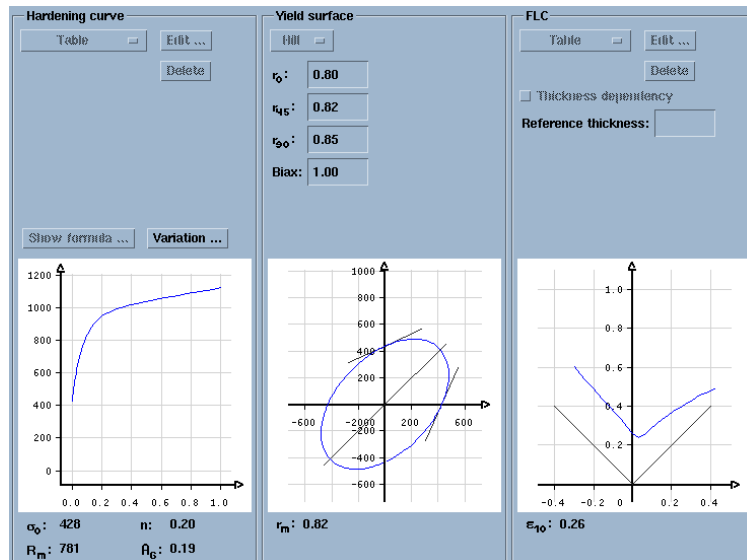
In Figure 3.3 there is a difference in the biaxial stress factor at the material model used in the AutoForm database a factor of 1.2 used, whereas in the one of Corus a factor 1 is used. Also one can see in Figure 3.3 that the FLC of the material model of Corus is situated lower than the one used in the database of AutoForm.

3.2.3 TRIP700

In Figure 3.4 another comparison is made between two models of one material namely TRIP700.



(a) AutoForm



(b) Corus

Figure 3.4: Material models of TRIP700

Conclusion

In Figure 3.4 there is a difference in the biaxial stress factor at the material model used in the AutoForm database a factor of 1.2 used, whereas in the one of Corus a factor 1 is used. This causes a difference in the yield surfaces of the material models. Also one can see in Figure 3.4 that the FLC of the material model of Corus is situated lower than the one used in the database of AutoForm.

3.3 Discussion

There are several reasons and explanations possible, for the differences in the FLC, yield surfaces and hardening curves. These possibilities will be shortly mentioned upon the three different material properties. This research is not going to look into the exact reasons why the material models are different. For the completeness of this research the Corus data sheets of the different materials are included in Appendix C.1.

Hardening Curve

Depending on the material behavior, the specimen fails at a plastic strain ϵ_{pl} in the range of 0.15 to 0.35. However, biaxial strain states encountered during deformation of a sheet may correspond to equivalent strain values greatly in excess of the failure strain. Therefore, the flow curve needs to be extrapolated, from experimentally determined values, up to a strain of 1.0. A few of the standard methods for approximation models are presented in Figure 3.5.

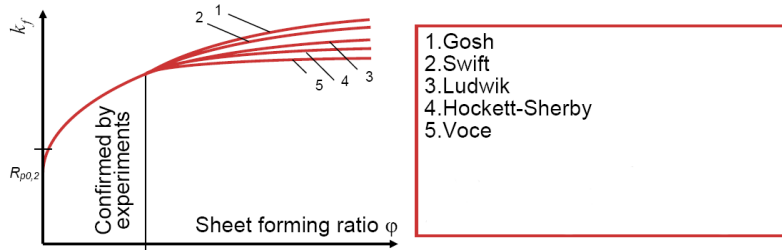


Figure 3.5: Extrapolation models for the yield curve [5]

In Figure 3.5 k_f is the true stress.

The flow curve in the AutoForm models, see Equation 3.1 from [3], is defined with help of a combination of Swift (Krupkowski), see Equation B.1 and Hocket-Sherby approximation, see Equation B.2, for more information see Appendix B.1.1.

$$\sigma = (1 - \alpha)\{C \cdot (\epsilon_{pl} + \epsilon_0)^m\} + \alpha\{\sigma_{Sat} - (\sigma_{Sat} - \sigma_i)e^{-a\epsilon_{pl}}\} \quad (3.1)$$

If the weight factor (α) is 0 then the approximation of the Swift equation is used, the upper limit. If the weight factor (α) is 1 then the approximation of the Hocket-Sherby equation is used. For more information about the hardening curve, see Appendix B.1.1.

The approximation formula, see Equation 3.1 is used in all the models of AutoForm. While in the material models of Corus, the hardening curve is generated with the data imported from a file. Therefore it is possible to determine if the material properties are different, which is the case with all the material models. But it is not possible to determine which approximation method they used for the flow curve.

Yield surfaces and biaxial stress factor

The yield surface determines the conditions for material flow in terms of stress components. The two yield surfaces models available are Hill and Barat [3]. In both the models only the Hill criterion is used and therefore further explained.

The Hill model is formulated in stress space. The yield surface is defined using the three r -values r_0 , r_{45} and r_{90} and the initial yield stress σ_0 in the rolling direction. If the biaxial stress factor is equal to 1.0, the classical Hill-48 model (quadratic function), see Equation 3.2 from [16], is used in AutoForm [3].

$$(r_{90} + r_0 r_{90}) \sigma_{f_x}^2 = r_0 \sigma_y^2 + r_{90} \sigma_x^2 + r_0 r_{90} (\sigma_x - \sigma_y)^2 + 2 \frac{r_0 + r_{90}}{\frac{1}{2} + r_{45}} \tau_{xy} \quad (3.2)$$

Where r_0, r_{45} and r_{90} are the ratio of the transverse to the thickness strain at $0^\circ, 45^\circ$ and 90° to the rolling direction, respectively. σ_x is the stress in the rolling direction, σ_y is the transverse stress and σ_{f_x} is the uniaxial flow stress in the rolling direction.

The biaxial stress factor allows the yield surface to be expanded or contracted near the equibiaxial stress points. Meaningful values of the biaxial stress factor range from 0.8 to 1.2. If a biaxial stress factor unequal to 1.0 is specified, a model similar to Hill-90 models is used. For a material whose reference system coincides with the principal axes of anisotropy this criterion has the form, see Equation 3.3 from [7];

$$\left| \sigma_x + \sigma_y \right|^m + \frac{\sigma_b^m}{\tau_s^m} \left| (\sigma_x - \sigma_y)^2 + 4\sigma_{xy}^2 \right|^{\left(\frac{m}{2}\right)-1} \left\{ -2a_{H90}(\sigma_x^2 - \sigma_y^2) + b_{H90}(\sigma_x^2 - \sigma_y^2)^2 \right\} = |2\sigma_b|^m \quad (3.3)$$

Where the Hill 90 parameters a_{H90} and b_{H90} are defined by, see Equation 3.4 and Equation 3.5;

$$a_{H90} = \frac{1}{4} \left[\left(\frac{2\sigma_b}{\sigma_{90}} \right)^m - \left(\frac{\sigma_b}{\sigma_0} \right)^m \right] \quad (3.4)$$

$$b_{H90} = \frac{1}{2} \left[\left(\frac{2\sigma_b}{\sigma_0} \right)^m - \left(\frac{\sigma_b}{\sigma_{90}} \right)^m \right] - \left(\frac{2\sigma_b}{\sigma_{45}} \right)^m \quad (3.5)$$

Where σ_b is the uniform biaxial yield stress, σ_0 and σ_{90} are the yield stresses along the anisotropic axis, and m is the non-quadratic yield exponent. The yield exponent for this formulation will vary for different materials and is loosely coupled to the r value. In general, a material with a $r > 1$ will have $m > 2$ whereas for $r < 1$, $1 < m < 2$ will hold.

For all the yield surface models AutoForm uses an anisotropic yield surface in conjunction with an isotropic hardening model [3].

The largest difference between the AutoForm and Corus models is that with all the material models, excluded the one for H340LAD, the Hill-48 criterion is used for creating the yield surfaces. Whereas in the models of AutoForm the "Hill-90" criterion is used. This is related to that in the AutoForm models a biaxial stress factor unequal to 1.0 is specified. Also there are difference between the the r values between Corus and AutoForm material models has some influence on the ellipse of the yield surface. Also it must be clear that, the differences in the hardening curves keeps on working in the yield surfaces.

FLC

It is important to understand, on account of the following facts, that the FLC for a material can never be accurately established [4].

- Influence of friction (for example, in the Nakazima tests)
- Accuracy of measurement of major and minor strains, especially on bent areas of the specimens

Besides that the FLC of a material is dependent of the specimens thickness [13, 4], and it also varies from one production run to another.

3.4 Conclusion

In general it can be said that the material models in the database of AutoForm are, “stronger” then the ones provided by Corus. This is caused by the differences in the FLC, yield surfaces and hardening curves.

4

FEM simulations

In the first part of this chapter the four design variables are varied one by one while the others are set to the reference setting, see Sections 4.3 to 4.5, while recording their effect on the responses in the so called scatter plots.

While in Section 4.6 two design variables are varied while the other two are set to the reference setting the so called surface plots.

In these sections only the scatter/surface plots that attracted our attention are presented. For all the scatter and surface plots of the responses in the two regions, see Appendix D. But before going any further into the subject the settings are described.

4.1 Settings

In Section 2.2 the number of design variables is reduced to 4 variables. The design variables that can be influenced are;

$$\begin{array}{rclcl} \min & \leq & \text{blank holder force} & \leq & \max \text{ kN} \\ 0 & \leq & x_{72} & \leq & 130 \text{ mm} \\ 0 & \leq & x_5 & \leq & 20 \text{ mm} \\ 0 & \leq & x_6 & \leq & 20 \text{ mm} \end{array}$$

For this FEM simulation 3 materials are available, 4 design variables are chosen and 3 response are chosen in 2 regions, namely failure, wrinkling and thickness. The two regions are pointed out for each material in Section 4.3.1-4.3.3.

As mentioned earlier, see Section 2.1.5, we consider the 3 different materials independently. So every variable is changed for the different material parameters, while the other variables are set at the reference value. Due to the fact that the materials are considered independently the maximum and minimum blank holder force is different for each material. This upper and lower limit of the blank holder force is determined for each material in Section 4.3.

4.1.1 Reference settings

The reference settings of the B-pillar are gained from the base simulation. The base simulation is gained from the owner of the dies AutoForm, see Table 4.1.

The difference between the simulations with the different materials is not only in the material model that is used. Also the rolling direction is different from one material to another. This is due to material dimensions that are available for the experimental validation tests. The rolling direction for DP600 and TRIP700 is 97° , while the rolling direction of H340LAD is 7°

| | | |
|--------------------|---|--------|
| Blank holder force | = | 600 kN |
| x_{72} | = | 0 mm |
| x_5 | = | 0 mm |
| x_6 | = | 0 mm |

Table 4.1: Reference settings

4.1.2 Variable settings

The 3 geometrical variables are all the same for the different material models, see Figure 4.1. The red lines are the maximum values for the variables.

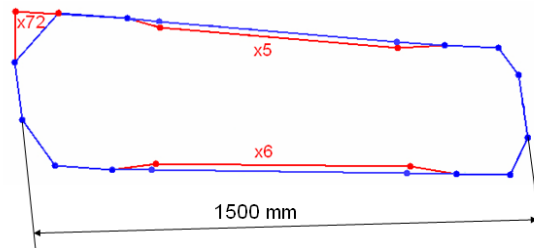


Figure 4.1: Blank size variables with global modification mode

The only setting that must be determined for each material model is the minimum and maximum blank holder force. This will be extensively discussed in Section 4.3.

4.1.3 Blank size

The reference blank length, see Figure 4.1, length is close to the sheet length (1500 mm) that are available for the experimental validation.

The blank is turned around the z -axis (7°) and then placed in the press. These dimensions are 1500 and 440 mm. So in theory the sheet length of 1500 mm fits precisely, but to be sure some calculations are performed to investigate the influence of the blank length on the problem areas which are pointed out in Section ???. The blank is varied from 1400 mm to 1600 mm. For the Pareto and scatter plots see Appendix A.2.

Conclusion

The problem areas are not sensitive for a variation in blank length. If the left side is set as reference point and the right side of the blank is varied.

4.2 Scatter plots

The four design variables are varied one by one while the others are set to the reference setting while recording their effect on the responses in the scatter plots. The scatter plots are made with the use of AutoForm. A scatter plot, see Figure 4.2 shows the raw result variable (RV) and the selected design variable (DV) in an xy-scatter plot for all the simulations of the current performance analysis.

| | |
|------------------------|---|
| Red circle | Individual simulation result |
| Blue bars | IQR_{normal} range for as DV as RV |
| Red lines | Median value(s) for as well DV as RV |
| Thin Green line | Nominal simulation value(s) |
| Thin Black line | Current simulation value(s) |
| Thick grey line | Visualization of the Sensitivity / partial derivative at the median / median crosshair position. |

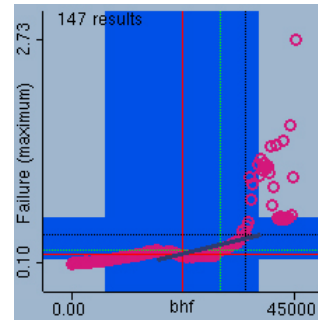


Figure 4.2: Scatter plot

Median: Center value of all the simulation results. 50 % of computed result values are smaller, and 50 % are larger than the median results.

Nominal: base simulation results.

IQR_{normal} range: 68.28% of the center values of the design/response variable are inside the blue box.

4.3 Blank holder force (Process Window)

The blank holder is used to hold the blank in position and to avoid wrinkling, see Figure 4.3.

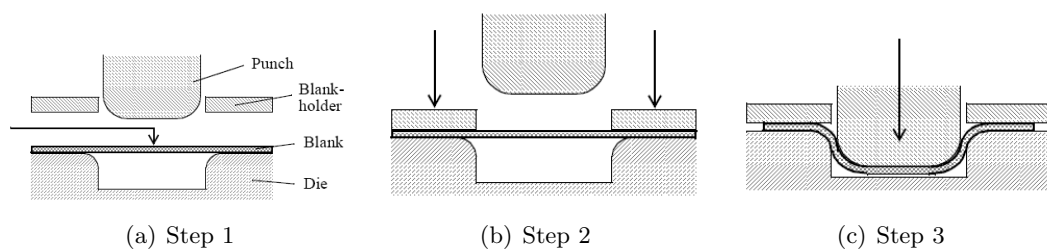


Figure 4.3: (a) Positioning of the blank (b) Closing of the blank holder, (c) Application of blank holder force, and forming

The lower limit of the process window is called the minimal blank holder force. This is the blank holder force which is caused by the reaction forces of the blank during the deformation of the blank to a B-pillar. The upper limit of the process window, the maximum blank holder force, is caused by the fact that the B-pillar starts to neck.

In Section 4.3.1 to 4.3.2 the process windows of the Corus material models are presented. The process windows of the AutoForm material parameters are also performed but not presented, these are summarized in Table 4.2.

4.3.1 H340LAD

In Figure 4.4 the FEM simulations with H340LAD are shown, one with the minimum (Figure 4.4(c)) and the other with the maximum (Figure 4.4(d)) blank holder force.

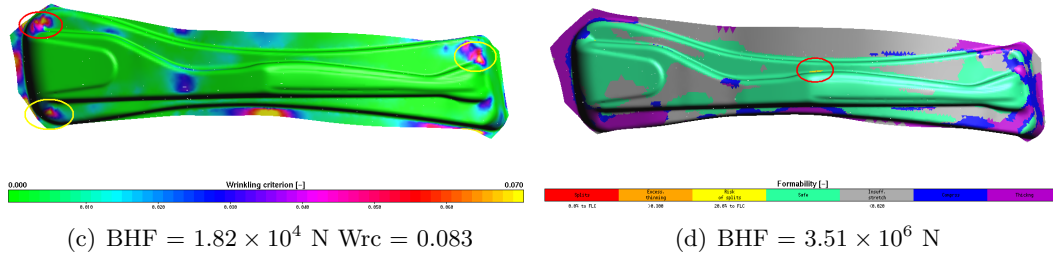


Figure 4.4: Lower(c) and upper(d) limit of the process window

In Figure 4.4(c) the red circled area is the one where the highest value of the wrinkling criterion occurs, Region B. The yellow circled areas are regions where the wrinkling criterion exceeds 0.05 in the product. The higher the value of the wrinkling criterion, the more chance that wrinkles occur. For more information about the wrinkling criterion see Appendix B.2.2.

The upper limit of the work domain is determined at which blank holder force the B-pillar starts to neck. In Figure 4.4(d) the FE simulation is shown with the critical blank holder force. In Figure 4.4(d) in the red circled area is the area where the strains in more than 5 elements are above the FLC, Region A. The used response in Figure 4.4(d) is the formability criterion, due to the fact that this is an on/off criterion, there is a split or there is no split. The response used in the scatter plots is failure. For the precise location of the 2 regions see Appendix D.1.

Of the two different regions, scatter plots are produced with three response variables; failure, wrinkling criterion and thickness, for all the plots of the different regions see Appendix D.2 on page 103. In the report only the failure in region A, see Figure 4.5(a) and the wrinkling criterion in region B, see Figure 4.5(b) is presented. In both cases the design variable is in a range of $0 \leq \text{BHF} \leq 4.5 \times 10^6$ N. If the failure criterion is above 1 the strain is above the forming limit curve and the product will crack. For more information about the failure criterion see Appendix B.2.1.

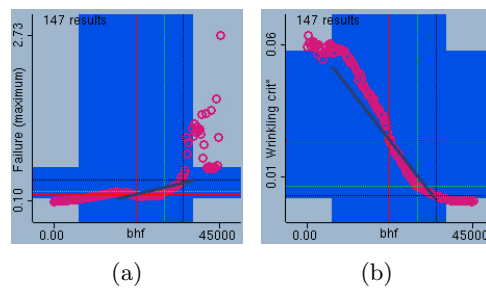


Figure 4.5: Scatter plots of region A (a) and region B (b)

4.3.2 DP600

In Figure 4.6 the FEM simulations with DP600 are shown, one with the minimum (Figure 4.6(c)) and the other with the maximum (Figure 4.6(d)) blank holder force.

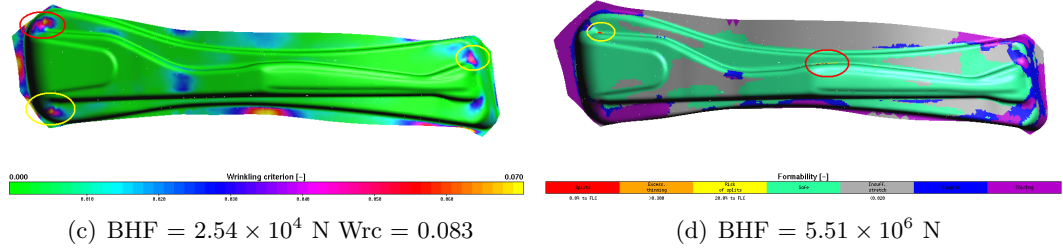


Figure 4.6: Lower(c) and upper(d) limit of the process window

In Figure 4.6(c) the red circled area is the one where the highest value of the wrinkling criterion occurs, Region B. The yellow circled areas are regions where the wrinkling criterion exceeds 0.05 in the product.

In Figure 4.6(d) the FE simulation is shown with the critical blank holder force. In Figure 4.6(d) in the red circled area is the area the strains in more than 5 elements are above the FLC, Region A. Also a yellow circled area is presented in this area only the strains in a few elements is above the FLC, this will be thoroughly discussed in Section 4.4. The used response in Figure 4.6(d) is the formability criterion. For the precise location of the yellow circled area in Figure 4.6(d) see Appendix D.1

Of the two different regions, scatter plots are produced with the three response variables; failure, wrinkling criterion and thickness, for all the plots of the different regions see Appendix D.2 on page 105. In the report only the failure in region A, see Figure 4.7(a) and the wrinkling criterion in region B, see Figure 4.7(b) is presented. In both cases the design variable is in a range of $0 \leq \text{BHF} \leq 6.0 \times 10^6 \text{ N}$.

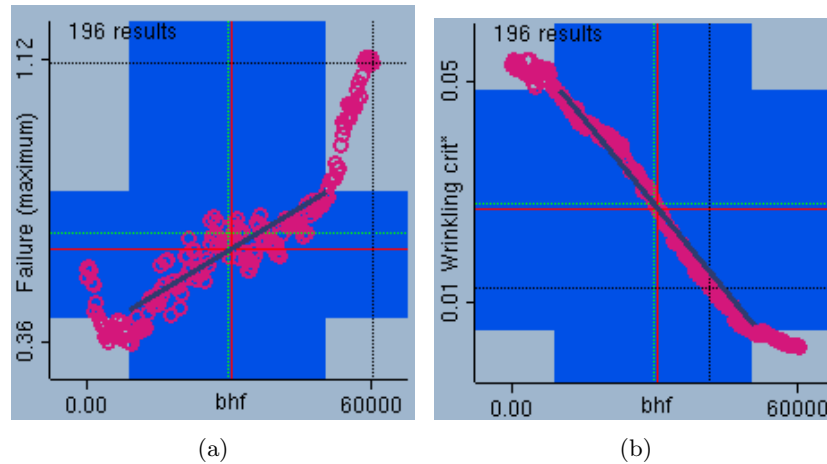


Figure 4.7: Scatter plots of region A (a) and region B (b)

4.3.3 TRIP700

In Figure 4.8 the FEM simulations with TRIP700 are shown, one with the minimum (Figure 4.8(c)) and the other with the maximum (Figure 4.8(d)) blank holder force.

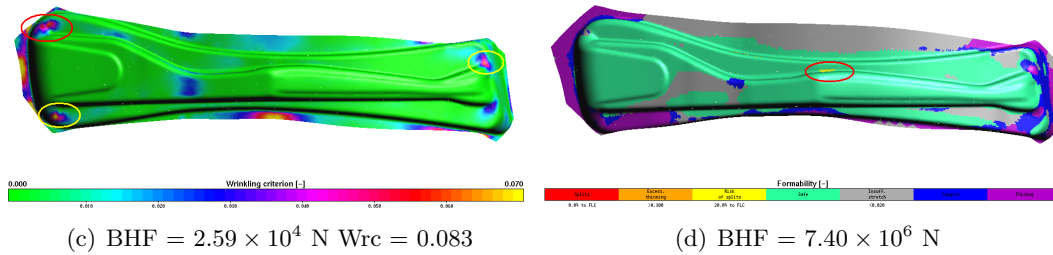


Figure 4.8: Lower(c) and upper(d) limit of the process window

In Figure 4.8(c) the red circled area is the one where the highest value of the wrinkling criterion occurs, Region B. The yellow circled areas are regions where the wrinkling criterion exceeds 0.05 in the product.

The upper limit of the work domain is determined at which blank holder force the B-pillar starts to neck. In Figure 4.8(d) the FE simulation is shown with the critical blank holder force. In Figure 4.8(d) the red circled areas are the one where the material first start to neck, Region A. The used response in Figure 4.8(d) is the formability criterion, due to the fact that this is an on/off criterion, there is a split or there is no split.

Of the two different regions, scatter plots are produced with the three response variables; failure, wrinkling criterion and thickness, for all the plots of the different regions see Appendix D.2 on page 106. In the report only the failure in region A, see Figure 4.9(a) and the wrinkling criterion in region B, see Figure 4.9(b) is presented. In both cases the design variable is in a range of $0 \leq BHF \leq 8.0 \times 10^6 \text{ N}$.

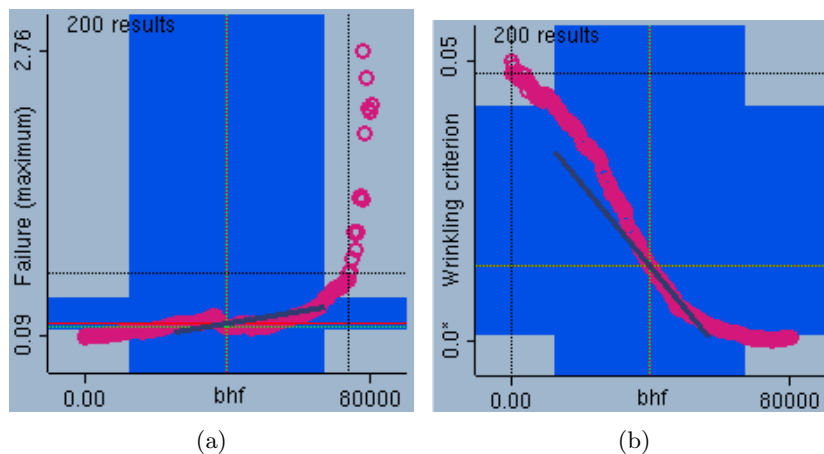


Figure 4.9: Scatter plots of region A (a) and region B (b)

4.3.4 Discussion

As one can clearly see, that how higher the blank holder force the less chance off wrinkles, see for example Figure 4.9(b) and at a certain point the product starts to crack in region A, see for example Figure 4.9(a).

In Section 4.3.1 to 4.3.3 the process windows of the Corus material models are presented. The process windows of the material models included AutoForm are also performed but not presented, these are summarized in Table 4.2. The differences between the blank holder forces (BHF in Table 4.2) at which the material starts to neck are mentioned. Also the minimal blank holder force is mentioned with the corresponding wrinkling criterion. In Table 4.2 the blank holder force in the second column is the force at which the material starts to neck. Wcr stands for wrinkling criterion. Also the blank thickness is mentioned (in mm) this stands directly under the material model.

| | | BHF at necking ($\times 10^6$ N) | Wrinkling criterion | | | |
|----------------------------|----------|--------------------------------------|------------------------|-------|------------------------|-------|
| | | | BHF ($\times 10^4$ N) | Wrc | BHF ($\times 10^6$ N) | Wrc |
| H340LAD 1.458 mm | Corus | 3.5-3.7 | 1.59 | 0.083 | 3.51 | 0.055 |
| | AutoForm | 4.0-4.2 | 1.70 | 0.083 | 4.00 | 0.053 |
| Trip700 1.716 mm | Corus | 7.4-7.8 | 2.42 | 0.074 | 7.5 | 0.050 |
| | AutoForm | 9.3-9.5 | 2.52 | 0.079 | 9.3 | 0.057 |
| DP600 1.807 mm | Corus | 5.4-5.6 | 2.55 | 0.081 | 3.37 | 0.061 |
| | AutoForm | 7.7-7.9 | 2.40 | 0.078 | 7.9 | 0.043 |

Table 4.2: Corus and AutoForm differences in blank holder forces

Some conclusion can be drawn from Table 4.2, the blank holder force at which the material models of Corus starts to neck are lower than the one used standard in AutoForm. In Section 3.4 there is mentioned that the materials used in AutoForm are stronger, this conclusion is verified by these results. The material models which are included in AutoForm are stronger. Another point is that the rolling direction at time of the "AutoForm" simulations was unknown. While with the material models of Corus the dimensions of the blanks were known and therefore the rolling direction of the blank is different.

The reason for this differences in the maximum blank holder force is clarified through the differences in the material models, see Section 3.2.

4.4 Blank holder force (Split in edges)

As mentioned in Table 4.2 the process windows of the three different materials were made. Only in Figure 4.6(d) a yellow circled area is presented. In this region the strains in the elements exceeds the FLC.

At a certain blank holder force the area in the upper left corner, region B, started to neck, see Figure 4.10(a), if the blank holder force was higher this area "disappeared". This was discovered with the reference blank shape. In Figure 4.10 one can see the specimen at the end of the deformation step, see Figure 4.10(a) a close up of the problem area in Figure 4.10(b).

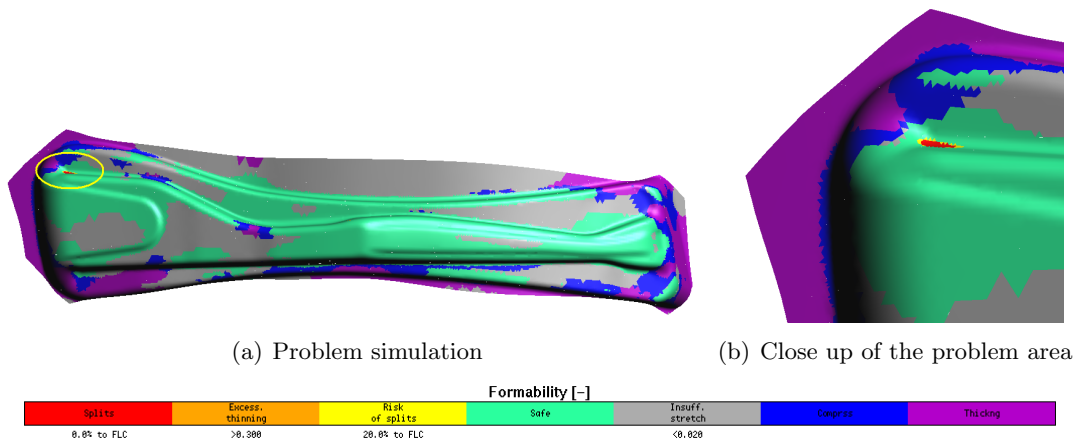


Figure 4.10: Blank holder force = 4.0×10^6 N with DP600

To investigate if this phenomenon also occurred by the other material models. Scatter plots are made of region B with response the failure criterion and the design variable the blank holder force, see Figure 4.11.

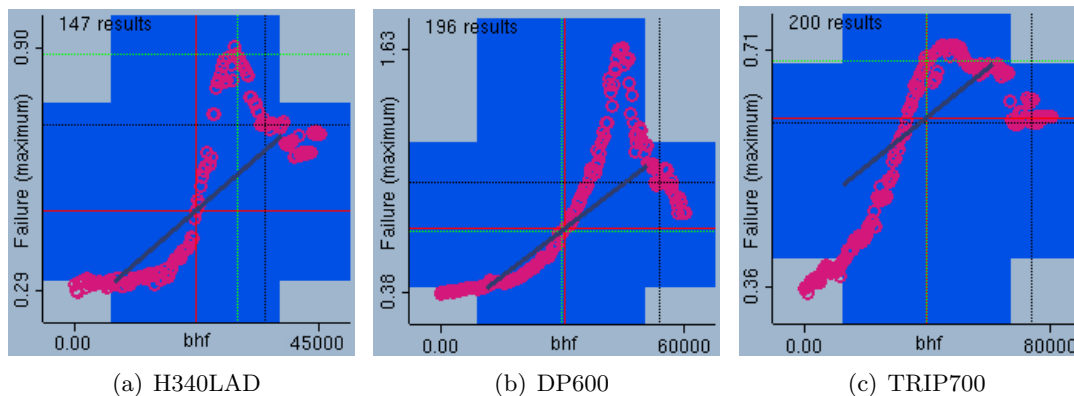


Figure 4.11: Failure plots of the left corner with different material models.

The black dotted line is the line of the edge of the process window. As one can see in Figure 4.11(a) and Figure 4.11(c) the failure(maximum) value never exceeds 1. This means

that the average value, of the failure criterion, in the selected elements never exceeds 1. Therefore it is possible that the maximum failure in 1 element in that zone exceeds 1. With the material models of H340LAD and TRIP700 an investigation is done to determine if the strain in the selected elements never exceeds the FLC. With the material model of TRIP700 the strains in the elements of region B never exceeds the FLC. The strain in the selected elements exceeds the FLC with the material model of H340LAD.

To make this non continuous trend obvious several plots are made with different blank holder force of the problem area, see Figure 4.10. This is done with the material model of H340LAD, see Figure 4.12 and DP600 see Figure D.2. The criterion that is used is the formability criterion.

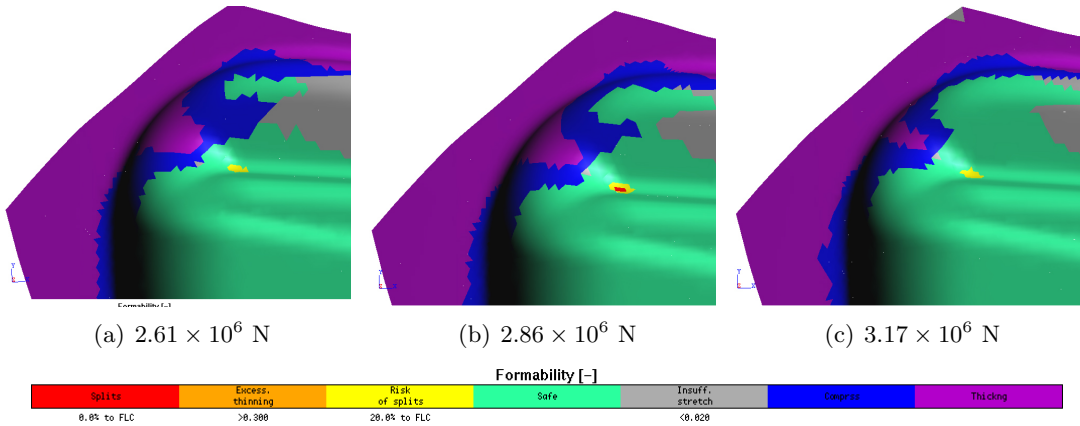


Figure 4.12: Formability plots of the left corner with different blank holder forces with H340LAD.

The non continuous trend in the scatter plots of response variable failure, see Figure 4.11 may be explained with the fact of "rotation" of the strains. If one looks at the scatter plots of the major and minor strain. One can see that there is change in minor strain, see Figure 4.13(b) and a slight increase in the major strain, see Figure 4.13(a). For example the material model of H340LAD is used, but this is the case with all the other material models.

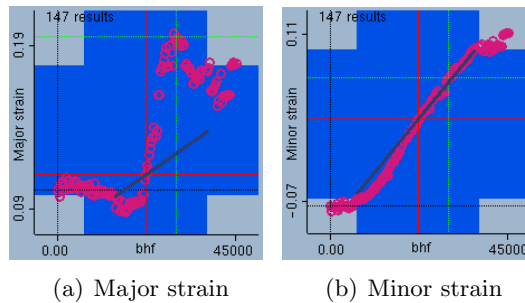


Figure 4.13: Forming limit diagrams of region B with different blank holder forces

To look if "rotation" is a possible explanation for the high peaks in the failure plots that are mentioned in Figure 4.11. A closer look is needed in the forming limit diagrams.

In Figure 4.14 the forming limit diagrams at the blank holder forces, that are mentioned in Figure 4.12 are presented. The red dots are the strains of the elements in region B. The failure value at this blank holder force is made the strains in the FLD. The average value of the strains is taken and the distance to the FLC is determined and the failure value is calculated. The failure value is than used in the scatter plot, see Figure 4.11(a).

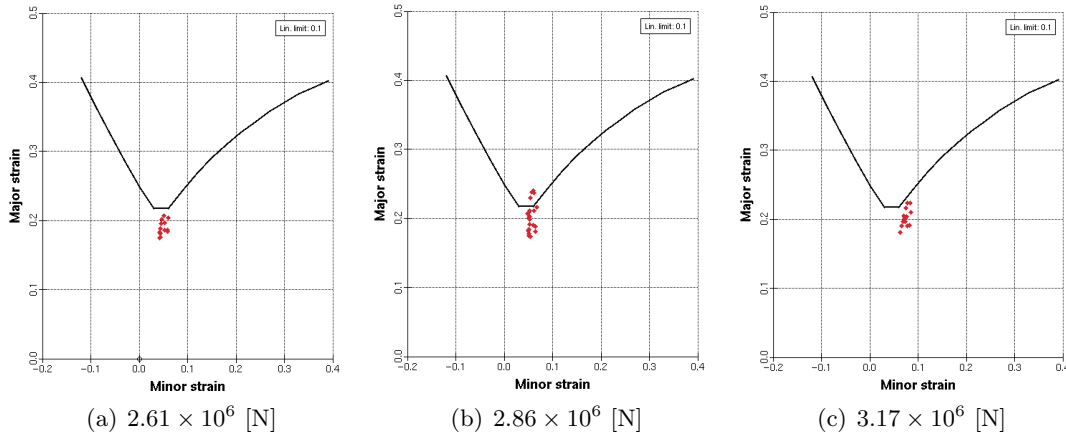


Figure 4.14: Forming limit diagrams of region B with different blank holder forces

It looks like that a slight increase in the minor strain, see the difference between Figure 4.14(b) and Figure 4.14(c). Causes the decrease in failure after the peak, see Figure 4.11(a).

To investigate the increase of the minor strain further, the following Figure 4.15 is made. This figure is made with the help of a couple of forming limit diagrams at different blank holder forces. The average value of the major and minor strain in the elements of region B is taken and set as a point in the FLD with the corresponding blank holder force in N, see Figure 4.15. As one can clearly see there is a trend visible. The reason that the points never lie above the FLC is caused by the fact that an average value over the elements in region B is taken.

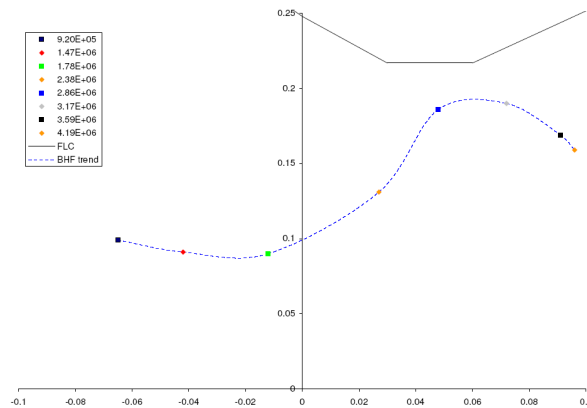


Figure 4.15: Major and minor strain in the elements of Region B at different blank holder forces

4.5 Scatter plots dependent on geometrical variables

In this section the FEM simulations of the geometrical variables is presented, only the trends in the scatter plots that attracted our attention are presented. For all the scatter plots see Appendix D.2, from page 107 to 121.

4.5.1 Scatter plots dependent of x_5

In Appendix D.2 from page 107 to 112 the scatter plots with variable x_5 of each material model are presented, with all the other variables set to there reference values (BHF = 600 kN). The following attracted attention, a trend is visible with the failure criterion in region B, see Figure 4.16.

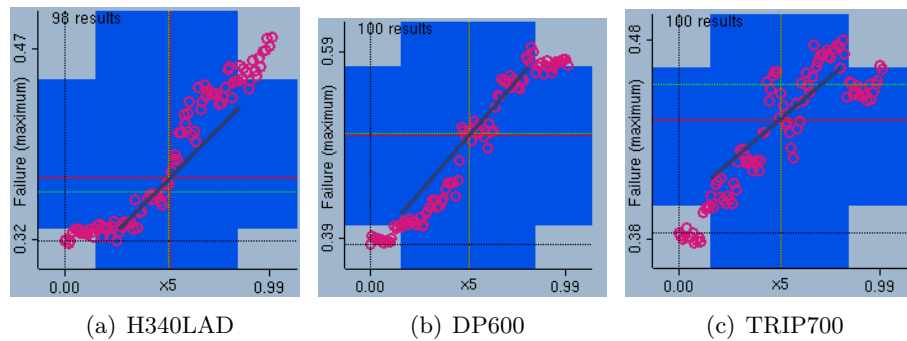


Figure 4.16: Variable x_5 , response is failure in region B

Due to the fact that the influence of x_5 might be larger if the blank holder force is higher. Simulations are done with the blank holder force set close to the maximum, in the case of H340LAD a force of 3.4×10^6 N and the variable x_5 . This is only done for H340LAD for the fact that of this material the most blanks were available for validation, see Section 5.1. The following attracted attention, the trends with the failure criterion in region A and B, see Figure 4.17. The trend that was visible with the blank holder force set to the reference setting in Region B, is changed, see Figure 4.17(b) vs Figure 4.16(a). Also the trend in region A is changed, see Figure 4.17(a) vs figure on page 107.

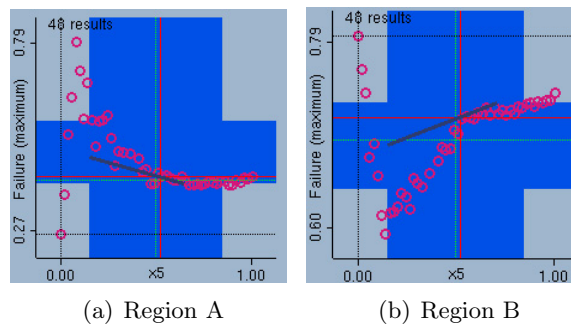


Figure 4.17: Variable x_5 and BHF = 3.4×10^6 N, response is failure in region B

4.5.2 Scatter plots dependent of x_6

In Appendix D.2 from page 113 to 118 the scatter plots with variable x_6 are presented. Because there are no obvious trends visible in the response of the two regions these are not included in the report.

Due to the fact that the influence of x_6 might be larger if the blank holder force is higher. Simulations are done with the blank holder force set close to the maximum, in the case of H340LAD a force of 3.4×10^6 N and a variable x_6 . With these settings a trends can be recognized in the response failure in region A, see Figure 4.18(a) and region B see Figure 4.18(b).

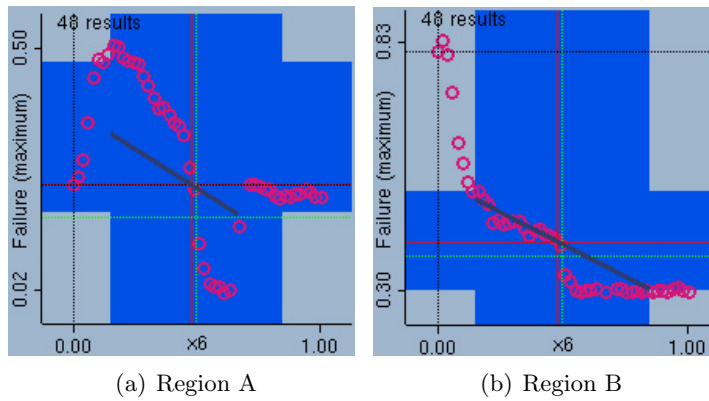


Figure 4.18: Scatter plots with variable x_6 and BHF 3.4×10^6 N, response is Failure in region B

4.5.3 Scatter plots dependent of x_{72}

In Appendix D.2 from page 119 to 121 the scatter plots with variable x_{72} are presented. The following attracted attention, a trend is visible with the failure criterion in region B, see Figure 4.19.

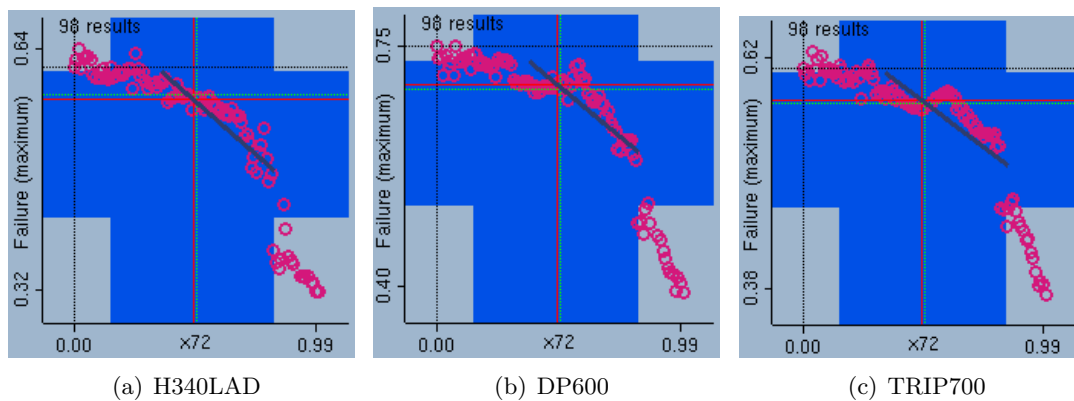


Figure 4.19: Scatter plots with variable x_{72} , response is Failure in region B

4.6 Surface plots

The surface plots dependent of 2 design variables are made with the use of MATLAB. Several sequences of steps are necessary to produce these plots, these are explained in Appendix D.3.

The AutoForm sigma analysis was set with 200 calculations. Due to some internal errors, not all the calculations are used in some cases, see for example simulation series 14. Also another remarkable point was discovered in the case of simulation series 18. The indrawn was becoming so large, that there was no material in region A, therefore this simulation series consist of reasonable less calculations than the rest of the simulation series.

The black squares in the figures are the points at which a simulation has taken place. The rest of the values is obtained through an interpolation function.

4.6.1 Surface plots dependent on BHF and x_5

In Appendix D.3 from page 123 to 125 the surface plots with variables BHF and x_5 are presented. A trend is visible in region A, see Figure 4.20 with as response the failure criterion. An increasing x_5 has a positive influence on the safety margin, the response of failure is descending. The influence of x_5 is increasing at a higher blank holder force in region A.

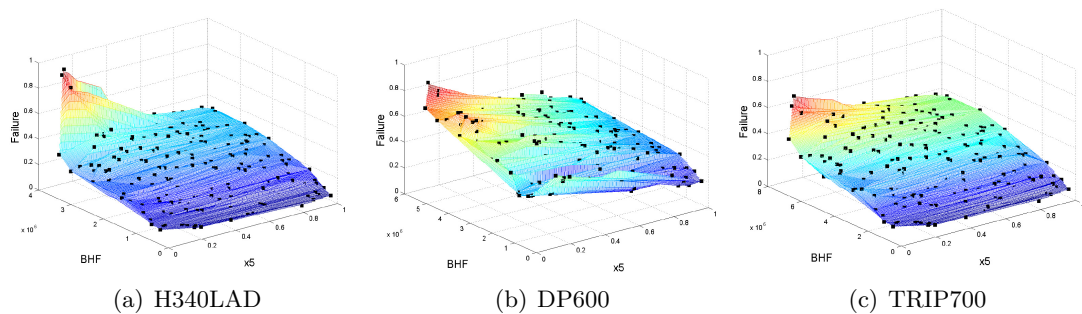


Figure 4.20: Surface plots with variables BHF and x_5 , response is failure in region A

4.6.2 Surface plots dependent on BHF and x_6

In Appendix D.2 from page 126 to 128 the surface plots with variables BHF and x_6 are presented. A trend is visible in region A, see Figure 4.21 with as response the failure criterion. An increasing x_6 has a positive influence on the safety margin, the response of failure is descending. The influence of x_6 is increasing at a higher blank holder force in region A.

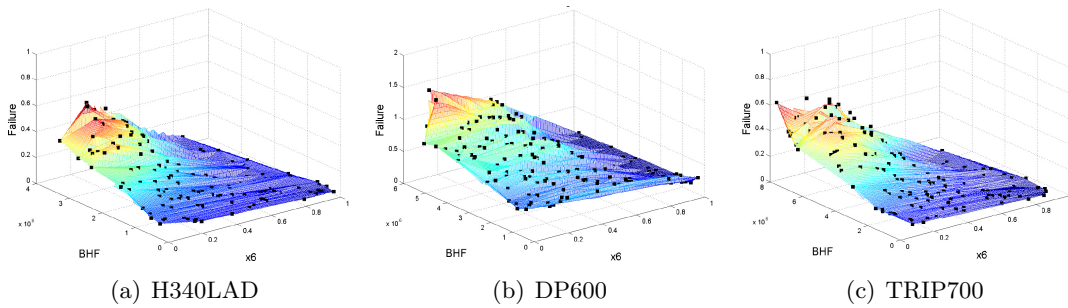


Figure 4.21: Surface plots with variables BHF and x_6 , response is failure in region A

4.6.3 Surface plots dependent on x_5 and x_6

In Appendix D.2 from page 129 to 131 the surface plots with variables x_5 and x_6 are presented. The most obvious trend was discovered with the response failure in region A. The surface plot are made with a blank holder force of 600 kN. Based on the figures presented with the variable blank holder force and x_5 and blank holder force and x_6 . The influence of the geometrical variables will be larger at a higher blank holder force. Therefore the trends in Figure 4.22 do not seem interesting, but the can be very useful at a higher blank holder force.

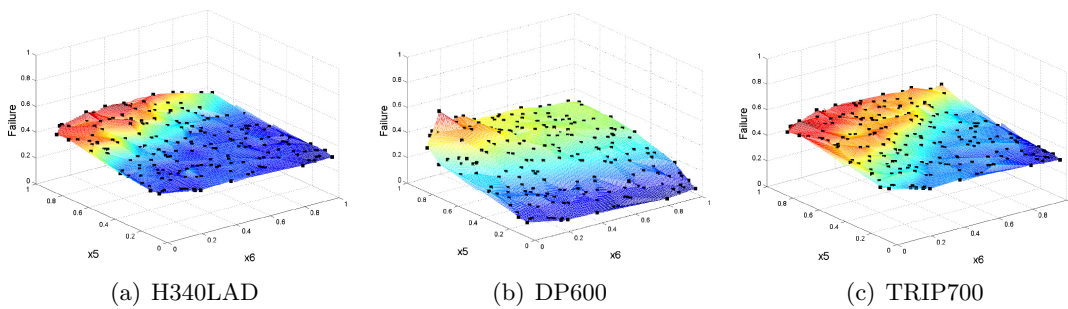


Figure 4.22: Surface plots with variables x_5 and x_6 , response is failure in region A

4.7 Discussion: scatter and surface plots

The scatter plots must also be found back in the surface plots made with the same variables. To make this statement clear the surface plot of H340LAD with the variables x_5 and BHF is evaluated.

If one looks at the scatter plot of x_5 and compares these to the surface plot of the BHF and x_5 , see Figure 4.23. The scatter plots are made at a blank holder force of 600 kN, see Figure 4.23(a) and at a blank holder force of 3400 kN, see Figure 4.23(b). Also the trend that occurred with $x_5 = 0$ and increasing blank holder force, see Figure 4.23(c) must be found back in the surface plot, see Figure 4.23(d).

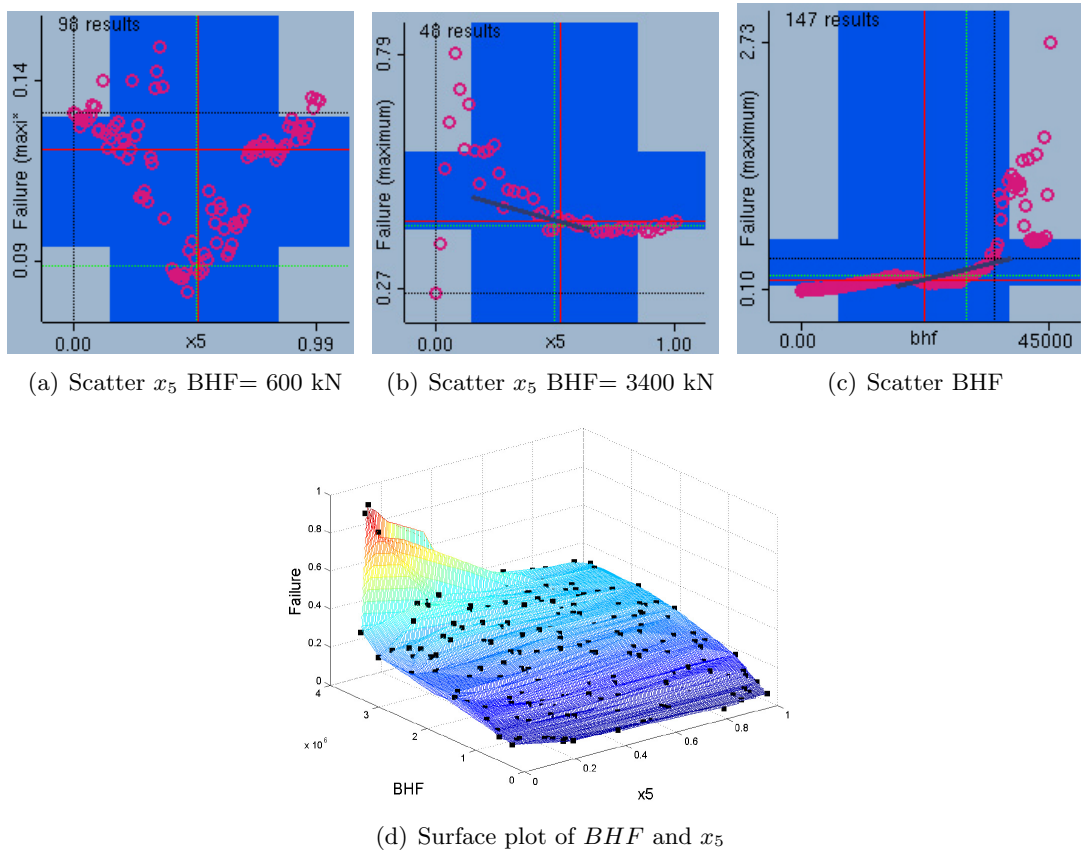


Figure 4.23: Scatter and surface plots of the response failure in region A.

The only difference can be seen in the values. This difference between the scatter plots and the surface plots can be explained through the fact that the focus area in the surface plots is larger. Therefore the average value in the area of the surface plots is less sensitive for differences. As one can see in Figure 4.11 of Section 4.4, the necking is very local. The reason that a large area is taken in the surface plots is for the fact that with MATLAB a 3D box is drawn. While in AutoForm one can selected a surface in 3D.

Another point is that the scatter plots produced with AutoForm takes the failure maximum of all the process time. While with the surface plots the failure value at the last increment is used.

4.8 Optimal settings

Based on the mathematical optimisation model which has been proposed in Section 2.2.4. All the trends of the design variables on the different responses and regions are presented in the last sections. A statement can be made with regard to the optimal settings.

The objective is to maximize the distance to the FLC therefore the blank holder force must be set to a minimum. This is namely the most "dominate" factor for the objective and the constraint, see Figure 4.5. Based on this factor, the blank holder force is set to 700 kN, in the case of H340LAD. Also with this blank holder force the product does not fail in region B.

If one looks at the response failure in region A, see Figure 4.24. The scatter plot of x_{72} is not included for the fact that this variable had no influence in region A, see Figure D.2 in Appendix D.2. Based on these graphs a setting must be chosen for x_5 and x_6 . If one looks at Figure 4.24(b) one can see that if x_6 becomes larger the risks of splits drops therefore x_6 is set to 1. The variable is set to 0.5 due to the fact that is one looks in Figure 4.24(a) a local minimum can be seen. For a more detailed view of this trend see Figure D.2 in Appendix D.2.

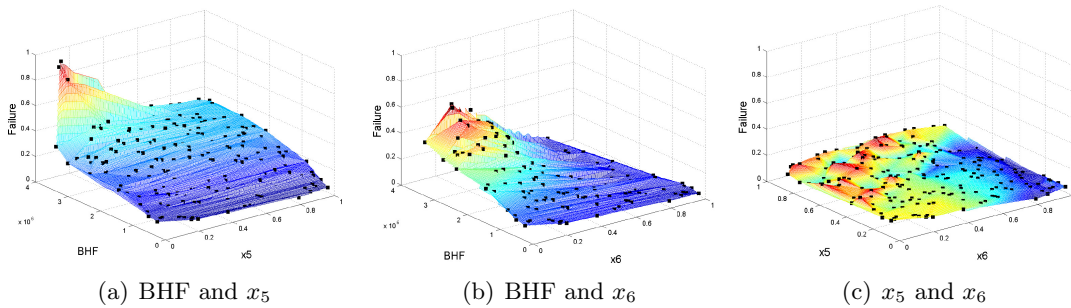


Figure 4.24: Surface plots with variables BHF, x_5 and x_6 , response is failure in region A

Now only the settings for the geometrical variables are determined for region A. For region B the variable with the most influence is x_{72} . If one looks at the effects of x_5 and x_6 on region B the settings which are determined with respect for region A are also here good, see Figure D.2 and D.2 in Appendix D.2. Due to the relative low blank holder force split in the edges is no issue. If one looks in Figure 4.25 one can see that an increasing x_{72} gives a higher change of wrinkles, see Figure 4.25(b), x_{72} is set 0.

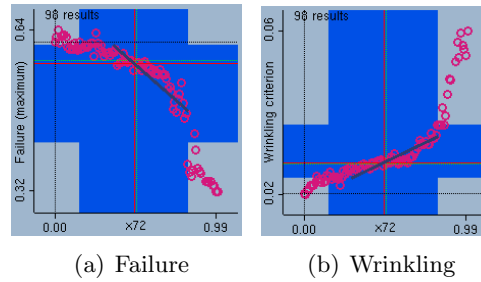


Figure 4.25: Scatter plots with variable x_{72} with BHF set to 6.0×10^5 in region B.

4.8.1 Discussion: Optimal settings

In AutoForm Sigma also an optimization mode is available. In the AutoForm release notes there optimisation option is referred as: A search of the best parameter set in a user defined design space in order to achieve a predefined quality target. An asynchronous algorithm is implemented for optimization analysis [3]. In Appendix A.3 the AutoForm Sigma optimisation is worked out here only the results of the optimisation are presented. The settings which are determined with the help of the scatter and surface plots are also included.

| | min | max | optimal | AF sigma |
|----------|-------|---------|---------|----------|
| BHF | 16 kN | 3400 kN | 700 kN | 150 kN |
| x_5 | 0 | 1 | 0.5 | 0.64 |
| x_6 | 0 | 1 | 1 | 0.98 |
| x_{72} | 0 | 1 | 0 | 0.04 |

The only clear difference can be seen in the blank holder force. The reason for this difference lies within AutoForm sigma due to the optimisation algorithm that is used in AutoForm. With this algorithm it is possible that there are points below the wrinkling line whereas with the self determined optimum all the points in the FLD are above the FLD. This means that in the optimum found with AutoForm a lot of thickening is taken place, a lot of point lie beneath the line of equal thickness, see Figure A.8(b).

4.9 Conclusion

The scatter and surface plots presented in this chapter give a good indication of the formability of the product as function of the process and geometrical variables. The attention point is the area where the product will crack. The calculations show that in region B only in a few elements the strains are above the FLC. The experiments will put an end to this discussion. An optimal setting for the deep drawing of the B-pillar has been obtained. This is only done with the help of the scatter and surface plots and not with the OptForm. Therefore one cannot give a clear answer for the differences between OptForm and AutoForm Sigma. What can be conducted is that the found optimum with the AutoForm Sigma optimisation mode is that is in the lower regions of the blank holder force. Also the optimum is evaluated with one material therefore one can only speculated over the effect of different materials.

5

Experimental validation

This chapter is concerned with the experimental validation tests which were conducted at the University of Dortmund. The equipment used at Dortmund is described in Section 5.2. Due to several reasons the tests are conducted with a different material batch than used in the FEM simulations, this is described in Section 5.1. The tests that are conducted and their results are described in two different sections. One is concerned with the blank holder force, see Section 5.4, the next section, Section 5.5, is concerned with the validation of the geometrical variables. In these sections the results of the test are presented. In Section 5.6, the results of the test are discussed and the most striking points are highlighted. The next section (5.8) is concerned with the verification of the experimental data. The following section (5.9) is used to verify the points that were discussed in Section 5.6. The last two sections are concerned with the discussion and conclusions.

5.1 Materials for experimental validation

Due to several different reason the materials that were used in the FEM simulations were not available for the experimental validation. In the case of TRIP700 the material was not available in the required dimensions. In the case of DP600 the selected batch was out of stock, therefore another batch is used for the experimental validation.

The following materials are used for the experimental validation; H340LAD and DP600, for the specific properties see Appendix C.2. With both materials the rolling direction is different than the ones used in the FEM simulations, see Chapter 4. The production width of the sheets was 1500 mm, see Table 5.1 therefore the rolling direction of the blank changes to 97^0 . However the trends that are discovered with the FEM simulations will not change dramatically for the materials that are available for validation.

| | | H340LAD | DP600 |
|----------------------------|----|----------------|--------------|
| Length (rolling direction) | mm | 1500 | 1500 |
| Width (production) | mm | 990 | 1100 |
| Thickness | mm | 1.458 | 1.807 |
| Number of sheets | | 29 | 5 |
| Number of blanks | | 58 | 10 |

Table 5.1: Sheet sizes for experimental validation

5.2 Equipment

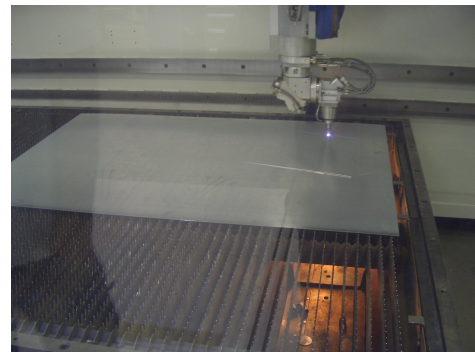
The tests are conducted at the University of Dortmund. The deep drawing press was a Müller Weingarten, see Figure 5.1(a). The blanks were cut with a laser a Lasercell 1005, see Figure 5.1(c). At several blanks a grid was applied, the circular grid pattern was marked into the surface of the blank using electrochemical-etching technique. The blanks were oiled by hand and put in by hand, see Figure 5.1(b). For the exact position of the blank on the blank holder see Appendix E.2



(a) Müller Weingarten



(b) Position of blank



(c) Lasercell 1005

Figure 5.1: Equipment at University of Dortmund.

Setting the variables

The first focus for the experimental validation was to validate the process windows and the second focus was to validate the trends of x_5 and x_6 .

This means that only one process variable must be set that is the blank holder force, this must be done with the press. The 2 geometrical variables are changed with the Lasercell, for the exact dimensions of all the blanks, see Appendix E.1.

5.3 Validation

At the experimental validation two measurements will be done namely a thickness measurement at the press. At Corus a FMTI grid analyzer is used to determine the major and minor strains in the part.

A point that must be addressed is the difference in focus areas in the FEM simulations and the measurement areas. Due to the fact that the focus areas in the FEM simulation are small and in corners of the B-pillar, see Appendix D.1. With the measurement equipment it is only possible to measure flat areas. Therefore the measurement areas are different than the focus areas in the FEM simulations.

The measurement points for the thickness measurements can be seen in Figure 5.2, with as short reminder the region A and B in Figure 5.2(b). The thickness measurements are conducted with an ultrasonic thickness gauge.

In order to produce a FLD, the circular grid pattern was marked into the surface of the blank using an electrochemical-etching method. The strains in region A are also measured in the areas pointed out in Figure 5.2(a). The strains in region B are measured around the flat areas pointed in Figure 5.2(c).

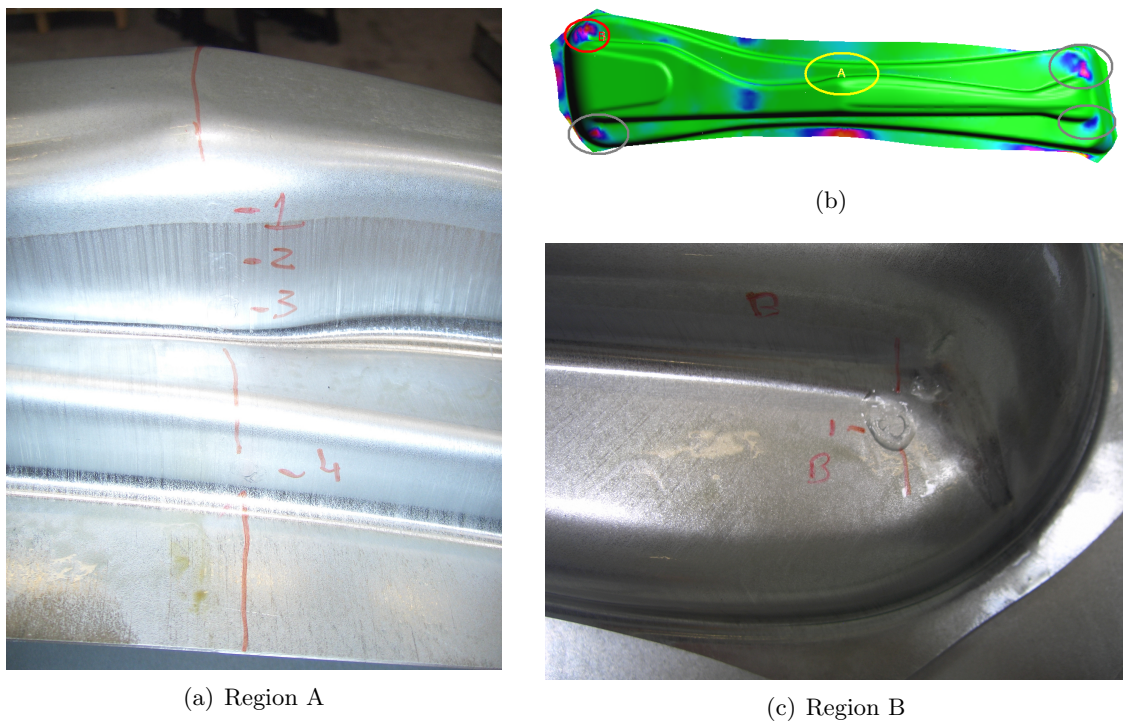


Figure 5.2: Measurement points for the measurements.

5.4 Blank holder force

The first objective was to determine the process windows, this has been done for both the materials, H340LAD, see Section 5.4.1, and DP600, see Section 5.4.2. Several test are conducted with different blank holder forces, first the thickness is presented after that the strains in the specific regions are presented.

5.4.1 H340LAD

In the FEM simulations, see Section 4.3.1, the process window was determined. The upper limit of the process window was determined at a blank holder force of 3500 kN and the lower limit at a blank holder force of 18 kN, see Table 4.2. The objective was to determine the upper and lower limit of the material with the experimental trials.

Some remarks must be made about the results of the experiments. Due to the factors that are still unknown there are differences between the experiments conducted at day 1 and day 2. The reasons for these differences will be discussed in Section 5.6. For now only the remark is made that at day 1 the product did not show any fractures at a blank holder force of 2200 kN (experiment number 10). While at day 2 the product did show a fracture in Region B at a blank holder force of 2200 kN (experiment number 16 in Table 5.4) for the picture of the crack see Figure E.30 in Appendix E.5.1. This is with the geometrical variable x_5 set to 1.

Another point to investigate was the lower limit of the process window, the wrinkling of the product, therefore 2 experiments are conducted one at a blank holder force of 100 kN, experiment number 8, and another at 500 kN, experiment number 9. The experiment with a blank holder force of 100 kN, the product shows wrinkles in region B of the B-pillar, see Figure E.27 in Appendix E.5.1. While at a blank holder force of 500 kN no wrinkles could be detected and therefore the blank holder force was set as reference blank holder force for wrinkling.

Thickness

In Table 5.2, the gray marked rows is where the product shows cracks, for experiment 7 see Figure E.29 and for experiment 18 see Figure E.30 both in Appendix E.5.1. One can conclude from these figures that at a blank holder force of 3400 kN the product fails at several points. While at experiment 18 with a blank holder force of 2600 kN only a crack can be seen in region B.

| BHF in kN | Experiment number | Thickness in mm | | | | |
|-----------|-------------------|-----------------|-------|-------|-------|----------|
| | | Region A | | | | Region B |
| | | 1 | 2 | 3 | 4 | 5 |
| DAY 1 | | | | | | |
| 100 | 8 | 1.451 | 1.423 | 1.377 | 1.504 | 1.507 |
| 500 | 9 | 1.363 | 1.352 | 1.407 | 1.478 | 1.477 |
| 1000 | 6 | 1.367 | 1.313 | 1.367 | 1.477 | 1.482 |
| 2200 | 10 | 1.273 | 1.280 | 1.337 | 1.447 | 1.450 |
| 3400 | 7 | 1.330 | 1.186 | 1.239 | 1.416 | 1.431 |
| DAY 2 | | | | | | |
| 1200 | 21 | 1.359 | 1.264 | 1.364 | 1.467 | 1.464 |
| 1400 | 20 | 1.367 | 1.301 | 1.351 | 1.464 | 1.455 |
| 1400 | 47 | 1.359 | 1.294 | 1.357 | 1.468 | 1.457 |
| 1400 | 48 | 1.353 | 1.293 | 1.361 | 1.468 | 1.458 |
| 1800 | 19 | 1.362 | 1.294 | 1.336 | 1.459 | 1.464 |
| 2600 | 18 | 1.160 | 1.243 | 1.296 | 1.439 | 1.465 |

Table 5.2: Process window thickness

For the graphical display of the values see Figure E.5 for day 1 and Figure E.6 for day 2 in Appendix E.3.1.

Several conclusions can be drawn from this table. The first point is the variation in thickness with exact the same settings. If one looks at the experiments 20, 47, 48 in Table 5.2. One can conclude that there is a difference of 0.01 mm. This is taken as the so called noise factor. This is due to deviation in the measurement equipment and the variance in the position of the measurement.

The other conclusion that can be drawn from this table is that there is a variance in thickness in region A. If one looks at experiments 20, 47 and 48 which are conducted at day 2. Specifically at the thicknesses at the measurement points 1, 2, 3. One can see a trend, see Figure 5.3 for the location of the measurement points see Figure 5.2(a).

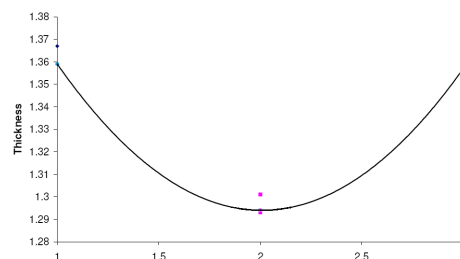


Figure 5.3: Variance in thickness in region A

Strains

Also the areas where the strains are measured are different than the focus areas of the FEM simulations. Due to the fractures in the focus area of experiment 7 the strains were not measured of this product. For all the forming limit diagrams see Appendix E.4.3.

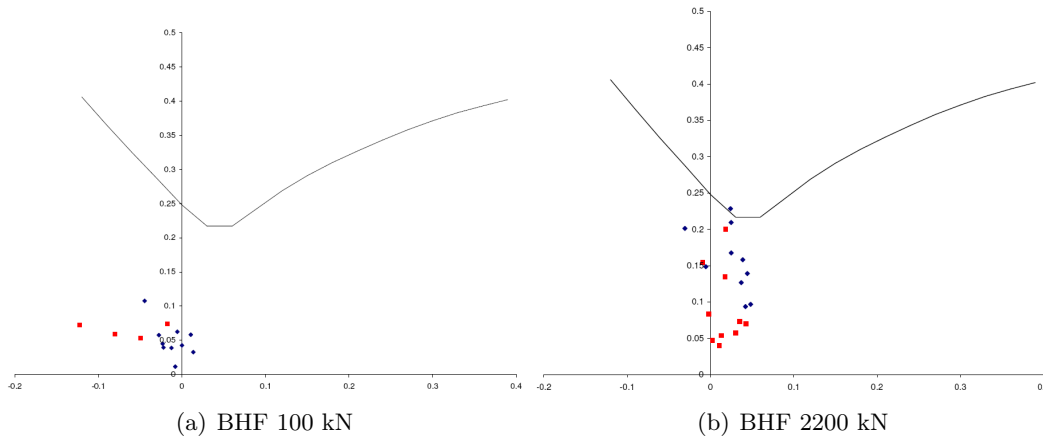


Figure 5.4: Forming limit diagram with strains in region A en B of day 1

One can conclude from Figure 5.23(a) that a lot of thickening is taking place in region B. The strains in the elements lie beneath the line of equal thickness ($\epsilon_{major} = -\epsilon_{minor}$). However the product at day 1 did not show cracks at a blank holder force of 2200 kN. The strains, which are measured with the FMTI grid analyzer, are above the FLC, this is caused by a measuring error.

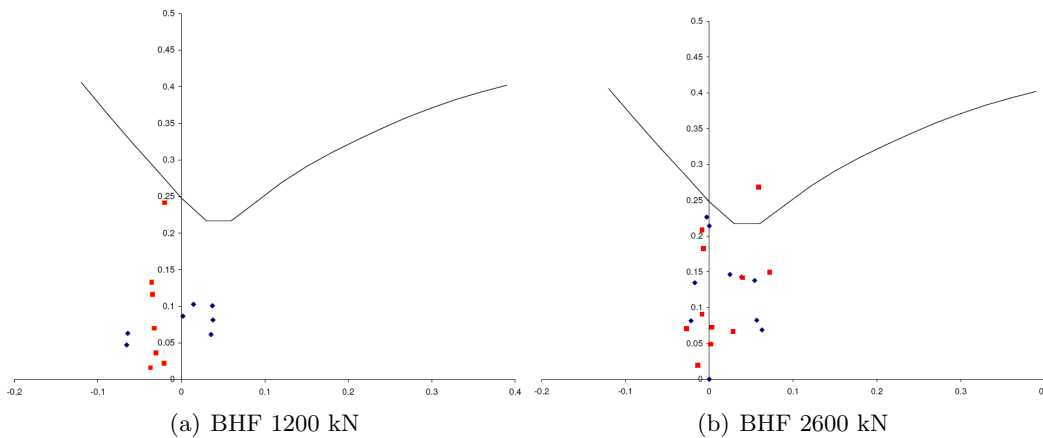


Figure 5.5: Forming limit diagram with strains in region A en B of day 2

If one takes a good look at the strains at a blank holder force of 2200 kN, see Figure 5.5(b). One can see that only one point is above the FLC, while the product showed a clear fracture in region B, see Figure E.31. Therefore one can conclude that the strains in region B are higher in the corners.

5.4.2 DP600

In the FEM simulations, see Section 4.3.2, the process window was determined of another batch, but this is still used as a guideline. The upper limit of the process window was determined at a blank holder force of 5400 kN, see Table 4.2. The objective was to determine the upper limit of the process window with the experimental trials.

Also some remarks must also be made about the results of the experiments of DP600. Due to factors that are still unknown there are differences between the experiments conducted at day 1 and day 2. The reasons for these differences will be discussed in Section 5.6. For now, only the remark is made that at day 1 the product did not show any fractures at a blank holder force of 3000 kN (experiment number 13) while at day 2 the product did show a fracture in Region B at a blank holder force of 1000 (experiment number 41, 43).

Thickness

In Table 5.3, the gray marked rows is where the product shows cracks, for experiment 14 see Figure E.32 in Appendix E.5.2.

| BHF in kN | Experiment number | Thickness in mm | | | | |
|-----------|-------------------|-----------------|-------|-------|-------|----------|
| | | Region A | | | | Region B |
| | | 1 | 2 | 3 | 4 | 5 |
| DAY 1 | | | | | | |
| 1000 | 11 | 1.376 | 1.381 | 1.437 | 1.515 | 1.479 |
| 2000 | 12 | 1.374 | 1.378 | 1.482 | 1.499 | 1.468 |
| 3000 | 13 | 1.361 | 1.325 | 1.367 | 1.485 | 1.461 |
| 4000 | 14 | 1.379 | 1.260 | 1.343 | 1.477 | 1.458 |
| DAY 2 | | | | | | |
| 1000 | 44 | 1.362 | 1.376 | 1.421 | 1.516 | 1.478 |
| 1000 | 45 | 1.416 | 1.388 | 1.416 | 1.521 | 1.478 |
| 1000 | 46 | 1.367 | 1.401 | 1.411 | 1.513 | 1.483 |
| 1500 | 41 | 1.380 | 1.335 | 1.384 | 1.507 | 1.481 |
| 1500 | 43 | 1.401 | 1.314 | 1.397 | 1.506 | 1.488 |

Table 5.3: Process window thickness

For the graphical display of the values see Figure E.7 for day 1 and Figure E.8 for day 2 in Appendix E.3.2.

One can conclude from this table that the thickness measurements which are conducted at the different regions do not give a good indication if the product fails. If one looks at, for example experiment 11 and 44, the thickness values are almost the same. While undergoing experiment 11 the product did not show fractures and during experiment 44 the product did show a crack in region B.

Strains

Also the areas where the strains are measured are different than the focus areas of the FEM simulations. Another point that must be addressed is the variance in the FLD, see Figure 5.7, for more forming limit diagrams see Appendix E.4.2.

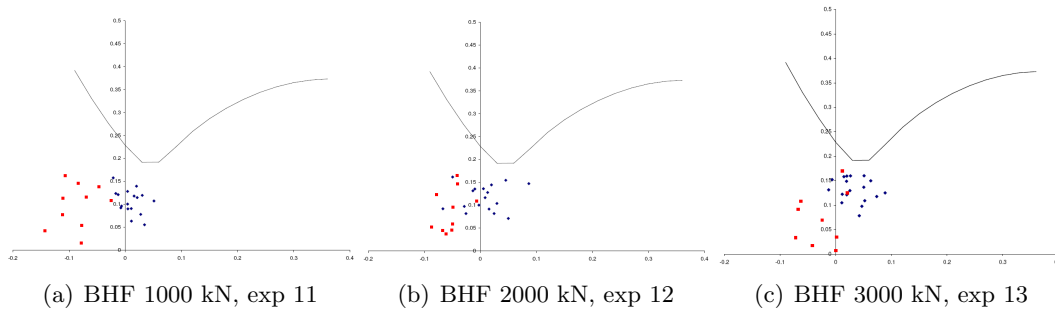


Figure 5.6: Forming limit diagram with strains in region A en B of day 1

One can conclude that the strains in region B at an increasing blank holder force seems to "rotate", see Figure 5.6. The minor strain is moving from negative to positive while the major strain stays in the same values for the strain.

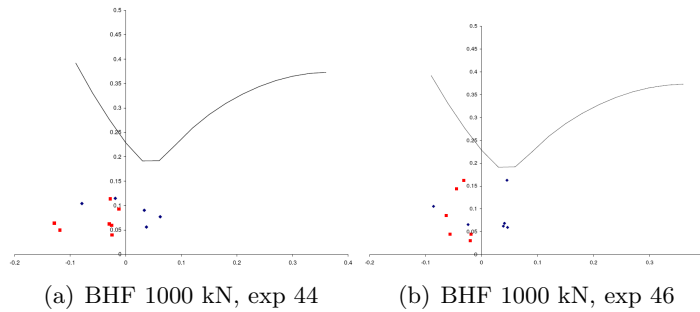


Figure 5.7: Forming limit diagram with strains in region A en B of day 2

One can conclude from Figure 5.7 that the measured strains of day 2 at a blank holder force of 1000 kN are in the same region as at day 1, see Figure 5.6(a). But at day 2 the B-pillar showed a crack in region B. The strains in the flat areas around in region B do not seem to increase. Therefore one must conclude that the strains in an edge in region B are increased while the strains in the flat areas in region B are not increased.

5.5 Geometrical variables x_5 and x_6

The second objective was to determine if the trends that were discovered with the FEM simulation can be validated, see Section 4.5 and Section 4.6. This has only been done with H340LAD, due to the lack of material of DP600.

Several tests are conducted with different blank holder forces and geometrical variables. For the validation of the scatter plots of x_5 , see Section 5.5.1, for the scatter plots of x_6 see Section 5.5.2. Also x_5 and x_6 are varied simultaneously at a specific blank holder force and in this way surface plots of the FEM simulations could be evaluated, see Section 5.5.3. Also in these sections the thickness is presented. After that the strains in the specific regions are presented.

The exact dimensions of the blanks with the variables x_5 and x_6 are included in Appendix E.1

5.5.1 Variation of geometrical variable x_5

In Section 4.5.1 the variable x_5 was varied and some interesting trends were discovered. The experiments must confirm whether these FEM simulation trends can be experimentally validated.

Thickness

In Table 5.4 experiments number 6 and 10 were conducted at day 1 while all the other experiments were conducted at day 2. The gray marked rows showed cracks in region B product, experiments 24 and 16.

| x_5 | Experiment number | Thickness [mm] | | | | Region B 5 |
|-------------|-------------------|----------------|-------|-------|-------|---------------|
| | | Region A | | | | |
| | | 1 | 2 | 3 | 4 | |
| BHF 1000 kN | | | | | | |
| 0 | 6 | 1.367 | 1.313 | 1.367 | 1.477 | 1.482 |
| 1/2 | 25 | 1.378 | 1.340 | 1.370 | 1.474 | 1.470 |
| 1 | 17 | 1.376 | 1.319 | 1.360 | 1.463 | 1.483 |
| BHF 1400 kN | | | | | | |
| 0 | 20 | 1.367 | 1.301 | 1.351 | 1.464 | 1.455 |
| 1/2 | 23 | 1.356 | 1.314 | 1.351 | 1.464 | 1.457 |
| 1 | 22 | 1.350 | 1.312 | 1.348 | 1.458 | 1.458 |
| BHF 2200 kN | | | | | | |
| 0 | 10 | 1.273 | 1.280 | 1.337 | 1.447 | 1.450 |
| 1/2 | 24 | 1.352 | 1.244 | 1.290 | 1.440 | 1.463 |
| 1 | 16 | 1.343 | 1.251 | 1.321 | 1.447 | 1.469 |

Table 5.4: x_5 variation at different blank holder forces.

For the fullness of this investigation the graphs for the thickness are included in Appendix E.3.3. For blank holder force; 1000 kN see Figure E.9, for 1400 kN see Figure E.10 and for 2200 kN see Figure E.11.

One can conclude from Table 5.4 that the influence of the geometrical variable x_5 on the thickness in Region A becomes larger if the blank holder force is increased. The same conclusion can be drawn with respect to the scatter plots, see Figure D.2 and Figure D.2.

While at the same, time the trend that can be seen in the thickness in region B in the FEM simulations, could not be seen back in Table 5.4. The trend that can be seen at a low blankholder force is a descending thickness in region B, see Figure D.2.

Strains

Also here the areas where the strains are measured are different than the focus area of the FEM simulations. Only the forming limit diagrams of the variation of x_5 at a blank holder force of 2200 kN is presented. For the other forming limit diagrams see Appendix E.4. For blank holder force; 1000 kN see Figure E.21, for 1400 see Figure E.22 and for 2200 kN see Figure E.23.

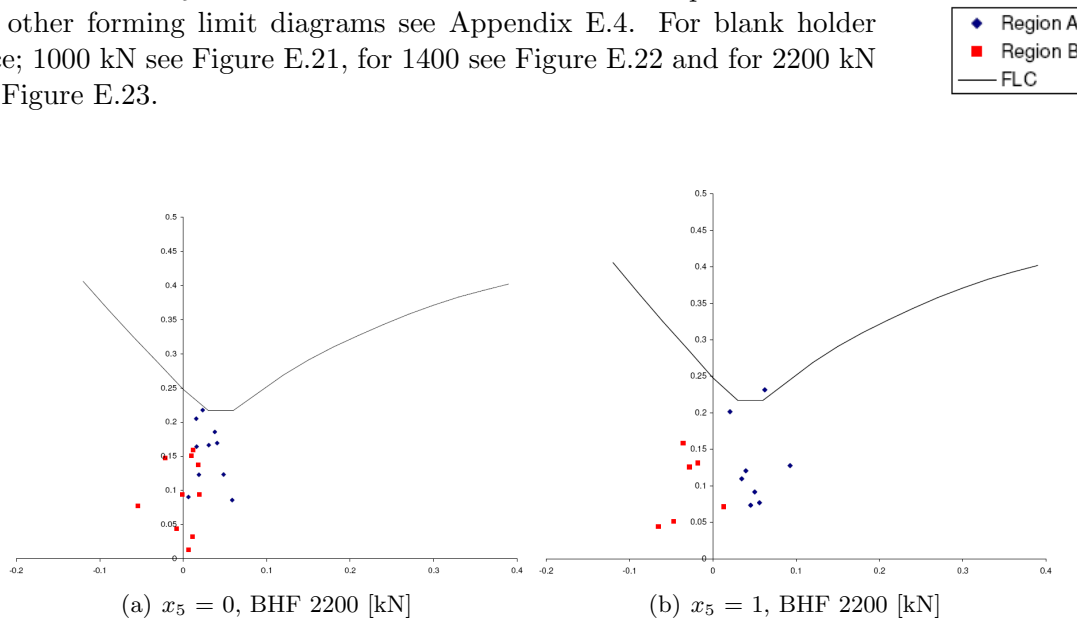


Figure 5.8: Forming limit diagram with strains in region A en B

It is not possible to draw a good conclusion if the variation of x_5 has effect on the strains in the product. If one takes a look at Figure 5.7 a lot of variation in measured strains can be seen at the same blank holder force.

5.5.2 Variation of geometrical variable x_6

In Section 4.5.2 the variable x_6 was varied and some interesting trends were discovered. The experiments must confirm whether these FEM simulation trends can be experimental validated.

Thickness

In Table 5.5 experiments number 6 and 10 were conducted at day 1 while all the other experiments were conducted at day 2. Also experiments 34 and 38 showed a crack in region B.

| x_6 | Experiment number | Thickness in mm | | | | |
|-------------|-------------------|-----------------|-------|-------|-------|----------|
| | | Region A | | | | Region B |
| | | 1 | 2 | 3 | 4 | 5 |
| BHF 1000 kN | | | | | | |
| 0 | 6 | 1.367 | 1.313 | 1.367 | 1.477 | 1.482 |
| 1/2 | 36 | 1.372 | 1.344 | 1.390 | 1.471 | 1.471 |
| 1 | 40 | 1.375 | 1.331 | 1.388 | 1.477 | 1.462 |
| BHF 1400 kN | | | | | | |
| 0 | 20 | 1.367 | 1.301 | 1.351 | 1.464 | 1.455 |
| 1/2 | 33 | 1.371 | 1.284 | 1.347 | 1.351 | 1.461 |
| 1 | 37 | 1.373 | 1.272 | 1.349 | 1.463 | 1.453 |
| BHF 2200 kN | | | | | | |
| 0 | 10 | 1.273 | 1.280 | 1.337 | 1.447 | 1.450 |
| 1/2 | 34 | 1.217 | 1.307 | 1.304 | 1.446 | 1.466 |
| 1 | 38 | 1.352 | 1.255 | 1.313 | 1.466 | 1.466 |

Table 5.5: x_6 variation at different blank holder forces.

For the completeness of this investigation the graphs are included in Appendix E.3.3. For blank holder force; 1000 kN see Figure E.12, for 1400 kN see Figure E.13 and for 2200 kN see Figure E.14.

One can conclude from Table 5.5 that the influence of the geometrical variable x_6 on the thickness in Region A is negligible at a blank holder force of 1000 kN and 1400 kN. If one looks at the scatter plots of the FEM simulations with the geometrical variation of x_5 , the same conclusion can be drawn: the influence is negligible at low blank holder force, see Figure D.2.

If one looks at the thickness in region B at a blank holder force of 2200 kN a trend can be seen, the sheet gets thicker if the x_6 is active. This trend at a higher blank holder force can also be found back in the scatter plot of the FEM simulations, see Figure D.2.

Strains

Also here the areas where the strains are measured are different than the focus area of the FEM simulations. Only the forming limit diagrams of the variation of x_6 at a blank holder force of 2200 kN is presented. For the other forming limit diagrams see Appendix E.4. For blank holder force; for 1400 see Figure E.24 and for 2200 [kN] see Figure E.25.

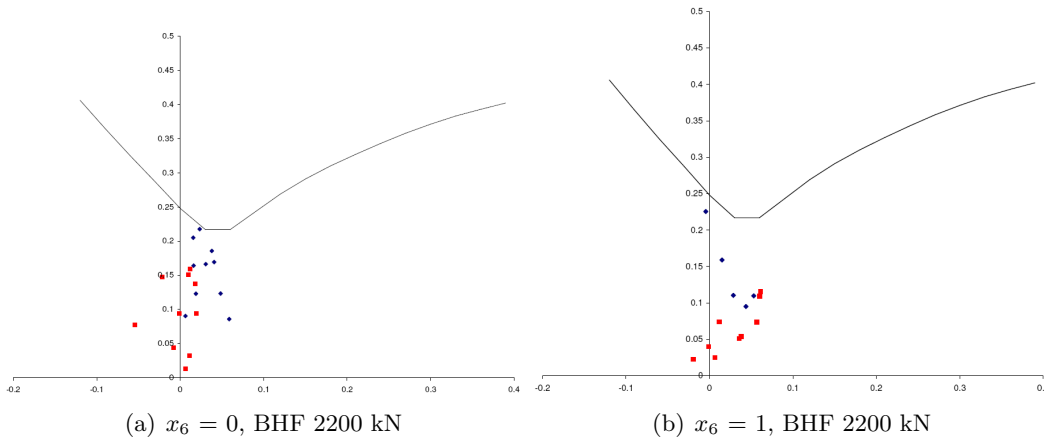
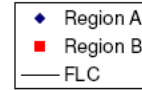


Figure 5.9: Forming limit diagram with strains in region A en B

One can conclude from Figure 5.9 that an increasing x_6 has the most effect on the strains in region B.

5.5.3 Variation of geometrical variable x_5 and x_6

In Section 4.6.3 the variable x_5 and x_6 was varied and some trends were discovered. The experiments must confirm these FEM simulation trends.

Thickness

In Table 5.6 all the experiments are conducted at day 2. Only experiment 31 showed a crack in region B.

| x_5 | x_6 | Experiment number | Thickness in mm | | | | |
|-------------|-------|-------------------|-----------------|-------|-------|-------|----------|
| | | | Region A | | | | Region B |
| | | | 1 | 2 | 3 | 4 | 5 |
| BHF 1400 kN | | | | | | | |
| 0 | 0 | 20 | 1.367 | 1.301 | 1.351 | 1.464 | 1.455 |
| 1/2 | 0 | 23 | 1.356 | 1.314 | 1.351 | 1.464 | 1.457 |
| 1 | 0 | 22 | 1.350 | 1.312 | 1.348 | 1.458 | 1.458 |
| 1/2 | 1/2 | 32 | 1.371 | 1.294 | 1.351 | 1.459 | 1.467 |
| 1/2 | 1 | 31 | 1.349 | 1.295 | 1.341 | 1.452 | 1.460 |
| 1 | 1/2 | 27 | 1.372 | 1.304 | 1.366 | 1.464 | 1.455 |
| 1 | 1/2 | 28 | 1.376 | 1.289 | 1.364 | 1.459 | 1.463 |
| 1 | 1 | 26 | 1.378 | 1.296 | 1.331 | 1.464 | 1.456 |
| 0 | 1/2 | 33 | 1.371 | 1.284 | 1.347 | 1.351 | 1.461 |
| 0 | 1 | 37 | 1.373 | 1.272 | 1.349 | 1.463 | 1.453 |

Table 5.6: x_5 and x_6 variation at blank holder force of 1400 kN.

As one can see the difference between the thickness are negligible therefore the surface plots do not reveal a certain trend, see Figure E.15 and Figure E.16 in Appendix E.3.4.

As one looks at the surface plots of the thickness in region A and B of the FEM simulations, see Figure D.3. The trend that can be seen in Figure D.3 is very light. So therefore it is also possible that the trend cannot be seen due to the noise which is caused by the measurements.

Strains

Due to the little variance in strains that can be seen at a blank holder force of 1400 kN, the forming limit diagrams are not presented in this section but but included in Appendix E.4 in Figure E.26.

5.6 Discussion: results experiments

The first point that must be addressed is the difference between the two days. Another point is the accuracy of the measurements. The last point that must be addressed is the difference between the lower limit of the experimental validation and the one calculated with AutoForm.

Differences between the two days;

In the case of DP600 there is a differences between the blank holder force at which the products cracks between the two dayss. Possible explanations for these difference can be put in the category of position or friction. Possible options for friction are;

- Oiling the blank by hand
- Difference in etchant
- Zinc deposition on the die and/or punch

Positioning; the blanks are positioned at the die by hand, therefore it is not possible to get the blank at the exact same position every time. Also if the blank holder is closed the blank moved a bit.

Friction; the blank is oiled by hand therefore it is possible that one blank is more oiled than another and therefore the friction between the die and the blank is lower/higher. In order to produce a FLD the circular grid is marked into the surface by an electrochemical-etching method. This etching causes differences between the experiments with a grid and the ones without a grid. Also between the gridded blanks there can be a difference due to the fact that the etching is done by hand. The etchant "eats" the circular pattern in the blank. The time that the etchant is applied to the product determines how deep the circular pattern is etched into the product. Therefore the friction which is caused by the circular pattern can be more or less depending on the time of etching. The depth of the circular pattern can also be a possible explanations for the influence of the electrochemical for etching, because two different chemicals were used, one at day 1 and the other at day 2. Another possibility is that the sheets of material were protected against corrosion with a layer of zinc. With every blank that is deformed a small layer of zinc is left on the die. Which is a possibility why the friction between the blank and die is larger when the next sheet is deformed.

A possibility that can be excluded is the temperature difference due to numbers of deep drawing. Our pace was too low to cause any temperature differences.

Accuracy of the measurements;

Due to the fact that it is not possible to measure, for example the thickness on exactly the right place, this will cause some variation in the results. This is also the case for the strain measurements. Another point is that the equipment only could measure on flat surfaces.

Minimal blank holder force;

Differences in minimal blank holder force are caused by the fact that AutoForm only takes into account the reaction forces of the blank during deformation. While in reality at a certain blank holder the product starts to wrinkle which causes the blank holder to open. As result the blank holder force must be set higher to protect the dies.

5.7 Conclusion: results experiments

There are some discussion points concerning the experiments but one thing can be concluded. In Section 4.4 the discussion was about whether the B-pillar starts to neck in region B or not. With the experiments is shown that for the B-pillar the strains exceeds the FLC and the B-pillar showed a crack in region B. Also in Section 4.4 is stated that only in a few elements the strains were above the FLC. If one looks at the FLC of the experiments which cracked in region B, see for example 5.9(b). The strain in the elements does not exceed the FLC while the product showed a clear crack in region B. One can conclude that the strain is higher in the edges of Region B this is predicted by the FEM simulations and confirmed with the experiments.

5.8 Verification of the experimental results

In Section 5.6 several possibilities are pointed out to explain the differences between the two days. The possible explanations must be found in the area of friction and position.

Position

Due to the fact that it is not possible to verify if every blank is put at the exact same position, the blanks are placed in by hand. One must look at the data which is obtained of the press.

At the beginning of the experiments the position of the blank is determined, to obtain a good product. The position of the blank is varied while the blank holder force is kept at a constant value. If one compares the press data of the variation of position one can determine the influence of the position on the effective punch force.

Friction

Two possibilities must be investigated; the influence of etching. The other is one to determine if friction is a possible explanations for the difference between day 1 and day 2.

Both of this explanations must be verified at the hand of the press data that is available.

The following press data is available from the Müller Weingarten; the blank holder force (ziehkissenkraft), blank holder path (ziehkissenweg), the pounder force (Stößelkraft) and the pounder path (Stößelweg) as can be seen in Figure 5.10.

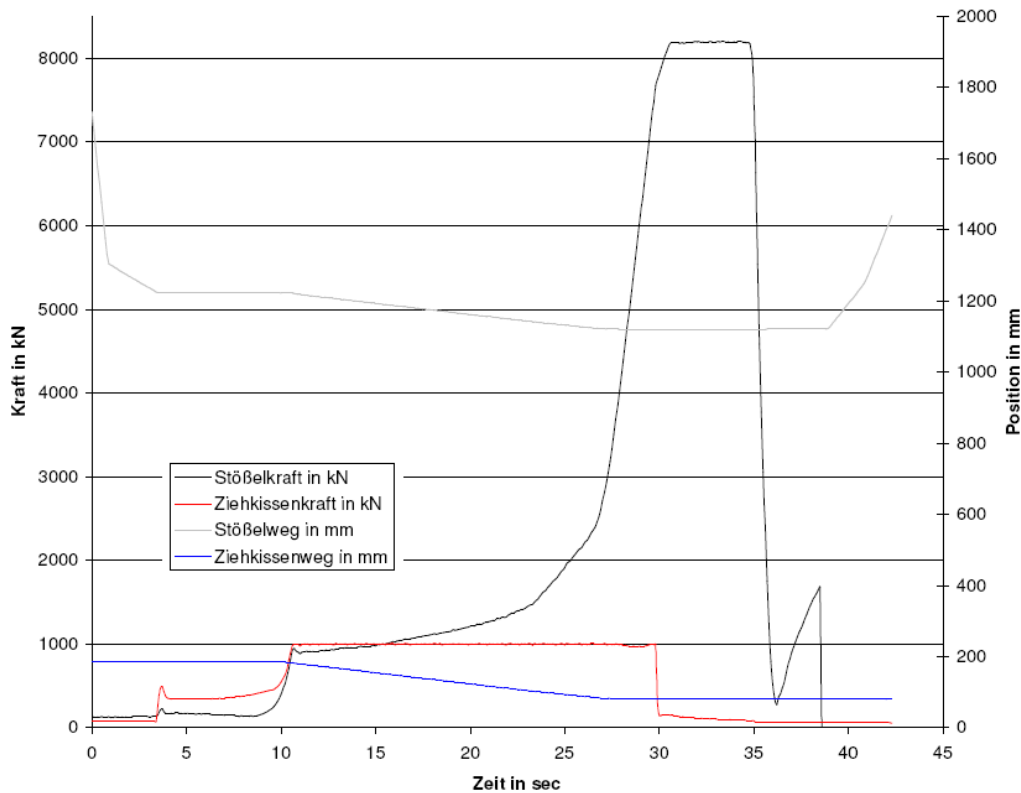


Figure 5.10: Press data of experiment 4; material H340LAD, BHF 1000 kN.

To determine the effect of friction and position one must analyze the effective punch force. The following statement is used; assumed is that the deformation of the part stops if the blank holder and the pounder stops moving. In Figure 5.10 the deformation start at a pounder path of 1220 mm and stops at 1119 mm, this is the so called deformation path. The force that is needed to deform the blank is the forces needed for the pounder minus the blank holder force, that is the effective punch force.

If we save the effective punch force at 0.4, 0.6 and 0.8 of the deformation path in a specific data file and the corresponding blank holder force. A graph can be made with the data of the same conditions, the only difference is the blank holder force, for example see Figure 5.11(a). If there is a possible influence of friction this must be the most obvious at the higher effective punch forces. So therefore a trend line is put through the effective punch force at 0.8 of the deformation path. If there is a difference in friction, for example etching and no etching, see Figure 5.11, there must be differences between the slope of the linear line. At this way one can concluded if there is a difference in friction. If the slope is higher the effective punch force will be higher at the end of the process.

5.8.1 Friction

In Section 5.6 several points were highlighted which all could have influence on the friction. These will all be investigated within the possible press data that is available.

Influence etching day 1

The first point that is addressed is the influence of etching substance. Causes the etching substance a difference in in the slope of the trend line, which is a explanations for higher friction factor.

Only the difference between a grid and no grid can be presented of day 1 of the material H340LAD. Due to the fact that a lot of experiments are conducted with a variation in geometrical variables.

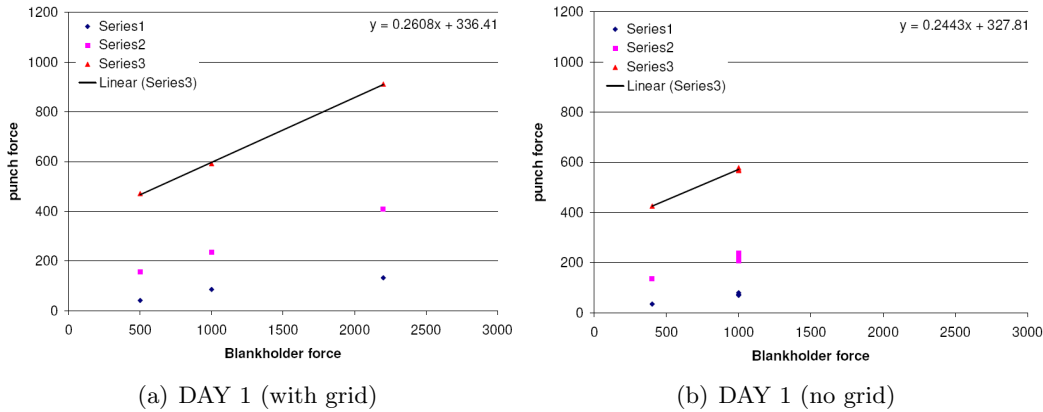


Figure 5.11: H340LAD day 1 difference in punch force with of without a grid

The slope of the trend line in the case that a grid was applied is 0.2608, see Figure 5.11(a). If there was no grid applied to the blank the slope is 0.2443 , see Figure 5.11(b). The difference in slope (0.0165) between the blanks with a grid and the ones without is not large. Therefore one can conclude that the etching substance does not have a great influence on the friction factor of the die and the blank.

day 1 vs day 2

The first point that was mentioned what could case the difference in the effective punch force between the two days is the is the etching substance. If one looks at the graphs of the two different days of the two materials, for H340LAD see Figure 5.12 and DP600 5.13. A trend line is added through the effective punch force at 0.8 of the deformation path.

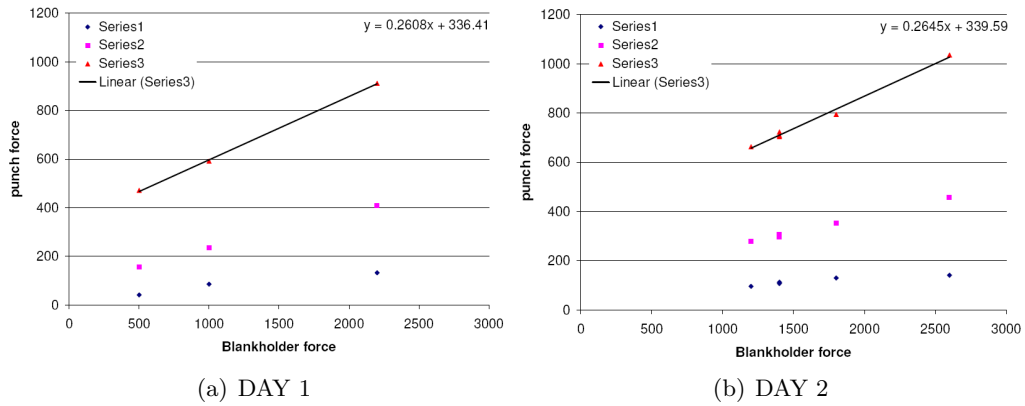


Figure 5.12: H340LAD day 1 and day 2 (in all cases a grid was applied to the blank)

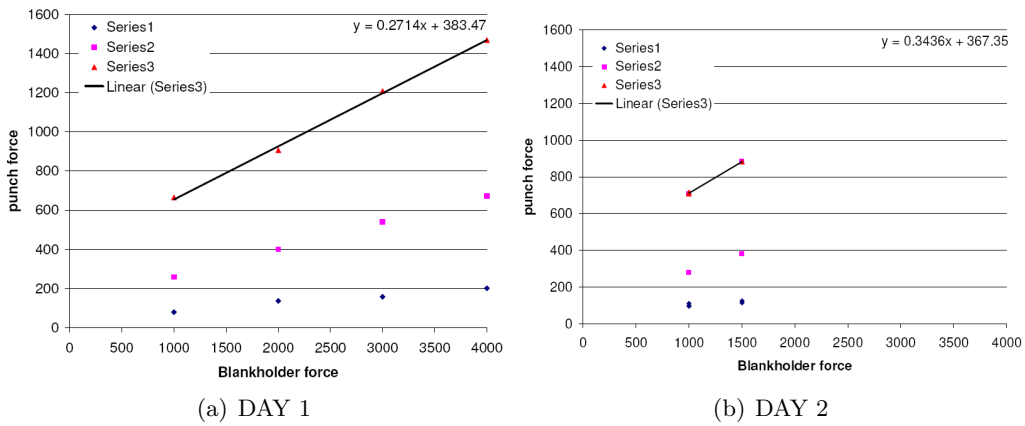


Figure 5.13: DP600 day 1 and day 2 (in all cases a grid was applied to the blank)

The difference between the two days with the material of H340LAD is negligible, for day 1, see Figure 5.12(a) the slope of the trend line is 0.2608 and for day 2, see Figure 5.12(b) 0.2645. It is most likely that this is caused by another factor than the etching substance. In the case of DP600 the difference between the slope of the trend line is a lot larger, for day 1 see Figure 5.13(a) 0.2714 and for day 2 see Figure 5.13(b) 0.3436. This difference is a good explanation why at day 2 the product started to neck at a much lower blank holder force. However the specific reason for this large difference in slope is lot harder to explain. A possible explanation is the difference in etching substance, this is highly unlikely due to the small difference in slope between day 1 and day 2 of H340LAD.

Conclusion

The etching substance seems to have an influence on the effective punch force, see Figure 5.11. This can be a possible explanation for the difference between thickness of blanks with and without a grid at day 1.

The difference in etching substance does not seem to influence the effective die force of H340LAD, see Figure 5.12. It has got a large influence on the effective punch force of DP600, see Figure 5.13. The difference in effective punch force is a good explanation for why the cracks occurred at a lower blank holder force at day 2.

5.8.2 Position

To determine the effect of the position of the effective punch force (EPF). One must look at the spread of the effective punch force in the first experiments (3, 4 and 5), see Table 5.7. The position of the blank is varied while the blank holder force is kept at a constant value.

| | EPF in kN | | |
|----------|-----------|-----|-----|
| | 0.4 | 0.6 | 0.8 |
| exp 3 | 69 | 207 | 567 |
| exp 4 | 73 | 236 | 570 |
| exp 5 | 80 | 226 | 578 |
| variance | 11 | 29 | 11 |

Table 5.7: Influence position on effective die force

As one can see the largest influence of the position on the effective punch force is at 0.6 of the deformation path. The influence of the position on the effective punch force at 0.8 at the deformation path is 11 kN.

Conclusion

One can conclude from Table 5.7 that the positioning of the blank has influence on the effective punch force.

5.8.3 Influence geometrical variables

As one can see in Table 5.5 in Section 5.5.3 that the geometrical variables have an influence on the thickness and the strains in the measured regions. A possible explanations can be a change in effective punch force. If one looks in the surface plots at the effective punch force with the blank holder force is 1400 kN. The following surface plots can be presented, see Figure 5.14.

One can see that the geometrical variables x_5 and x_6 have a certain influence on the effective punch force. If the blank holder force is higher the same trends must be seen, then one can conclude the trends are caused by the geometrical variables.

At a blank holder force of 2200 kN the geometrical variables were also varied. Only there are not enough experiments done to make a surface plot, x_5 and x_6 are not varied simultaneously. So therefore only the trends with a variable x_5 and $x_6 = 0$ can be presented, see Figure 5.15(a) and variable x_6 and $x_5 = 0$, see Figure 5.15(b).

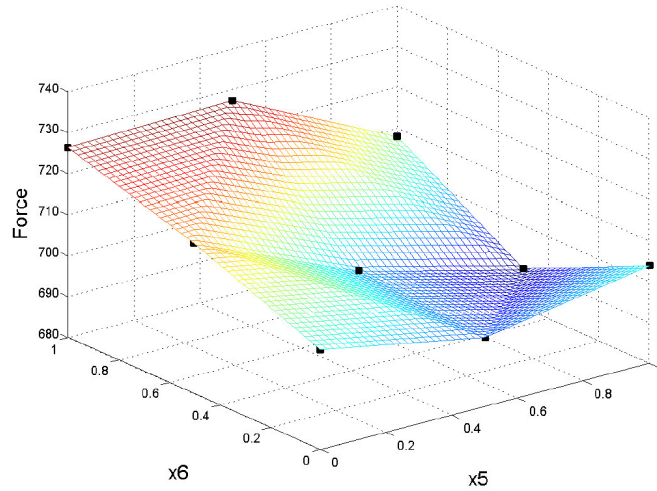


Figure 5.14: Influence of x_5 and x_6 at a BHF of 1400 kN

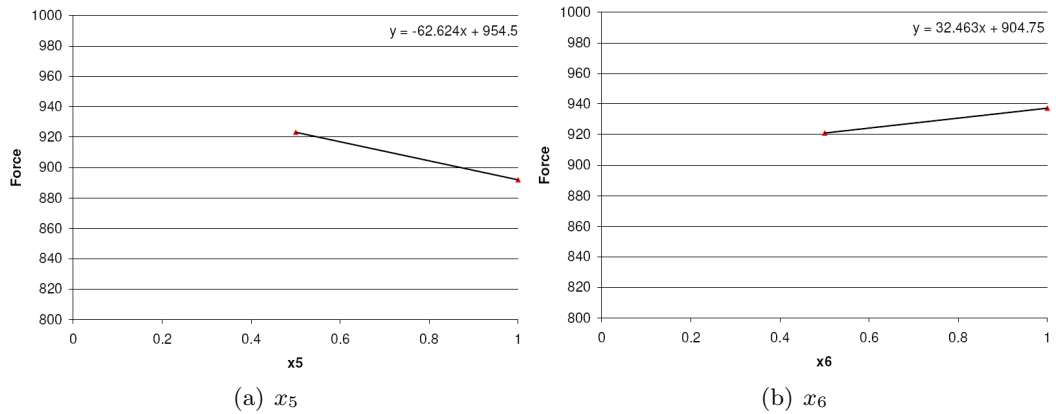


Figure 5.15: Influence of x_5 and x_6 at a BHF of 2200 kN

Conclusion

One can conclude from Figure 5.15(a) the trend with x_5 in this graph does not comply with the trend in the surface plot, if one looks at $x_6 = 0$ and increasing x_5 . In Figure 5.15(a) a descending trend is visible between $x_5 = 0.5$ and $x_5 = 1$. While in Figure 5.14 between $x_5 = 0.5$ and $x_5 = 1$ the effective punch force increases. If one takes in mind the variance in effective punch force which can be caused by the positioning of the blank. One must conclude that the geometrical variable x_5 has little influence on the effective punch force.

If one looks at the trend with increasing x_6 and $x_5 = 0$, see Figure 5.14 this is the same as in Figure 5.15(b). This can be a possible explanation for the fact that x_6 has a larger influence on the focus areas, see Figure 4.18 in Section 4.5.2. While the influence of x_5 is smaller see Figure 4.17 in Section 4.5.1.

5.9 Comparison of the experimental results with FEM

However the trends that are found with the FEM simulations are confirmed with the experiments. The values of the responses are different this is due to different rolling direction and other factors which are discussed in Section 5.6.

Due to the fact that the scatter plots and surface plots of the FEM simulations in Chapter 4 are done with different material properties, another series of FEM simulations is done with the correct material properties, see Appendix C.2 and rolling direction in a late stage of this thesis work. In the case of DP600 the material of the first batch is "stronger" then the used for the experimental validation, see Figure ?? in Appendix ??.

Also the focus area of the focus areas in the FEM simulation of Chapter 4 is different then the measurement areas of the experiments. This is done to compare the thickness and strains which are gained from the experiments.

In Section 5.9.1 the process windows are determined with the new material properties. Due to the fact that the focus area of the first FEM simulations is different then the area were thickness and strains are measured during the experiments. The focus area is changed so that FEM calculated and experimental validated thickness can be compared. Also the measured strains during the experiments can be validated with the strains obtained from the FEM simulation program. This will be done in Section 5.9.2 for the thicknesses and for the strains are compared in Section 5.9.3.

In Section 5.6 several points were highlighted which could have influence on the deep drawing process. To investigated if these points have influence on the deep drawing of the B-pillar. The several points are varied to research if this points have an influence on the measured regions, this has been done in Section 5.9.4.

The last point that will be discussed is the thickness variation in Region A which has been discussed in Section 5.4.1, comes back in the FEM simulation this will be done in Section 5.9.5.

5.9.1 Process window

As mentioned earlier the process window of the new material parameters are determined. In the case of DP600 a new batch of material parameters is used, while in the case of H340LAD only the rolling direction is changed. The focus area for the response failure(maximum) is the area were the product first started to neck, see for example Figure E.30 in Appendix E.5.1. In the AutoForm Sigma mode this region is pointed, see Figure 5.16 for the exact coordinates, see Appendix D.4.1.



Figure 5.16: Focus area in AutoForm Sigma

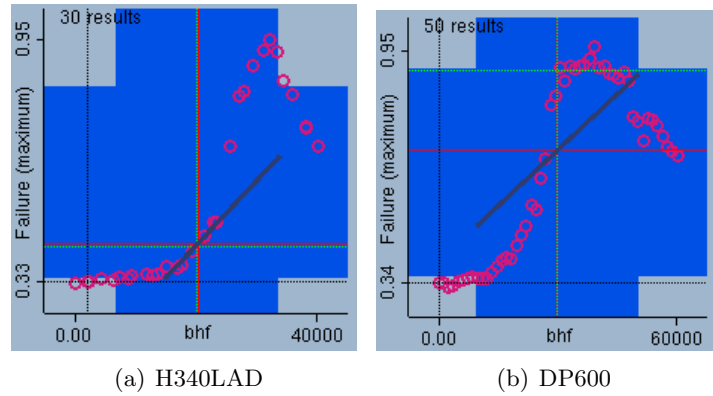


Figure 5.17: Failure(maximum) with as design variable BHF.

As one can see in Figure 5.17(a) the failure(maximum) value never exceeds 1. This should mean that the product does not fail. In the case of AutoForm an average value is taken over the zone. Therefore it is possible that the maximum failure in that zone exceeds 1. In the case of H340LAD this happens at a blank holder force of 2690 kN, see Figure 5.18 for the part and the corresponding FLD.

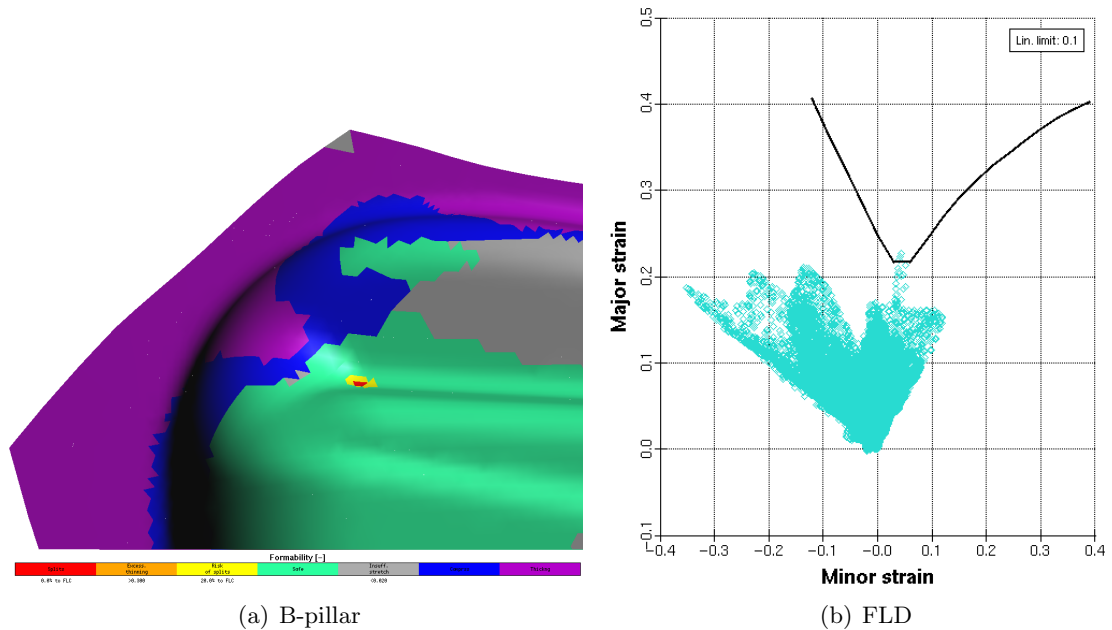


Figure 5.18: Blank holder force = 2690 kN (H340LAD)

Now one can compare the new FEM simulations with the experiments which have been presented in Section 5.4.1. At the first day (experiment number 7) at a blank holder force the B-pillar showed severe cracking. While at day 2 the B-pillar a small crack occurred at a blank holder force of 2600 kN (experiment number 18). In this case the experiments and the calculation are closely together. If one compares this FEM calculation with the one

done with the original rolling direction, see Figure 4.12 in Section 4.4. The product fails in the corner around a blank holder force of 2700 kN. So one can conclude that the rolling direction has little influence on the necking in region B.

As one takes a look at Figure 5.19(b) also in the case of DP600 the failure(maximum) value never exceeds 1 in region B. If one takes a good look at the simulations one can see that the strain in 5 elements exceeds the FLC, see Figure 5.19(b). In the case of DP600 this happens at a blank holder force of 3060 kN, see Figure 5.19 for the part and the corresponding FLD.

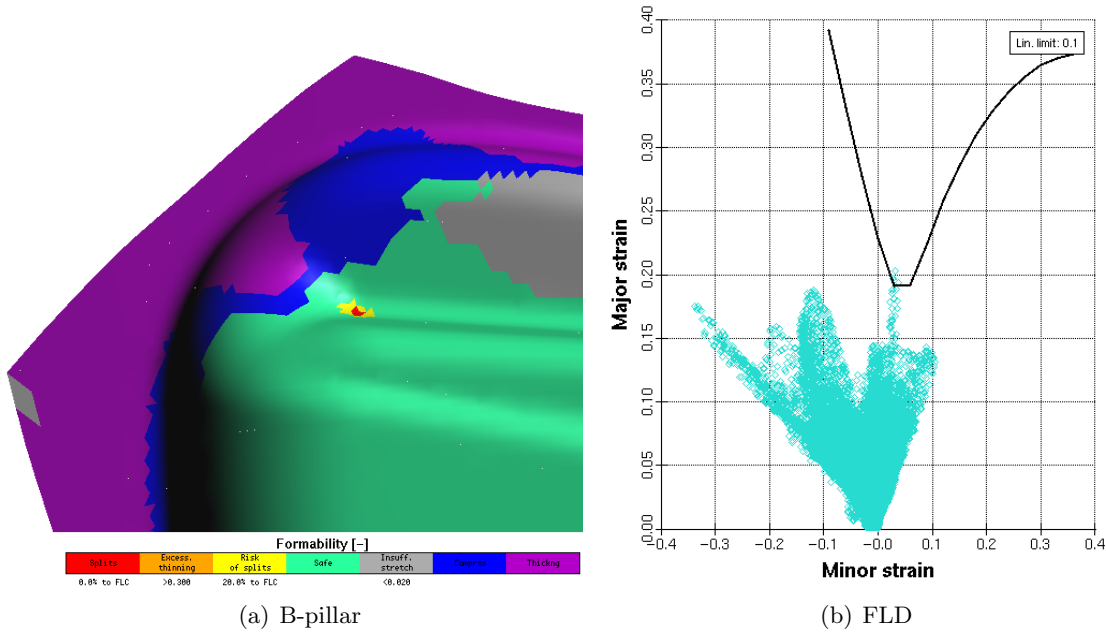


Figure 5.19: Blank holder force = 3060 kN (DP600)

Now one can compare the new FEM simulations with the experiments which have been presented in Section 5.4.2. At the first day (experiment number 14) at a blank holder force of 4000 kN a small crack occurred in region B of the B-pillar. While at day 2 the B-pillar showed a small crack at a blank holder force of 1000 kN (experiment number 44). In this case the experiment values are widely distributed. Therefore not a clear answer can be given with respect to the experiments and the FEM simulations.

If one compares this FEM calculation with the one done with the original material properties in Section 4.4. One can see in Figure D.2 in Appendix D.1.3 that the original batch fails in region B at a blank holder force of 3500 kN. While with the "new" material batch the Batch 2 fails in Region B at a blank holder force of 3060 kN. The difference in the blank holder force at which the products starts to neck in region B is clarified through the differences in the original batch and the new batch, see Figure C.1 in Appendix C.2.1

5.9.2 Thickness

A general remark must be made with respect to the thickness in the product. At Corus one B-pillar is taken through a PHASTTM measurement. PHASTTM involves photographing a pressed panel from different positions using a digital camera and then processing the data. The software is capable of linking all the photographic measurements automatically, calculating the thickness in the pressed part. The results are typically available within 1-3 hours [6]. The result is shown in Figure 5.20, the more red the thinner the area. It can be clearly seen that the thickness rapidly decreases at the edges of the product. Resulting in the fact that the thickness that are presented in Appendix D.2 and D.3 could not be compared with the thickness which are measured. Due to the fact that the focus area in the FEM simulations was located in the edge of the product, see Figure 5.16 and the measurements were taken on a flat area, see Figure 5.2(c) for Region B.

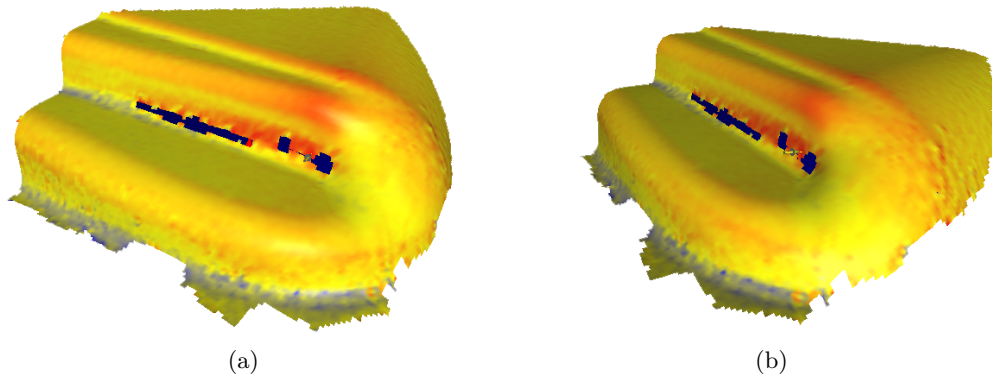


Figure 5.20: PHASTTM measurements in Region B

Due to the fact that the measurements are taken in another region, see Figure 5.2, than the one used during the FEM simulations, see Section D.1. A large difference will occur if one takes in mind the information in Figure 5.20. To compare the FEM simulations with the experiments two new focus areas are prescribed in AutoForm, see Appendix D.4.1.

The thickness that is presented is the average thickness in the regions which are pointed out in Appendix D.4.1.

H340LAD

The thicknesses measured during the experiments are presented in Section 5.4 in the case of H340LAD these are presented in Table 5.2. For the thickness in region A for the experiments we take the average value of measurement 1, 2 and 3. For region B only one measurement is done. In Table 5.8 one can find the average thickness which has been obtained from the FEM simulations is presented.

| BHF in kN | Exp num | Thickness in mm | | | |
|-----------|----------|-----------------|-------|----------|-------|
| | | Region A | | Region B | |
| | | Exp. | FEM | Exp. | FEM |
| DAY 1 | | | | | |
| 100 | 8 | 1.417 | 1.335 | 1.507 | 1.446 |
| 500 | 9 | 1.374 | 1.323 | 1.477 | 1.440 |
| 1000 | 6 | 1.349 | 1.301 | 1.482 | 1.431 |
| 2200 | 10 | 1.297 | 1.212 | 1.450 | 1.422 |
| 3400 | 7 | 1.252 | 1.151 | 1.431 | 1.407 |
| DAY 2 | | | | | |
| 1200 | 21 | 1.329 | 1.284 | 1.464 | 1.417 |
| 1400 | 20,47,48 | 1.340 | 1.288 | 1.457 | 1.427 |
| 1800 | 19 | 1.331 | 1.271 | 1.464 | 1.419 |
| 2600 | 18 | 1.233 | 1.195 | 1.465 | 1.423 |

Table 5.8: Thickness experiments vs FEM

As one can conclude from Table 5.8 the thickness in the FEM simulation in region A, is a monotonous descending function, see Figure 5.21(a). This is also the case in the thickness measured at day 1 in Region A. The variation in thickness in region A of the measured thickness maybe caused by the noise variation in the measurements.

The thickness in the FEM simulation of region B is not a monotonous, see Figure 5.21(b). Another conclusion that can be drawn from Table 5.8 is that the thickness calculated with the FEM simulations come close to thickness measured on day 1 in region B. Also the fluctuation in thickness, see day 2 region B, is also predicted with the FEM simulations.

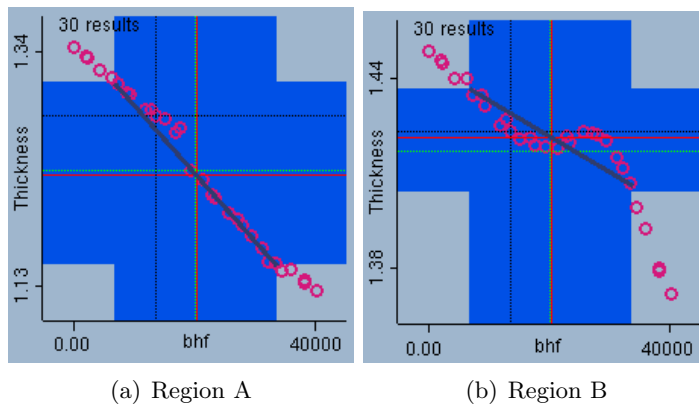


Figure 5.21: Thickness in Region A and Region B

DP600

In the case of DP600 a slight other approach has been taken. Due to the fact that the experiments of day 2 did not match at all with the process window FEM simulations, see Section 5.9.1. Day 2 is eliminated from Table 5.9. Also here the same approach, to obtain the thickness in region A is taken, in comparison with H340LAD is used.

| BHF in kN | Exp. num | Thickness in mm | | | |
|-----------|----------|-----------------|-------|----------|-------|
| | | Region A | | Region B | |
| | | Exp. | FEM | Exp. | FEM |
| DAY 1 | | | | | |
| 1000 | 11 | 1.398 | 1.369 | 1.479 | 1.464 |
| 2000 | 12 | 1.411 | 1.345 | 1.468 | 1.448 |
| 3000 | 13 | 1.351 | 1.285 | 1.461 | 1.446 |
| 4000 | 14 | 1.327 | 1.236 | 1.458 | 1.423 |

Table 5.9: Thickness experiments vs FEM

In region A the measured thickness do not coincide with the ones predicted with FEM. Also the trends in region A do not coincide with each other. A possible explanation is a measurement error in experiment 12.

As one can conclude from Table 5.9 the thickness in the FEM simulation in region B comes close to the ones measured on the B-pillar. Also the not monotonous descending trend in thickness of region B can be found back with the FEM simulations, see Figure 5.22(b).

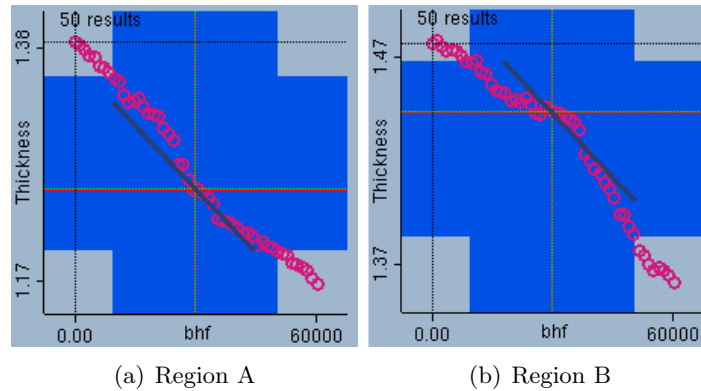


Figure 5.22: Thickness in Region A and Region B

Conclusion

As one can conclude from Table 5.8 and Figure 5.20 of H340LAD however the exact values do not match, the trends in thickness are similar.

This is not the case with the thickness in the FEM simulations and the measured thickness with the experiments of DP600. The thickness do not match and the trend in region A. But the trend measured thickness in Region B does compile with the FEM simulations.

5.9.3 Strains

In Section 5.4 the forming limit diagrams were presented. In this section the FLD of the experiments are compared with the ones of the same conditions in the FEM simulations. The only point that is investigated is the strain in region B. At the same region were the strain were measured with FMTI, the strains in the FLD are presented by red dots, see Figure 5.24.

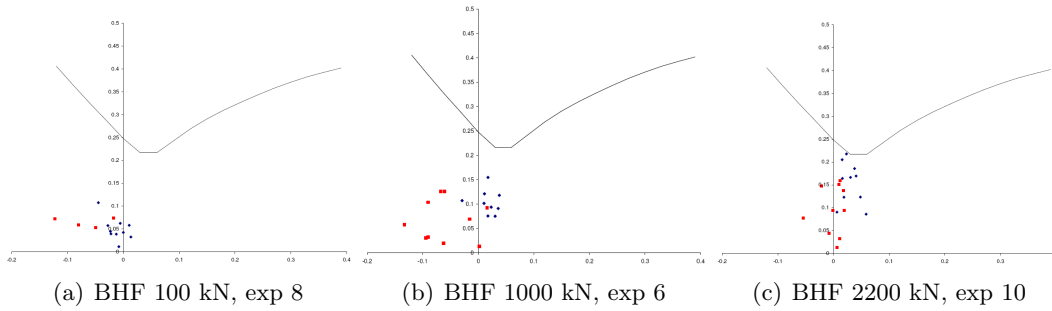


Figure 5.23: Forming limit diagram with strains in region A en B of day 1

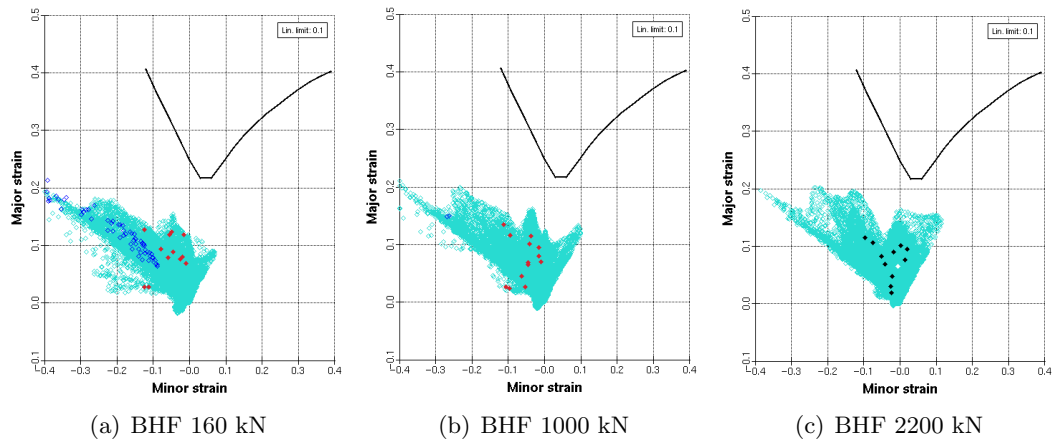


Figure 5.24: Forming limit diagram with strains in region B with FEM

As one can conclude from Figure 5.23 and Figure 5.24 that the strains obtained with the FMTI measurements are in the same region as the ones in the FLD of the FEM simulations. It is hard to conclude if the strains are exactly the same. This is caused through the fact that the circular pattern, which is etched on the blank with the experiments, has the dimension of 2 x 2 mm. While the elements can be a lot smaller. Therefore the strain in the elements is in the same region but not the exact values can be found back.

5.9.4 Sensitivity for noise variables

Additional research has been done with the following variables; the blank position and the friction factor. The range of the variables; in the case of blank position both the x-coordinate and y-coordinate was varied ± 20 mm, in the case of friction factor was varied from 0.05 up to 0.15. These ranges were chosen, in the case of blank position for experience that have been gained during the experiments. In the case of the friction factors due to the experience of user of AutoForm, due to several different reasons the factor is varied from 0.05 till 0.15. The analysis have been done with the material H340LAD, due to the fact that most of the experiments were conducted with this material. 3 scatter plots are made with the same response variable failure and the design variables are x-position, y-position and lubrication. The focus area for this research, was the area were the product first started to neck, see Figure D.4(b) in Appendix D.4.1.

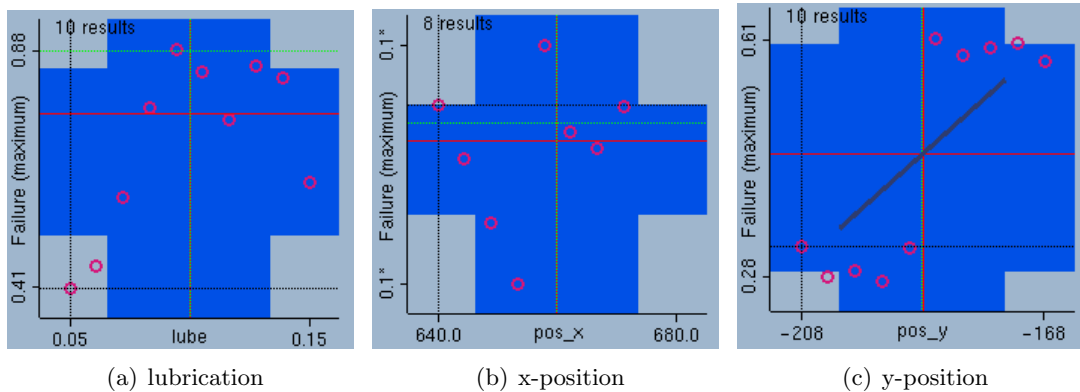


Figure 5.25: Failure(maximum) with as design variable the 3 noise variables.

A remark one must take a close look to the y-axis of the scatter plots. The range of the y-axis is not all the same, for example in Figure 5.25(b) the range is 0.04. As one can see in Figure 5.25 that the lubrication, see Figure 5.25(a) and the y-position, see Figure 5.25(c) has a large influence on the focus area. Also it looks likes if the influence of the y-position is bivalent.

If one compares these results to the data of the experiments one can conclude that the influence of the y-position is a good explanation for the variance in effective blank holder force, see Section 5.8.2. The influence of lubrication is one of the possibilities that causes the difference between the two days. Another explanation between the difference, based on the performed calculations, in the two days is not found.

5.9.5 Variation in region A

If one looks closer at Table 5.2 a trend can be seen in thickness of region A, see Figure 5.3. A small research is done if this is also the case for the FEM simulations. At the specific blank holder forces that are mentioned in Table 5.2. To confirm of this trend is also the case with the FEM simulations the thickness of region A is evaluated, see Figure 5.26.

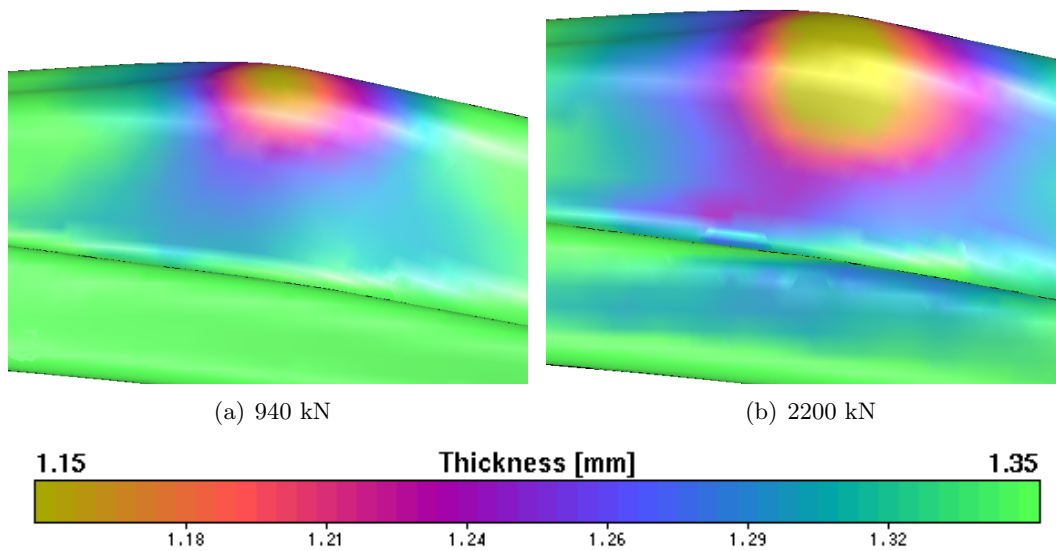


Figure 5.26: Thickness in region A at different blank holder forces

As can be clearly seen the trend that was discovered at the experiments cannot be found back in the FEM simulations.

5.10 Conclusion

With the material DP600 a difference is found between the two days at which blank holder force the B-pillar started to neck. The reason that at the same blank holder force the B-pillar started to neck is caused by an increase in friction. An explanation about what caused the increase in friction is not found. However the experimental tests that are conducted with the material of H340LAD match the FEM simulations. The influence of the geometrical variables on the thickness is also confirmed with the experiments. The influence on the strains in the B-pillar is not so very present in the experiments. The one thing that is stated with the experiments is that the strains and the thickness rapidly decreases in the corners of region B.

The one thing that is confirmed with the experiments that the strains and the thickness rapidly decreases in the corners of region B.

The possible factors that could influence the manufacturing process are investigated which yielded in a good explanation for the influence of the position on the effective punch force. Also the influence of friction on the manufacturing process is confirmed.

6

Conclusion & recommendations

The goal of this thesis was to provide useful information about the optimisation strategy. This goal has been achieved by;

1. The 7 step methodology is applied to the B-pillar and the design variables with the most influence on the manufacturing process of the B-pillar are determined.
2. The difference between the material models of AutoForm and Corus are pointed out and the effect of the differences on the material properties is determined.
3. Design variables are varied over a range to determine the effect on several responses with FEM simulations.
4. Experimental tests are conducted at the University of Dortmund which confirm the trends of the FEM simulations. Only the exact value did not match.

6.1 Conclusions

The following conclusions can be drawn from this thesis:

- Based on the 7 step methodology the B-pillar manufacturing process has been analyzed. The problem has been modeled. With OptForm and AutoForm the problem has been screened and the final optimisation model has been presented.
- In general it can be said that the material models in the database of AutoForm are, “stronger” than the ones provided by Corus. This is caused by the differences in the FLC, yield surfaces and hardening curves.
- The scatter and surface plots presented in Chapter 4 give a good indication of the formability of the product as function of the process and geometrical variables. The attention point is the area where the product will crack. The calculations show that in region B only in a few elements the strains are above the FLC. The experiments will put an end to this discussion. An optimal setting for the deep drawing of the B-pillar has been obtained. This is only done with the help of the scatter and surface plots and not with the OptForm. Therefore one cannot give a clear answer for the differences between OptForm and AutoForm Sigma. What can be conducted is that the found

optimum with the AutoForm Sigma optimisation mode is that is in the lower regions of the blank holder force. Also the optimum is evaluated with one material therefore one can only speculated over the effect of different materials.

- With the material DP600 a difference is found between the two days at which blank holder force the B-pillar started to neck. The reason that at the same blank holder force the B-pillar started to neck is caused by an increase in friction. An explanation about what caused the increase in friction is not found. However the experimental tests that are conducted with the material of H340LAD match the FEM simulations. The influence of the geometrical variables on the thickness is also confirmed with the experiments. The influence on the strains in the B-pillar is not so very present in the experiments. The one thing that is stated with the experiments is that the strains and the thickness rapidly decreases in the corners of region B.
- The possible factors that could influence the manufacturing process are investigated which yielded in a good explanation for the influence of the position on the effective punch force. Also the influence of friction on the manufacturing process is confirmed.

6.2 Recommendations

The following recommendations are given for further investigation:

- To make a 3d scan of the dies of the B-pillar to check if the dimensions of the dies match the data of the model in AutoForm.
- With the FEM simulations a non-linear trend is shown in region B. This could not be experimental validate, but what is come clear is that the product showed cracks in region B. This confirms that the FEM simulations did predict the strains in the elements of region B of above the FLC is right. A recommendation is to investigate the trends that are predicted in region B with more experiments. To confirm that a slightly higher blank holder force causes lower strains in region B.
- Possible explanations for the difference between the experiments are looked into, such as friction and position. Other factors not included in the FEM model may give another look for example; local friction, local roughness, non homogeneous material properties. A recommendation is to investigate these possibilities in a follow up project.
- The result of the performed activities is a good starting point for an improved optimisation. The recommendation is to execute the optimisation with OptForm and AutoForm Sigma. Several conclusions can then be drawn regarding the setting of the design variables and efficiency of both the methods.

Bibliography

- [1] M.H.A. Bonte. *Optimisation strategies for metal forming process*. PhD thesis, Universiteit Twente, Faculteit der construerende technische wetenschappen, June 2007. ISBN 978-92-365-2523-7.
- [2] Vincent T. Ciulla. Website. <http://autorepair.about.com/library/glossary/bldef-027a.htm>.
- [3] AutoForm Engineering GMBH. *AutoForm Release Notes*, 4.0 edition.
- [4] AutoForm Engineering GMBH. *AutoForm User's Manual*, 2.04 edition.
- [5] Dr. habil. Fabian Duddeck. Website. <http://www.baume.bauwesen.tu-muenchen.de>.
- [6] D Hamels. Website. <http://www.corusautomotive.com>.
- [7] E.T. Harpel. Numerical prediction of limiting draw ratio in aluminum cylindrical cup drawing. Master's thesis, Carleton University, Ottawa-Carleton Institute for Mechanical and Aerospace Engineering, May 1997.
- [8] R. Hill. Constitutive modelling of orthotropic plasticity in sheet metals. *J. Mech. Phys. Solids*, 38(3):405–417, 1990.
- [9] R. Hill. A theoretical perspective on in-plane forming of sheet metal. *J. Mech. Phys. Solids*, 39(2):295–307, 1991.
- [10] R. Hill. A user-friendly theory of orthotropic plasticity in sheet metals. *Int. J. Mech. Sci.*, 35(1):19–25, 1993.
- [11] J. Huétink, T. Meinders. Solid mechanics ii, plasticity. Technical report, Universiteit Twente, Faculteit der construerende technische wetenschappen, Opleiding Werktuigbouwkunde, Vakgroep TM, April 2005. Vakcode: 115776.
- [12] M.H.A.Bonte. Solving optimisation problems in metal forming using fem: A metamodel based optimisation algorithm. Technical report, N.I.M.R., April 2005. Document number CTW.04/TM-5475.
- [13] R.Narayanasamy, C.S. Narayanan. Forming limit diagram for interstitial free steels supplied by ford india motors. *Materials and Design*, 28:16–35, 2005.

BIBLIOGRAPHY

- [14] R.Narayanasamy, C.S. Narayanan. Forming, fracture and wrinkling limit diagram for if steel sheets of different thickness. In proceeding of ESAFORM, 2006.
- [15] R. Pearce. *Sheet Metal Forming*. The Adam Hilger Series on New Manufacturing Processes and Materials. Adam Hilger, Bristol, England, cop. 1991. ISBN 0-7503-0101-5.
- [16] Henk Vegter, Carel H.L.J. ten Horn, Yoguo An, Eisso H. Atzema, Herman H. Pijlman, Ton H. van den Boogaard, Han Huétink. Characterisation and modelling of the plastic material behaviour and its application in sheet metal forming simulation. In *International Conference on Computational Plasticity*, 2003.
- [17] M.H.A. Bonte, A.H. van den Boogaard, B.D. Carleer. Optimising towards robust metal forming processes. In proceeding, 2006.
- [18] M.H.A.Bonte, A.H. van den Boogaard, J. Huétink. An optimisation strategy for industrial metal forming processes. *Moddelling, screening and solving of optimisation problems in metal forming*. In proceeding, September 2006.
- [19] M.H.A.Bonte, A.H. van den Boogaard, R. van Ravenswaaij. The robust optimisation of metal forming processes. In proceeding, 2006.
- [20] E. Veldman. Using optimisation techniques to solve a production problem *with application to the deep drawing process of an automotive part*. Master's thesis, Universiteit Twente, Faculteit der construerende technische wetenschappen, Opleiding Werktuigbouwkunde, Vakgroep TM, November 2006.
- [21] K. Yang and B. El-Haik. *Design For Six Sigma; A roadmap for Product Development*. McGraw-Hill Inc, New York, USA, 2003. ISBN 0-07-141208-5.

FEM simulations

A.1 Springback

Preliminary calculations showed a significant amount of springback. In this appendix this will be treated.

Springback occurs after all the deformation processes when sheet is removed from between the punch and die. There are several different ways of analyzing springback computed during a simulation. In this analysis the free springback option is used. Under this option the springback sheet is compared to the sheet before the springback. The result values make up the shift vector between material-fixed point before and after springback. In this analysis the material displacement of the sheet in normal direction due to springback is evaluated. A remark, the material used for this simulation is one of database of AutoForm namely DP600.

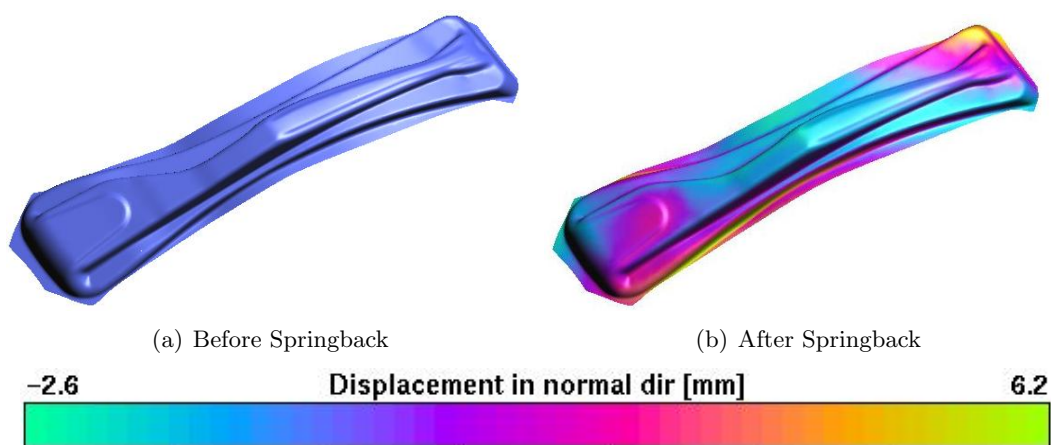


Figure A.1: Springback analysis of DP600

A.2 Blank size

The reference blank shape, see Figure A.2(a), the length is close to the maximum blank length that are available for the experimental validation.

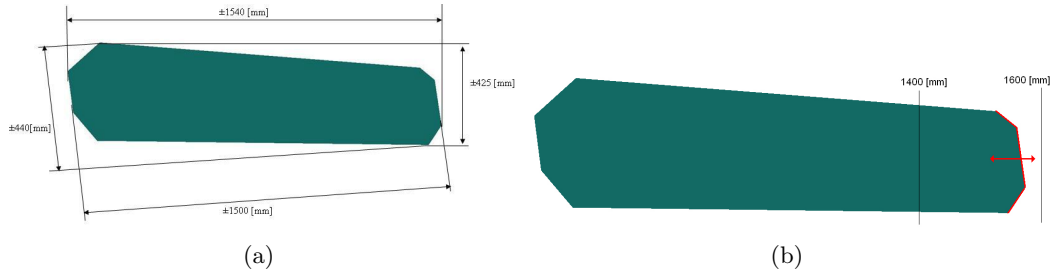


Figure A.2: (a) Reference blank shape, (b) length variation.

Some remarks, there are 2 different lengths and widths mentioned in Figure A.2(a). This is done because the blank is turned around the z - axis and then placed in the press. These dimensions are 1500 and 440. So in theory it fits precisely, but the be sure some influence calculation are preformed to investigate the influence of the blank length on the problem areas which are pointed out in Section 4.3.1. The blank is varied from 1400 mm to 1600 mm. As a short reminder the problem areas are shown in Figure A.3.

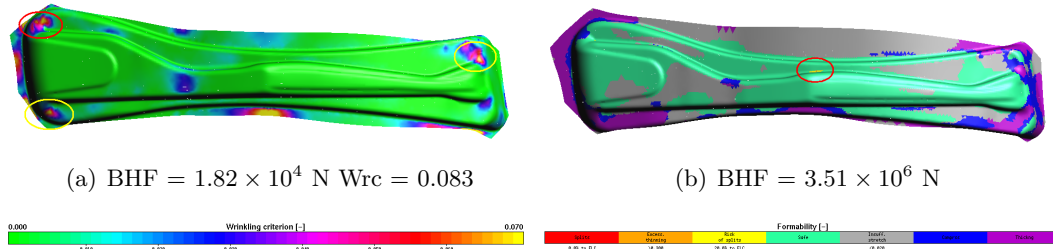


Figure A.3: Lower(a) and upper(b) limit of the process window

The red circled areas are the one where the highest wrinkling criterion occurs (Zone Wrinkling), Figure A.3(a) and the one where the material first starts to neck (Zone Failure), Figure A.3(b). The focus lies on these areas two areas with the AutoForm Sigma sensitivity/influence calculations, these sensitivity calculation are preformed with as variable the blank size, see Figure A.2(b), with a regular grid of 50.

In the following figures, the sensitivity in the problem areas, Figure A.4 for zone wrinkling and Figure A.5 for zone failure, are pointed out.

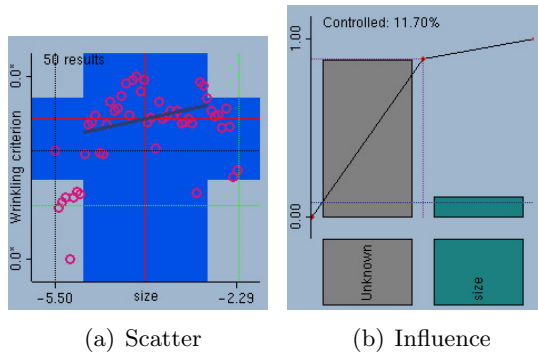


Figure A.4: Zone wrinkling

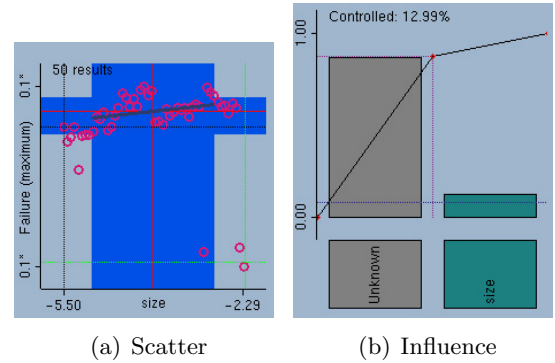


Figure A.5: Zone Failure

In the graphs is clearly to see that the blank size has a little influence on the problem. As expected the sensitivity of the variance in blank size, decreases if the area is further of the right side of the product.

Conclusions

If the blank is not exact 1500 mm it will not be a problem, because the problem areas aren't highly sensitive for this factor.

A.3 AutoForm Sigma Optimisation

A remark must be made with the AutoForm Sigma Optimization mode the hole product is used while with the scatter and surface plots a specific area was used. Also this is only done for H340LAD and not for the other materials.

How the blank variables are varied in AutoForm Sigma is explained in Section 4.1.2. Only the range of the blank holder force must be set. Due to the fact that if the blank area is set to the maximum ($x_{72} = 1, x_6 = 0, x_5 = 0$), the minimum required blank holder force is larger. Therefore the minimum blank holder force is set to 20 kN. The objective and constraint are defined in the target sheet of the sigma tab, see Figure A.6.

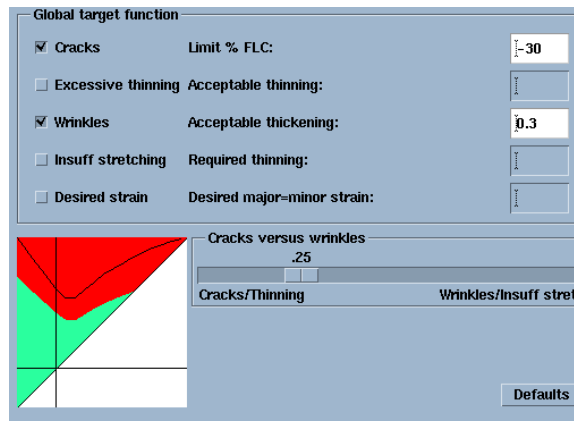


Figure A.6: Target sheet of AutoForm Sigma(b)

The objective function is set in the target sheet as a minimal distance to the FLC. In this case a factor of 30 % is taken if the factor is larger then the distance to the FLC will be larger. As one can see the constraint wrinkling is set to thickness which also been done in the mathematical model in Table 2.6. Only the limit is not taken set to 0.37 which has been proposed in the model but to 0.3. This is done for the fact that a global target function is used. Not the specific regions which are pointed out in Section 4.3.1.

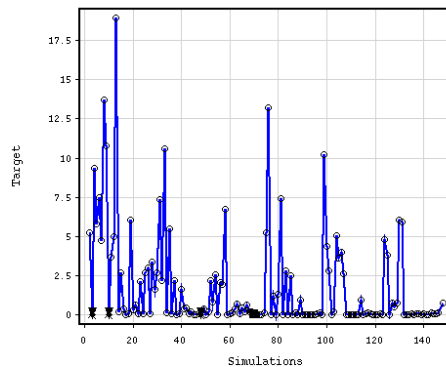


Figure A.7: Convergence plot AutoForm Sigma Optimisation

As mentioned earlier AutoForm uses an asynchronous algorithm to solve this optimisation model. The corresponding convergence plot of the sigma analysis is presented in Figure A.7. The convergence plot provides an overview of the number of simulations calculated, the convergence behavior and the best simulation result.

The simulations are characterized by a point, the best simulation by a square, others close to the best are triangles. The individual proportions of the target function are wrinkles and cracks, see Figure A.6. As one can see the best result is obtained with simulation 70. The other simulations which are indicated by a triangle are also examined. The difference between these simulations and the best simulation must be looked into differences between in a slight difference in blank holder force. The geometrical settings have a larger dispersion. So therefore one can conclude that the must dominated factor is the blank holder force. The settings of this simulation are, see Figure A.8(a).

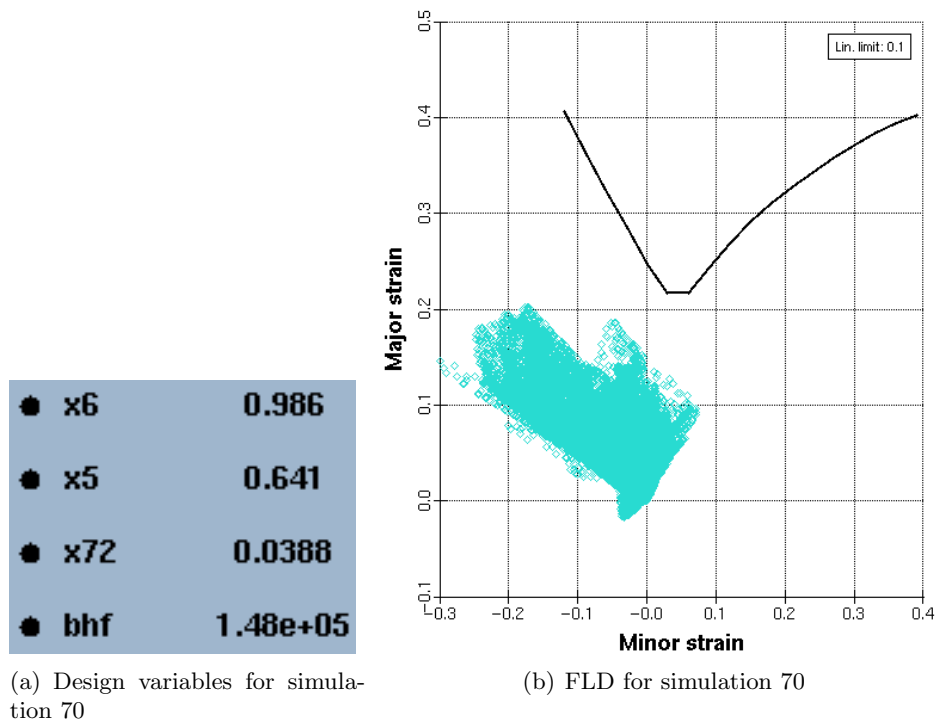


Figure A.8: Optimal value for the design variables and corresponding FLD

The corresponding FLD with these variables settings looks as follows, see Figure A.8(b).

Appendix B

AutoForm

This appendix gives some more background information about the FE simulation program AutoForm and the used functions.

B.1 Material models

The material models in AutoForm consists of three material parameters which are explained in the upcoming sections.

B.1.1 Hardening Curve

Depending on the material behavior, the specimen fails at a plastic strain ϵ_{pl} in the range of 0.15 to 0.35. However, biaxial strain states encountered during deformation of a sheet may correspond to equivalent strain values greatly in excess of the failure strain. Therefore, the flow curve needs to be extrapolated, from experimentally determined values, up to a strain of 1.0. Figure B.1 shows a schematic of an extrapolation to a value of $\epsilon_{pl} = 1.0$.

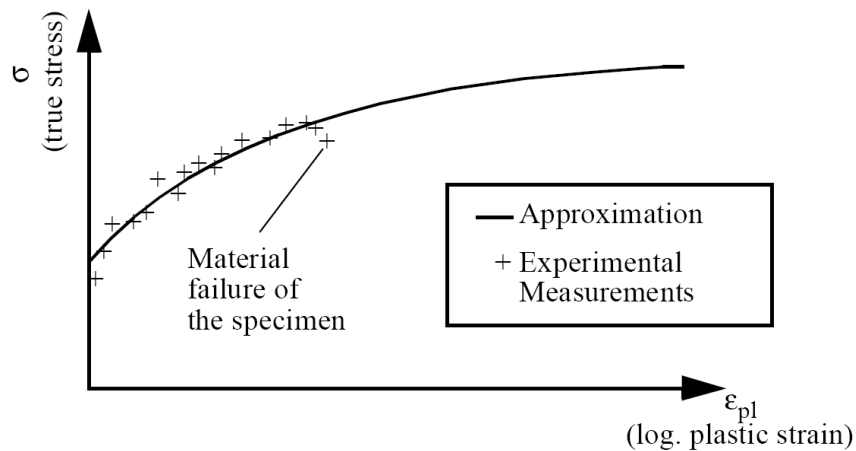


Figure B.1: Approximation of the hardening curve, from [4]

Standard methods for approximation of the hardening curve are Swift(Krupkowski), see Equation B.1 and the Hocket-Sherby, see Equation B.2.

$$\sigma = C \cdot (\varepsilon_{pl} + \varepsilon_0)^m \tag{B.1}$$

$$\sigma = \sigma_{Sat} - (\sigma_{Sat} - \sigma_i)e^{-a\varepsilon \frac{p}{pl}} \tag{B.2}$$

The methods of approximation the flow curve are described in AutoForm [3] with the a combined formula in Equation B.3.

$$\sigma = (1 - \alpha)\{C \cdot (\varepsilon_{pl} + \varepsilon_0)^m\} + \alpha\{\sigma_{Sat} - (\sigma_{Sat} - \sigma_i)e^{a\varepsilon \frac{p}{pl}}\} \tag{B.3}$$

This is combination of the Swift(Krupkowski), see Equation B.1 and the Hocket-Sherby, see Equation B.2 with a wight factor (α).

If the wight factor is 0 the upper line (blue), see Figure B.2 and the approximation of the Swift equation is used. If the wight factor is 1 the lower line (grey), see Figure B.2 and the Hocket-Sherby equation is used. Because these are generally expected as upper and lower limit. One can change the wight factor to come to there. The area between the 2 green lines is the experimental data imported with a data table.

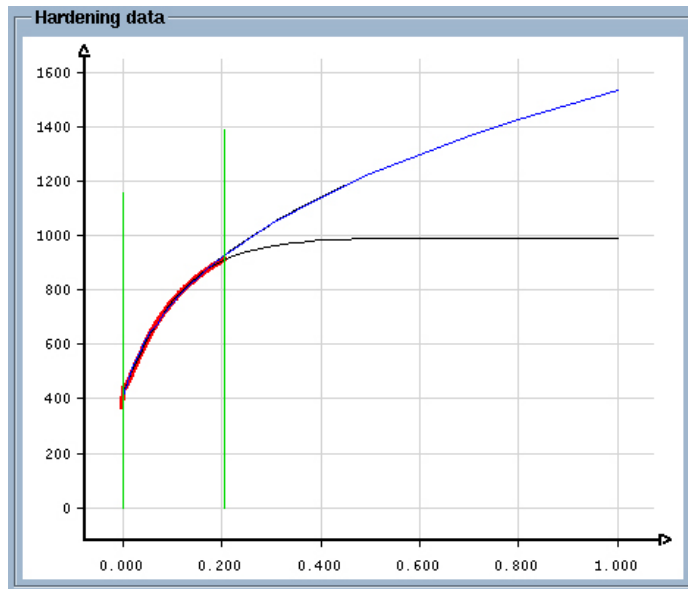


Figure B.2: Hardening Curve Trip 700

The form of the flow curve gives a good idea of the formability of the material [4]. The lower the curve (i.e., the lower the yield stress) and the steeper it is, the more formable the material.

B.1.2 Yield surfaces

The hardening curves shows relevant material properties, but has little resemblance with multi axial stress & strain states. Therefore a biaxial stress states is considered with both σ_1 and $\sigma_2 \neq 0$ and σ_3 is zero this is to so called plane stress state, for example sheet metal forming is a plane stress state.

This will lead to a yield surface, the deformation rate is perpendicular to the yield surface. The transition from elastic to plastic behavior is characterized by the yield surface. It's also a fact that the yield surface has to be convex [11].

The von Mises criterion is based on the observation that a hydrostatic pressure cannot cause plastic yielding of the material, this is also the cause in all the other models. The criterion is formulated as follows; the material passes from an elastic to a plastic state if the elastic energy of distortion reaches a critical value that is independent of the type of stress state. On the assumption that $\sigma_3 = 0$ for sheet metal, the plane-stress yield criterion is an elliptical section through the von Mises cylinder which leads to;

$$\sigma_y = (\sigma_1^2 - \sigma_1\sigma_2 + \sigma_2^2)^{1/2} \quad (\text{B.4})$$

This equation represents an ellipse in the plane of the principal stresses σ_1 and σ_2 .

This theory was re-presented with the influence of the r value in Equation B.5, the so called *Hill-48* model. The yield surface is a quadratic function, and is defined using the three r values, r_0 , r_{45} and r_{90} .

$$\sigma_y = (\sigma_1^2 - \frac{2r}{r+1}\sigma_1\sigma_2 + \sigma_1^2)^{1/2} \quad (\text{B.5})$$

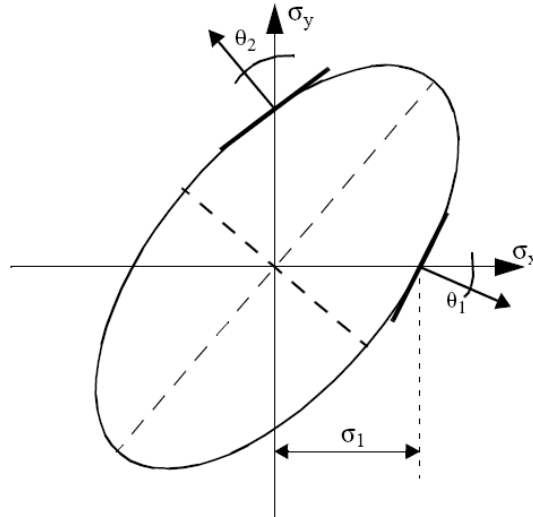


Figure B.3: Yield surface in the Hill-48 model

The two angles θ_1 and θ_2 , may be determined from the r_0 and r_{90} as follows:

$$\tan(\theta_1) = \frac{r_0}{1 + r_0} \tag{B.6}$$

$$\tan(\theta_2) = \frac{r_{90}}{1 + r_{90}} \tag{B.7}$$

Hill-79 model produces an yield surface based on a non-quadratic function: however the three r -values are assumed to be identical here ($r_0 = r_{45} = r_{90}$). This implies that the yield surface is an ellipse that expands along its major (longer) axis, see Figure B.4

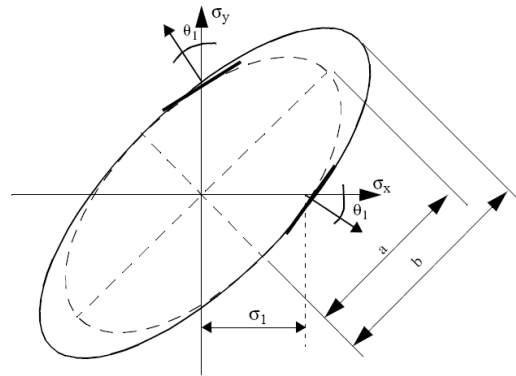


Figure B.4: Yield surface in the Hill-79 model

The advantage of this model is that it utilizes the material flow conditions under biaxial stress. This model uses, however, only the average r -value r_m . The biaxial stress factor directly controls the elongation of the yield ellipse in stress space.

$$\alpha = \frac{b}{a} \tag{B.8}$$

Meaningful values of the stress factor are in the range 0.8 to 1.2

B.2 AutoForm responses

In AutoForm 3 responses are used; thickness, failure and wrinkling criterion. Thickness speaks for itself and failure and wrinkling criterion is further explained.

B.2.1 Failure

The post-variable failure is defined as the ratio between the maximum major strain computed at an element and the major strain at which the FLC predicts failure at the corresponding minor strain (minor strain in the element). In equation form, this may be written as:

$$Failure(maximum) = \frac{a}{b} \quad (B.9)$$

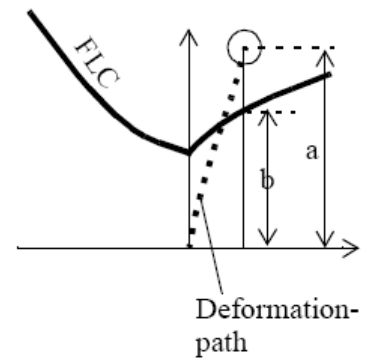


Figure B.5: Definition of the post-variable Failure

This implies that failure (splits) may be anticipated at a failure value of 1.0 or more, and that successful deformation may be anticipated at smaller values of failure [4]. However it's important that the FLC curve is determined under the assumption of linear deformation paths (i.e. based upon experimental procedures using linear deformation paths) [15].

Failure (maximum) is the maximum value of the failure criterion encountered at the element during its entire deformation history (or deformation path) [4].

B.2.2 Wrinkling criterion

The larger the value of the wrinkling criterion is at a given location on the sheet, the greater is the possibility that wrinkles occur at that location. Once the location of the danger zones have been identified, the user must then ascertain if these locations are in two-sided or one sided contact with tools, or if they are free.

In addition, the following considerations need to be taken into account when deciding whether the computed wrinkling criterion really predicts unacceptable wrinkling.

- 1: Wrinkles seldom arise in portions of the deformed sheet that have a complex three dimensional shape/geom
- 2: The blankholder stabilizes the sheet through application of pressure; therefore, there is a lesser danger of w

Critical values of the wrinkling criterion

The following table, provides reference values of the wrinkling criterion in different zones of the sheet.

| Location of wrinkles on sheet | Critical value |
|---|----------------|
| Planar zone | 0.001 |
| Bent zones | ~ 0.02 |
| Zones supported between blank holder and die surfaces | > 0.05 |

This values are dependent upon sheet thickness, a thinner sheet may be expected to wrinkle at smaller values than one that is thicker.

Appendix C

Materials models and properties

In this appendix the material properties data sheets of the material used during the first simulation series are included, see Section C.1. As well as the data sheet of DP600 used with the experimental validation, see Section C.2. The differences between the two material models of DP600 are pointed out in Section C.2.1.

C.1 Material properties used in FEM

H340LAD

| | | | | | | |
|--|-------------|-------|-------|-------|-------|-------|
| Material: 20020108 | | | | | | |
| Corus Strip Products IJmuiden Steelcode 1N82 Standards Steel Steel ColdRolled Coated Strength Steel Standards Steel EN EN 10 292 (CR BH- and P- Steel) H340LAD | | | | | | |
| PAC Stock | | | | | | |
| Owner | Vrenken | | | | | |
| Location | M51 | | | | | |
| Arrival date | 26 Mar 2002 | | | | | |
| Number of sheets | 50 | | | | | |
| Length (rolling direction) [mm] | 1500 | | | | | |
| Width (production) [mm] | 990 | | | | | |
| Thickness (production) [mm] | 1.458 | | | | | |
| Destination | | | | | | |
| Customer(s) | | | | | | |
| Project Number | | | | | | |
| Reference source links | | | | | | |
| 112099 112462 112852 112985 113207 113277 | | | | | | |
| Tensile Test (Uni Axial) | | | | | | |
| | avg | 0 | 30 | 45 | 60 | 90 |
| R _{p0.2} | [MPa] | 406 | 393 | 411 | 410 | 410 |
| R _{eL} | [MPa] | 398 | 385 | 402 | 403 | 403 |
| R _{eH} | [MPa] | 413 | 398 | 415 | 424 | 424 |
| R _m | [MPa] | 458 | 456 | 457 | 461 | 461 |
| A _e | [%] | 2.8 | 2.1 | 2.6 | 3.9 | 3.9 |
| A _g | [%] | 14 | 15.4 | 14.3 | 12.2 | 12.2 |
| A ₅₀ | [%] | | | | | |
| A ₈₀ | [%] | 24.9 | 27.3 | 27.1 | 18.2 | 18.2 |
| A ₂₀₀ | [%] | | | | | |
| D _{p5} | [%] | | | | | |
| C | [MPa] | 681 | 693 | 681 | 670 | 670 |
| r | | 1.004 | 0.891 | 1.037 | 1.053 | 1.053 |
| n | | 0.131 | 0.142 | 0.132 | 0.119 | 0.119 |
| BH ₀ | [MPa] | | | | | |
| BH ₂ | [MPa] | | | | | |
| Origin of Data | | | | | | |
| Datasheet for FEM | | | | | | |
| Contact Person | | | | | | |
| Test Notes | | | | | | |
| Files | | | | | | |
| Tensile Test, Basic Curve | | | | | | |

TRIP700

Material: 20060097

Corus Strip Products IJmuiden | Steelcode | 3QAE
 Standards Steel | Steel | TRIP Steel | Trip 700
 Standards Steel | EN | EN 10 336 (DP, TRIP and PM Steel) | TRIP | HT 700T

PAC Stock

| | |
|---------------------------------|-------------|
| Owner | Droog |
| Location | D51 |
| Arrival date | 24 Mar 2006 |
| Number of sheets | 13 |
| Length (rolling direction) [mm] | 1900 |
| Width (production) [mm] | 1500 |
| Thickness (production) [mm] | 1.716 |
| Destination | |
| Customer(s) | |
| Project Number | 896728 |

Tensile Test (Uni Axial)

| | | avg | 0 | 30 | 45 | 60 | 90 |
|-------------------|-------|---------------------------------------|-------|----|-------|----|-------|
| R _{p0.2} | [MPa] | 458 | 446 | | 462 | | 461 |
| R _{eL} | [MPa] | | | | | | |
| R _{eH} | [MPa] | | | | | | |
| R _m | [MPa] | 793 | 781 | | 797 | | 798 |
| A _e | [%] | | | | | | |
| A _g | [%] | 17.3 | 18.4 | | 16.8 | | 17.1 |
| A ₅₀ | [%] | | | | | | |
| A ₈₀ | [%] | 21.5 | 23.4 | | 21 | | 20.7 |
| A ₂₀₀ | [%] | | | | | | |
| D _{p5} | [%] | | | | | | |
| C | [MPa] | 1360 | 1352 | | 1366 | | 1357 |
| r | | 0.824 | 0.796 | | 0.825 | | 0.85 |
| n | | 0.206 | 0.212 | | 0.205 | | 0.203 |
| BH ₀ | [MPa] | | | | | | |
| BH ₂ | [MPa] | | | | | | |
| Origin of Data | | KRN | | | | | |
| Datasheet for FEM | | | | | | | |
| Contact Person | | | | | | | |
| Test Notes | | Kop Keur | | | | | |
| Files | | | | | | | |
| | | Tensile Test kop Keur | | | | | |

DP600

| |
|---|
| Material: 20060082 |
| External User Renault XE 360 B (DP600) Corus Strip Products IJmuiden Steelcode 3FAA Standards Steel EN EN 10 336 (DP, TRIP and PM Steel) DP HT 600X+Z |

| | |
|---------------------------------|-------------|
| PAC Stock | |
| Owner | Peeters |
| Location | M82 |
| Arrival date | 14 Mar 2006 |
| Number of sheets | 46 |
| Length (rolling direction) [mm] | 1500 |
| Width (production) [mm] | 1100 |
| Thickness (production) [mm] | 1.807 |
| Destination | |
| Customer(s) | |
| Project Number | 8282 |
| Reference source links | |
| 121024 | |

| | | | | | | | |
|--|-------|-------|-------|----|-------|----|-------|
| Tensile Test (Uni Axial) | | | | | | | |
| | | avg | 0 | 30 | 45 | 60 | 90 |
| R _{p0.2} | [MPa] | 402 | 400 | | 408 | | 393 |
| R _{eL} | [MPa] | | | | | | |
| R _{eH} | [MPa] | | | | | | |
| R _m | [MPa] | 620 | 619 | | 619 | | 623 |
| A _e | [%] | | | | | | |
| A _g | [%] | 14.1 | 14.8 | | 13.7 | | 14.3 |
| A ₅₀ | [%] | | | | | | |
| A ₈₀ | [%] | 22.1 | 22.3 | | 21.2 | | 23.6 |
| A ₂₀₀ | [%] | | | | | | |
| D _{p5} | [%] | | | | | | |
| C | [MPa] | 949 | 963 | | 938 | | 955 |
| r | | 0.939 | 0.91 | | 0.877 | | 1.091 |
| n | | 0.144 | 0.153 | | 0.139 | | 0.146 |
| BH ₀ | [MPa] | | | | | | |
| BH ₂ | [MPa] | | | | | | |
| Origin of Data | | KRN | | | | | |
| Datasheet for FEM | | | | | | | |
| Contact Person | | | | | | | |
| Test Notes | | | | | | | |
| Files | | | | | | | |
| Tensile Test Basic Curve | | | | | | | |

C.2 Material properties for experimental validation

DP600

Material: 20070117

External User | FIAT | FE 600 DP
 Corus Strip Products IJmuiden | Steelcode | 3FAE
 Standards Steel | Steel | Dual Phase | Cold Rolled DP | DP 600
 Standards Steel | EN | EN 10 336 (DP, TRIP and PM Steel) | DP | HCT600X+Z

General Properties

| | |
|---------------------------|-----------|
| Owner | Scholting |
| Thickness (production) | [mm] 1.5 |
| Location | D20 |
| Number of sheets | 20 |
| Coating type | GI |
| Surface texture type | MM |

General mechanical properties

| | | |
|-------------------|-------|-------|
| | | avg |
| R _{p0.2} | [MPa] | 371 |
| R _m | [MPa] | 627 |
| A _e | [%] | |
| A ₈₀ | [%] | 21.1 |
| r | | 0.929 |
| n | | 0.162 |

Tensile Test (Uni Axial)

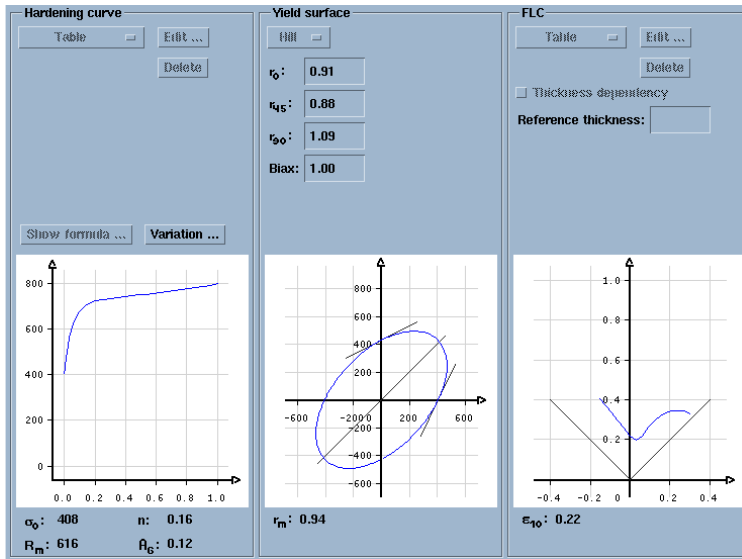
| | | avg | 0 | 30 | 45 | 60 | 90 |
|-------------------|-------|-------|-------|----|-------|----|-------|
| R _{p0.2} | [MPa] | 371 | 365 | | 377 | | 366 |
| R _{eL} | [MPa] | | | | | | |
| R _{eH} | [MPa] | | | | | | |
| R _m | [MPa] | 627 | 611 | | 633 | | 629 |
| A _g | [%] | | | | | | |
| A ₉ | [%] | 14.4 | 15 | | 14.3 | | 13.8 |
| A ₅₀ | [%] | | | | | | |
| A ₈₀ | [%] | 21.1 | 27.6 | | 19.4 | | 18.1 |
| A ₂₀₀ | [%] | | | | | | |
| D ₉₅ | [%] | | | | | | |
| C | [MPa] | | 976 | | | | |
| r | | 0.929 | 0.956 | | 0.821 | | 1.117 |
| n | | 0.162 | 0.167 | | 0.158 | | 0.164 |
| BH ₀ | [MPa] | | | | | | |
| BH ₂ | [MPa] | | | | | | |
| Origin of Data | | KRN | | | | | |
| Datasheet for FEM | | | | | | | |
| Contact Person | | | | | | | |

Test Notes
 Kop van rol 7998571
 thick 1.491 mm

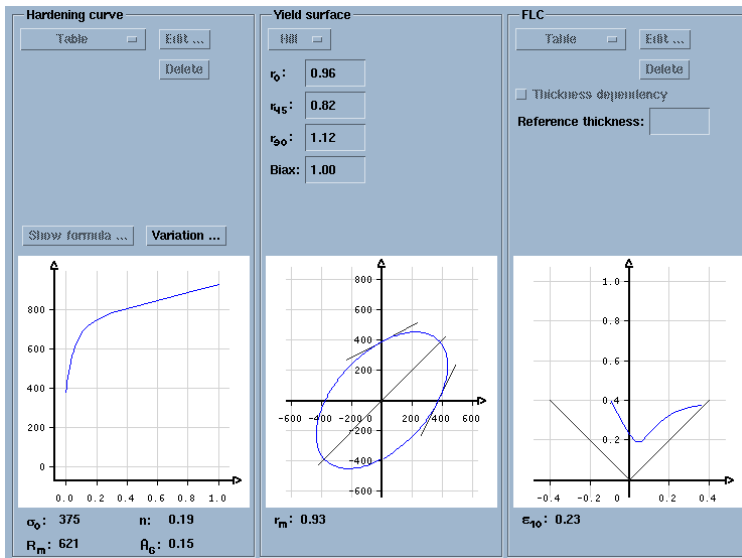
Files

[tensile test_20042007](#)

C.2.1 DP600 batch FEM against Experiments



(a) DP600 FEM



(b) DP600 EXP

Figure C.1: DP600 batch FEM against Experiments

Appendix D

Simulation series

In the beginning there were 3 materials available for the experimental validation, 4 design variables are chosen and 3 response are chosen in 2 regions. Therefore a simulation diagram is made with all the variables and a combination of variables.

| | Material | Design variable | Nominal setting |
|----|----------|--------------------------|-----------------|
| 1 | H340LAD | BHF | x5, x6, x72 |
| 2 | DP600 | BHF | x5, x6, x72 |
| 3 | TRIP700 | BHF | x5, x6, x72 |
| 4 | H340LAD | x5 BHF 6.0×10^5 | BHF, x6, x72 |
| 4A | H340LAD | x5 BHF 3.4×10^6 | BHF, x6, x72 |
| 5 | DP600 | x5 | BHF, x6, x72 |
| 6 | TRIP700 | x5 | BHF, x6, x72 |
| 7 | H340LAD | x6 BHF 6.0×10^5 | BHF, x5, x72 |
| 7A | H340LAD | x6 BHF 3.4×10^6 | BHF, x5, x72 |
| 8 | DP600 | x6 | BHF, x5, x72 |
| 9 | TRIP700 | x6 | BHF, x5, x72 |
| 10 | H340LAD | x72 | BHF, x5, x6 |
| 11 | DP600 | x72 | BHF, x5, x6 |
| 12 | TRIP700 | x72 | BHF, x5, x6 |
| 13 | H340LAD | BHF and x5 | x6, x72 |
| 14 | DP600 | BHF and x5 | x6, x72 |
| 15 | TRIP700 | BHF and x5 | x6, x72 |
| 16 | H340LAD | BHF and x6 | x5, x72 |
| 17 | DP600 | BHF and x6 | x5, x72 |
| 18 | TRIP700 | BHF and x6 | x5, x72 |
| 19 | H340LAD | x5 and x6 | BHF, x72 |
| 20 | DP600 | x5 and x6 | BHF, x72 |
| 21 | TRIP700 | x5 and x6 | BHF, x72 |

Table D.1: Simulation series

In the following pages one can find the responses in the regions which are pointed out in Section D.1.

D.1 Exact location of the Regions

In AutoForm Sigma a poly 3D curve can be generated, the average value of the response in that region is used in the scatter plots. For the three different responses in two different regions the following poly 3D curves are used.

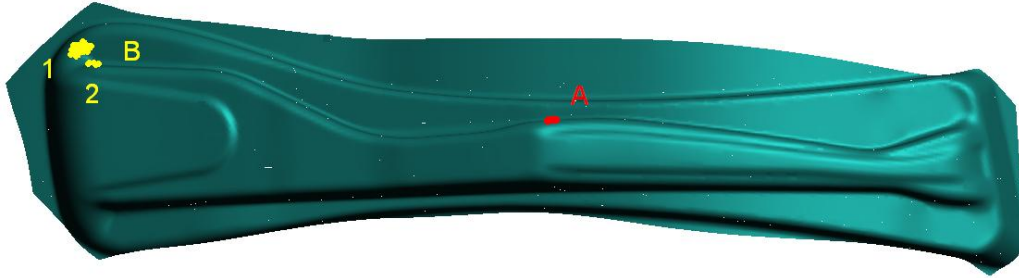


Figure D.1: B-pillar with region A and B

D.1.1 Region A

| Region A | | | |
|----------|-----------|-----------|-----------|
| | x_{pos} | y_{pos} | z_{pos} |
| 0 | -82.502 | 39.343 | 150.89 |
| 1 | -82.468 | 37.722 | 152.71 |
| 2 | -81.495 | 37.383 | 153.73 |
| 3 | -79.373 | 37.509 | 154.08 |
| 4 | -74.717 | 37.837 | 154.55 |
| 5 | -71.241 | 38.134 | 154.69 |
| 6 | -68.773 | 38.694 | 154.17 |
| 7 | -69.93 | 40.241 | 152.31 |
| 8 | -73.417 | 40.03 | 151.88 |
| 9 | -74.328 | 39.806 | 151.88 |
| 10 | -78.67 | 39.466 | 151.38 |
| 11 | -82.502 | 39.343 | 150.89 |

D.1.2 Region B

For region B two regions are pointed out 1 region where the wrinkling criterion was the highest at the lower limit of the blank holder force, see Figure D.1 number 1. The other was specified was determined with the position of were only a few elements were above the FLC, see Section 4.4 in Figure D.1 number 2.

| Region B (Failure & thickness) | | | | Region B (wrinkling) | | | |
|--------------------------------|-----------|-----------|-----------|----------------------|-----------|-----------|-----------|
| | x_{pos} | y_{pos} | z_{pos} | | x_{pos} | y_{pos} | z_{pos} |
| 0 | -710.64 | 129.29 | 33.162 | 0 | -732.13 | 161.07 | 25.239 |
| 1 | -714.72 | 127.08 | 36.463 | 1 | -745.67 | 156.97 | 19.246 |
| 2 | -724.4 | 128.87 | 34.469 | 2 | -748.74 | 149.54 | 20.74 |
| 3 | -724.19 | 131.19 | 31.316 | 3 | -749.12 | 143.51 | 24.212 |
| 4 | -717.55 | 131.26 | 30.428 | 4 | -742.05 | 140.65 | 27.714 |
| 5 | -710.64 | 129.29 | 33.162 | 5 | -726.05 | 146.75 | 26.94 |
| | | | | 6 | -720.54 | 154.55 | 28.833 |
| | | | | 7 | -732.13 | 161.07 | 25.239 |

D.1.3 Split in edge (DP600)

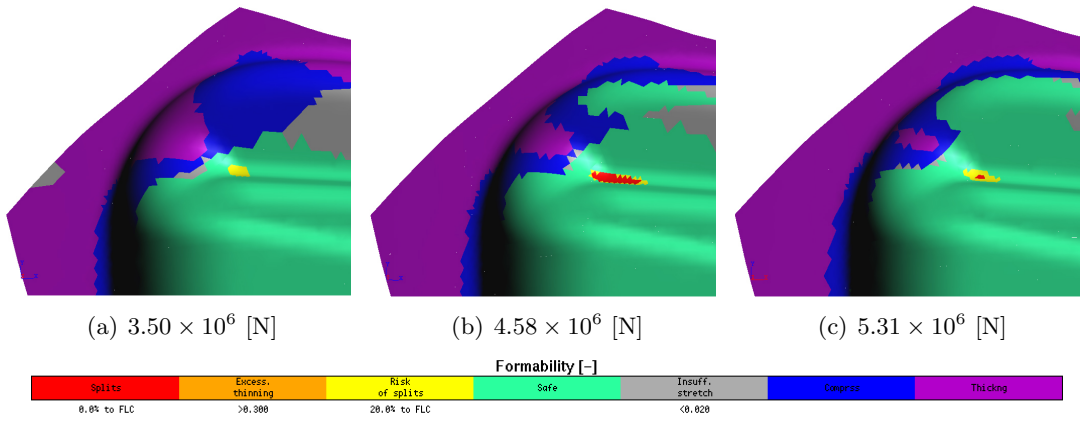
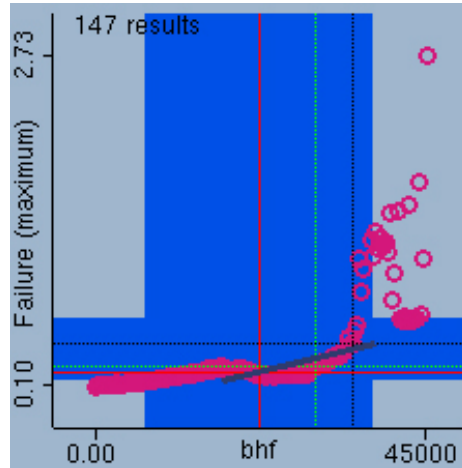


Figure D.2: Formability plots of the left corner with different blank holder forces with DP600.

D.2 Scatter plots

The following scatter plots are made with the use of AutoForm. A scatter plot shows the raw result variable (RV) and the selected design variable(DV) in an xy-scatter plot for all the simulations of the current performance analysis.



| | |
|-------------------------------|---|
| Red circle | Individual simulation result |
| Blue bars | IQR_{normal} range for as DV as RV |
| Red lines | Median value(s) for as well DV as RV |
| Thin dashed green line | Nominal simulation value(s) |
| Thin dashed black line | Current simulation value(s) |
| Thick grey line | Visualization of the Sensitivity / partial derivative at the median / median crosshair position. |

1:Scatter plots dependent on BHF for material H340LAD

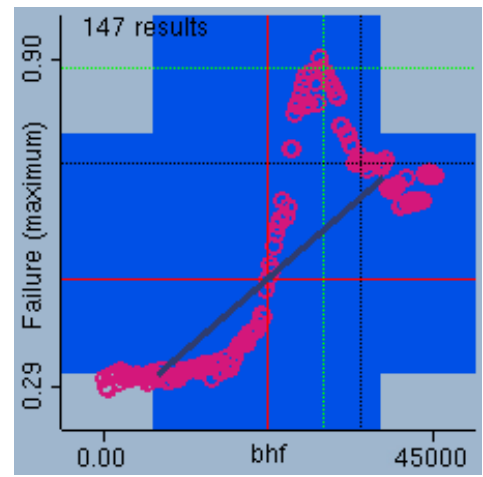
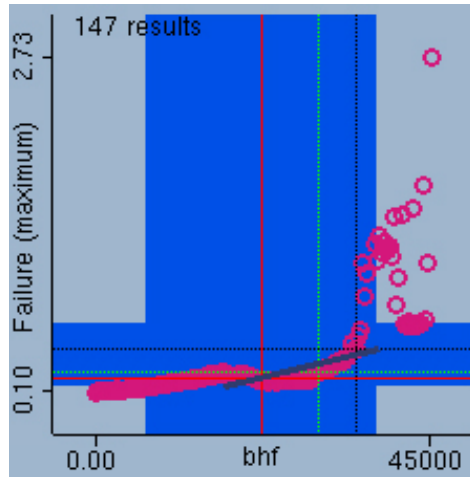
147 simulations dependent on BHF with x5, x6 and x72 to nominal settings.

147 sim

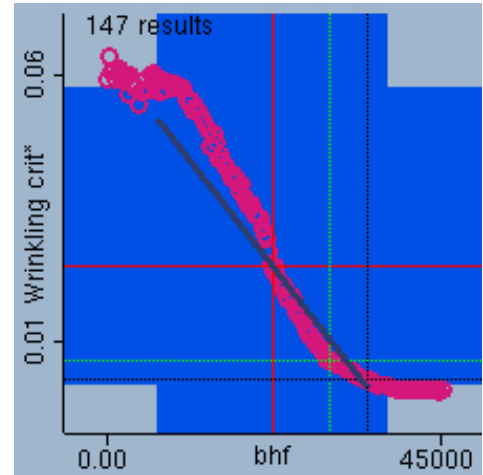
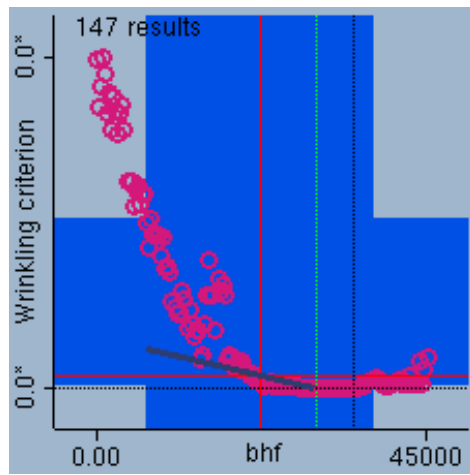
Region A

Region B

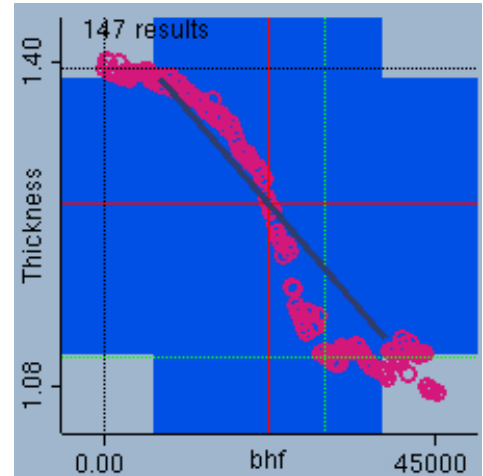
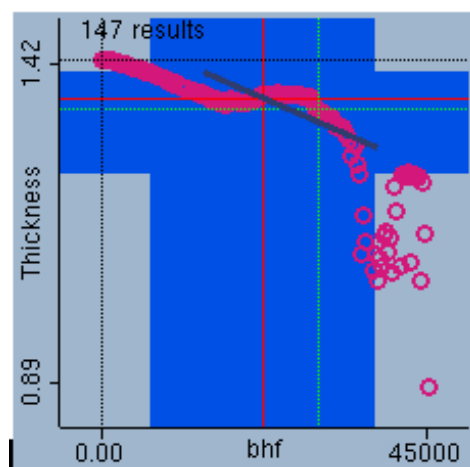
Failure



Wrinkling



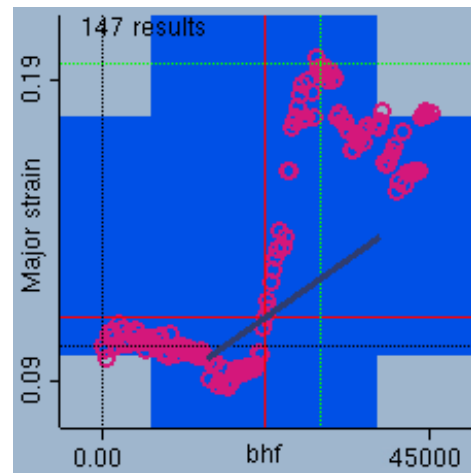
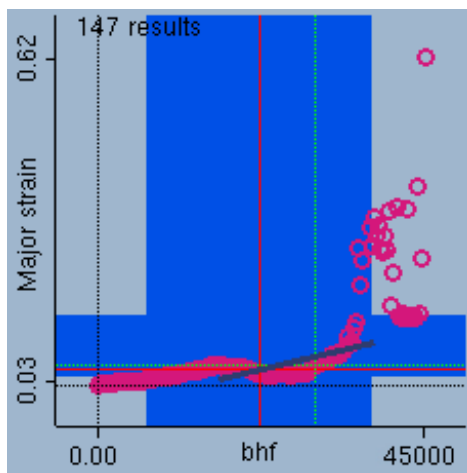
Thickness



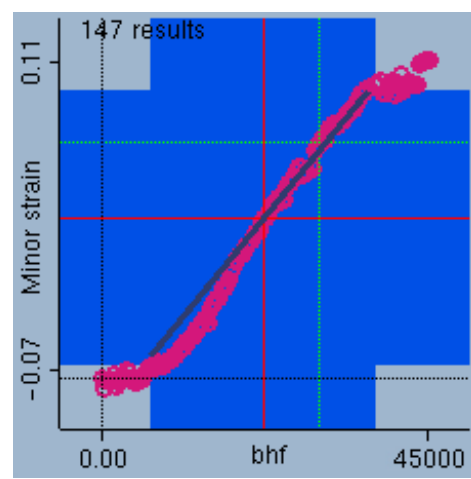
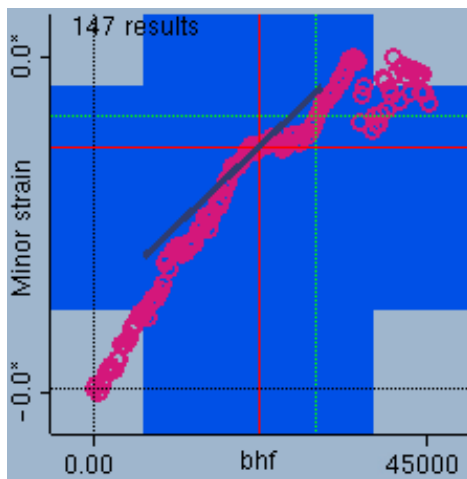
Region A

Region B

Major Strain



Minor strain



2:Scatter plots dependent on BHF for material DP600

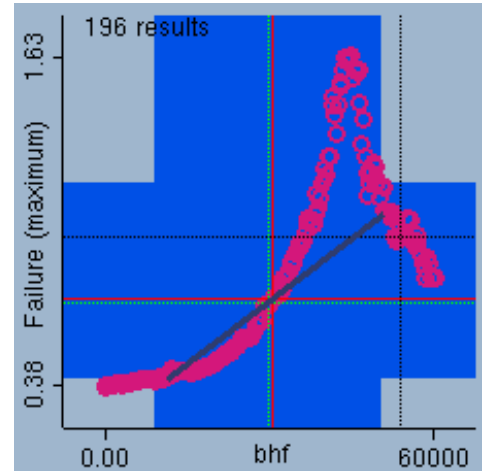
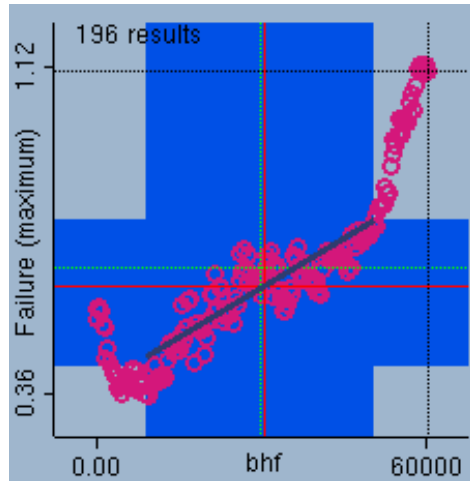
196 simulations dependent on BHF with x5, x6 and x72 to nominal settings.

196 sim

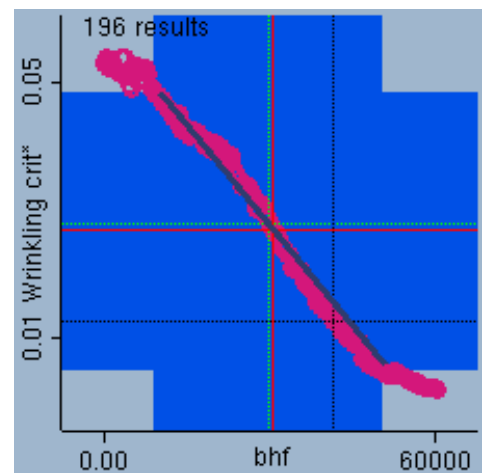
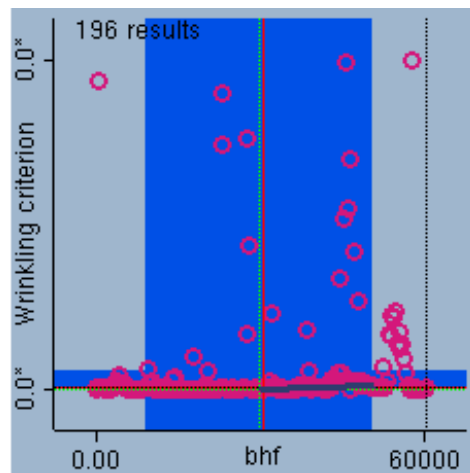
Region A

Region B

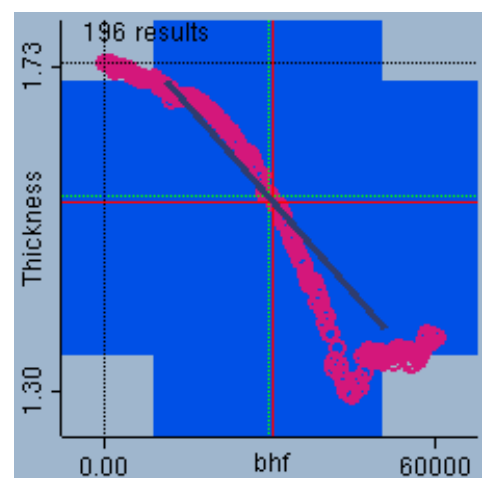
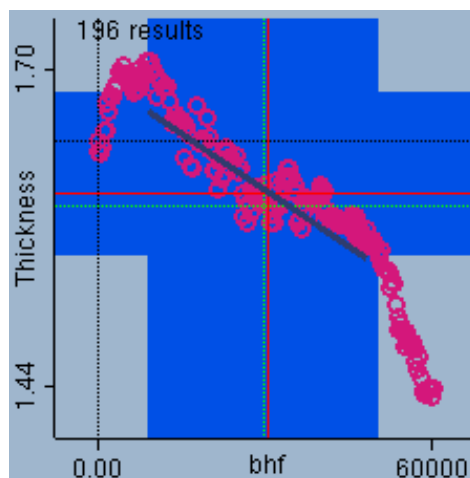
Failure



Wrinkling



Thickness



3:Scatter plots dependent on BHF for material TRIP700

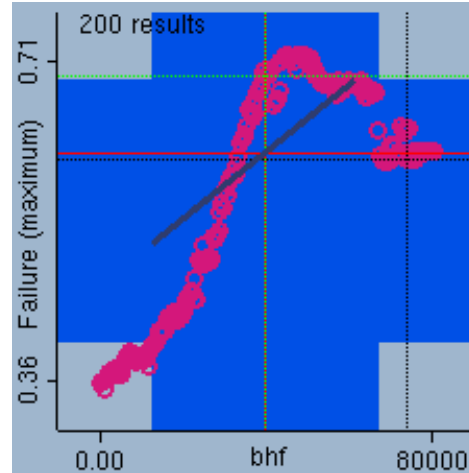
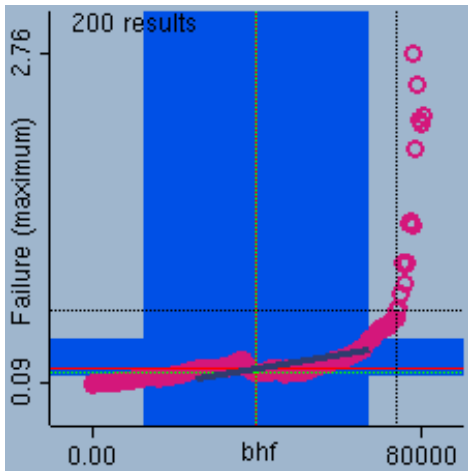
200 simulations dependent on BHF with x5, x6 and x72 to nominal settings.

200 sim

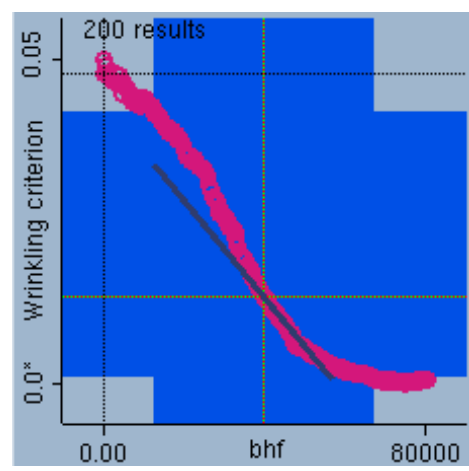
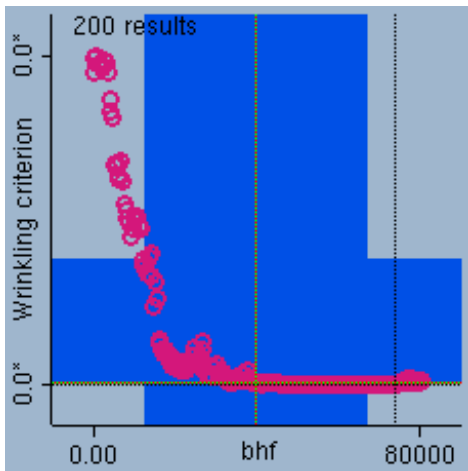
Region A

Region B

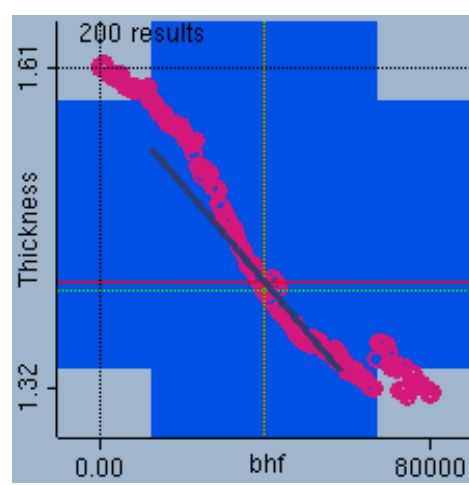
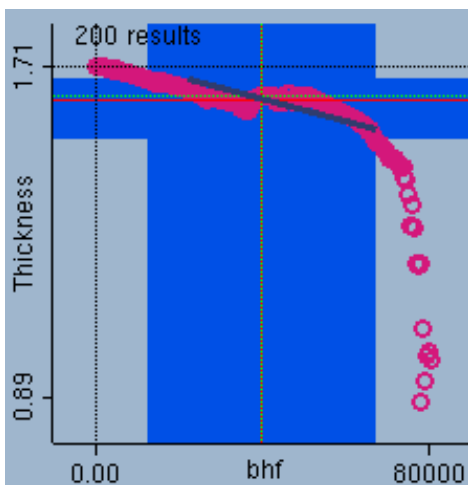
Failure



Wrinkling



Thickness



4:Scatter plots dependent on x5 for material H340LAD

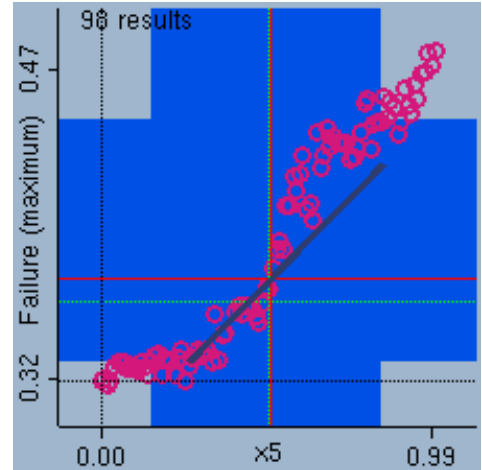
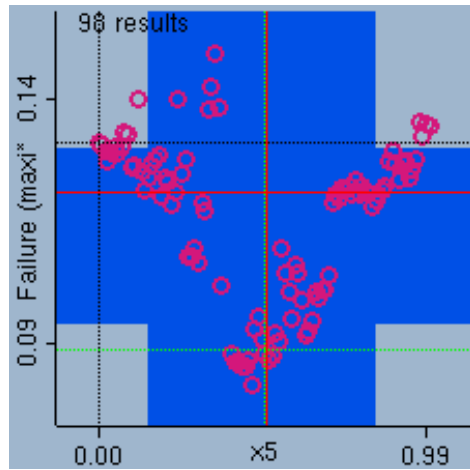
98 simulations dependent on x5 with BHF 6.0×10^5 , x6 and x72 to nominal settings.

98 sim

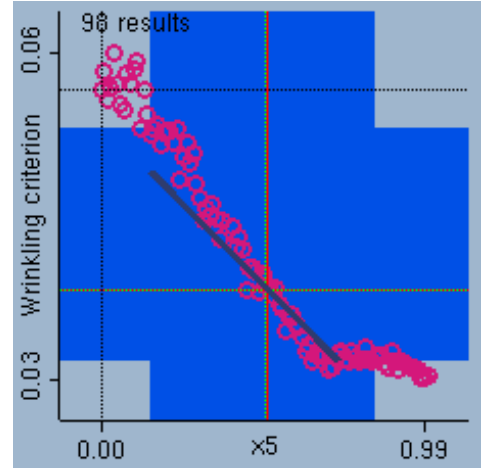
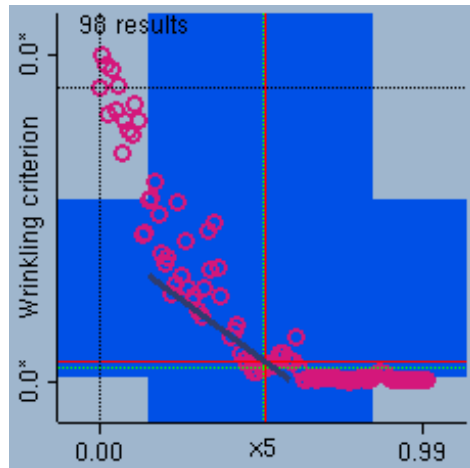
Region A

Region B

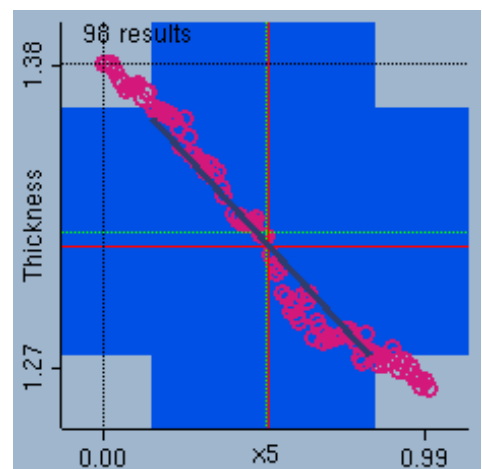
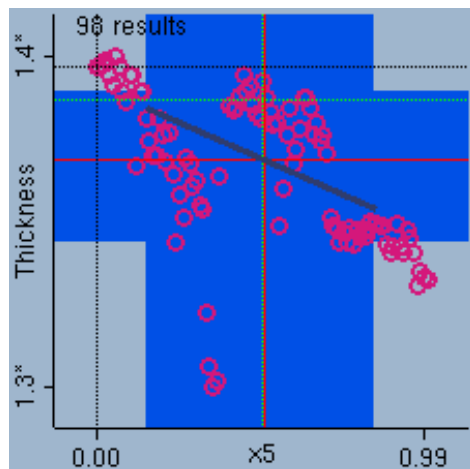
Failure



Wrinkling



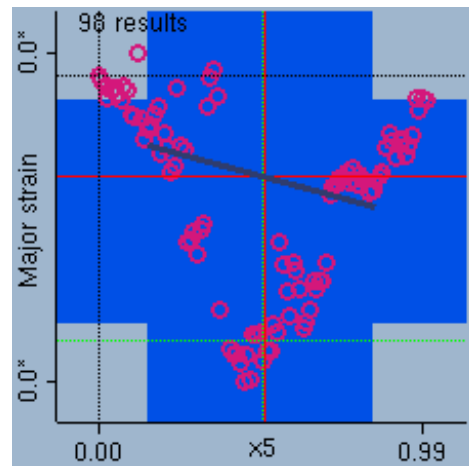
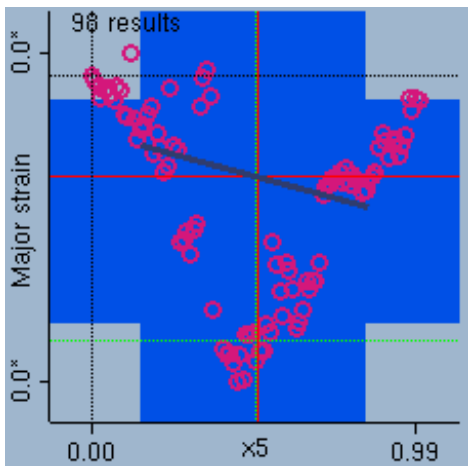
Thickness



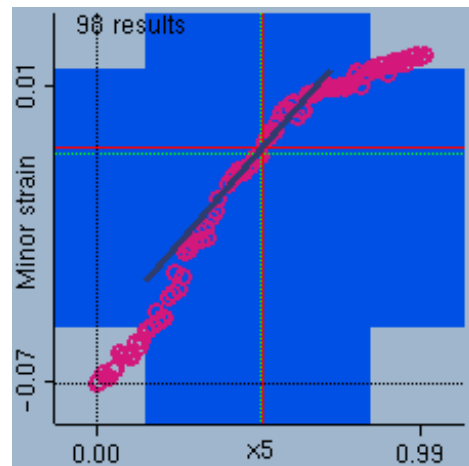
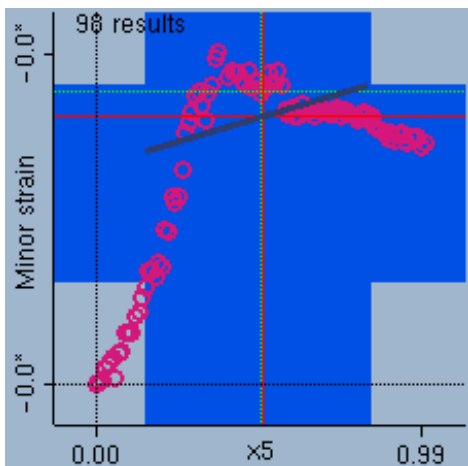
Region A

Region B

Major Strain



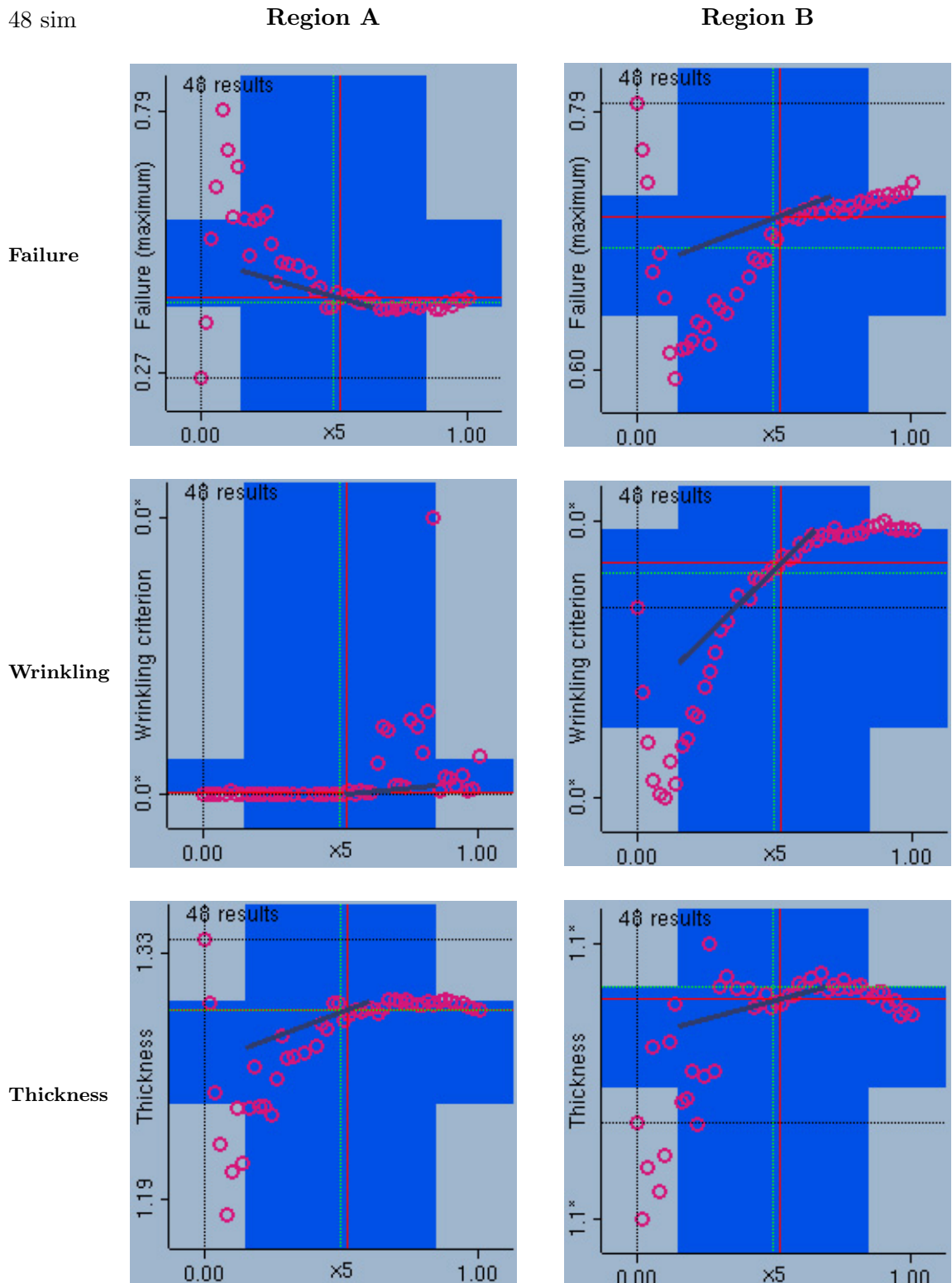
Minor Strain



4 A: Scatter plots dependent on x5 for material H340LAD

48 simulations dependent on x5 with BHF 3.4×10^6 , x6 and x72 to nominal settings.

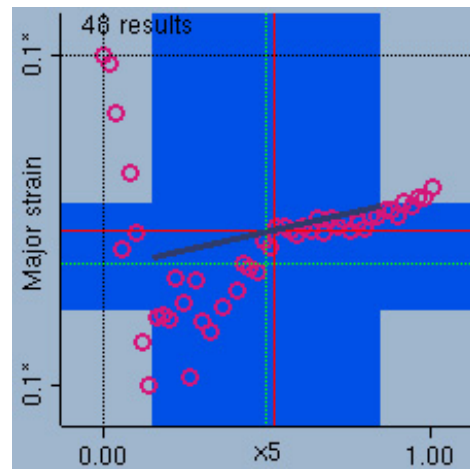
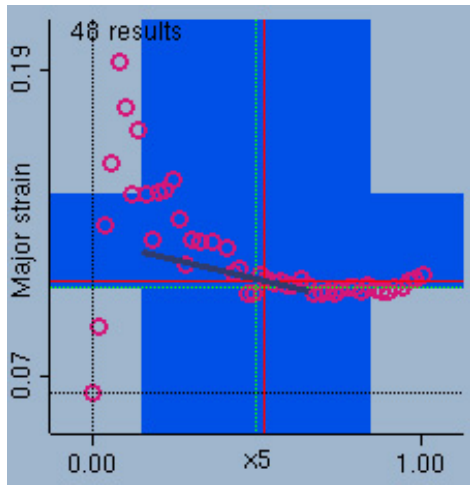
48 sim



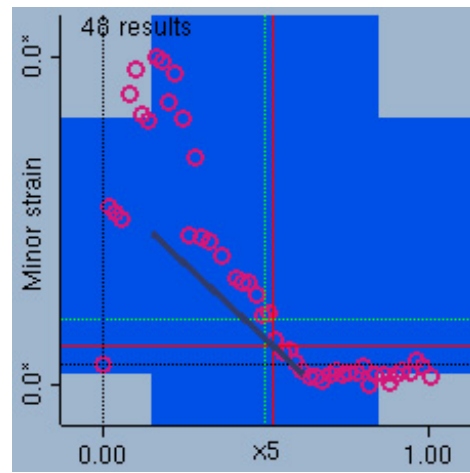
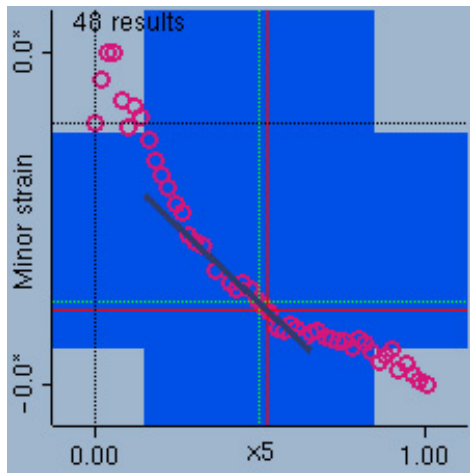
Region A

Region B

Major Strain



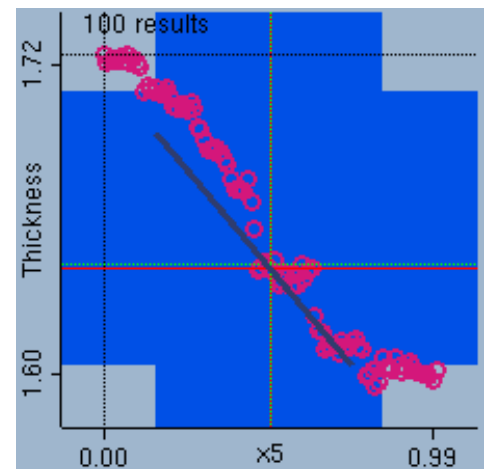
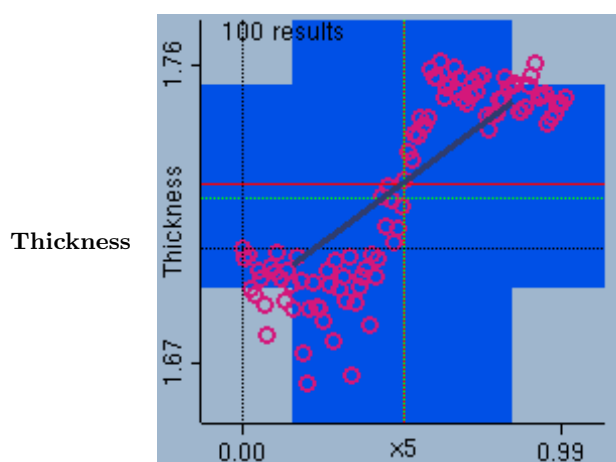
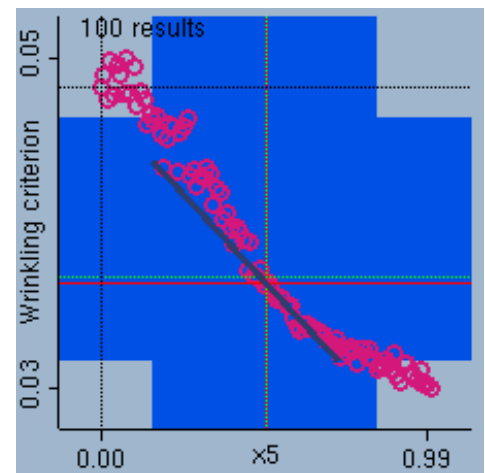
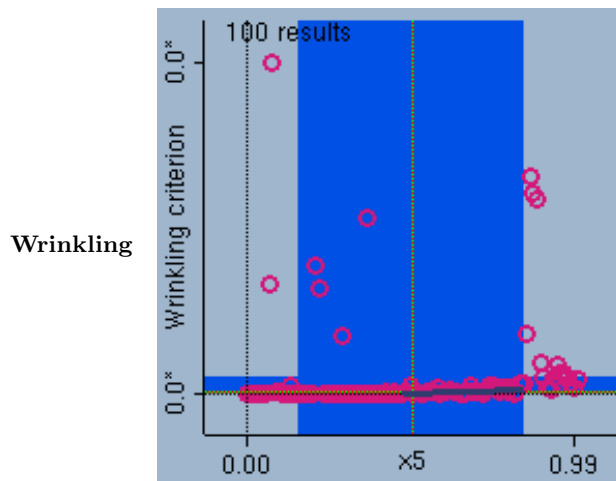
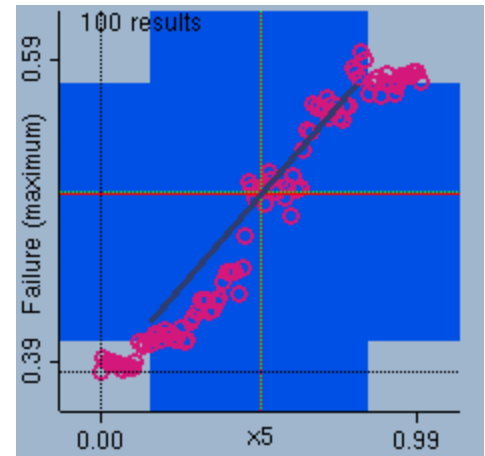
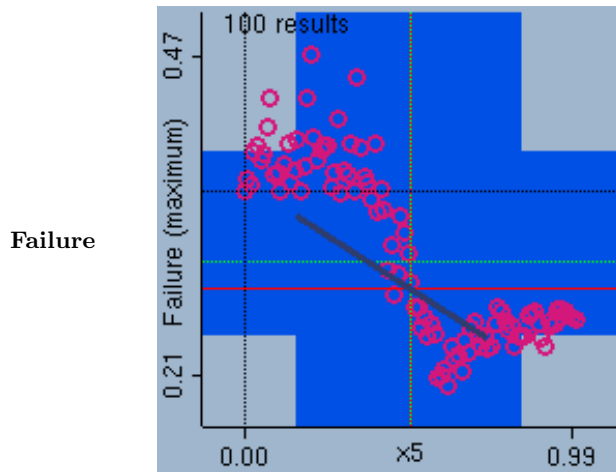
Minor Strain



5:Scatter plots dependent on x5 for material DP600

100 simulations dependent on x5 with BHF, x6 and x72 to nominal settings.

100 sim

Region A**Region B**

6:Scatter plots dependent on x5 for material TRIP700

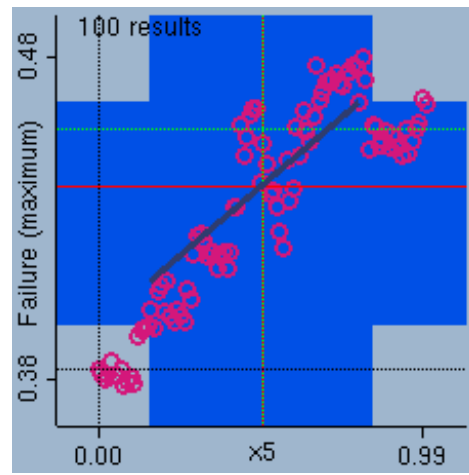
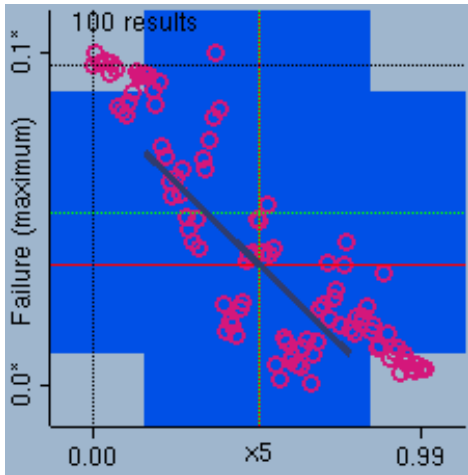
100 simulations dependent on x5 with BHF, x6 and x72 to nominal settings.

100 sim

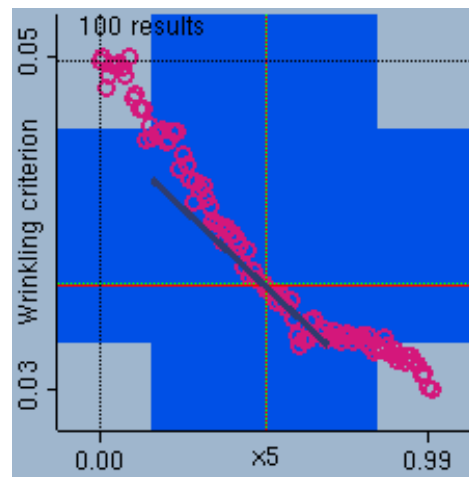
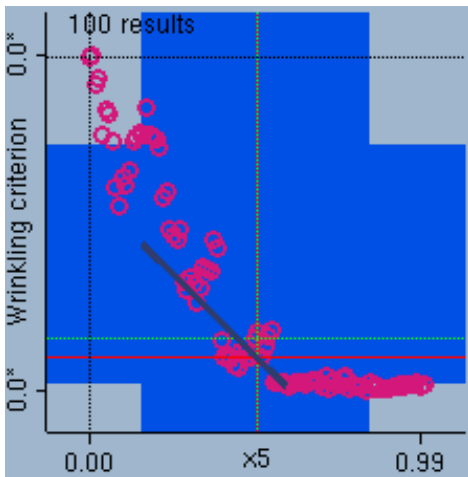
Region A

Region B

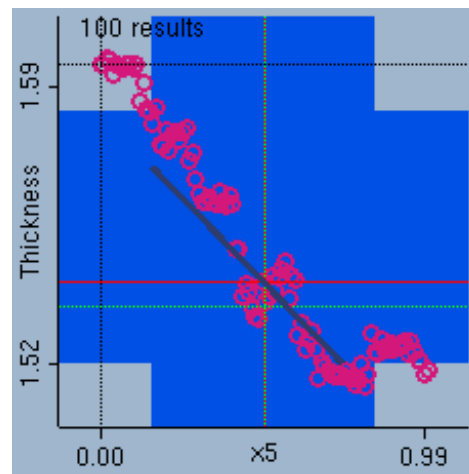
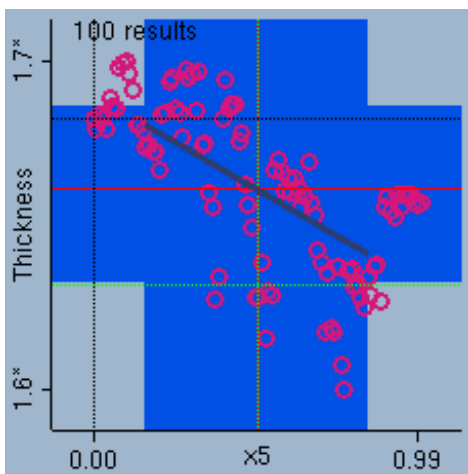
Failure



Wrinkling



Thickness



7: Scatter plots dependent on x6 for material H340LAD

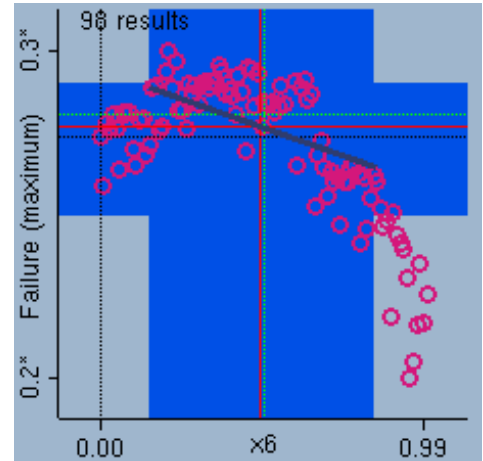
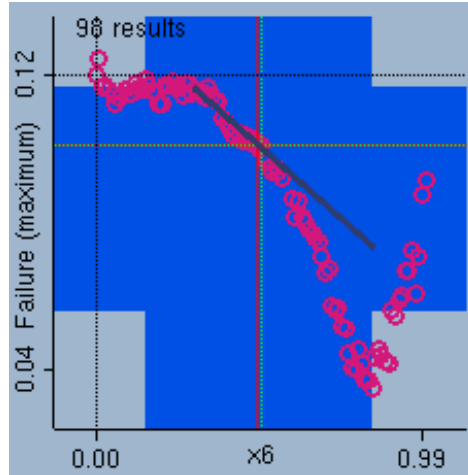
98 simulations dependent on x6 with BHF 6.0×10^5 , x5 and x72 to nominal settings.

98 sim

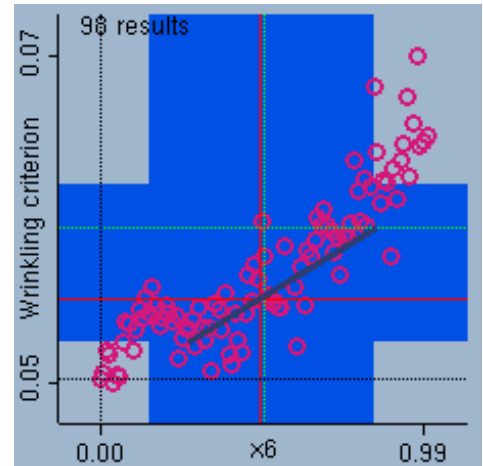
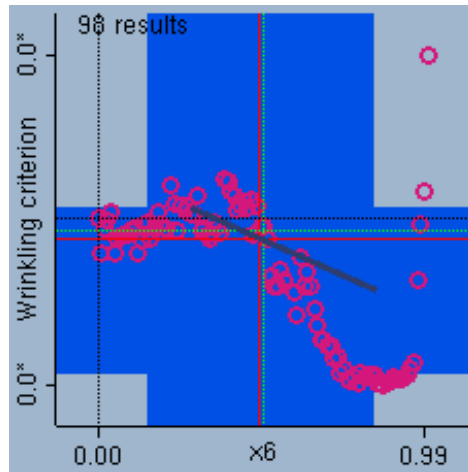
Region A

Region B

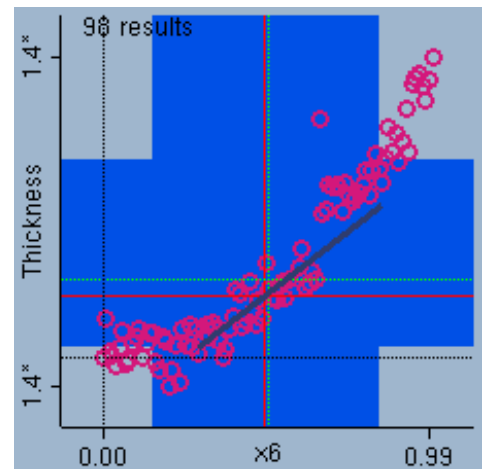
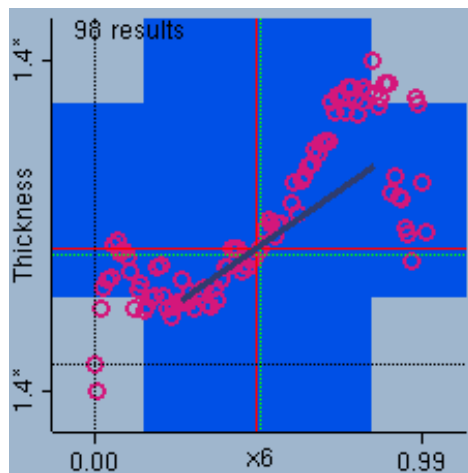
Failure



Wrinkling



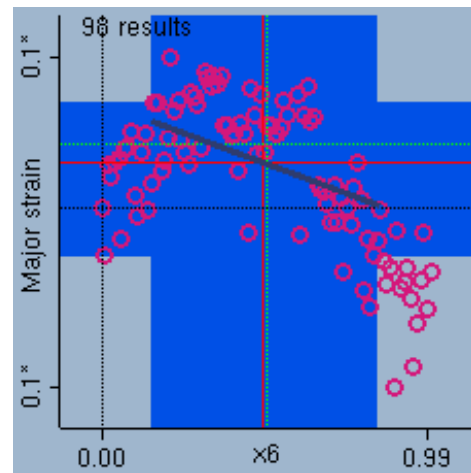
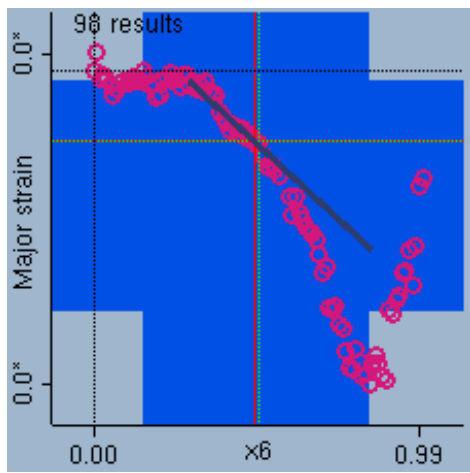
Thickness



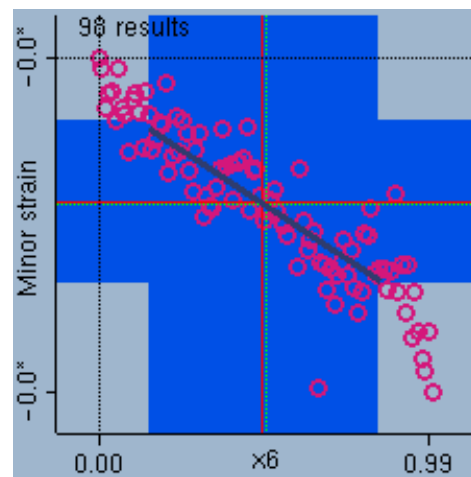
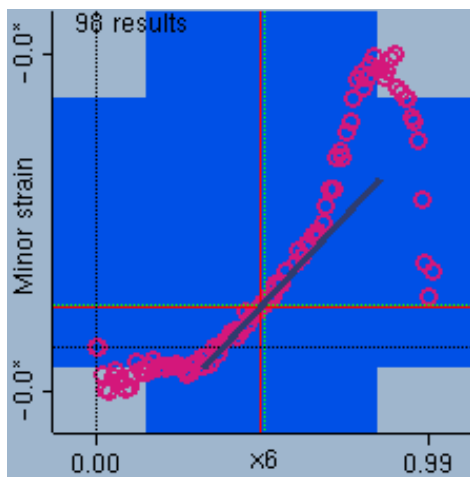
Region A

Region B

Major Strain



Minor Strain



7 A: Scatter plots dependent on x6 for material H340LAD

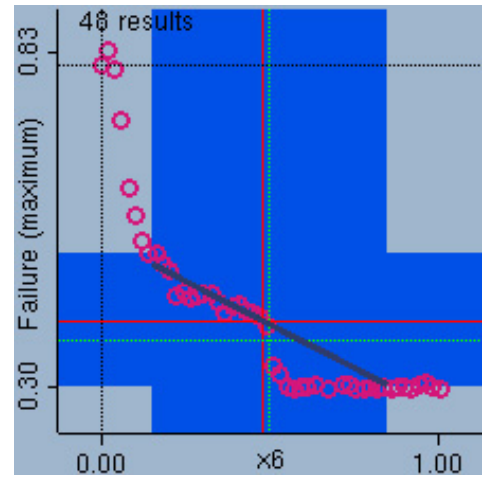
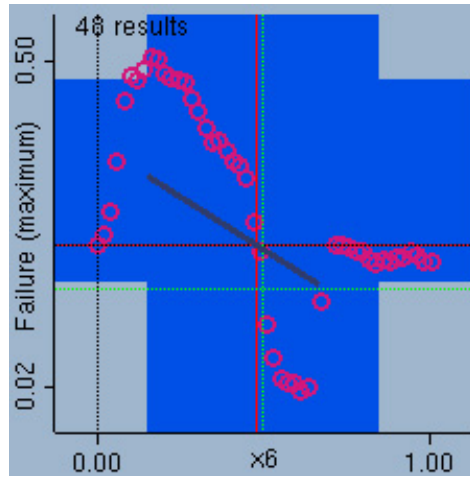
48 simulations dependent on x6 with BHF 3.4×10^6 , x5 and x72 to nominal settings.

48 sim

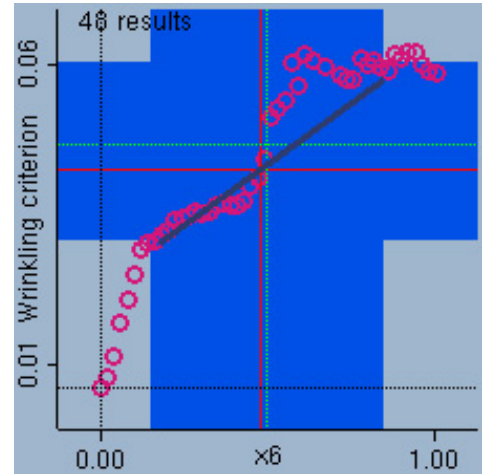
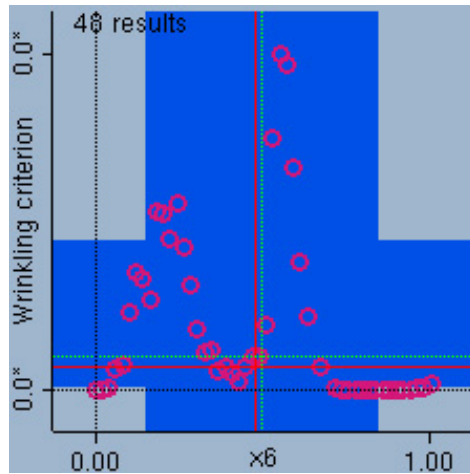
Region A

Region B

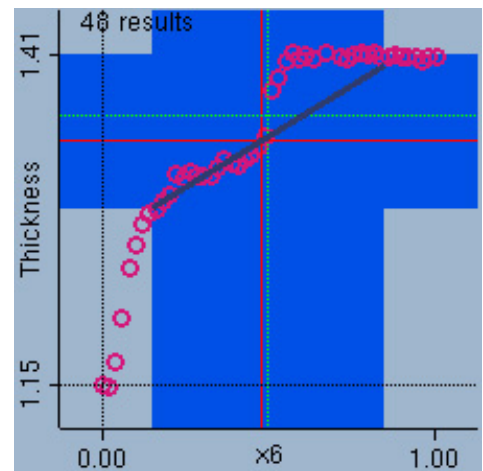
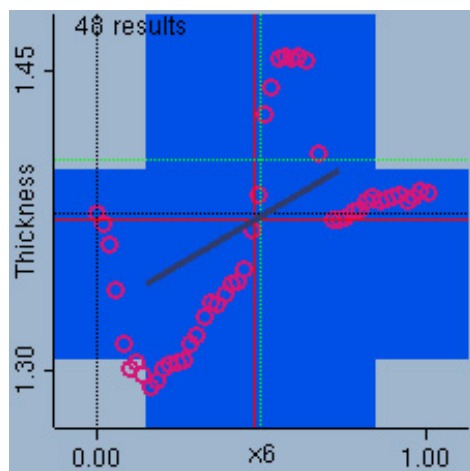
Failure



Wrinkling



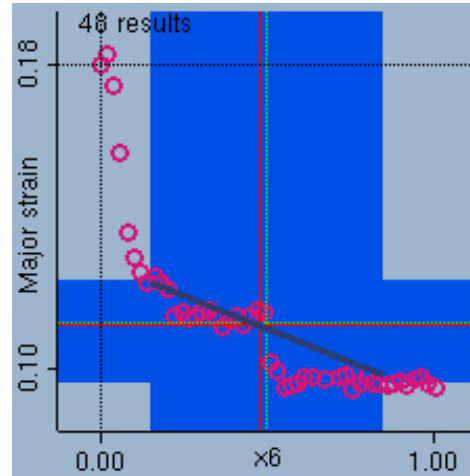
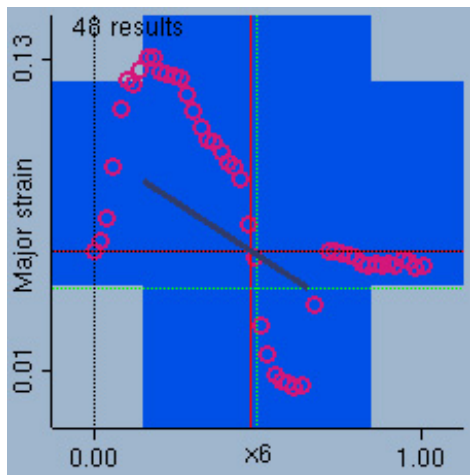
Thickness



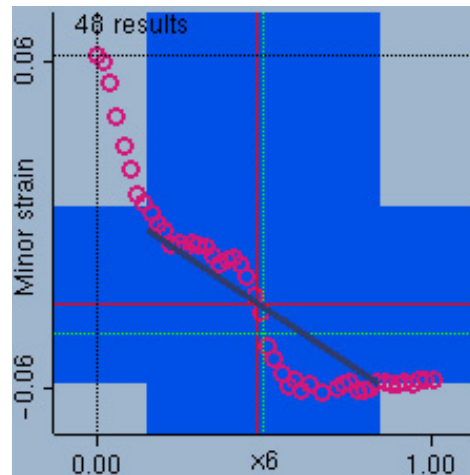
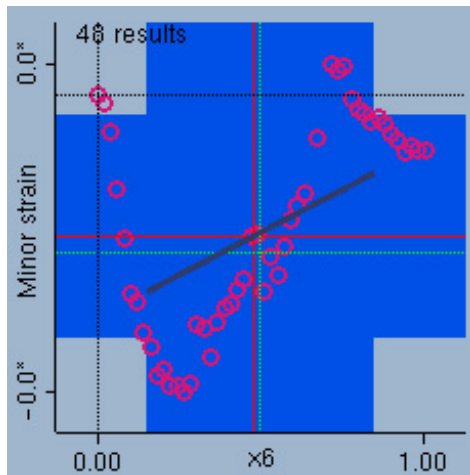
Region A

Region B

Major Strain



Minor Strain



8:Scatter plots dependent on x6 for material DP600

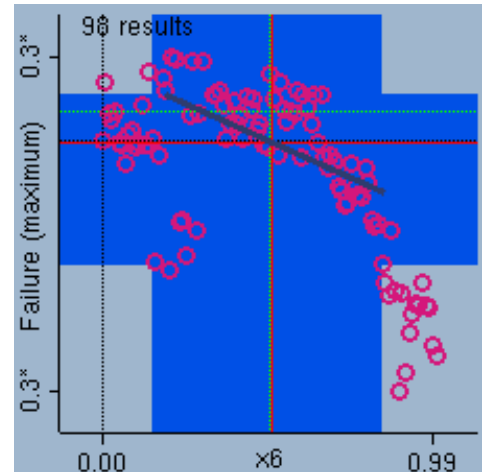
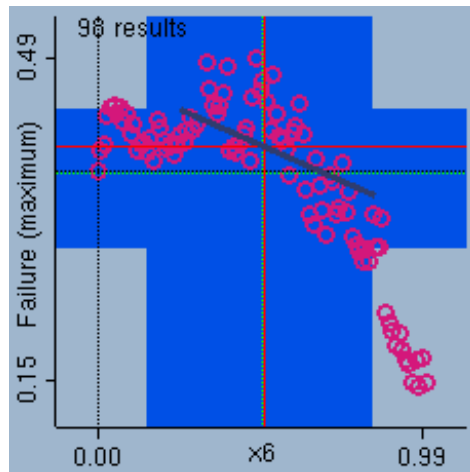
98 simulations dependent on x6 with BHF, x5 and x72 to nominal settings.

98 sim

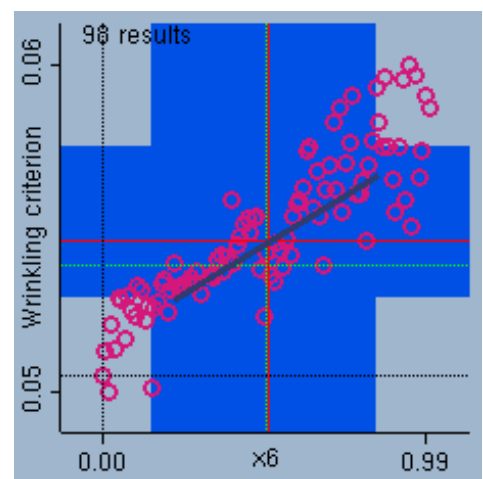
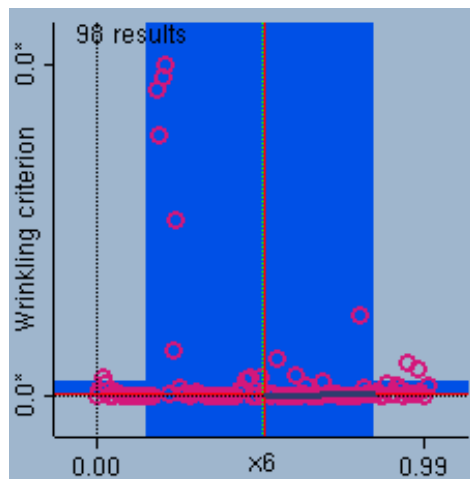
Region A

Region B

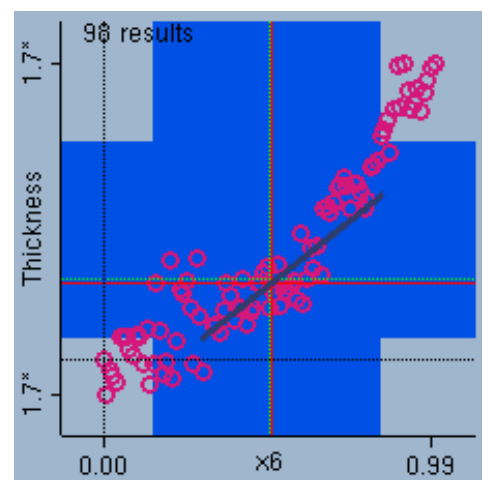
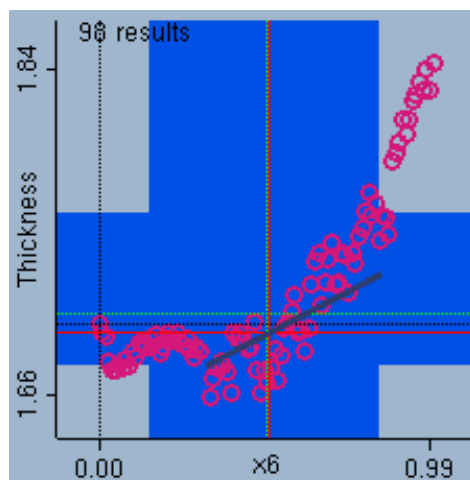
Failure



Wrinkling



Thickness



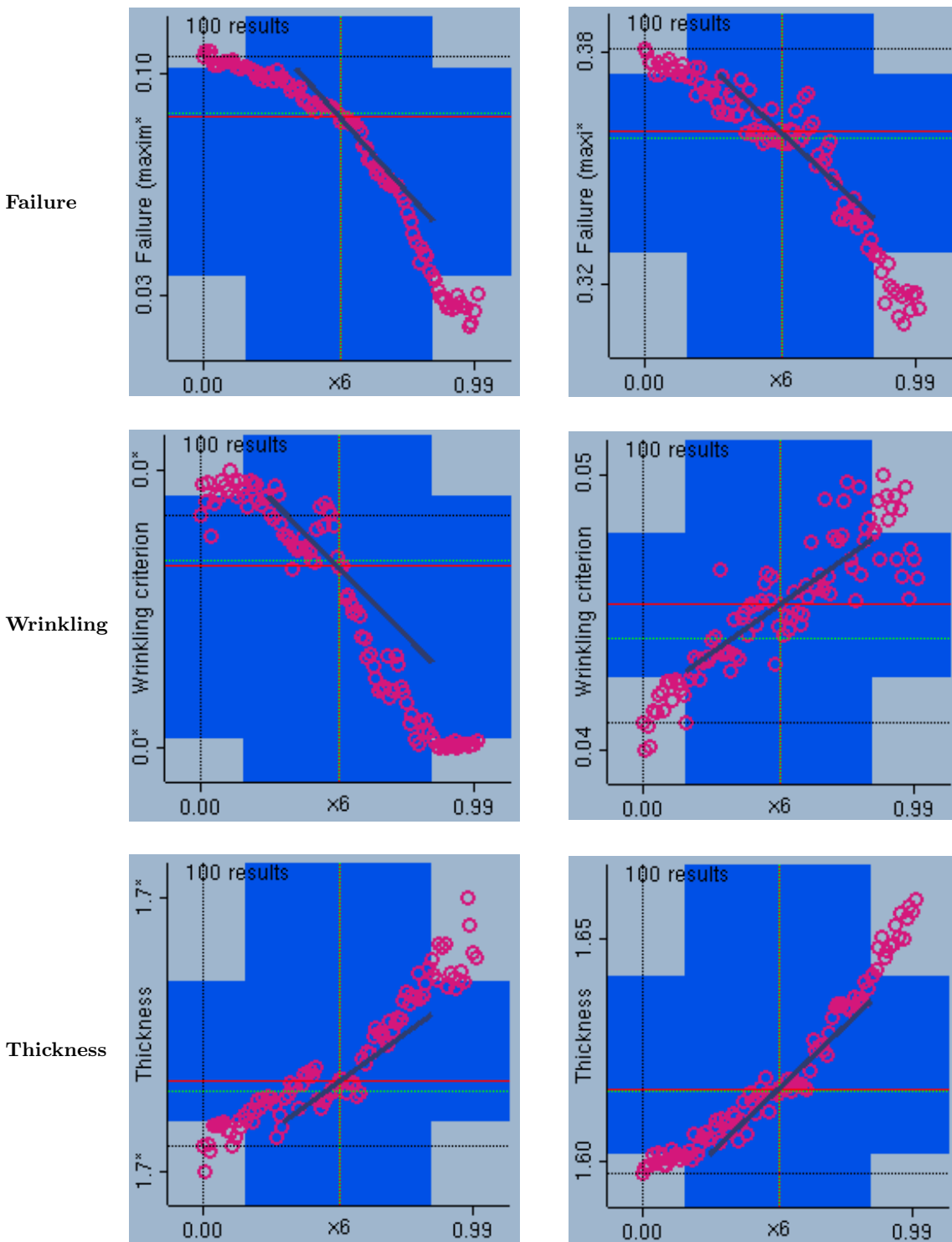
9:Scatter plots dependent on x6 for material TRIP700

100 simulations dependent on x6 with BHF, x5 and x72 to nominal settings.

100 sim

Region A

Region B



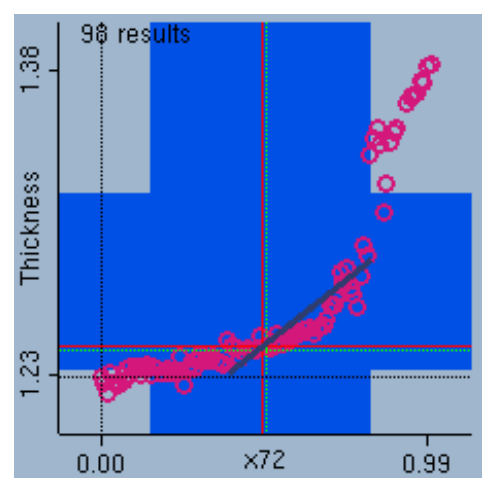
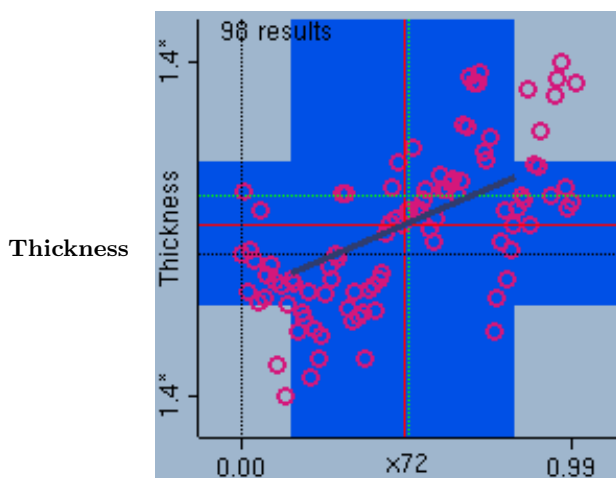
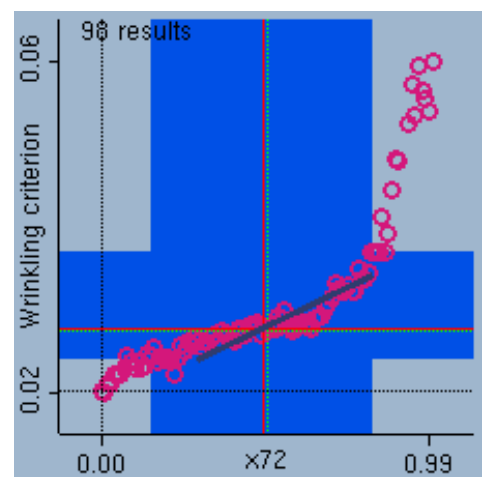
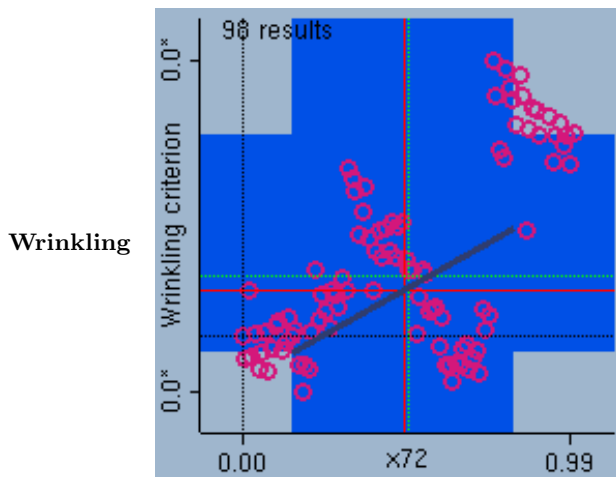
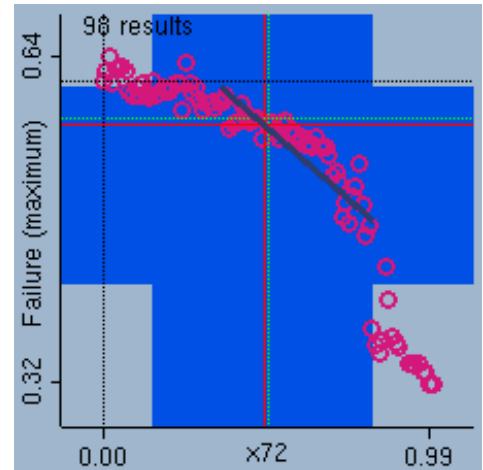
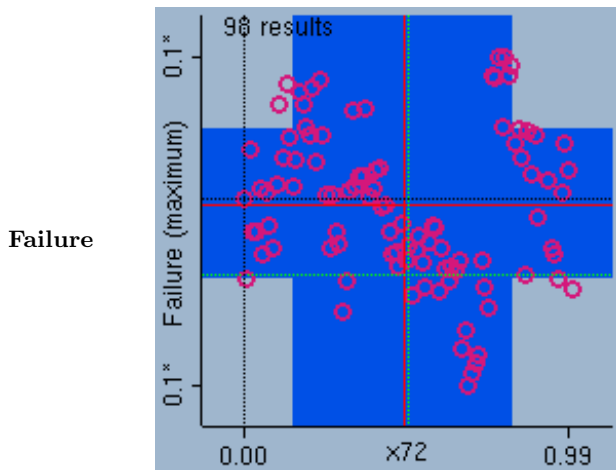
10:Scatter plots dependent on x72 for material H340LAD

100 simulations dependent on x72 with BHF, x5 and x6 to nominal settings.

98 sim

Region A

Region B



11:Scatter plots dependent on x72 for material DP600

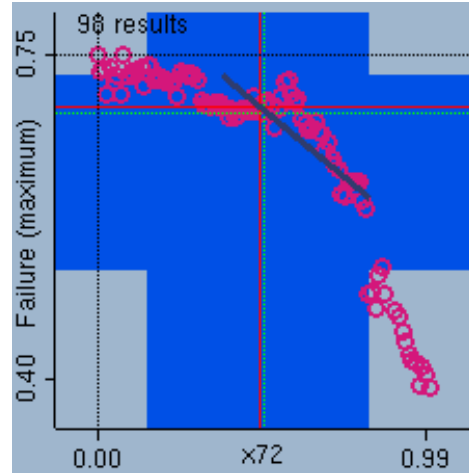
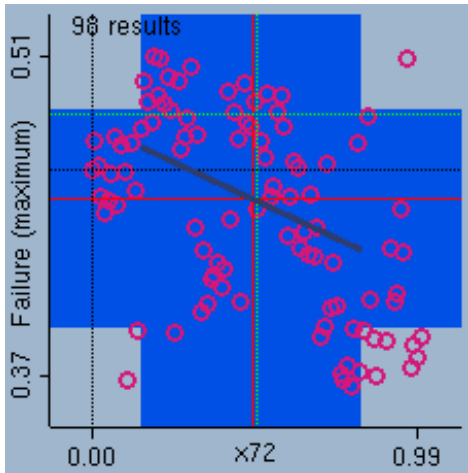
98 simulations dependent on x72 with BHF, x5 and x6 to nominal settings.

98 sim

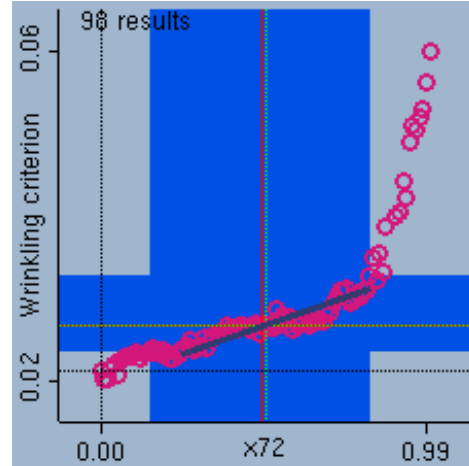
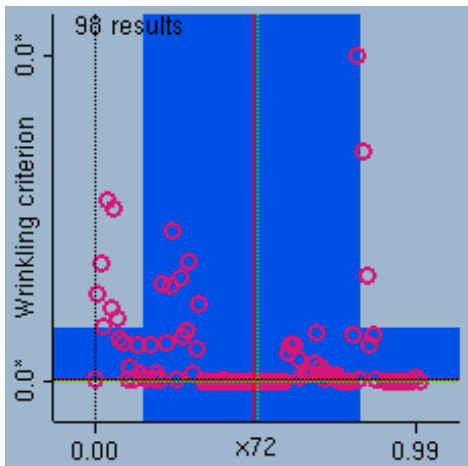
Region A

Region B

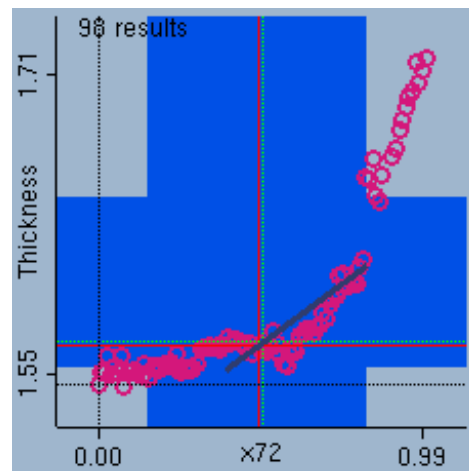
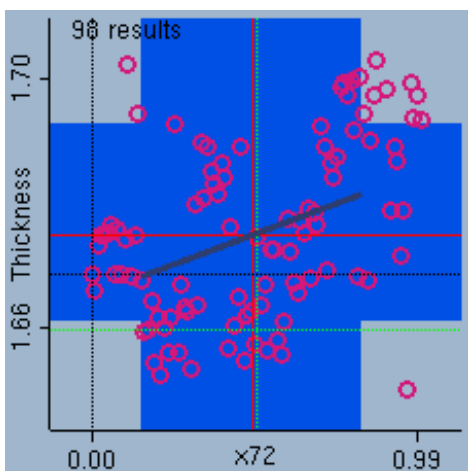
Failure



Wrinkling



Thickness



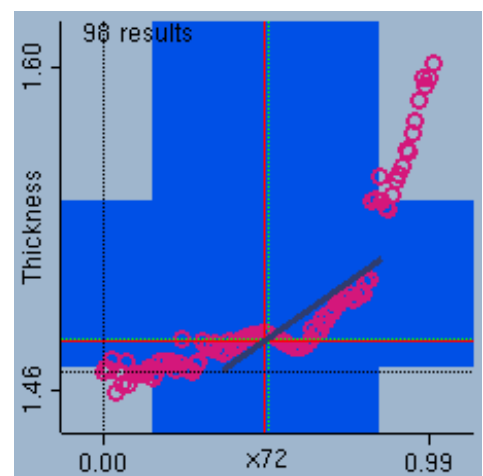
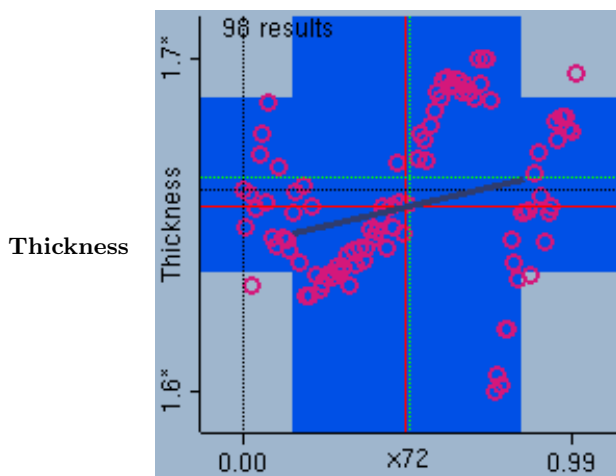
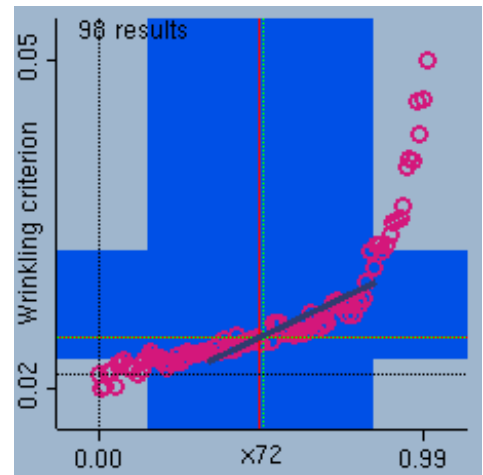
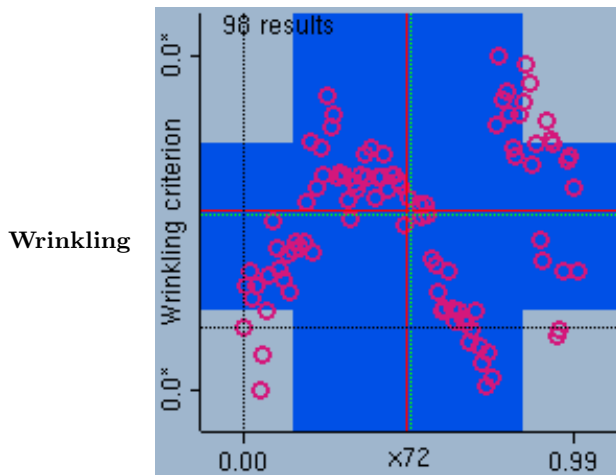
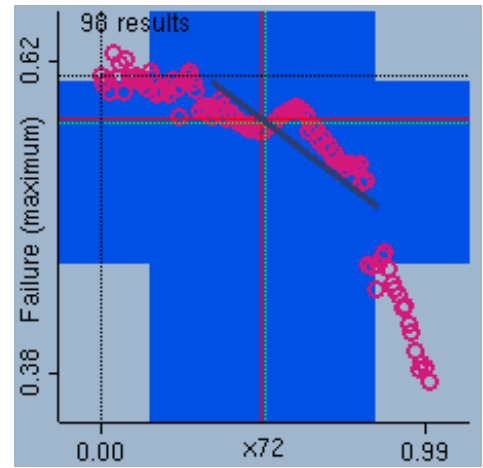
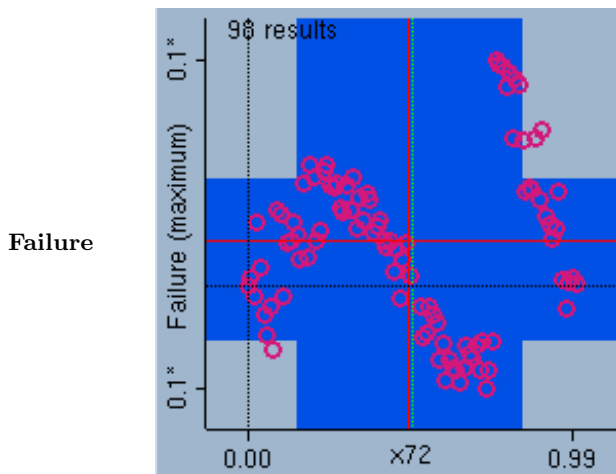
12:Scatter plots dependent on x72 for material TRIP700

98 simulations dependent on x72 with BHF, x5 and x6 to nominal settings.

98 sim

Region A

Region B



D.3 Surface plots

The following surface plots dependent of 2 design variables are made with the use of MATLAB. Several sequences of steps are necessary to produce these plots, these will be shortly explained.

The first sequence is to determine the values of the two design variables. In AutoForm-Sigma a performance analysis is used with the option of DESIGN. This means that the design parameters are non-uniformly distributed over a range from min to max. If the Sigma analysis is started the variables are written to a so called *.opl file.

- 1 Read *.opl in Matlab
- 2 Determine values of the design variables

The second sequence is to get the data from the simulation files and import into MATLAB. These consist of the following steps

- 1 Get data with AFprint
- 2 Read data in Matlab
- 3 Determine elements in region A and B
- 4 Determine response for elements in Region A and B

The following sequence is to produce the surface plots. Because the design variables are not uniformly distributed. Several steps have to be done to produce the surface plots.

- 1 Produce a uniformly spaced data
- 2 Generate a uniformly spaced grid
- 3 Interpolate the values of the responses at uniformly spaced points, based on the values of the function at the original data points.
This statement uses triangle-based linear interpolation to generate the new data
- 4 Plot the interpolated and nonuniform data

The black squares in the figure are the measuring points.

The AutoForm sigma analysis was set with 200 calculations. Due to some internal errors, not all the calculations are used in some cases, see for example simulation series 14. Also another remarkable point was discovered in the case of simulation series 18. The indrawn was becoming so large, that there was no material in region A, therefore this simulation series consist of reasonable less calculations then the rest of the simulation series.

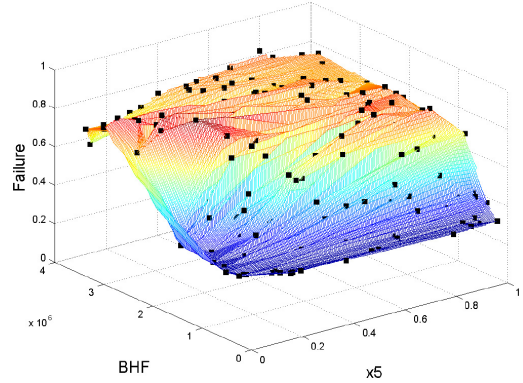
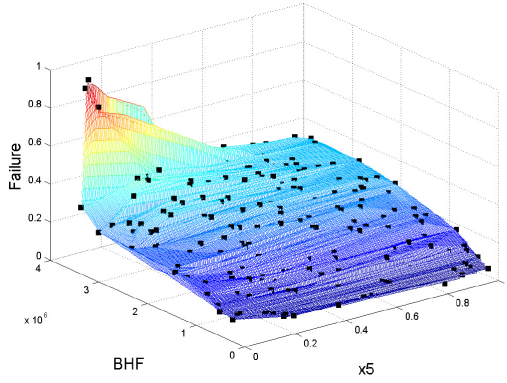
13:Surface plots dependent on BHF and x5 for material H340LAD
 200 simulations dependent on BHF and x5 with x6 and x72 to nominal settings.

200 sim

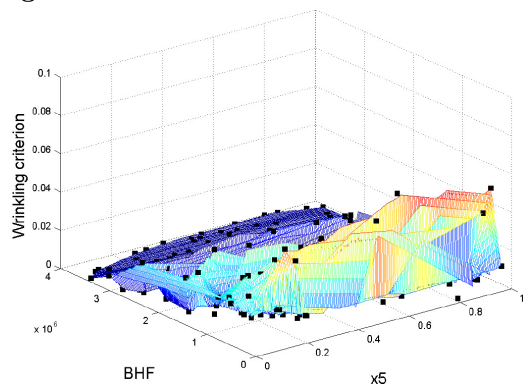
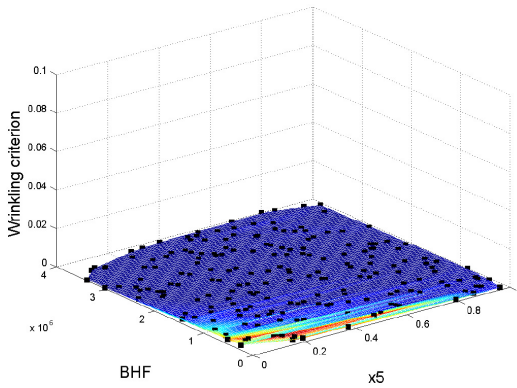
Region A

Region B

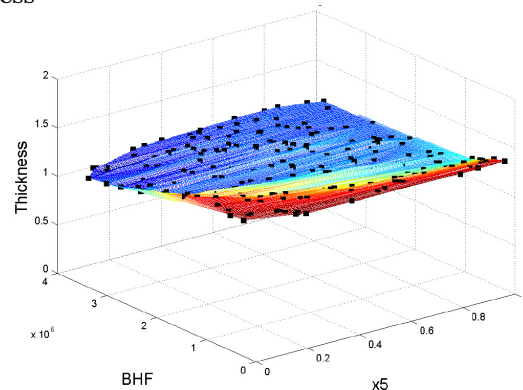
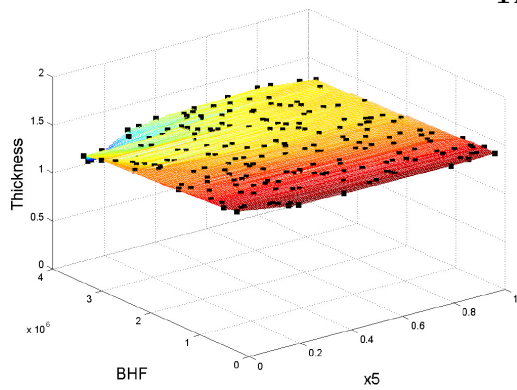
Failure



Wrinkling



Thickness



14:Surface plots dependent on BHF and x5 for material DP600

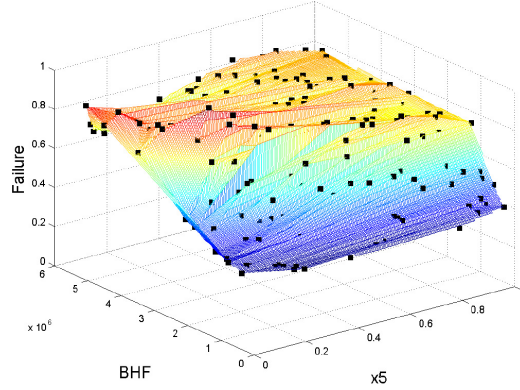
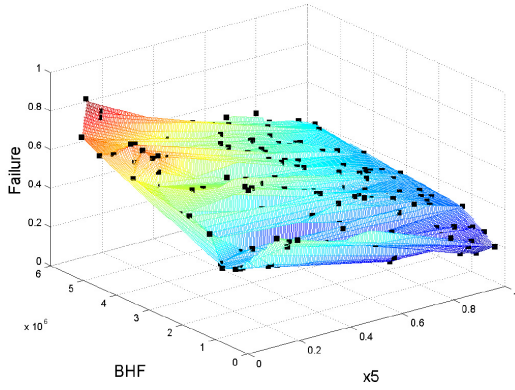
197 simulations dependent on BHF and x5 with x6 and x72 to nominal settings.

197 sim

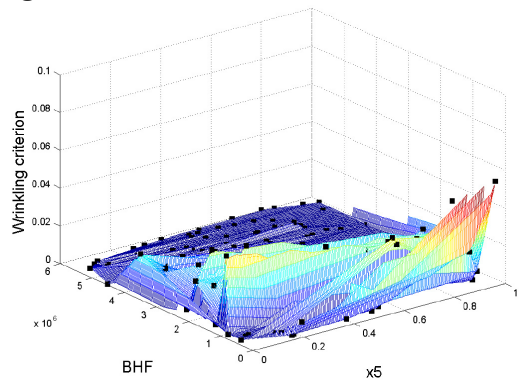
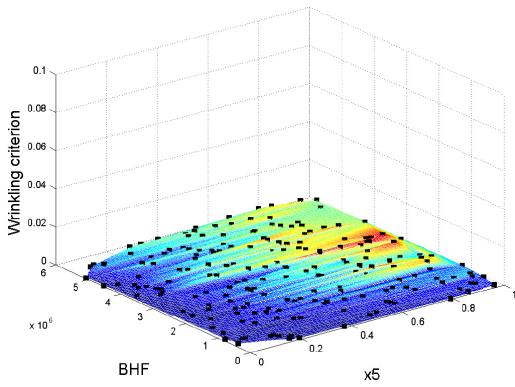
Region A

Region B

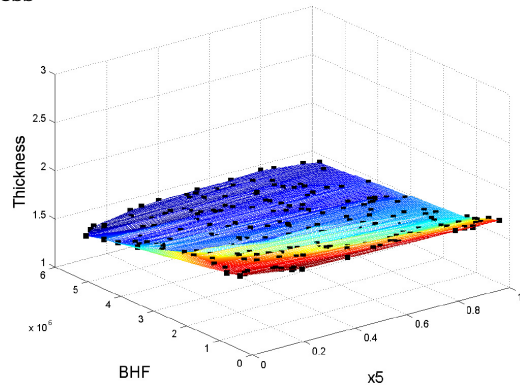
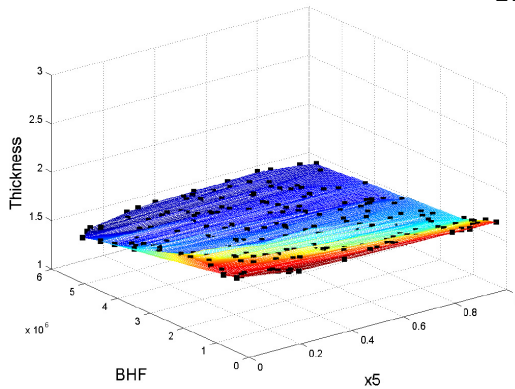
Failure



Wrinkling



Thickness



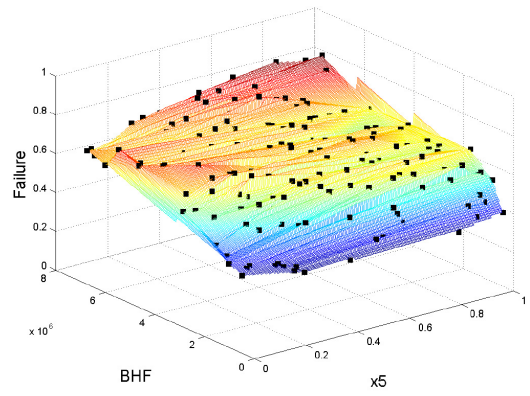
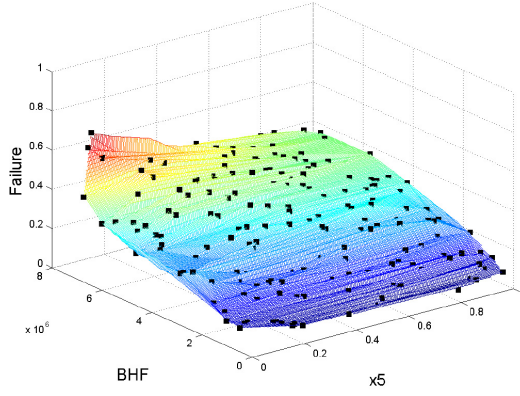
15:Surface plots dependent on BHF and x5 for material TRIP700
 200 simulations dependent on BHF and x5 with x6 and x72 to nominal settings.

200 sim

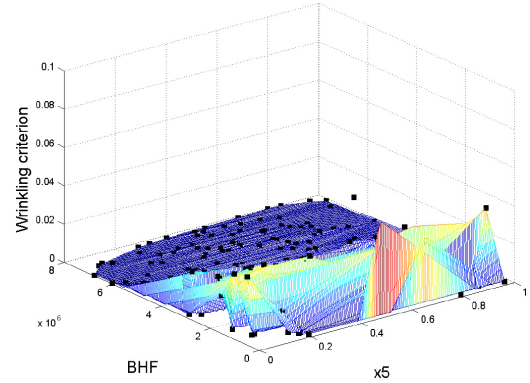
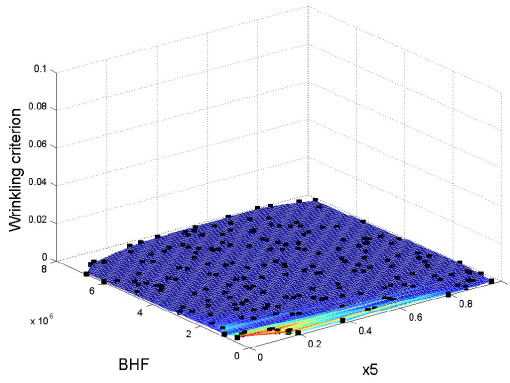
Region A

Region B

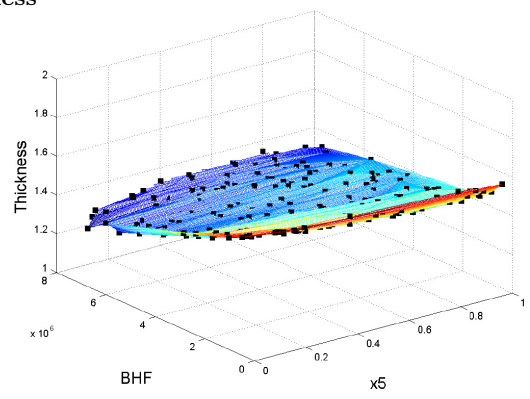
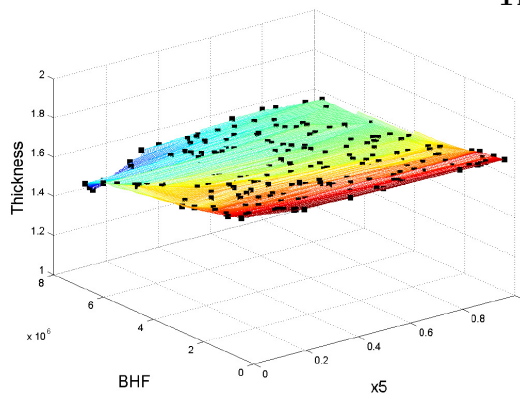
Failure



Wrinkling



Thickness



16:Surface plots dependent on BHF and x6 for material H340LAD

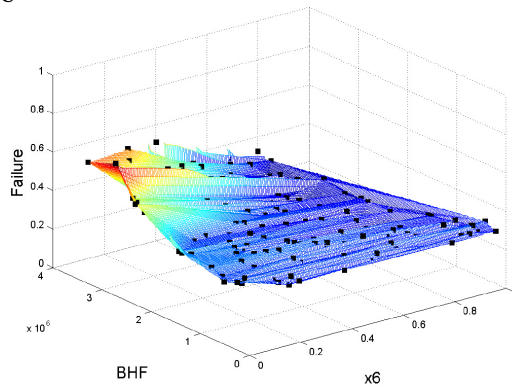
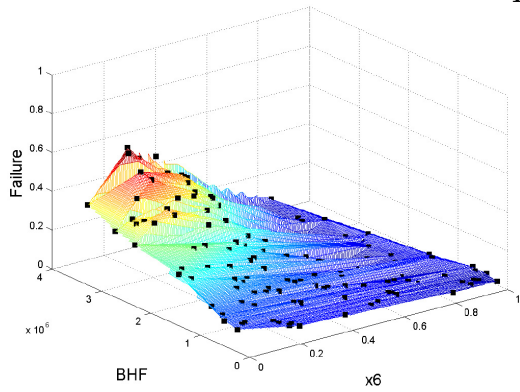
200 simulations dependent on BHF and x6 with x5 and x72 to nominal settings.

200 sim

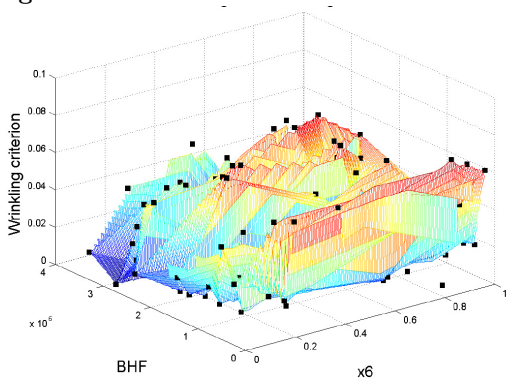
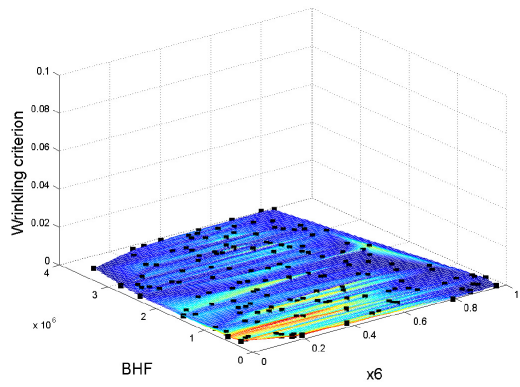
Region A

Region B

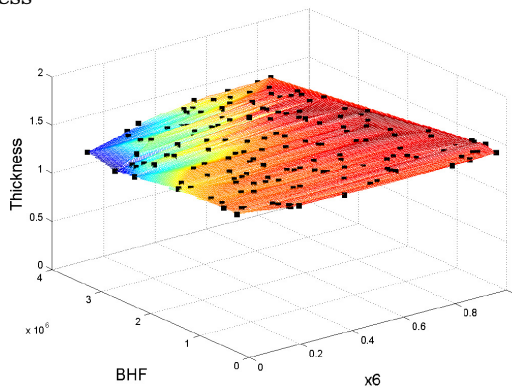
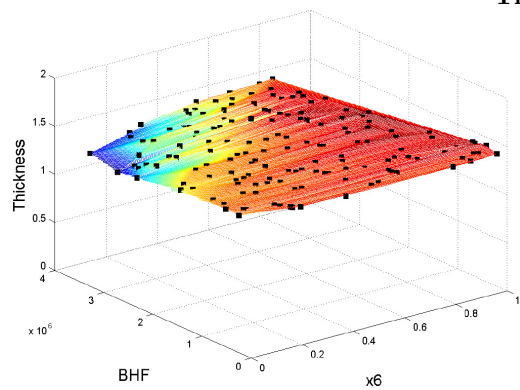
Failure



Wrinkling



Thickness



17:Surface plots dependent on BHF and x6 for material DP600

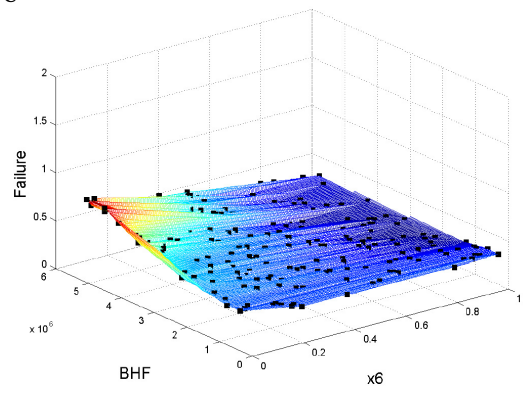
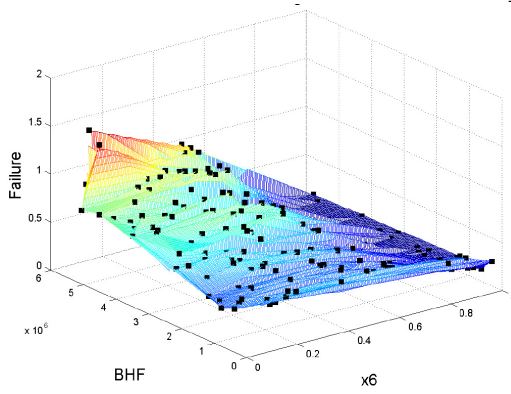
200 simulations dependent on BHF and x6 with x5 and x72 to nominal settings.

200 sim

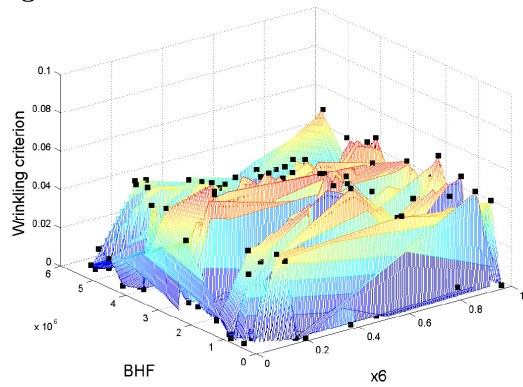
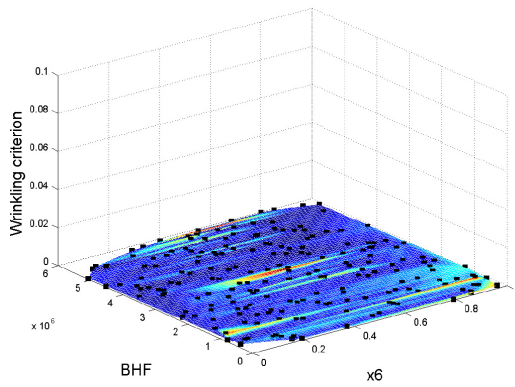
Region A

Region B

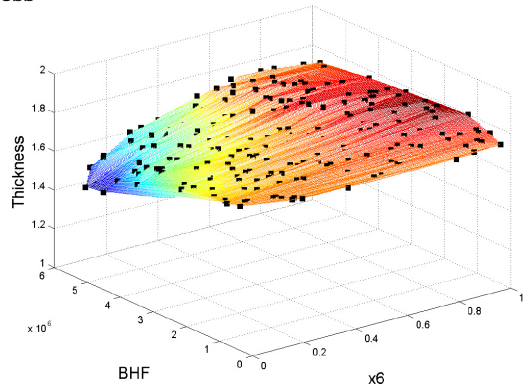
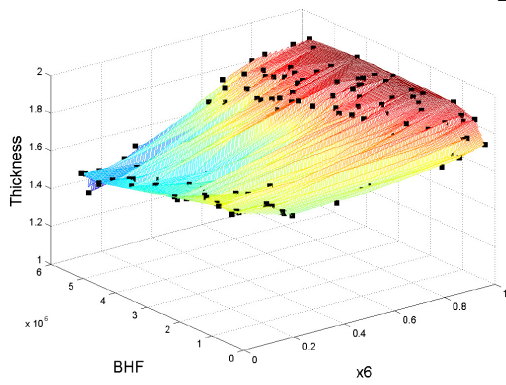
Failure



Wrinkling



Thickness



18:Surface plots dependent on BHF and x6 for material TRIP700

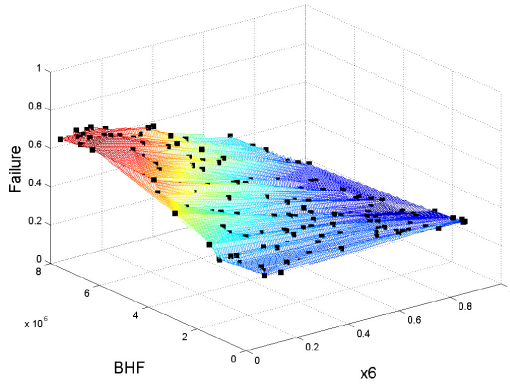
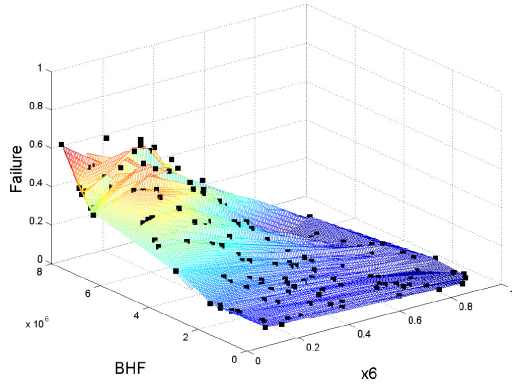
172 simulations dependent on BHF and x6 with x5 and x72 to nominal settings.

172 sim

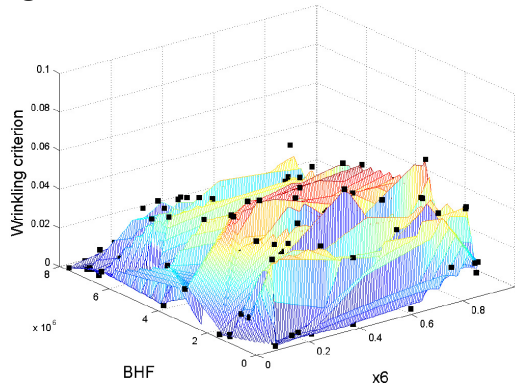
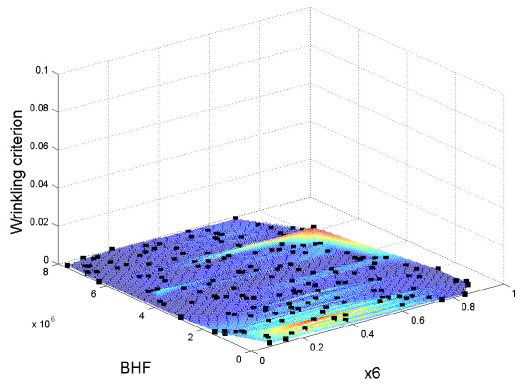
Region A

Region B

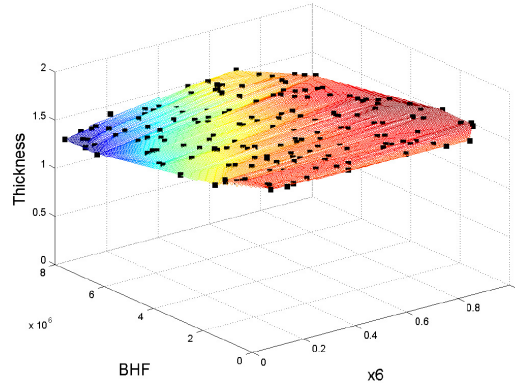
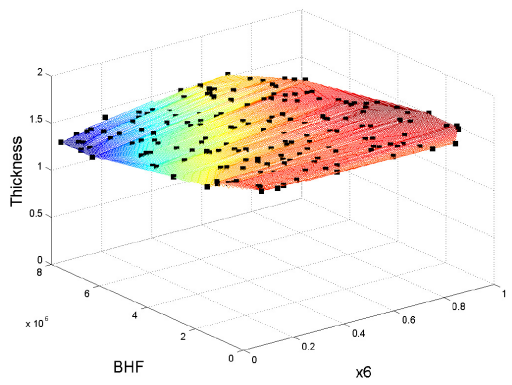
Failure



Wrinkling



Thickness



19:Surface plots dependent on x5 and x6 for material H340

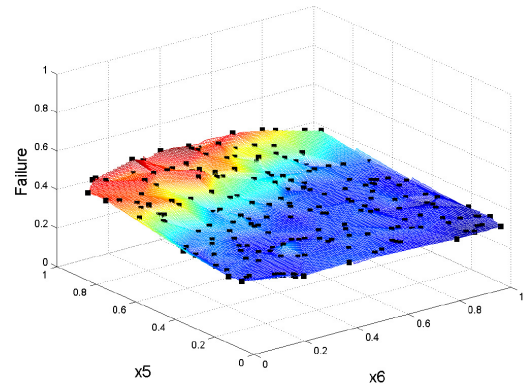
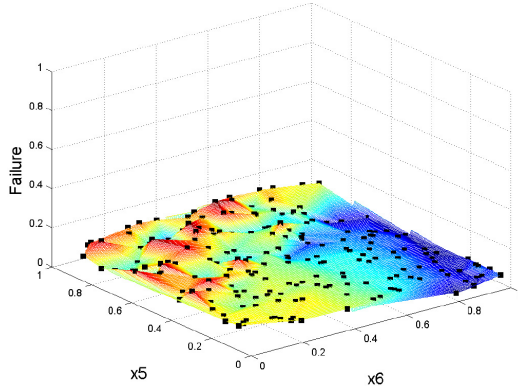
196 simulations dependent on x5 and x6 with BHF and x72 to nominal settings.

196 sim

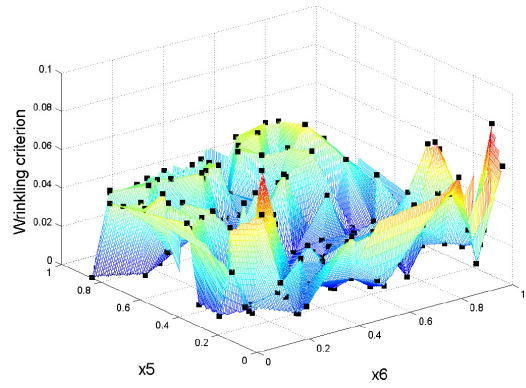
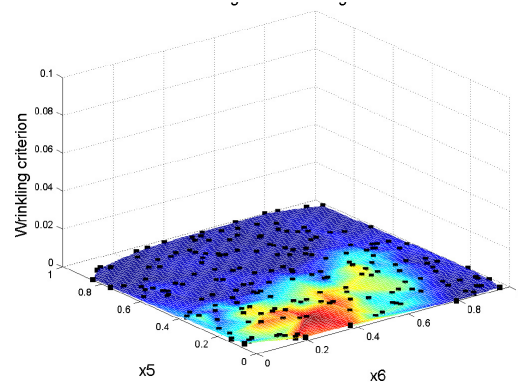
Region A

Region B

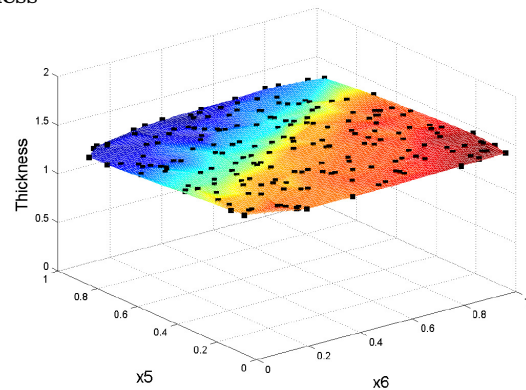
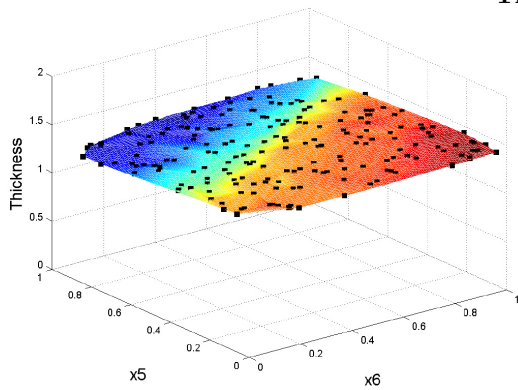
Failure



Wrinkling



Thickness



20:Surface plots dependent on x5 and x6 for material DP600

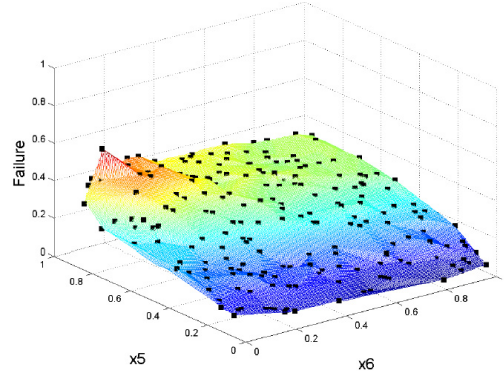
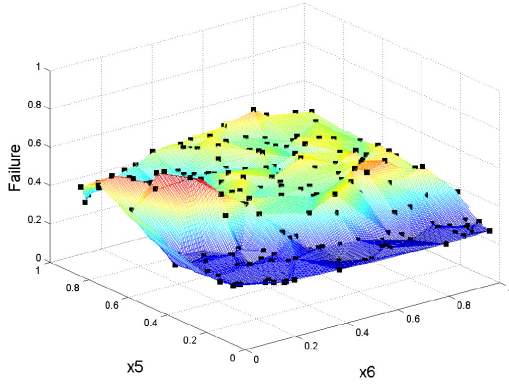
200 simulations dependent on x5 and x6 with BHF and x72 to nominal settings.

200 sim

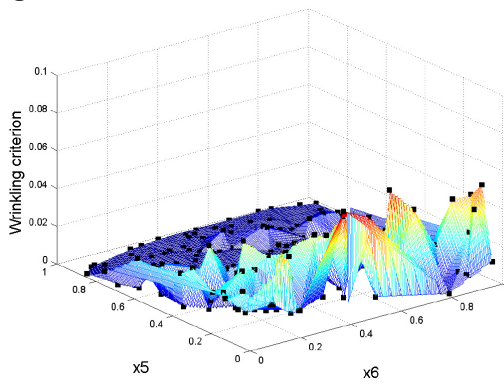
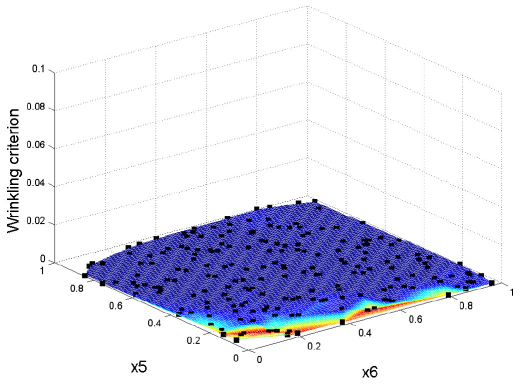
Region A

Region B

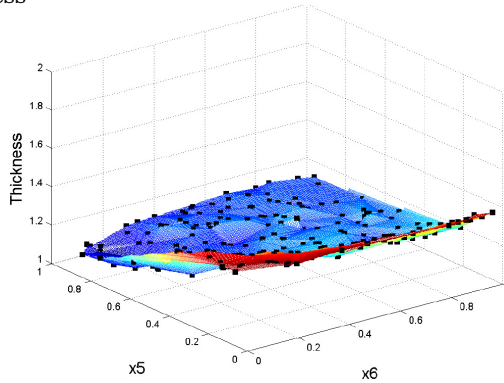
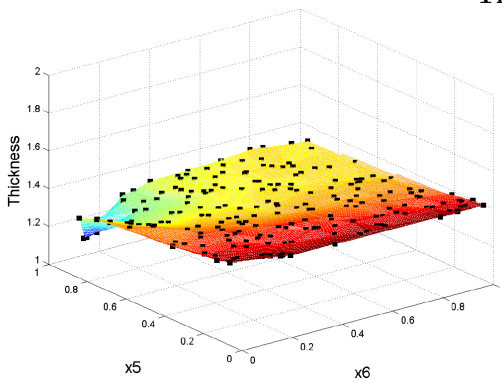
Failure



Wrinkling



Thickness



21:Surface plots dependent on x5 and x6 for material TRIP700

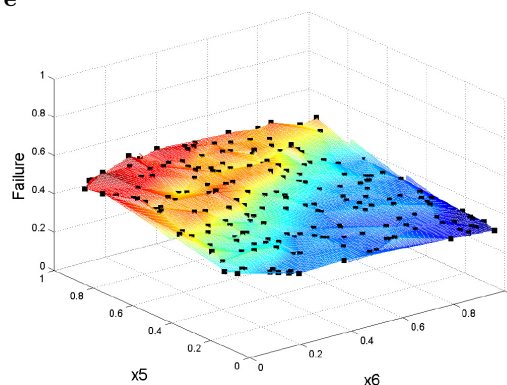
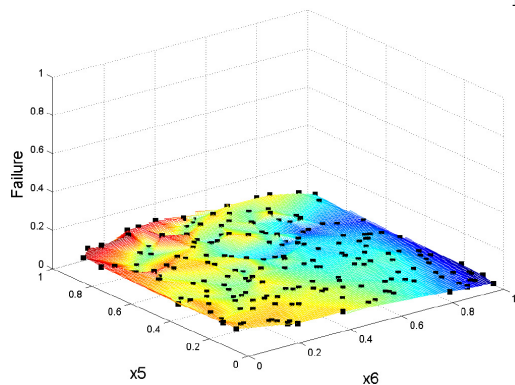
198 simulations dependent on x5 and x6 with BHF and x72 to nominal settings.

198 sim

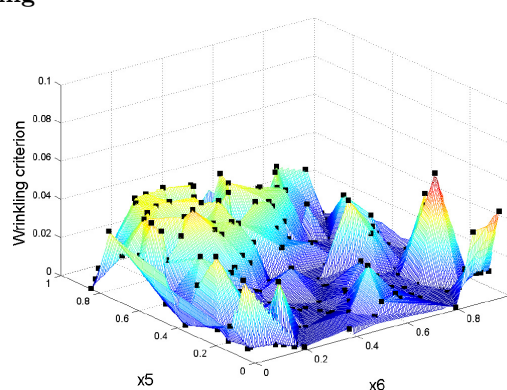
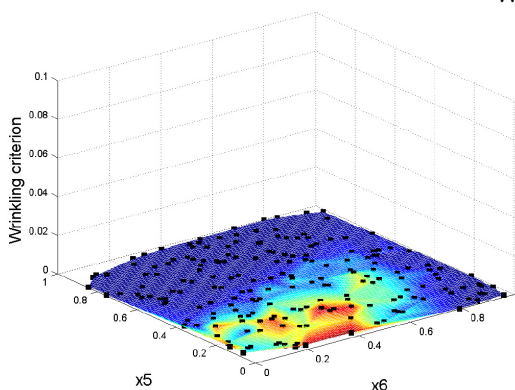
Region A

Region B

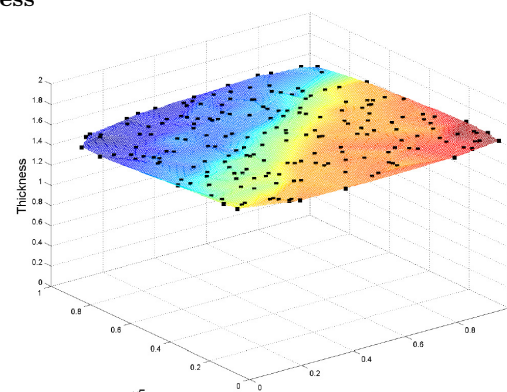
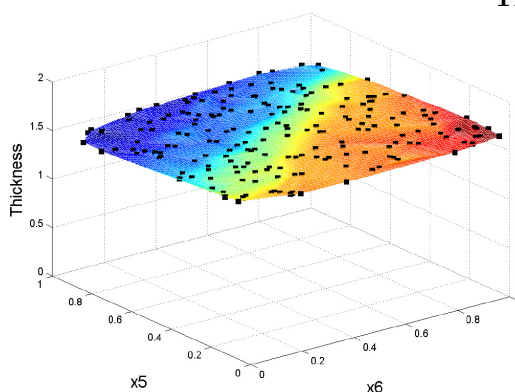
Failure



Wrinkling



Thickness



D.4 FEM simulations 2

Due to several different reason the materials that were used in the FEM simulations were not available for the experimental validation. In the case of TRIP700 the material was not available in the required dimensions. In the case of DP600 the selected batch was out of stock, therefor another batch is used for the experimental validation.

The following materials are used for the experimental validation; H340LAD and DP600, for the specific properties see Appendix C.2.

2 design variables are chosen and 2 response are chosen in 2 regions.

| | Material | Design variable | Nominal setting |
|---|----------|-----------------|-----------------|
| 1 | H340LAD | BHF | x5, x6, x72 |
| 2 | DP600 | BHF | x5, x6, x72 |

Table D.2: Simulation series 2

D.4.1 Exact location of the Regions (simulation series 2)

Due to the experiences that have been gained with the experiments the focus area changed. For the measurement that have been done with FMTI and the thickness gauge, the measurement area is different then the focus area for the specific areas, which are pointed out in Section D.1. The focus area for the scatter plot is changed to see if the results can match the ones which are obtained with the experiments.

The red marked area in Figure D.3 is the new focus area for region B. The blue marked area is the focus area for region A. For the exact location of the different zones see Figure D.4(a) for region A and Figure D.4(b) for Region B. The thickness in region B is measured at a specific region see Figure 5.2(c), so therefor the thickness values in region B are taken in a specific area see Figure D.4(c).

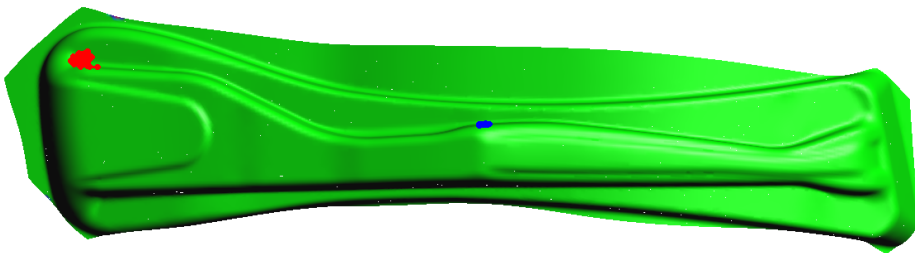


Figure D.3:

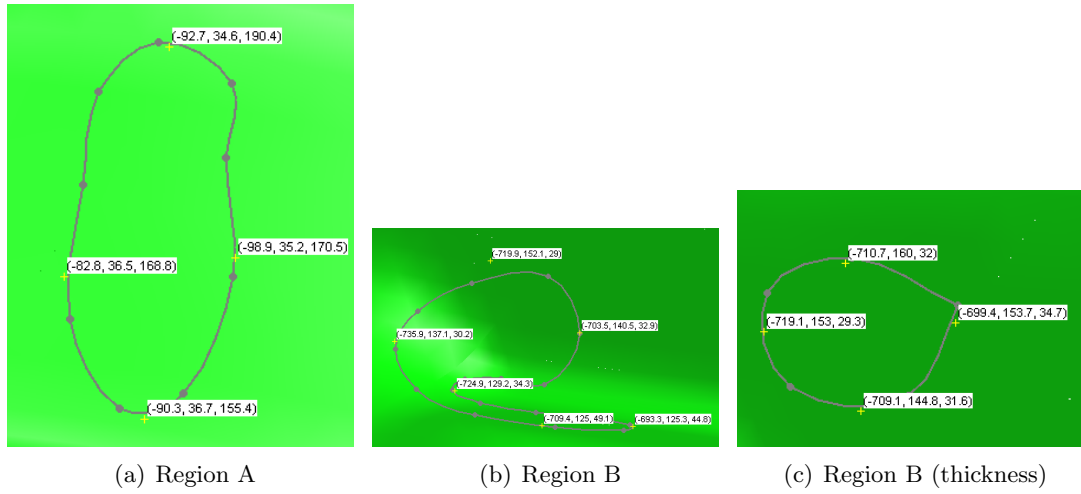


Figure D.4: Exact location for the focus areas A and B

In AutoForm Sigma a poly 3D curve is generated, the average value of the response in that region is used in the scatter plots. For the three different responses in two different regions the following poly 3D curves are used.

D.4.2 Region A

| Region A | | | |
|----------|-----------|-----------|-----------|
| | x_{pos} | y_{pos} | z_{pos} |
| 0 | -98.541 | 34.184 | 186.93 |
| 1 | -98.036 | 34.625 | 180 |
| 2 | -98.636 | 35.331 | 168.75 |
| 3 | -94.032 | 36.361 | 157.8 |
| 4 | -88.072 | 36.821 | 156.43 |
| 5 | -83.412 | 36.666 | 164.83 |
| 6 | -84.621 | 35.872 | 177.39 |
| 7 | -86.121 | 35.303 | 186.1 |
| 8 | -91.72 | 34.653 | 190.75 |
| 9 | -98.541 | 34.184 | 186.93 |

D.4.3 Region B

| Region B (strains) | | | | Region B (thickness) | | | |
|--------------------|-----------|-----------|-----------|----------------------|-----------|-----------|-----------|
| | x_{pos} | y_{pos} | z_{pos} | | x_{pos} | y_{pos} | z_{pos} |
| 0 | -720.39 | 127.5 | 36.664 | 0 | -699.07 | 155.58 | 34.846 |
| 1 | -725.31 | 129.31 | 34.37 | 1 | -704.31 | 146.31 | 32.96 |
| 2 | -723.29 | 131.1 | 31.333 | 2 | -716.38 | 147.23 | 29.743 |
| 3 | -716.83 | 131.56 | 30.493 | 3 | -718.64 | 156.92 | 29.629 |
| 4 | -709.16 | 130.97 | 32.443 | 4 | -709.96 | 160.45 | 32.153 |
| 5 | -703.51 | 140.38 | 32.872 | 5 | -699.07 | 155.58 | 34.846 |
| 6 | -709.5 | 150.1 | 31.75 | | | | |
| 7 | -722.93 | 147.92 | 28.008 | | | | |
| 8 | -732.22 | 142.4 | 27.068 | | | | |
| 9 | -735.83 | 135.86 | 31.063 | | | | |
| 10 | -731.75 | 129.29 | 36.943 | | | | |
| 11 | -721.16 | 125.94 | 44.778 | | | | |
| 12 | -707.05 | 124.85 | 49.751 | | | | |
| 13 | -694.9 | 124.85 | 48.003 | | | | |
| 14 | -693.84 | 125.57 | 43.284 | | | | |
| 15 | -710.54 | 126.55 | 39.388 | | | | |
| 16 | -720.39 | 127.5 | 36.664 | | | | |

D.5 Scatter plots

The following scatter plots are made with the use of AutoForm. A scatter plot shows the raw result variable (RV) and the selected design variable(DV) in an xy-scatter plot for all the simulations of the current performance analysis.

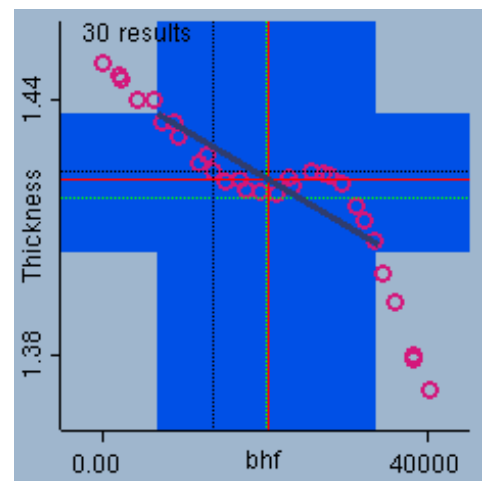
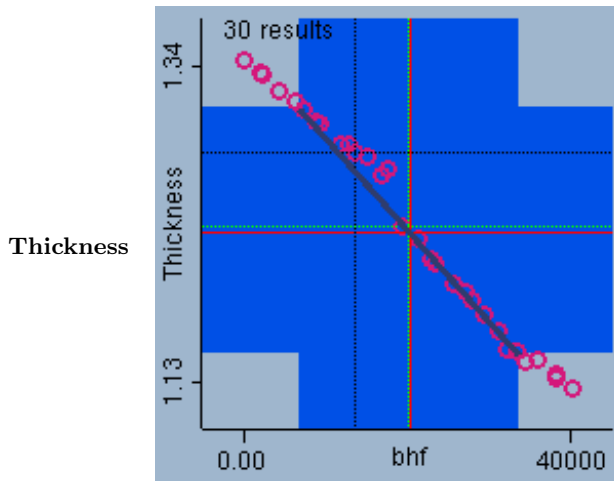
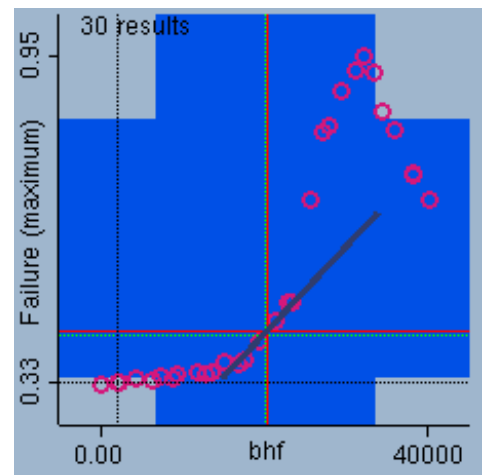
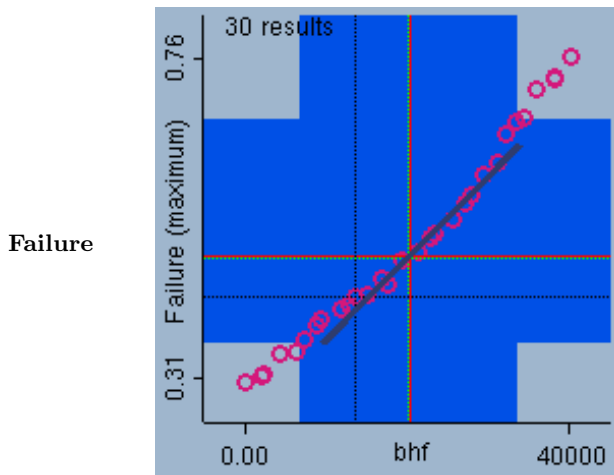
Scatter plots dependent on BHF for material H340LAD

30 simulations dependent on BHF with x5, x6 and x72 to nominal settings.

30 sim

Region A

Region B



Scatter plots dependent on BHF for material DP600

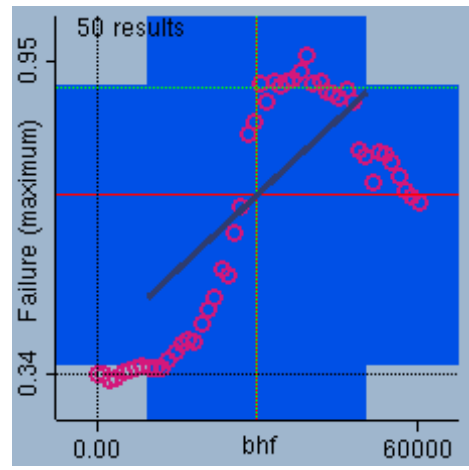
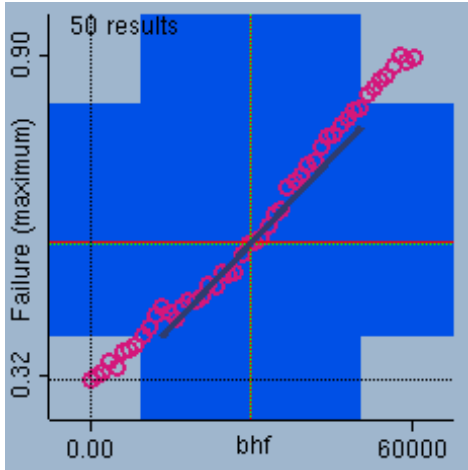
50 simulations dependent on BHF with x5, x6 and x72 to nominal settings.

50 sim

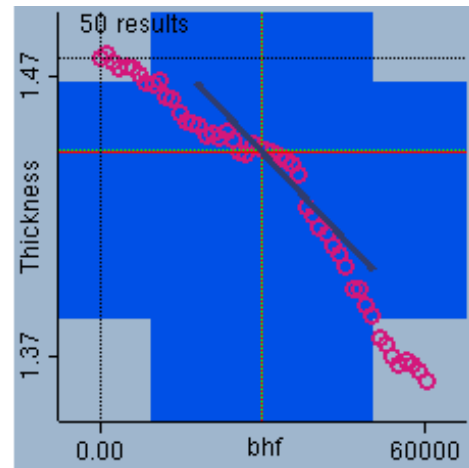
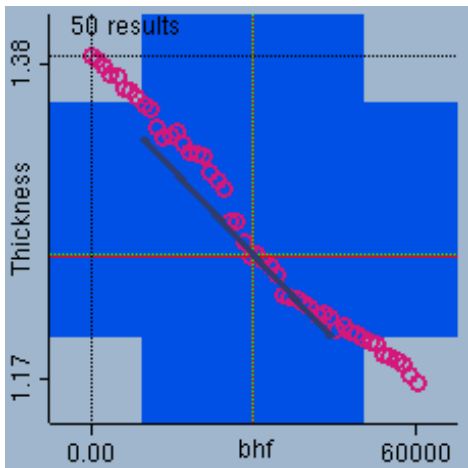
Region A

Region B

Failure



Thickness



Appendix E

Experimental information

In this appendix extra information of the experiments can be found.

E.1 Blank dimensions

The reference blank shape is cut out of the sheet. The following dimensions are used.

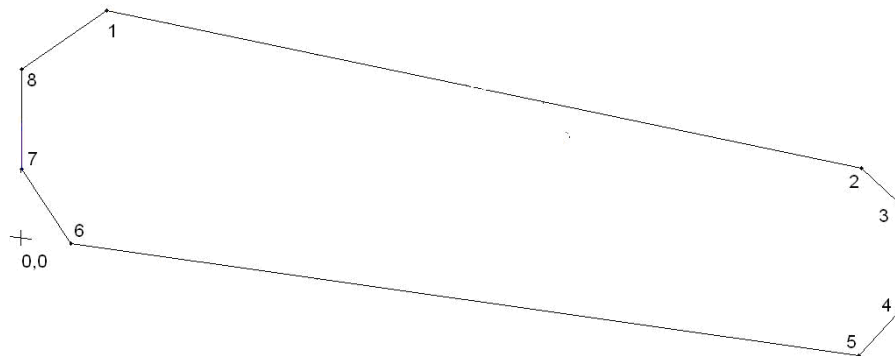


Figure E.1: Reference blank dimensions

| Nod | x_{pos} | y_{pos} |
|-----|-----------|-----------|
| 1 | 145 | 591 |
| 2 | 1438 | 320 |
| 3 | 1500 | 261 |
| 4 | 1500 | 73 |
| 5 | 1433 | 0 |
| 6 | 83 | 191 |
| 7 | 0 | 319 |
| 8 | 0 | 491 |

The geometrical variables are also varied the exact dimensions are pointed out, for x_5 and x_6 .

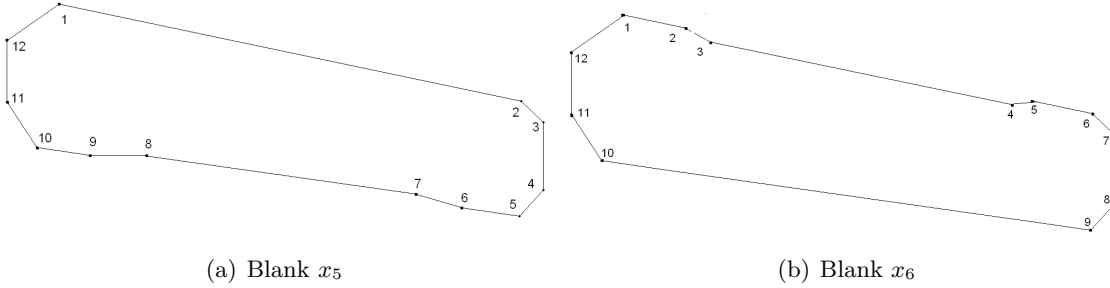


Figure E.2: Reference blank shape for x_5 (a) and x_6 (b)

| Nod | x_{pos} | $x_5 = 0.5$ | | $x_5 = 1$ | |
|-----|-----------|-------------|-----------|-----------|-----------|
| | | y_{pos} | x_{pos} | y_{pos} | x_{pos} |
| 1 | 145 | 591 | 591 | 591 | 591 |
| 2 | 1438 | 320 | 320 | 320 | 320 |
| 3 | 1500 | 261 | 261 | 261 | 261 |
| 4 | 1500 | 73 | 73 | 73 | 73 |
| 5 | 1433 | 0 | 0 | 0 | 0 |
| 6 | 1274 | 22 | 22 | 22 | 22 |
| 7 | 1137 | 52 | 62 | 62 | 62 |
| 8 | 382 | 159 | 169 | 169 | 169 |
| 9 | 251 | 168 | 168 | 168 | 168 |
| 10 | 83 | 191 | 191 | 191 | 191 |
| 11 | 0 | 319 | 319 | 319 | 319 |
| 12 | 0 | 491 | 491 | 491 | 491 |

| Nod | x_{pos} | $x_6 = 0.5$ | | $x_6 = 1$ | |
|-----|-----------|-------------|-----------|-----------|-----------|
| | | y_{pos} | x_{pos} | y_{pos} | x_{pos} |
| 1 | 145 | 591 | 591 | 591 | 591 |
| 2 | 364 | 549 | 549 | 549 | 549 |
| 3 | 444 | 518 | 508 | 508 | 508 |
| 4 | 1143 | 371 | 361 | 361 | 361 |
| 5 | 1281 | 352 | 352 | 352 | 352 |
| 6 | 1438 | 320 | 320 | 320 | 320 |
| 7 | 1500 | 261 | 261 | 261 | 261 |
| 8 | 1500 | 73 | 73 | 73 | 73 |
| 9 | 1433 | 0 | 0 | 0 | 0 |
| 10 | 83 | 191 | 191 | 191 | 191 |
| 11 | 0 | 319 | 319 | 319 | 319 |
| 12 | 0 | 491 | 491 | 491 | 491 |

E.2 Position of the blank on the die

The distance from the blank to the die are measured. Two points were taken as reference points for the deep drawing of the B-pillar. The upper left corner, see Figure E.4(a) and the lower right corner E.4(b). How the blank is situated on the die see Figure E.3



Figure E.3: Position of the blank on the die



(a) Left upper corner

(b) Right lower corner

Figure E.4: Position of the blank with respect to the die.

E.3 Thickness measurements

In the report the thickness tables are included in this section a graphical display is made of this information.

E.3.1 Blank holder force(H340LAD)

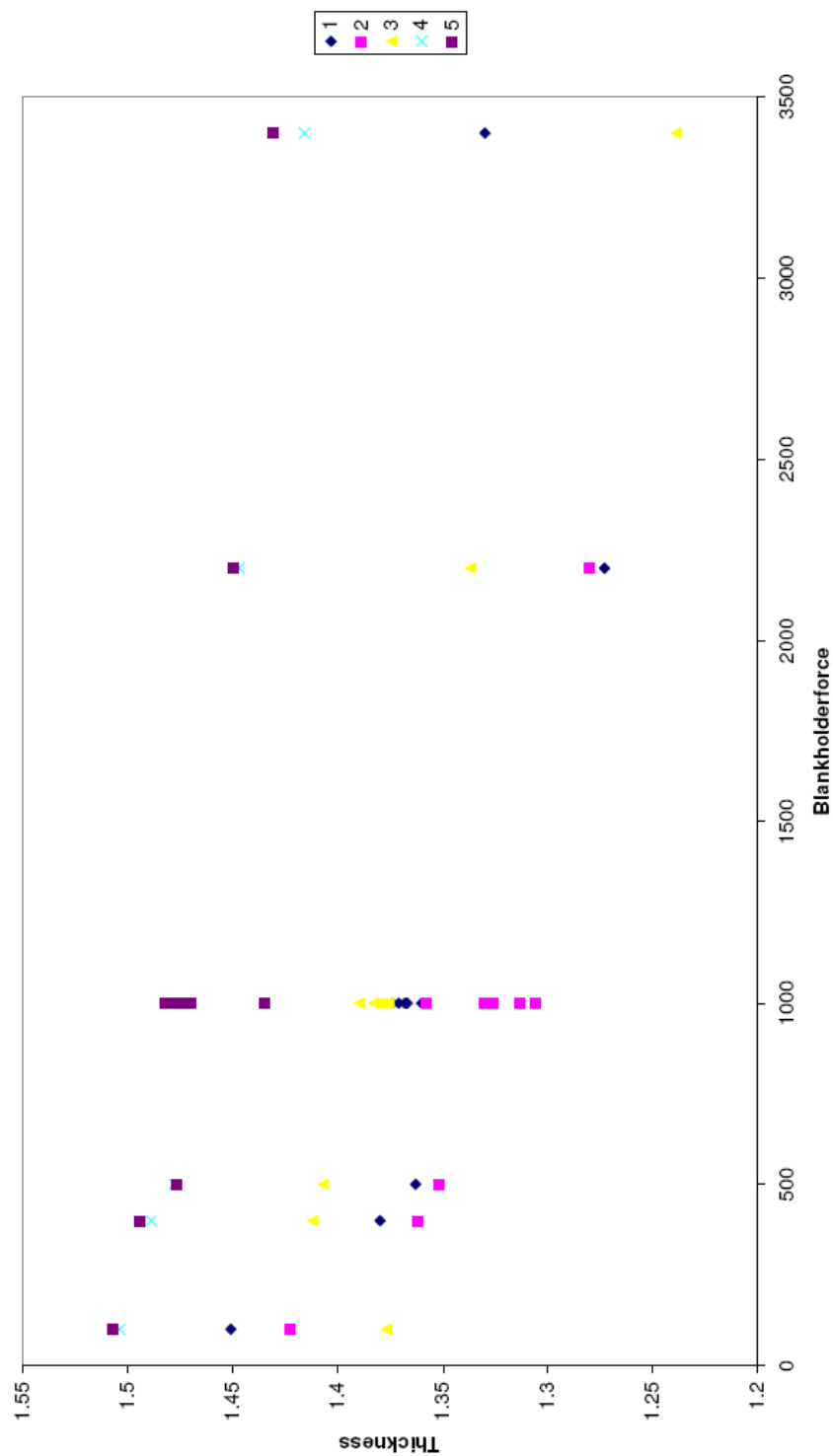


Figure E.5: Thickness measurements of H340 day 1

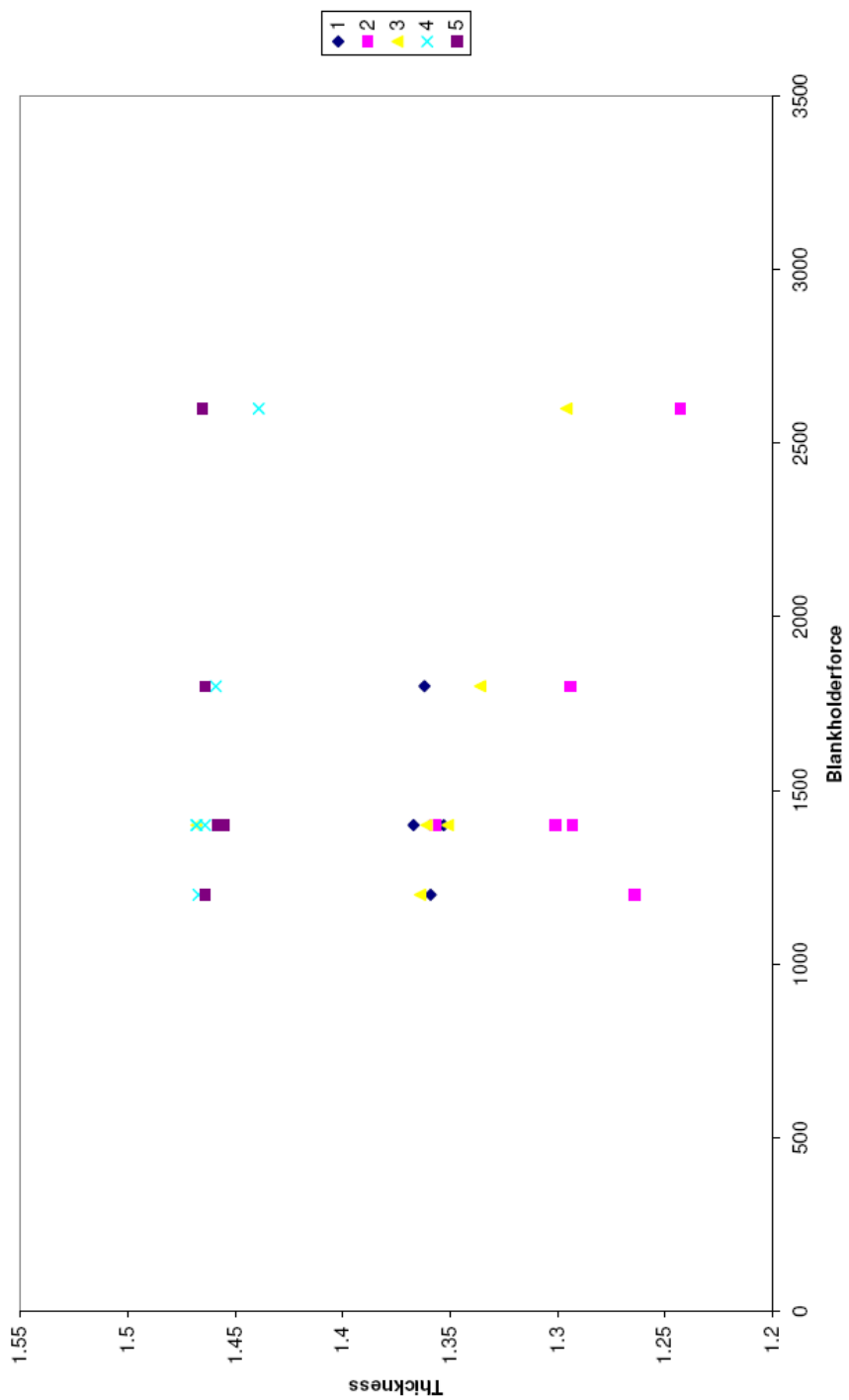


Figure E.6: Thickness measurements of H340 day 2

E.3.2 Blank holder force(DP600)

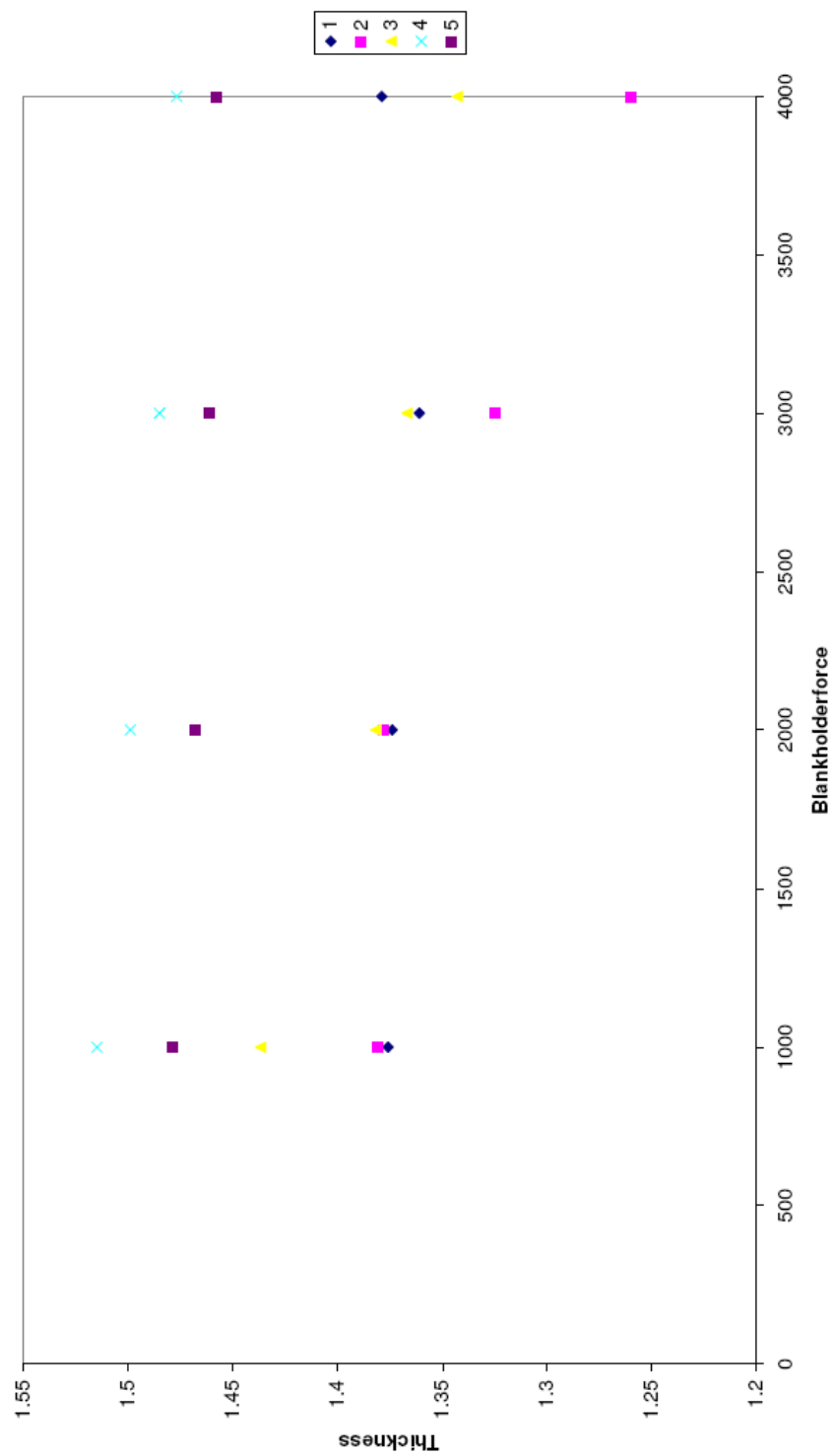


Figure E.7: Thickness measurements of DP600 day 1

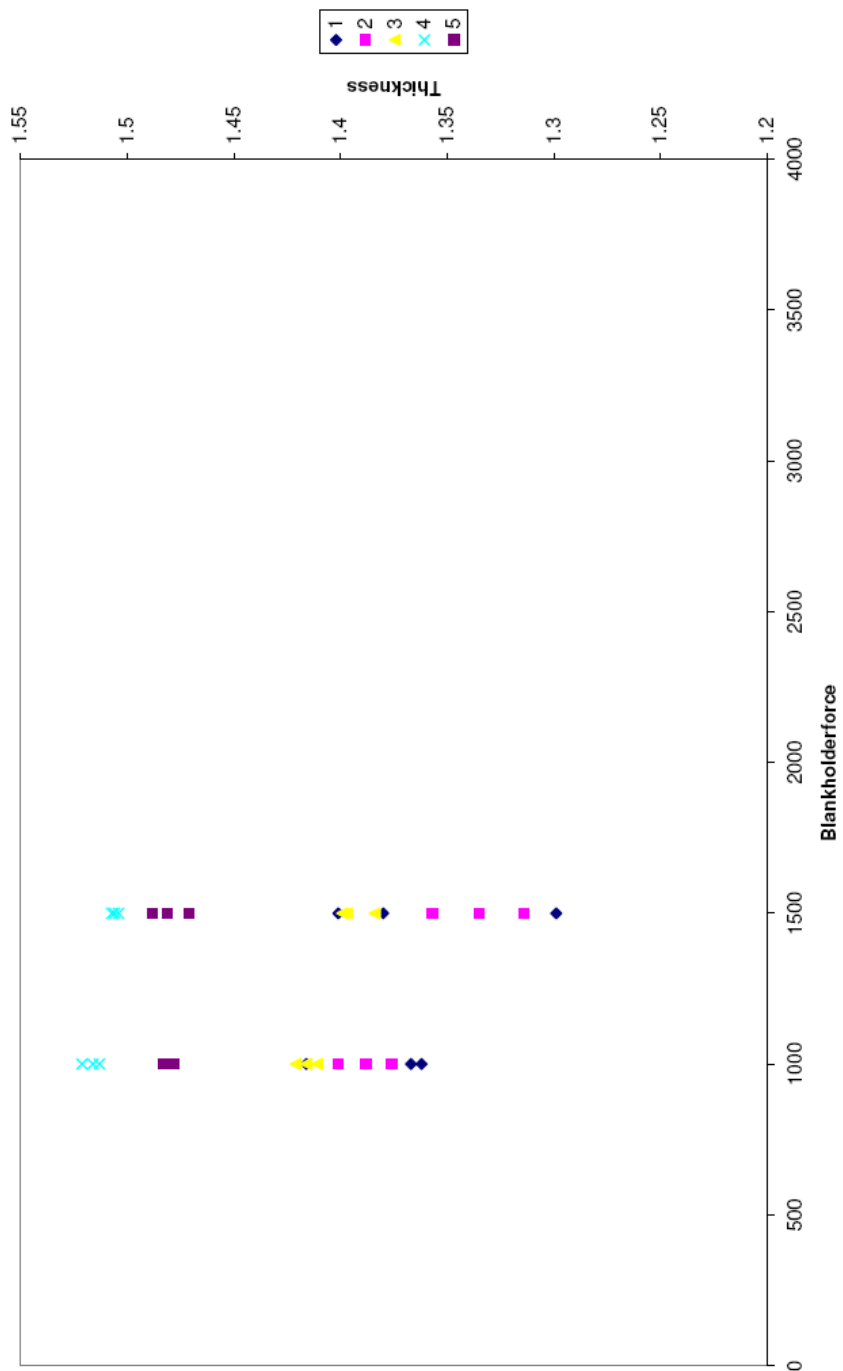


Figure E.8: Thickness measurements of DP600 day 2

E.3.3 Scatter plots dependent of the geometrical variables

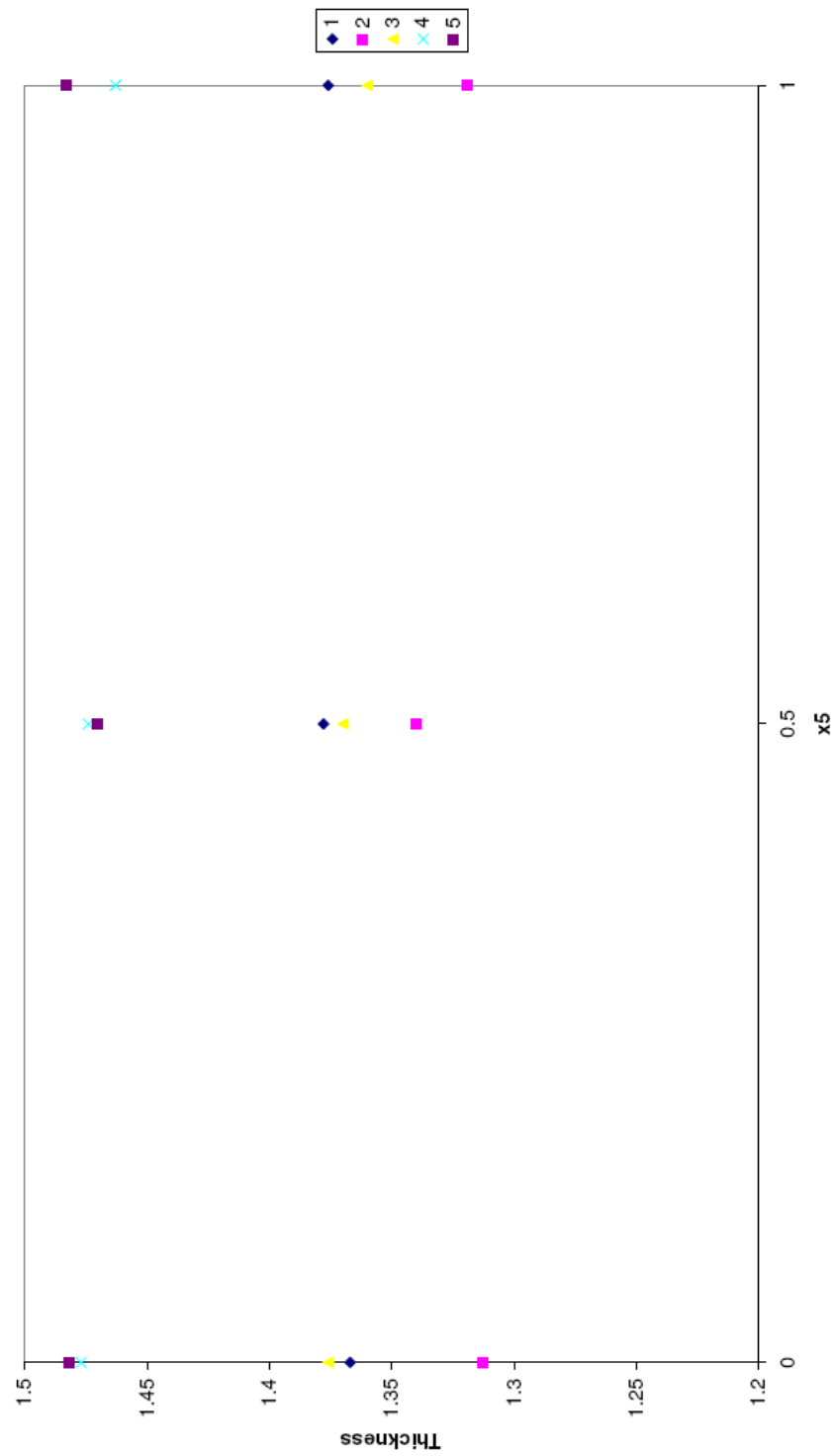


Figure E.9: Thickness measurements of H340LAD at a blank holder force of 1000 [kN]

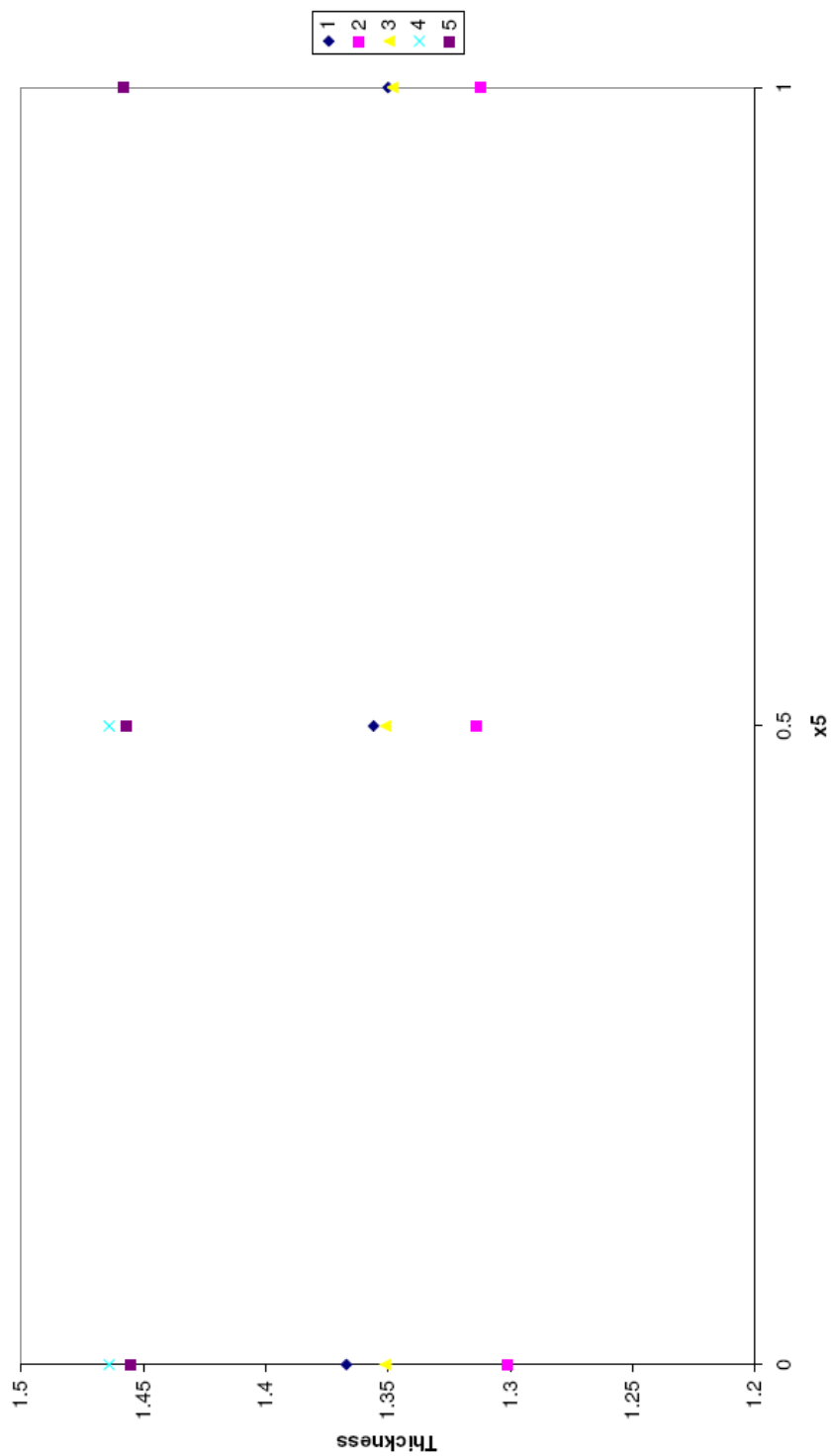


Figure E.10: Thickness measurements of H340LAD at a blank holder force of 1400 [kN]

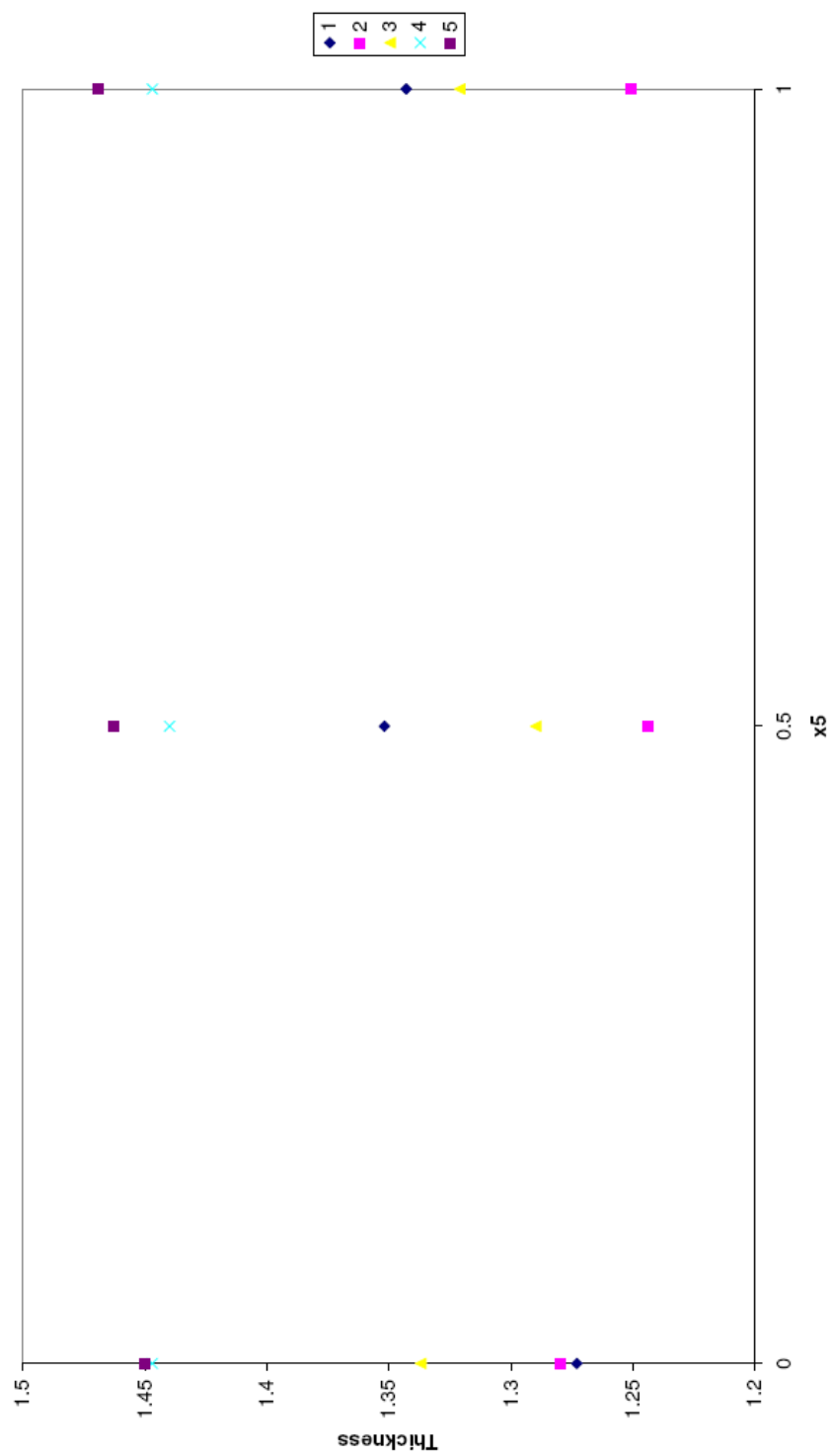


Figure E.11: Thickness measurements of H340LAD at a blank holder force of 2200 [kN]

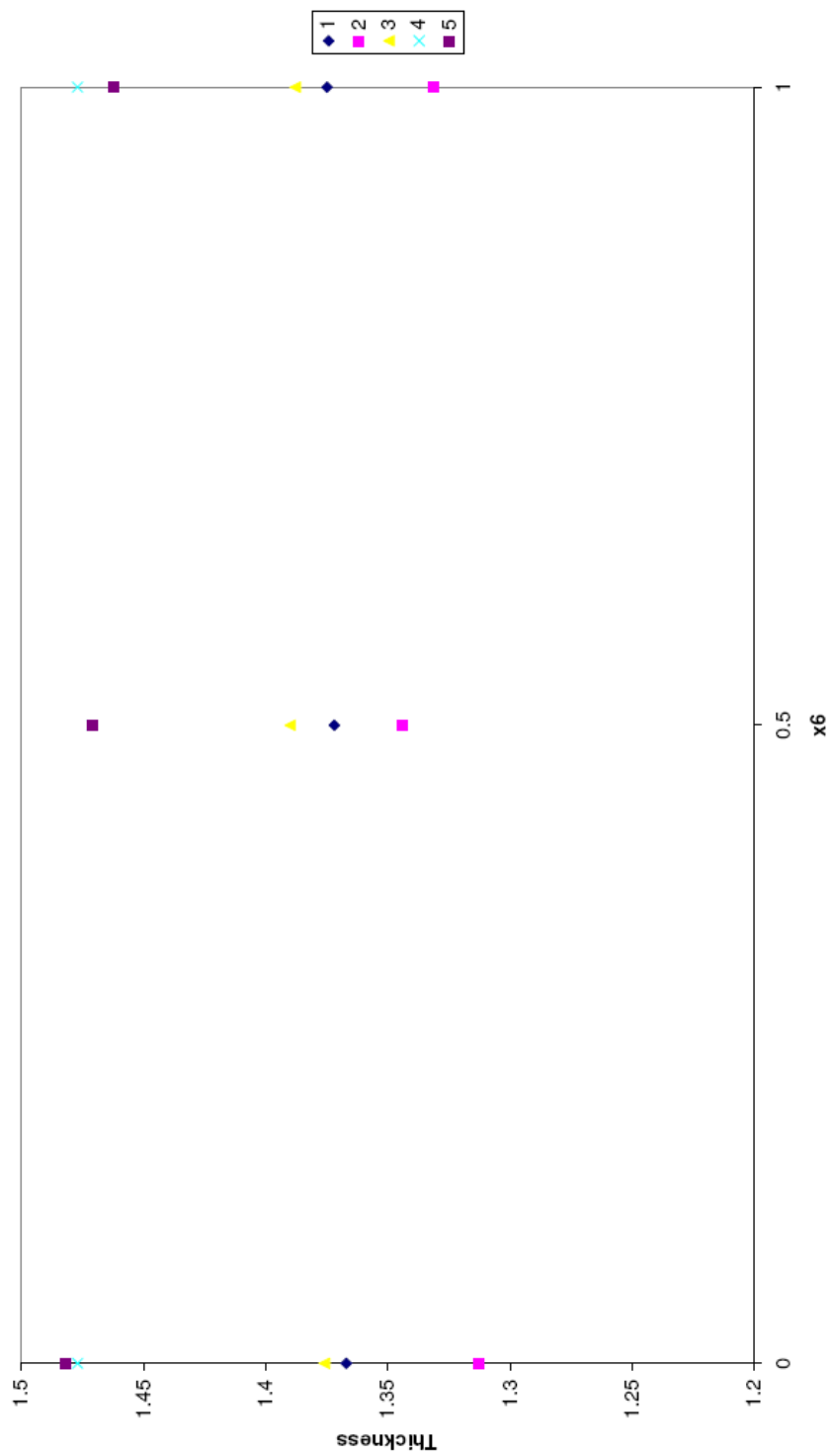


Figure E.12: Thickness measurements of H340LAD at a blank holder force of 1000 [kN]

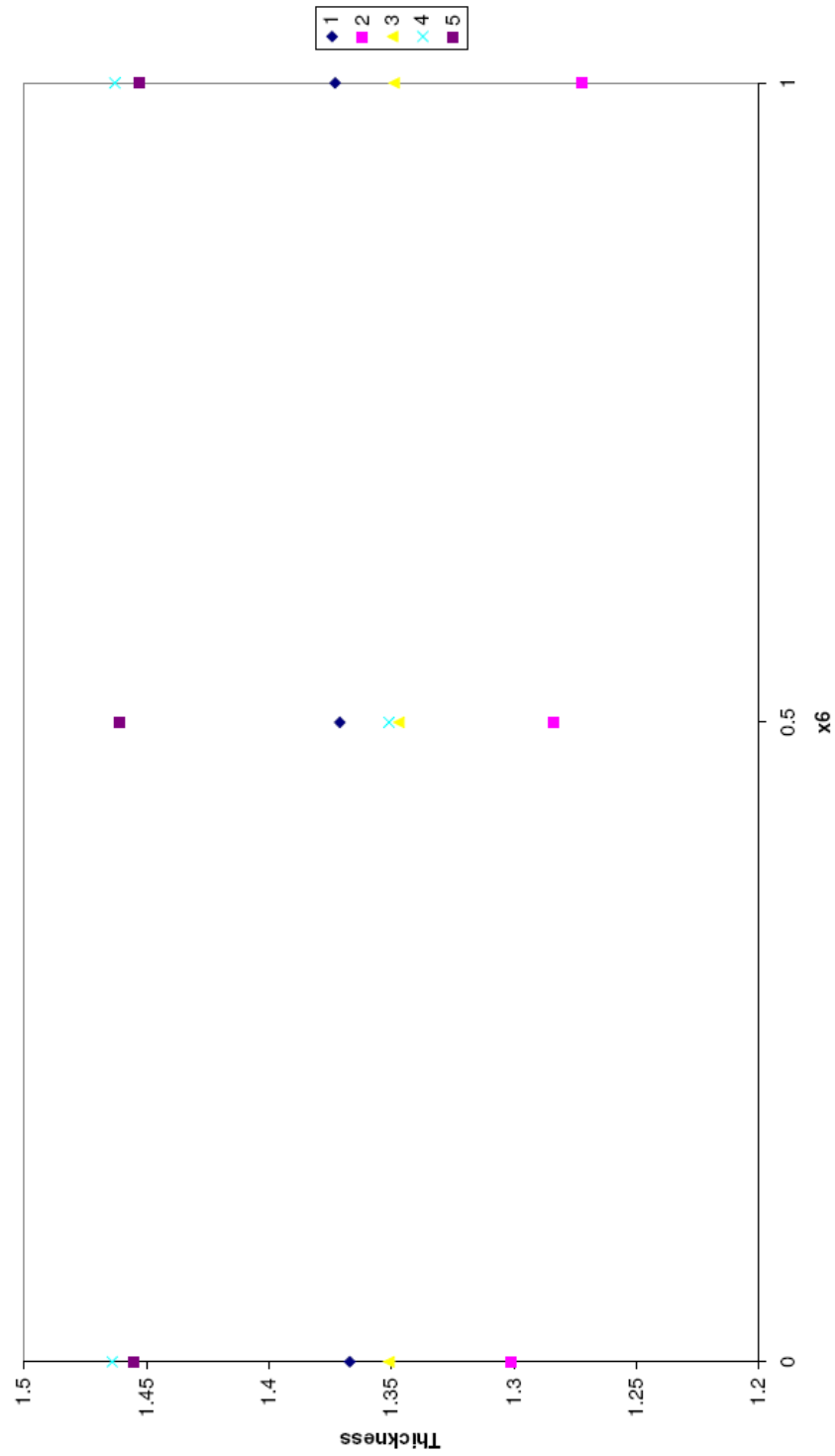


Figure E.13: Thickness measurements of H340LAD at a blank holder force of 1400 [kN]

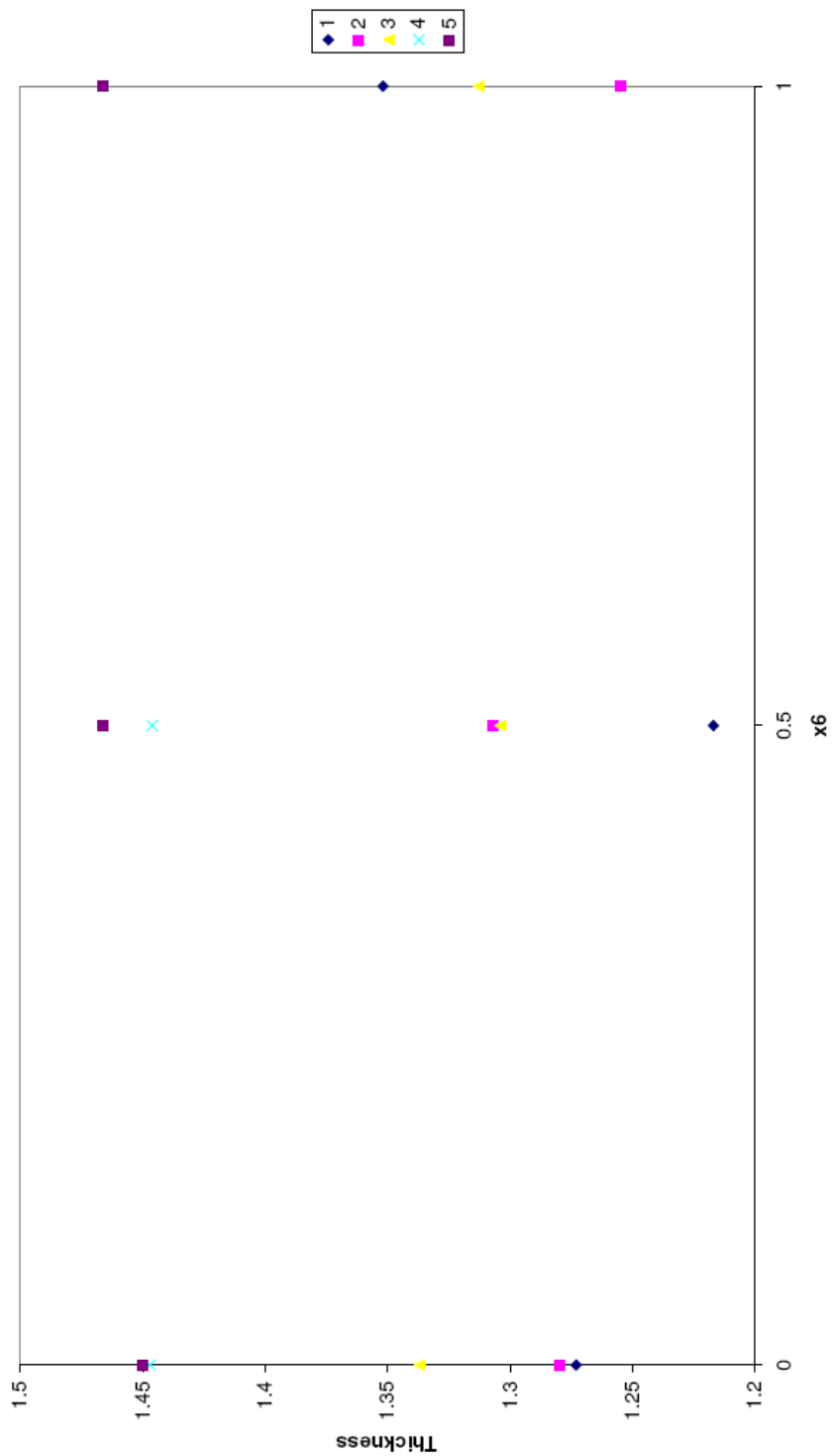


Figure E.14: Thickness measurements of H340LAD at a blank holder force of 2200 [kN]

E.3.4 Surface plots dependent of the geometrical variables

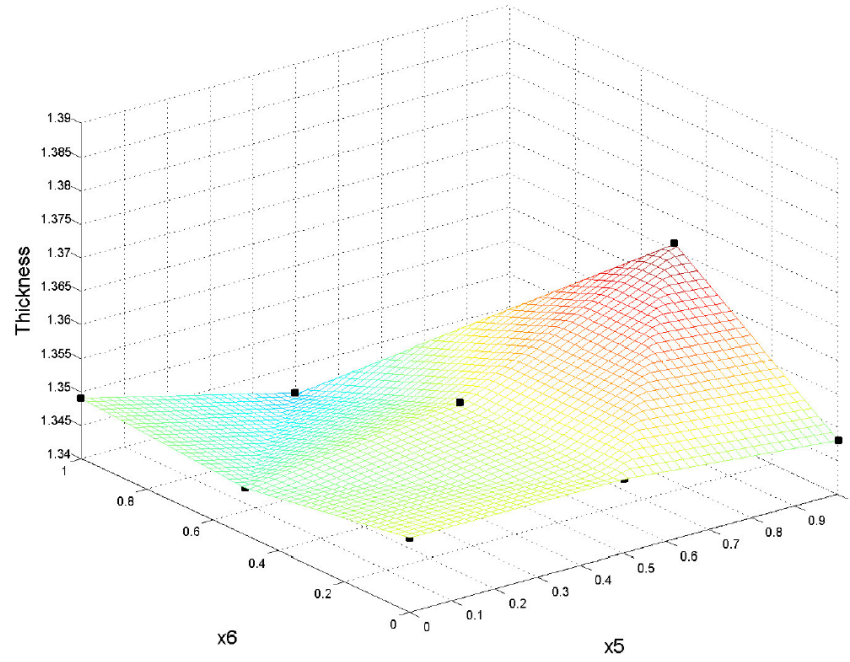


Figure E.15: Thickness in region A at a blank holder force of 1400 kN

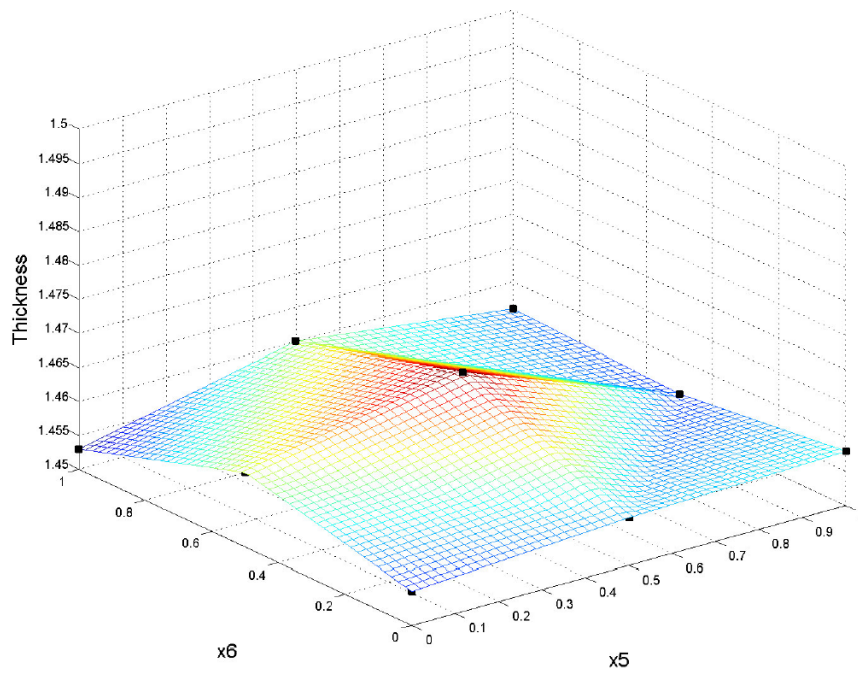
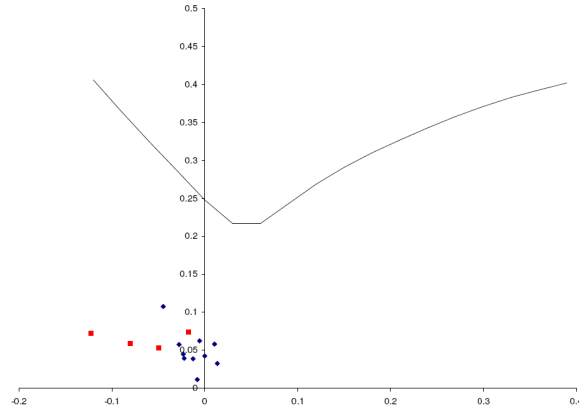


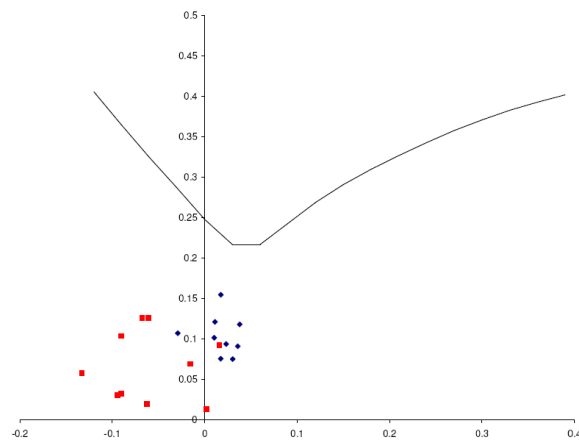
Figure E.16: Thickness in region B at a blank holder force of 1400 kN]

E.4 Forming limit diagrams

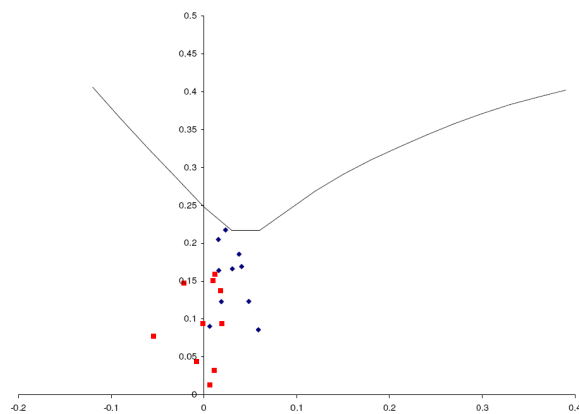
E.4.1 Blank holder force (H340LAD)



(a) BHF 100 [kN], exp 8

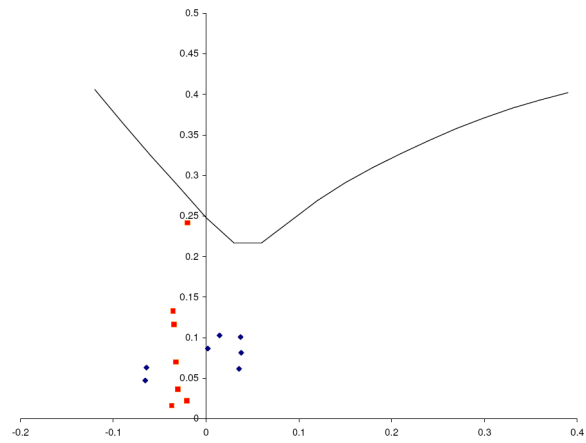


(b) BHF 1000 [kN], exp 6

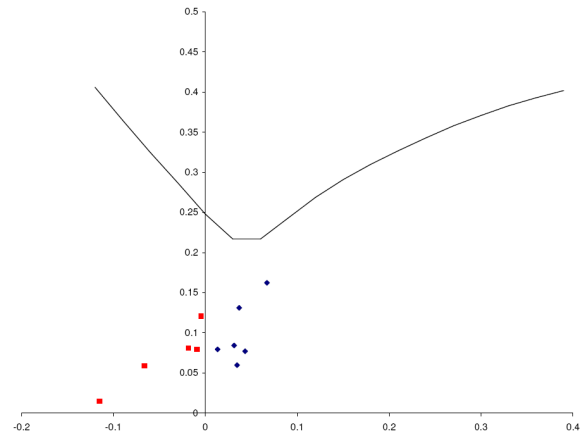


(c) BHF 2200 [kN], exp 10

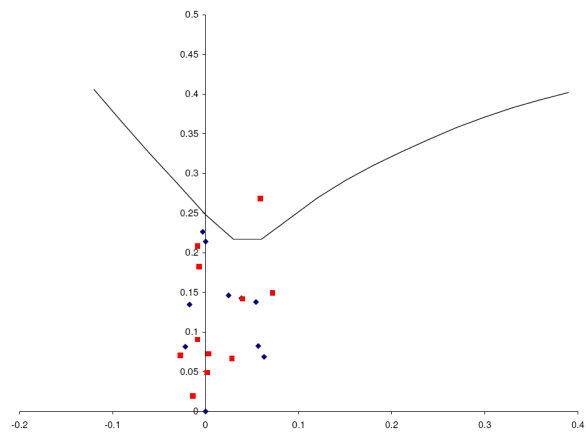
Figure E.17: Forming limit diagram with strains in region A en B of day 1



(a) BHF 1200 [kN], exp 21



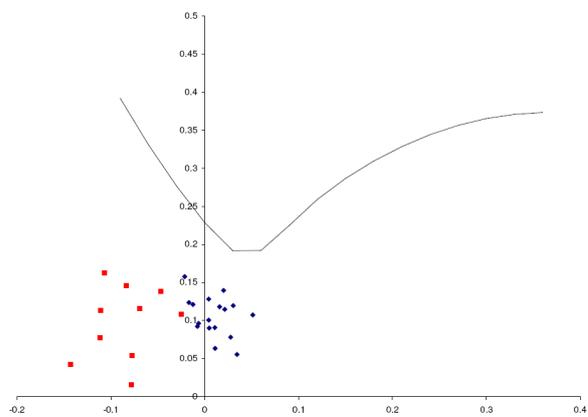
(b) BHF 1400 [kN], exp 20



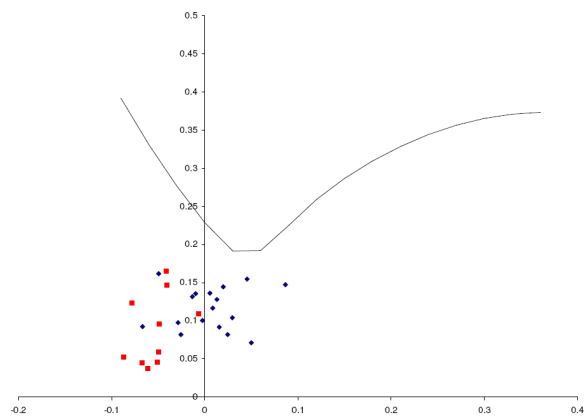
(c) BHF 2600 [kN], exp 18

Figure E.18: Forming limit diagram with strains in region A en B of day 2

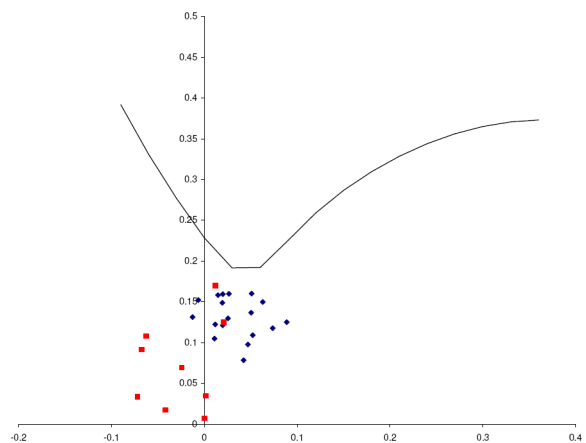
E.4.2 Blank holder force (DP600)



(a) BHF 1000 [kN], exp 11

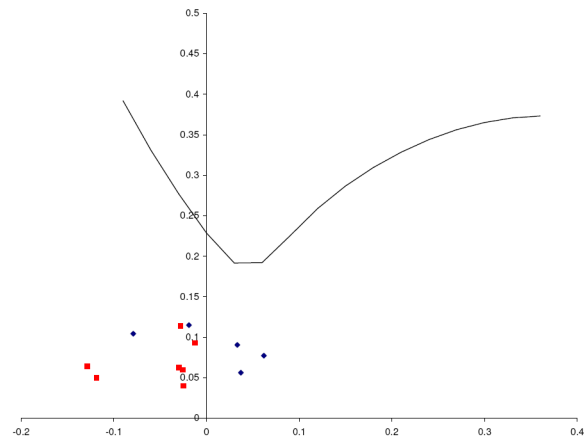


(b) BHF 2000 [kN], exp 12

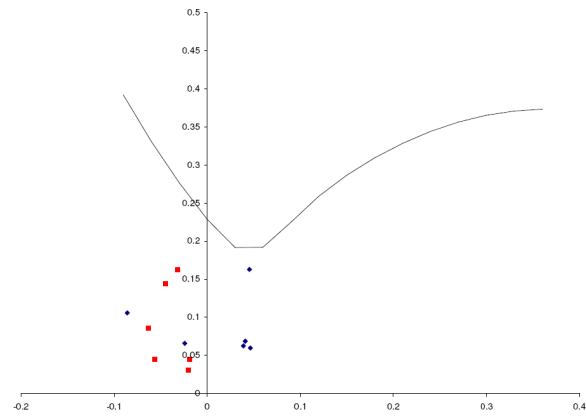


(c) BHF 3000 [kN], exp 13

Figure E.19: Forming limit diagram with strains in region A en B of day 1



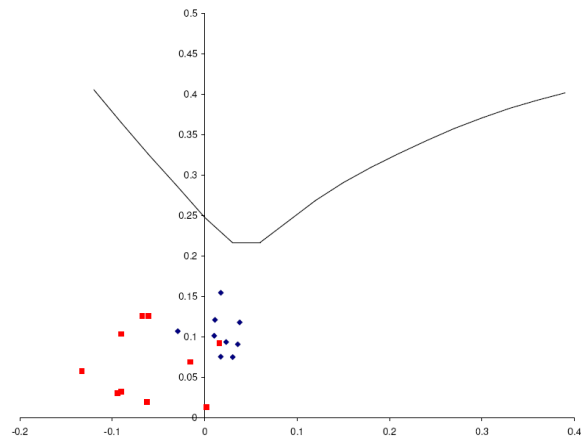
(a) BHF 1000 [kN], exp 44



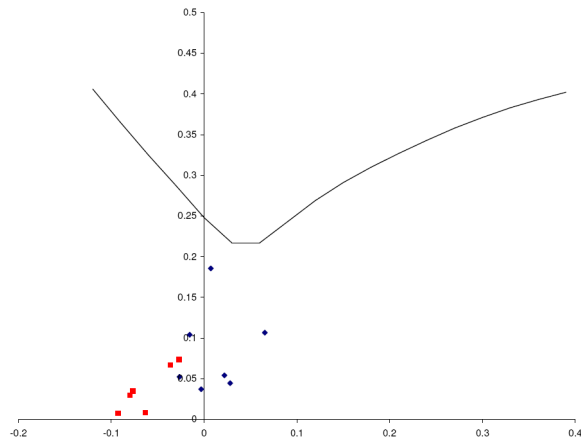
(b) BHF 1000 [kN], exp 46

Figure E.20: Forming limit diagram with strains in region A en B of day 2

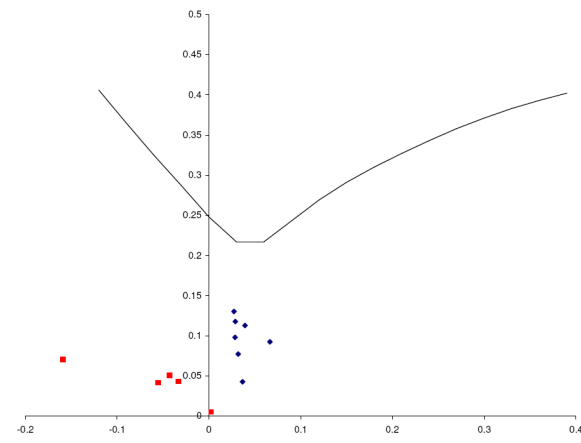
E.4.3 Geometrical variation(H340LAD)



(a) BHF 1000 [kN], $x_5=0$ exp 6



(b) BHF 1000 [kN], $x_5=1/2$ exp 25



(c) BHF 1000 [kN], $x_5=1$ exp 17

Figure E.21: Forming limit diagram with strains in region A en B, with variable x_5 and blank holder force 1000 [kN]

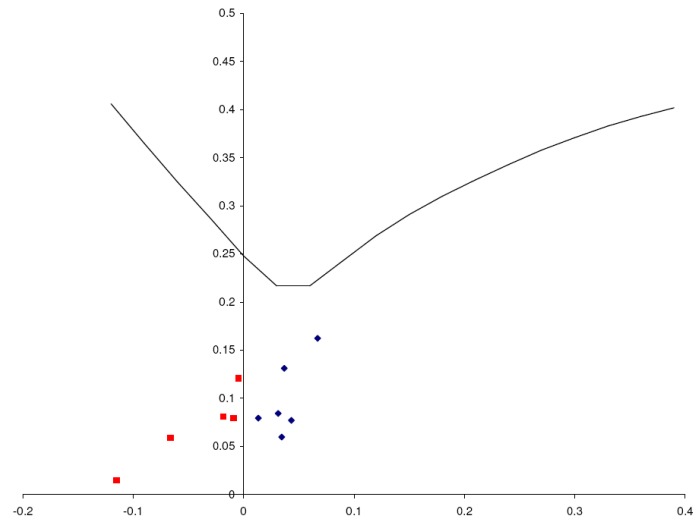
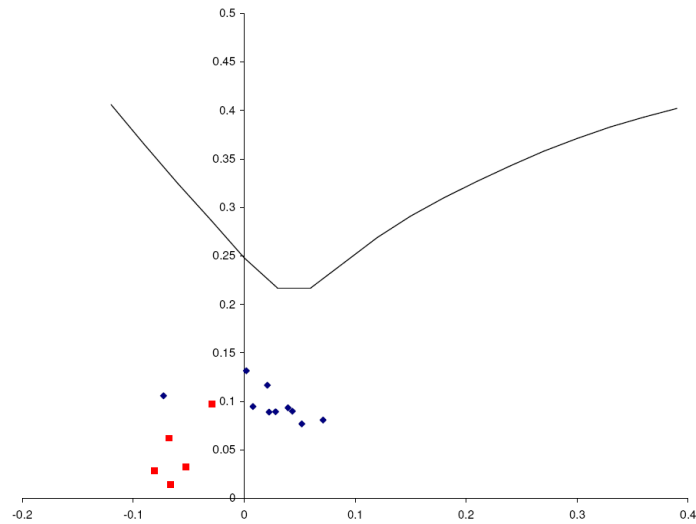
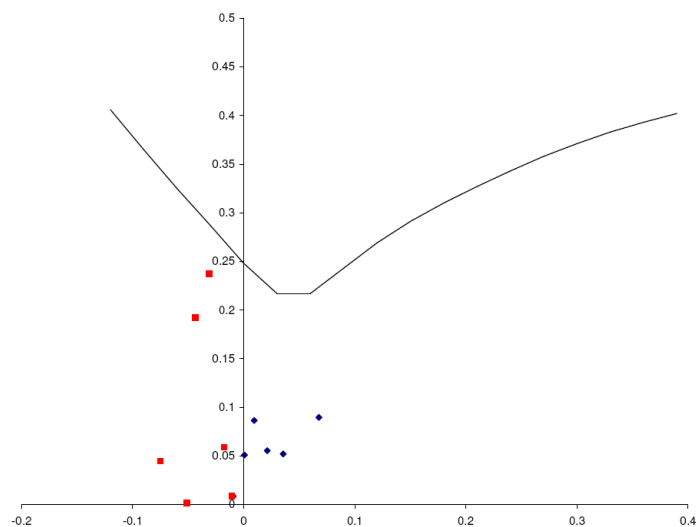
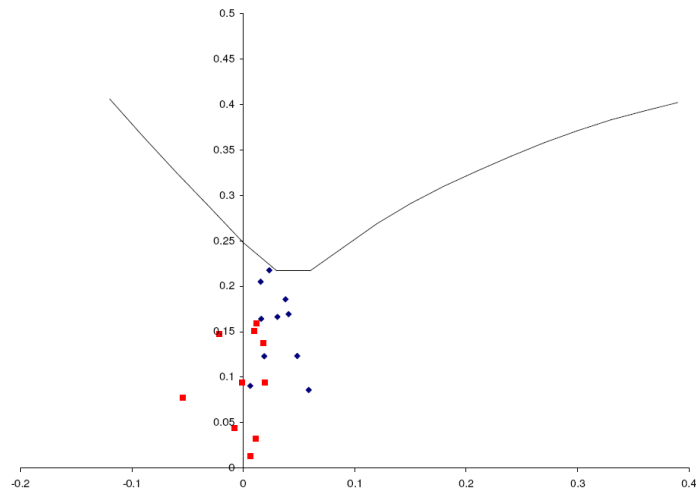
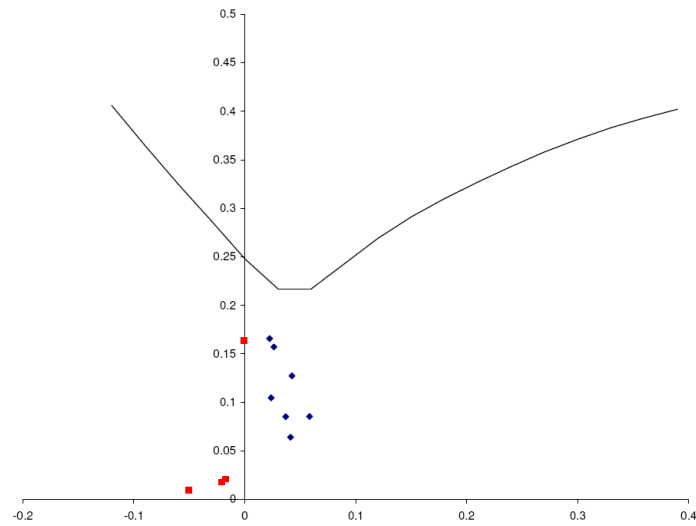
(a) BHF 1400 [kN], $x_5=0$ exp 20(b) BHF 1400 [kN], $x_5=1/2$ exp 23(c) BHF 1400 [kN], $x_5=1$ exp 22

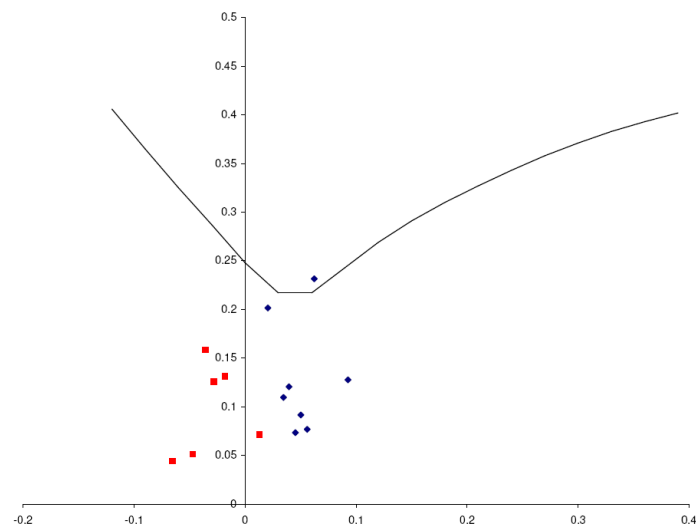
Figure E.22: Forming limit diagram with strain ϵ_{11} in region A en B, with variable x_5 and blank holder force 1400 [kN]



(a) BHF 2200 [kN], $x_5=0$ exp 10



(b) BHF 2200 [kN], $x_5=1/2$ exp 24



(c) BHF 2200 [kN], $x_5=1$ exp 16

Figure E.23: Forming limit diagram with strains in region A en B, with variable x_5 and blank holder force 2200 [kN]

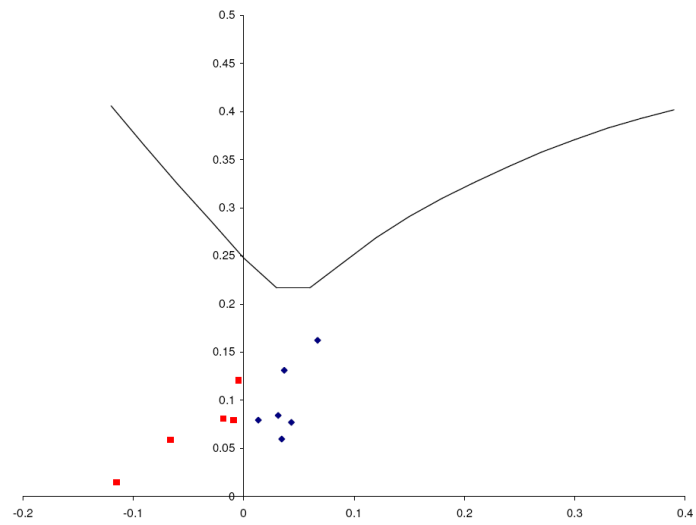
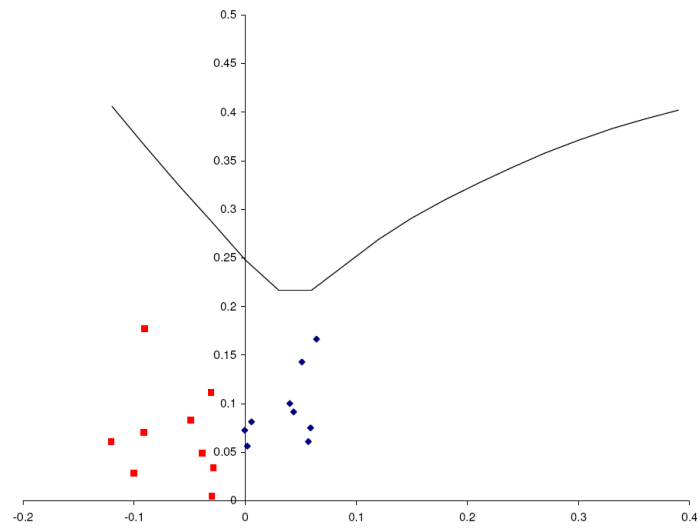
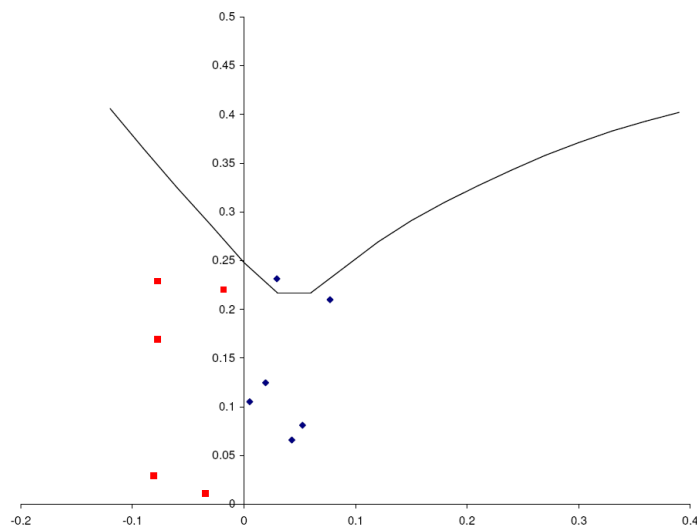
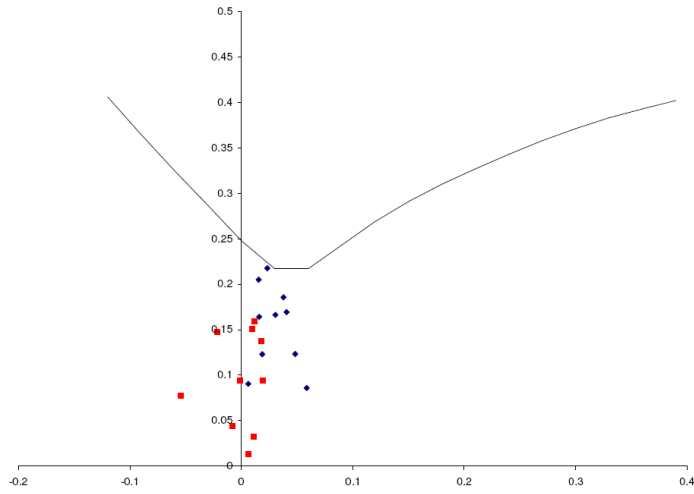
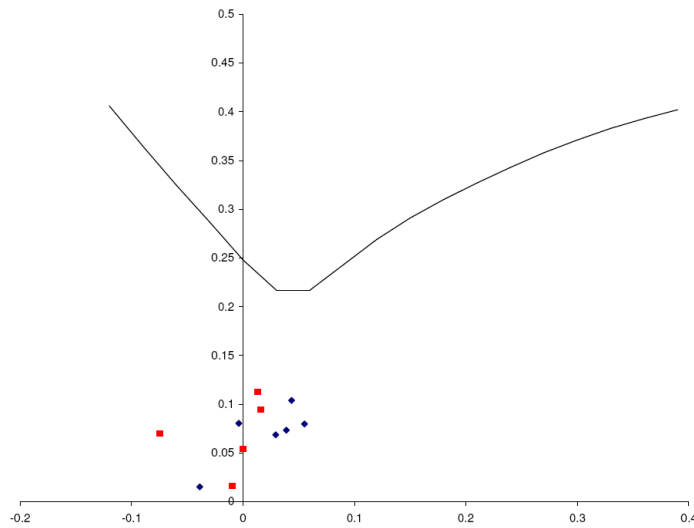
(a) BHF 1400 [kN], $x_6=0$ exp 20(b) BHF 1400 [kN], $x_6=1/2$ exp 33(c) BHF 1400 [kN], $x_6=1$ exp 37

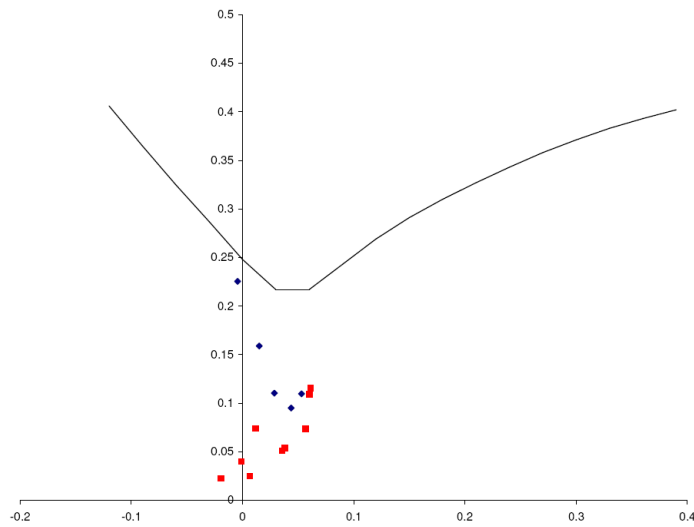
Figure E.24: Forming limit diagram with strains in region A en B, with variable x_5 and blank holder force 1400 [kN]



(a) BHF 2200 [kN], $x_6=0$ exp 10



(b) BHF 2200 [kN], $x_6=1/2$ exp 34



(c) BHF 2200 [kN], $x_6=1$ exp 38

Figure E.25: Forming limit diagram with strains in region A en B, with variable x_5 and blank holder force 2200 [kN]

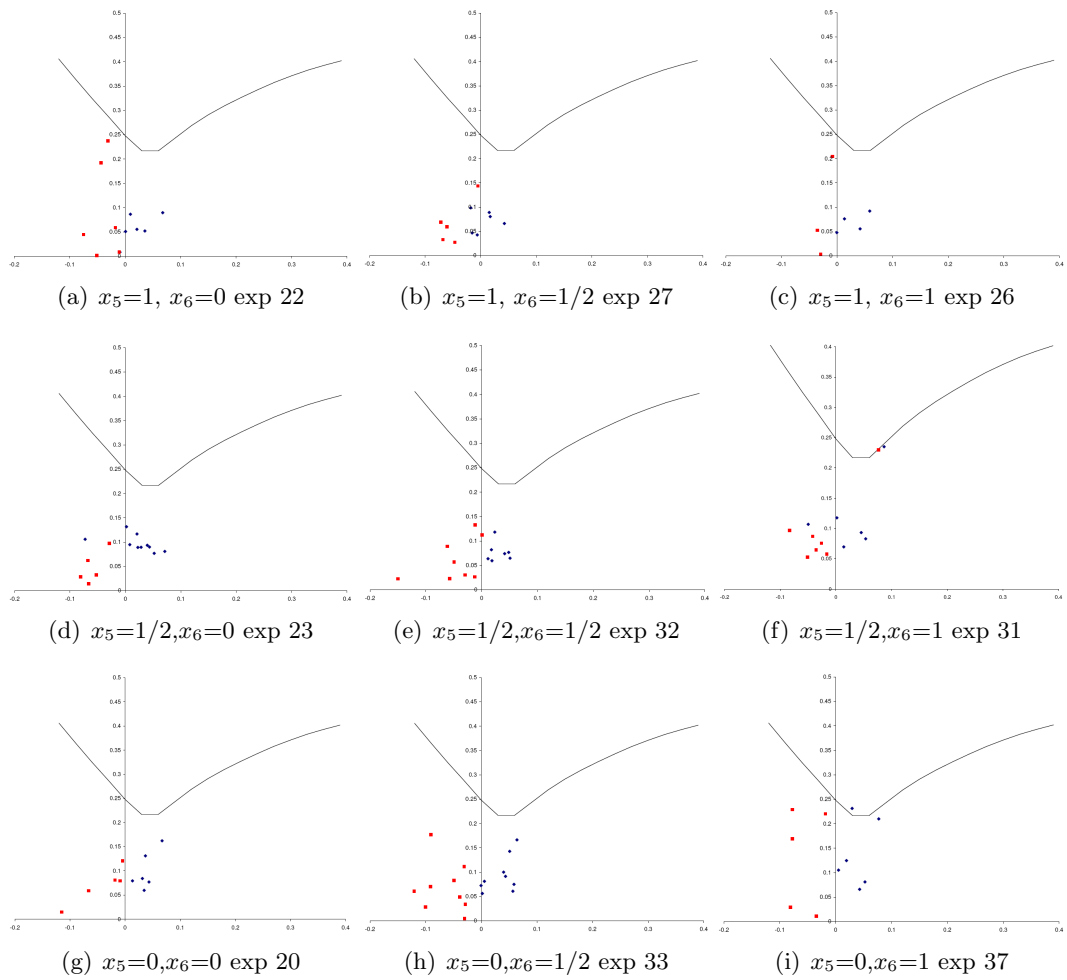


Figure E.26: Forming limit diagram with strains in region A en B, with variable x_5, x_6 blank holder force 1400 [kN]

E.5 Pictures of the experiments

E.5.1 H340LAD



Figure E.27: Experiment number 8 BHF = 100 [kN], day 1



Figure E.28: Experiment number 6 BHF = 1000 [kN], day 1

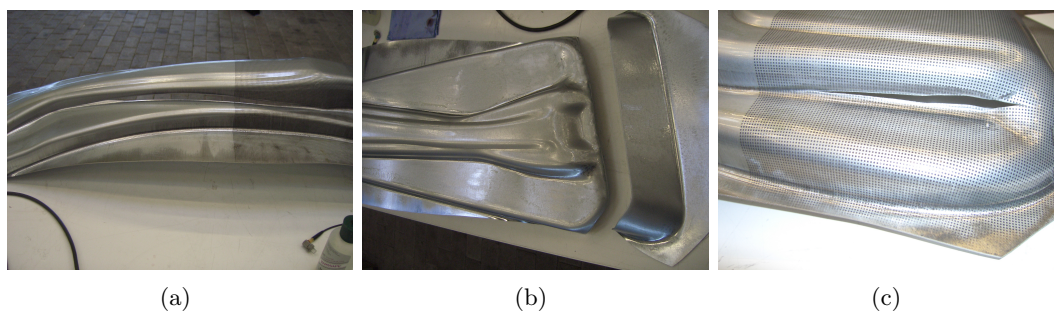


Figure E.29: Experiment number 7 BHF = 3400 [kN], day 1



Figure E.30: Experiment number 16 BHF = 2200 [kN], day 2



Figure E.31: Experiment number 18 BHF = 2600 [kN], day 2

E.5.2 DP600



Figure E.32: Experiment number 14 BHF = 4000 [kN], day 1

